

# Stimuli-Responsive Hydrogels and Hydrogel Pore-Filled Composite Membranes

(Stimuli-responsive Hydrogele und  
Poren-gefüllte Hydrogel-Kompositmembranen)

- D I S S E R T A T I O N -

*by*

Nadia Binti Adrus  
*from Perlis, Malaysia*

*Dissertation submitted to the*

Department of Chemistry of  
Universität Duisburg-Essen, in partial fulfilment of  
the requirements of the degree of  
Dr. rer. nat.

Essen, 2012

ULBRICHT  
GROUP



UNIVERSITÄT  
DUISBURG  
ESSEN

Approved by the examining committee on: 10.04.2012

Chair: Prof. Dr. Georg Jansen

Advisor: Prof. Dr. Mathias Ulbricht.

Reviewer: Prof. Dr. Christian Mayer.

This work was performed during the period from November 2007 to February 2012 at the Institute of Technical Chemistry (Lehrstuhl für Technische Chemie II), Department of Chemistry, Universität Duisburg-Essen, under the supervision of Prof. Dr. Mathias Ulbricht.

I declare that this dissertation represents my own work, except where due acknowledgement is made.

A handwritten signature in blue ink, appearing to read 'Nadia Binti Adrus', is written above a horizontal line.

Nadia Binti Adrus

## ***Abstracts***

Classical bulk temperature-responsive poly(*N*-isopropylacrylamide) (PNIPAAm) hydrogels were prepared *via* free radical polymerization in the presence of *N,N'*-methylenebisacrylamide (MBAAm) as a crosslinker. Two different initiation methods were studied: redox and photoinitiation. It was demonstrated that the desired final properties of resulting hydrogels, i.e., high monomer conversion and adjustable swelling were only achieved by selecting best suited initiation conditions. For redox polymerization, this was done by tuning the ratio of accelerator *N,N,N',N'*-tetramethylethylenediamine to initiator ammonium persulfate. The key parameters for achieving optimum photopolymerization conditions were photoinitiator concentration and UV irradiation time. With the help of *in situ* rheological measurements, optimum conditions could be further verified and quantified by monitoring the liquid-to-gel transition. Overall, photoinitiated crosslinking copolymerization was postulated to offer better options for *in situ* preparation of tailored functional hydrogels. Therefore the classical photopolymerized bulk PNIPAAm hydrogels were characterized in more details (swelling and mesh size, swelling recovery, volume expansion factor relative to synthesis state, morphology and partitioning of test solutes) as compared to redox hydrogels (swelling and mesh size). Rheology was also used to investigate the hydrogel after *ex situ* preparation, revealing “perfect” soft-rubbery behaviour. A good correlation between the mesh sizes determined from swelling and rheology was also found. Rheology has been found to be a powerful tool because it provides valuable data on polymerization and gelation kinetics as well as information about the hydrogels microstructure based on their viscoelastic character. The resulting optimum conditions from this part were utilized towards preparation and characterization of smart hydrogels that can respond to multiple stimuli and also functional pore-filling composite membranes.

Temperature-responsive PNIPAAm hydrogels were imprinted with lysozyme *via in situ* photoinitiated crosslinking copolymerization. The three-dimensional network of the hydrogels was tailored by tuning the ionic content through methacrylic acid (MAA) as template-binding comonomer while keeping the ratio between crosslinker (MBAAm) and *N*-isopropylacrylamide (NIPAAm) fixed. The rheological data demonstrated that the onset of gelation was delayed with increasing MAA content. Moderate salt concentrations (0.3 M NaCl) were found to be suited for template removal without phase separation of the hydrogel. Swelling and protein (lysozyme and cytochrome C) binding were investigated for molecularly imprinted (MIP) and non-imprinted polymers (NIP) gels at temperatures below and above the lower critical solution temperature of PNIPAAm (32 °C). MIP gels showed a much higher affinity, selectivity and binding capacity for lysozyme compared to the NIP reference materials. Protein binding capacity was strongly reduced above 32 °C, to zero for NIP and to small values for imprinted gels. Most important, specific lysozyme binding to the MIP gels caused a large concentration dependent deswelling. This effect was much smaller for NIP gels, and the response could be

modulated by the content of the comonomer methacrylic acid. It is envisioned that the alteration of swollen state of stimuli-responsive MIP hydrogels as functions of specific protein or temperature may govern the recognition-ability and binding-specificity towards establishment of novel biomimetic materials.

A copolymer of PNIPAAm and 4-vinylbenzo-18-crown-6 (vCE) was synthesized *via* redox-initiation polymerization. The influence of vCE content on the copolymerization efficiency and also on the ion-recognition properties was investigated. The copolymerization was relatively efficient in a more loosely crosslinked network (rheology and Fourier transform infrared analyses). The swelling of PNIPAAm-*co*-vCE at 37 °C was higher in the presence of cations; i.e.  $\text{Ba}^{2+} > \text{K}^+$  than in pure water. The hydrogel copolymers were more sensitive at the higher ion concentration (0.02 M). The cation recognition and selectivity were further enhanced by the increase of vCE content in the hydrogel copolymers. Overall, this approach is interesting for the development of novel sensors or materials for controlled release applications.

Hydrogel pore-filled composite membranes (HPFCM) based on polyethylene terephthalate (PET) track-etched membranes with pore diameters between 200 and 5000 nm and temperature-responsive PNIPAAm hydrogels were successfully prepared. A prefunctionalization of the pore walls by grafted linear PNIPAAm lead to stable anchoring of crosslinked PNIPAAm prepared in a subsequent step. Proper tuning of photopolymerization conditions resulted in desired microstructure of the hydrogels and thus tailored barrier properties of the composite membranes. The very interesting separation performance of HPFCM was due to diversification of the hydrogel network as function of its composition that caused adjustable sieving properties *via* synthesis conditions and also largely switchable barrier properties in response to the temperature. The interplay between the immobilized hydrogel and various pore sizes of the membrane support was also investigated. The base membrane provides mechanical support and confines the hydrogel within its pores, and it thus allows using the hydrogel mesh size for size-selective solute transport. Completely stable and selective HPFCM were only obtained with base pore sizes of about 2  $\mu\text{m}$  or smaller. The size-selectivity (molecular weight cut-off) of the same HPFCM was higher under diffusive than under convective flow conditions; this is presumably mainly caused by elastic deformation of the hydrogel network. The cut-off from diffusion experiments was well correlated to mesh-size of the hydrogel determined from the Darcy model applied to permeability data obtained under convective flow conditions. Upon temperature increase beyond 32 °C, flux increased and rejection decreased very strongly; this remarkable change between macromolecule-size selective ultrafiltration and microfiltration/filtration behaviour was fully reversible. The smart performance of HPFCM could be interesting for the separation of multi-component mixtures or for controlled release due to the tunability of the sieving coefficient by changing the temperature.

- The art of being wise is the art of knowing what to overlook. The art of love is largely the art of persistence -

*To my husband (Nazri) and my son (Nafiz), who are always be there for me and for loving me so much*

## *Acknowledgements*

I would like to express my gratitude to those who gave me the possibility to complete this dissertation.

First and foremost, my advisor, Prof. Dr. Mathias Ulbricht has always been a role model to me. I am deeply impressed with his profound knowledge in the field of membrane technology and polymer science. He has been a noble guide with his novel ideas and inspiring discussions throughout the research period. He is generous with his time and his encouragement. His patience and support helped me to overcome countless problems. My deepest gratitude is especially dedicated to him. I hope that one day I would become as good an advisor to my students as Mathias Ulbricht has been to me.

Secondly, I would like to acknowledge the other two members of my oral defence committee; Prof. Dr. Christian Mayer and Prof. Dr. Georg Jansen.

Many thanks to Dr. Abdul Halim Mohd Yusof for being the first person I met the first time I landed in Germany (Halle Saale) in 2005. He always provides a great assistance to me and my family. I am also thankful to him for his valuable comments.

I feel privileged to have been able to work with all members (previous and current) of the Lehrstuhl für Technische Chemie II. Particularly I wish to acknowledge Dr. Heru Susanto, Dr. Eva Maria Berndt, Dr. Monica Sallai, Dr. Haofei Guo, Dr. Polina Peeva, Karin Klingelhöller and Jing Lei.

I would like to express my appreciation to Tobias Hennecke, Fatih Özcan, Annie Froeschner, Tobias Grees and also Kevin Bojaryn who devoted contributions on the collaborative works. I wish a good success to Tobias Hennecke for his doctoral study.

I am highly indebted to Inge Danielzik, Claudia Schenk, Tobias Kallweit and Jürgen Schulze-Braucks for providing the technical support. Inge and Claudia have done a great help to improve my practical skills. To Frau Nordmann, I gratefully acknowledge for the secretarial work.

I wish to thank Smail Boukercha for SEM measurement and also Dieter Jacobi for GPC analysis.

I would like to express my gratitude to the Universiti Teknologi Malaysia and Ministry of Higher Education Malaysia for granting me sponsorship to accomplish my doctoral study at Universität Duisburg Essen, Essen, Germany.

To my best friends, Yusliza Md Yunus and Noraina Suyanti Md. Aris, I greatly value their friendship and motivation.

To my fellowmates, Noor Ashrina Hamid and Nurharniza Abd Rahman (also cousin), I cherish their magical words. I wish a good success to them for their doctoral study.

My family has been a truly inspirational. To my father Haji Adrus Ismail, whom I shared the same interest (Chemistry). To my mother, Hajjah Naemah Saad, who raised me with a love of science. To my one and only sister, Aliya Adrus, I am grateful for our memorable childhood. And to my brothers, Khairi and Fauzi Adrus, I appreciate for their belief in me. My deepest appreciation also goes to my parents-in-law for their support and prayers from afar.

Especially, I would like to convey my heart-felt gratitude to my dear husband Nazri whose love and patience encouraged and enabled me to complete this work. He has been a great companion through happiness and sadness. Words alone cannot express what I owe him. To my son Nafiz, I owed him the time that I spent in the lab or in front of computer to finish this doctoral study. One thing for sure, his smile faded away my sorrow.

Finally, all the praises and thanks be to Allah.



The main parts of this dissertation have been published (submitted) in the following publications:

- [1] N. Adrus and M. Ulbricht. Rheological studies on PNIPAAm hydrogel synthesis *via in situ* polymerization and on resulting viscoelastic properties, *React. Func. Polym.* (2012) submitted.
- [2] N. Adrus and M. Ulbricht. Novel hydrogel pore-filled composite membranes with tunable and temperature-responsive size-selectivity, *J. Mater. Chem.* **12** (2012) 3088.
- [3] N. Adrus and M. Ulbricht. Molecularly imprinted stimuli-responsive hydrogels for protein recognition, *Polymer* (2012) submitted.

# TABLE OF CONTENT

<i>Title Page</i> .....	<i>i</i>
<i>Abstracts</i> .....	<i>iv</i>
<i>Acknowledgements</i> .....	<i>vii</i>
<i>Table of Content</i> .....	<i>x</i>
<i>List of Figures</i> .....	<i>xvi</i>
<i>List of Tables</i> .....	<i>xxiv</i>
<i>List of Schemes</i> .....	<i>xxvii</i>
<b>1. INTRODUCTION</b> .....	<b>1</b>
1.1 Introduction .....	1
1.2 Problem Statement.....	2
1.3 Objective of the Research .....	4
1.4 Scope of the Research .....	5
<b>2. THEORY AND LITERATURE REVIEW</b> .....	<b>8</b>
2.1 Polymer-Based Hydrogels.....	8
2.1.1 The Gelation.....	9
2.1.2 Study of Hydrogel Network Structure .....	11
2.1.3 Separation Functions of Hydrogels .....	16
2.2 Stimuli-Responsive Polymer Hydrogel Systems.....	18
2.2.1 General Properties and Classification.....	18
2.2.2 Classical Temperature-Responsive Hydrogels.....	19
2.2.3 Temperature-Responsive and Protein-Selective Hydrogels.....	21
2.2.4 Temperature-Responsive and Ion-Selective Hydrogels.....	22
2.3 Membranes and their Functionalization .....	25
2.3.1 Basic Principles of Conventional Ultrafiltration and Microfiltration Membranes .....	26
2.3.2 Surface Functionalization <i>via Grafting-From</i> .....	28
2.3.3 Pore-Filling Functionalization .....	29
2.3.3.1 Concept and overview .....	29
2.3.3.2 Preparation of composite membranes.....	31
2.3.3.3 Performance and function .....	31

<b>3. EXPERIMENTAL</b> .....	<b>33</b>
<b>3.1 Chemicals and Materials</b> .....	<b>33</b>
3.1.1 Hydrogel Compositions .....	33
3.1.1.1 Hydrogel compositions for classic hydrogels .....	34
3.1.1.2 Hydrogel compositions with ionic comonomer .....	35
3.1.1.3 Hydrogel compositions with macrocyclic comonomer .....	35
3.1.2 Membranes.....	36
3.1.3 Information on Test Solutes .....	36
3.1.4 Others .....	37
<b>3.2 Synthesis of Stimuli-Responsive Bulk Hydrogels</b> .....	<b>38</b>
3.2.1 Redox-Polymerization of Poly( <i>N</i> -Isopropylacrylamide) Hydrogels .....	38
3.2.1.1 Preliminary experiments .....	38
3.2.1.2 Synthesis of conventional and phase-separated hydrogel.....	39
3.2.1.3 Rheology monitoring <i>in situ</i> redox-polymerization .....	39
3.2.2 Photopolymerization of Poly( <i>N</i> -Isopropylacrylamide) Hydrogels.....	40
3.2.2.1 Preliminary experiments: efficiency of photoinitiator .....	40
3.2.2.2 Optimization of photopolymerization conditions.....	42
3.2.2.3 Synthesis of hydrogels various compositions .....	42
3.2.2.4 Rheology monitoring <i>in situ</i> photo-polymerization .....	42
3.2.3 Synthesis of Molecularly Imprinted and Non-Imprinted Poly( <i>N</i> -Isopropylacryl amide- <i>co</i> - Methacrylic Acid) Hydrogels <i>via</i> Photopolymerization .....	43
3.2.4 Synthesis of Poly( <i>N</i> -Isopropylacrylamide- <i>co</i> -4-vinylbenzo-18-crown-6) Hydrogels <i>via</i> Redox-Polymerization .....	44
<b>3.3 General Characterization of Hydrogels</b> .....	<b>45</b>
3.3.1 Washing and Conversion .....	45
3.3.2 Evidence of Copolymerization .....	46
3.3.3 Swelling Experiments .....	46
3.3.4 Rheology and Viscoelasticity of Hydrogels.....	46
3.3.5 Determination of the Mesh Size .....	46
3.3.6 Morphology Investigation of Hydrogels.....	46
<b>3.4 Functional Characterization of Hydrogels</b> .....	<b>47</b>
3.4.1 Partitioning Test for Non-ionic Hydrogels .....	47
3.4.2 Sorption Experiments for Molecular-Imprinted and Non-Imprinted Hydrogels.....	47
3.4.2.1 Rebinding Tests with Template-Protein .....	47

3.4.2.2	Rebinding Tests with Competitive-Protein.....	47
3.4.3	Ion-Sensitivity Test for Poly( <i>N</i> -Isopropylacrylamide- <i>co</i> -4-vinylbenzo-18-crown-6) Hydrogels.....	48
<b>3.5</b>	<b>Functionalization of Membranes.....</b>	<b>48</b>
3.5.1	Prefunctionalization <i>via Grafting-From</i> Photoinitiator Adsorption Method .....	48
3.5.2	Pore-Filling Functionalization .....	49
3.5.3	Degree of Functionalization.....	50
3.5.4	Scanning Electron Microscopy .....	50
<b>3.6</b>	<b>Functional Characterization of Base, Prefunctionalized and Pore-Filled Composite Membranes.....</b>	<b>50</b>
3.6.1	Water Permeability.....	50
3.6.1.1	Determination of Hydrodynamic Layer Thickness .....	51
3.6.1.2	Determination of Darcy Void-Spacing .....	51
3.6.1.3	Permporometry.....	51
3.6.2	Stability Tests.....	52
3.6.3	Switchability Tests .....	52
3.6.4	Size-Selectivity Tests <i>via</i> Convective Fractionation of Solute .....	52
3.6.5	Size-Selectivity Tests <i>via</i> Solute Diffusion.....	53
<b>4.</b>	<b><i>RESULTS AND DISCUSSION</i>.....</b>	<b>54</b>
<b>4.1</b>	<b>Poly(<i>N</i>-isopropylacrylamide) Bulk Hydrogels .....</b>	<b>54</b>
4.1.1	Redox-Polymerization .....	54
4.1.1.1	Hydrogel washing and calculation of conversion .....	54
4.1.1.2	Optimization of accelerator to initiator ratio.....	57
4.1.1.3	Physical properties of redox hydrogels.....	58
4.1.1.3.1	<i>Effect of crosslinker</i> .....	58
4.1.1.3.2	<i>Effect of synthesis temperature</i> .....	59
4.1.1.3.3	<i>Effect of solvent/porogen</i> .....	59
4.1.1.4	Rheology.....	61
4.1.1.4.1	<i>Gelation point and reproducibility of gelation</i> .....	61
4.1.1.4.2	<i>Influence of accelerator to initiator ratio</i> .....	62
4.1.1.5	Equilibrium swelling degree and mesh size.....	63
4.1.2	Photopolymerization.....	66
4.1.2.1	Kinetics of photoinitiator .....	66

4.1.2.2	Optimization of photopolymerization conditions.....	67
4.1.2.2.1	Effect of photoinitiator concentration .....	67
4.1.2.2.2	Effect of UV irradiation time.....	68
4.1.2.3	Conversion and physical properties of various compositions of photopolymerized hydrogels.....	69
4.1.2.4	Rheology.....	72
4.1.2.4.1	<i>Influence of UV intensity</i> .....	72
4.1.2.4.2	<i>Influence of UV irradiation time</i> .....	73
4.1.2.4.3	<i>Influence of UV as a trigger of photopolymerization</i> .....	74
4.1.2.4.4	<i>Influence of monomer content</i> .....	75
4.1.2.4.5	<i>Influence of crosslinker content</i> .....	76
4.1.2.4.6	<i>Temperature-responsivity</i> .....	77
4.1.2.4.7	<i>Viscoelasticity of hydrogels and their mesh sizes</i> .....	78
4.1.2.5	Equilibrium swelling degree as function of temperature and recovery of swelling.....	80
4.1.2.6	Structure of hydrogels .....	83
4.1.2.7	Partitioning of test solutes.....	84
<b>4.2</b>	<b>Molecularly Imprinted and Non-Imprinted Poly(<i>N</i>-Isopropylacryl amide) Bulk Hydrogels</b> .....	<b>86</b>
4.2.1	Rheology Investigation of Gelation Kinetics .....	86
4.2.2	Template-Protein Removal and Conversion .....	87
4.2.3	Physical Properties and Temperature-Responsivity .....	89
4.2.4	Protein Binding .....	92
4.2.4.1	Binding capacity and imprinting factor .....	92
4.2.4.2	Protein sorption isotherm.....	93
4.2.4.3	Protein binding selectivity .....	94
4.2.4.4	Temperature-induced binding response.....	95
4.2.4.5	Specific volume change induced by protein-responsivity .....	96
<b>4.3</b>	<b>Ion-Selective Poly(<i>N</i>-Isopropylacrylamide-<i>co</i>-4-vinylbenzo-18-Crown-6) Bulk Hydrogels</b>	<b>98</b>
4.3.1	Conversion and Copolymerization Efficiency .....	98
4.3.2	Rheology Investigation of Gelation Kinetics .....	100
4.3.3	Equilibrium Swelling Degree.....	101
4.3.4	Ion-Responsivity .....	102

<b>4.4</b>	<b>Characterization of Base Membranes .....</b>	<b>105</b>
4.4.1	Average Pore Size, Pore Size Distribution and Pore Properties.....	105
4.4.2	Water Permeability.....	106
<b>4.5</b>	<b>Prefunctionalization and Characterization of Prefunctionalized Membranes.....</b>	<b>107</b>
4.5.1	Selections of Suitable Prefunctionalization .....	107
4.5.2	Degree of Grafting.....	109
4.5.3	Switchability of Membrane Pore after Prefunctionalization.....	110
<b>4.6</b>	<b>Pore-Filling and Characterization of Pore-Filled Composite Membranes.....</b>	<b>111</b>
4.6.1	Pore-Filling under 'Open' System.....	111
4.6.1.1	Permeability .....	111
4.6.1.2	Switchability and Stability .....	112
4.6.1.3	Scanning electron microscopy .....	114
4.6.1.4	'Open' pore-filling: some remarks for improvement.....	114
4.6.2	Pore-filling under 'Closed' System: General Characterization.....	115
4.6.2.1	Degree of pore-filling .....	115
4.6.2.2	Scanning electron microscopy .....	116
4.6.3	Pore-filling under 'Closed' System: Functional Characterization.....	119
4.6.3.1	Water permeability .....	119
4.6.3.2	Microstructure of pore-filled hydrogel composite membranes .....	121
4.6.3.3	Stability.....	123
4.6.3.4	Temperature-responsive permeability .....	124
4.6.3.5	Size-selectivity of pore-filled composite membranes under diffusion .....	127
4.6.3.5.1	<i>Effect of base membranes .....</i>	<i>127</i>
4.6.3.5.2	<i>Effect of hydrogel composition .....</i>	<i>128</i>
4.6.3.5.3	<i>Effect of temperature.....</i>	<i>129</i>
4.6.3.6	Size-selectivity of pore-filled composite membranes under ultrafiltration...	130
4.6.3.6.1	<i>Effect of UV-irradiation time.....</i>	<i>130</i>
4.6.3.6.2	<i>Effect of base membranes .....</i>	<i>131</i>
4.6.3.6.3	<i>Effect of transmembrane pressure.....</i>	<i>131</i>
4.6.3.6.4	<i>Effect of temperature.....</i>	<i>134</i>
4.6.3.6.5	<i>Effect of composition.....</i>	<i>134</i>
4.6.3.7	Mechanism for tunable and switchable size-selectivity of composite membranes .....	136

**5. CONCLUSIONS..... 138**

**REFERENCES..... 141**

*Abbreviations and Symbols.....xxviii*

*List of Awards and Publications ..... xxxii*

*Curriculum Vitae..... xxxv*

## List of Figures

Figure 1.1	Membrane modification (a) on the outer surface, (b) and (c) on the pore wall surface; the pore diameter does not change effectively in the case of (c).....	3
Figure 1.2	Chemical structures of PNIPAAm, PNIPAAm- <i>co</i> -MAA and PNIPAAm- <i>co</i> -vCE hydrogels.....	6
Figure 1.3	Schematic illustration of pore-filling functionalization <i>via in situ</i> photopolymerization; (a) filling and equilibration of membrane with reaction mixture, sealing and pressing with two glass plates on top and bottom sides; (b)-(d) cross-section view of prefunctionalized membrane pore, obtained <i>via grafting-from</i> of linear functional polymer chains ( <i>c.f.</i> <sup>[32, 43]</sup> ), (b) during equilibration with reaction mixture, (c) during UV initiated <i>in situ</i> crosslinking polymerization, and (d) after complete reaction toward hydrogel pore-filled composite membrane (HPFCM). ....	7
Figure 2.1	Schematic representation of chemical and physical gels. ....	8
Figure 2.2	Swollen, crosslinked structure of hydrogel by a thermodynamically compatible liquid, indicating the number average molecular weight between crosslinks, $M_c$ and the average mesh size, $\zeta$ . Figure adapted from <sup>[48, 68]</sup> . ....	12
Figure 2.3	Various types of crosslinked networks; ideal versus network imperfections (left; from ref. <sup>[66]</sup> ), and conventional versus macroporous network of hydrogels (right; from ref. <sup>[17]</sup> ). ....	12
Figure 2.4	Dynamic mechanical behaviour of polybutadiene samples <sup>[73]</sup> .....	15
Figure 2.5	Reversible volume phase transition of stimuli-responsive gels. From ref. <sup>[49]</sup> .....	18
Figure 2.6	Phase separation mechanisms of PNIPAAm below and above its LCST <sup>[101]</sup> . ....	19
Figure 2.7	Principles of molecular imprinting (1 = functional monomers, 2 = crosslinker monomer, 3 = template molecule; a = self-assembly, b = polymerization, c = removal of template molecule). Adapted from ref. <sup>[115]</sup> .....	21
Figure 2.8	Chemical structures of common crown ethers: (a) 12-crown-4 (CE-12,4), (b) 15-crown-5 (CE-15,5) and (c) 18-crown-6 (CE-18,6). (d) and (e) are nitrogen-substitutes aza crown ether of CE-18,6 family members.....	23
Figure 2.9	Formation of 2 : 1 (left <sup>[138]</sup> ) and 1 : 1 (right <sup>[144]</sup> ) stable complexes of PNIPAAm copolymerized either with CE-15,5 (left) or CE-18,6 (right) in the presence of potassium ion that induced negatively or positively LCST shift, respectively. ....	24



Figure 2.10	Schematic depiction of three main composite membrane types: (a) thin-film, (b) pore-filling and (c) pore-surface functionalization <sup>[1]</sup> .....	25
Figure 2.11	Schematic illustration of different pressure-driven membrane processes according to size of pores in the selective barrier and size of exemplaric targets for separation <sup>[1]</sup> .....	26
Figure 2.12	Morphology of MF membrane prepared by phase inversion (left) <sup>[156]</sup> , stretching (middle) <sup>[157]</sup> , and track-etching (right) <sup>[32]</sup> .....	27
Figure 2.13	A two-step UV-assisted graft copolymerization ( <i>grafting-from</i> ) applicable to various functional monomers according to Ulbricht <sup>[44]</sup> .....	28
Figure 2.14	The pore-filling concept according to Yamaguchi <i>et al.</i> <sup>[163]</sup> .....	29
Figure 2.15	Using water permeabilities in combination with Hagen-Poiseuille and Darcy models to characterize the unmodified, prefunctionalized and hydrogel pore-filled composite membrane. $J$ is water flux through the membrane [ $l/m^2h$ ], $V$ is volume of permeate [l], $A$ is membrane outer surface area [ $m^2$ ], $\epsilon_{mem}$ is membrane porosity [%], $\eta$ is viscosity of water [Pa.s], $\Delta P$ is transmembrane pressure [bar], $\Delta t$ is time [s] and $\Delta x$ is membrane thickness [m]. .....	30
Figure 3.1	The chemical structure of PET.....	36
Figure 3.2	Molecular weight distribution of feed used for diffusion and filtration experiment. ....	37
Figure 3.3	Reaction vessel for synthesis of PNIPAAm- <i>co</i> -vCE hydrogels.....	44
Figure 3.4	Illustration of prefunctionalization experimental set-up <i>via grafting-from</i> . ....	48
Figure 3.5	Illustration of 'open' pore-filling functionalization steps. The membrane was equilibrated with the monomer solution between 2 glass plates and then subjected to UV irradiation. ....	49
Figure 3.6	Illustration of 'closed' pore-filling functionalization steps. The membrane equilibrated with the monomer solution was sealed in a plastic bag, pressed between 2 glass plates and then subjected to UV irradiation. ....	49
Figure 4.1	Sum of the washed carbon per washing step in PNIPAAm hydrogels with and without PEG as a porogen. The monomer was not recrystallized prior to the synthesis. The argon deaeration step was omitted during the preparation of hydrogels. The polymerization was performed for 24 h, at 15 °C using TEMED/APS 4.0 : 1.....	55

Figure 4.2	Influence of TEMED to APS ratio towards gelation of hydrogels with 15 wt% NIPAAm and 5 wt% MBAAm (M15DC05). From here the polymerization was performed under Argon conditions and using recrystallized monomer. Other conditions <i>c.f.</i> Figure 4.1. ....	57
Figure 4.3	Photograph showing the appearance of hydrogels obtained without PEG (PEG0, left-hand side) or with PEG (PEG40, right-hand side).....	60
Figure 4.4	Gelation point (cross-over between $G'$ and $G''$ ) and reproducibility of the online rheological monitoring. <i>In situ</i> polymerization toward PNIPAAm hydrogels was performed using initiator TEMED/APS 0.5 : 1. Other conditions were as for bulk gels ( <i>c.f.</i> Figure 4.1). Arrows indicate the further development of storage and loss moduli (in first run).....	61
Figure 4.5	<i>In situ</i> polymerization toward PNIPAAm hydrogels with variation in TEMED/APS ratio (arrows indicate acceleration of $G'$ due to "gel-effect"). Other conditions were as for bulk gels ( <i>c.f.</i> Figure 4.1) .....	62
Figure 4.6	Equilibrium swelling degree of PNIPAAm hydrogels as a function of temperature: (a) influence of TEMED/APS ratio (M15DC05); (b) influence of crosslinker content (TEMED/APS 4.0 : 1); and (c) conventional vs. macroporous PNIPAAm hydrogels (macroporous hydrogels were prepared either above LCST or using PEG as a porogen, TEMED/APS 4.0 : 1).....	63
Figure 4.7	The kinetic plots of photoinitiator Irgacure-2959® fit the first reaction order. ....	67
Figure 4.8	Influence of PI concentration and UV time toward conversion (TOC) of PNIPAAm hydrogels (M15DC05). The polymerization was performed at 4 °C.....	68
Figure 4.9	Photograph showing the appearance of hydrogels (M15DC05) obtained with 2 wt% of PI, irradiated 15.0 (left) and 20 min (right). ....	69
Figure 4.10	Photograph showing the conventional hydrogel (left; M15DC05) as well as the influence of crosslinker (middle; M15DC10) and porogen content (right; M15DC05PEG40) on the appearance of hydrogels. ....	70
Figure 4.11	<i>In situ</i> photopolymerization towards PNIPAAm hydrogels (UV time 15 min; hydrogel composition: M15DC05, 2 wt% PI) performed at different UV intensities. Other conditions were as for bulk gels ( <i>c.f.</i> Table 4.8). ....	72
Figure 4.12	Investigation of UV irradiation time to achieve complete reaction to crosslinked PNIPAAm hydrogel (UV time 15 min; hydrogel composition: M15DC05, 2 wt% PI). Measurement was performed at constant UV intensity	

	of 1 mW/cm <sup>2</sup> , and UV irradiation was kept “on” for the described time followed by another period with UV “off”.....	73
Figure 4.13	Investigation of photopolymerization toward PNIPAAm hydrogels using interrupted UV irradiation at constant intensity of 1 mW/cm <sup>2</sup> . Experiment 1 is a control experiment (analogous to Figure 4.12).....	74
Figure 4.14	Influence of monomer content (M_ <sub>-</sub> DC05) on the onset of gelation. Measurement was performed at constant UV intensity of 1 mW/cm <sup>2</sup> (analogous to Figure 4.12).....	75
Figure 4.15	Influence of crosslinker content (M15DC_ <sub>-</sub> ) on the onset of gelation. Measurement was performed at constant UV intensity of 1 mW/cm <sup>2</sup> (analogous to Figure 4.12).....	76
Figure 4.16	Monitoring temperature-responsivity of PNIPAAm hydrogels (bulk gels prepared with 15 min photopolymerization, $\omega = 1$ rad/s, $\gamma = 1$ %, $F_N = 5$ N) using different heating rates.....	77
Figure 4.17	Storage modulus at 20 °C as a function of shear frequency for PNIPAAm hydrogels (a) prepared at different UV irradiation times (hydrogel composition: M15DC05); and (b) various compositions (obtained at 15 min UV time). ....	78
Figure 4.18	Equilibrium swelling degree of PNIPAAm hydrogels as a function of temperature: influence of irradiation time for hydrogels obtained with (a) 2.0 and (b) 3.5 wt % PI concentration respectively (hydrogel composition: M15DC05); and (c) influence of compositions (hydrogels were obtained using 2.0 wt% PI concentration and 15 min irradiation time).....	81
Figure 4.19	SEM micrographs of swollen hydrogels in freeze-dried state: (a) M15DC02; (b) M15DC10; and (c) M15DC05PEG40.....	83
Figure 4.20	ESEM micrograph of swollen hydrogel in a wet state (M15DC02). ....	83
Figure 4.21	The comparison between experimental (solid line) and calculated data (dashed-line; <i>c.f.</i> 2.1.3) of the reflection coefficient of test solutes: (i) dextran from various molecular weights, and (ii) lysozyme, in M15DC05 gel. ....	85
Figure 4.22	The reflection coefficient of dextran from various gel compositions (calculated data; <i>c.f.</i> 2.1.3).....	85
Figure 4.23	Influence of template-monomer content on the gelation time for NIP and MIP hydrogels. Measurement was performed at constant UV intensity of 1 mW/cm <sup>2</sup> (analogous to Figure 4.12). ....	86

Figure 4.24	Photograph showing the effect of sodium chloride concentration used for washing of MIP and NIP hydrogels prepared with 5 wt% MAA.....	88
Figure 4.25	Photograph showing the influence of MAA content on properties of MIP and NIP gels (washing: 0.3 M NaCl).....	90
Figure 4.26	Degree of swelling for MIP and NIP hydrogels prepared with 2 wt% of MAA as a function of temperature.....	90
Figure 4.27	Degree of swelling for MIP and NIP hydrogels at two temperatures as a function of MAA content.....	91
Figure 4.28	Binding capacities and resulting imprinting factor obtained with 0.5 g/l lysozyme in tris-HCl buffer (10 mM, pH 7.0) at RT.....	92
Figure 4.29	Binding isotherms for MIP and NIP with lysozyme in tris-HCl buffer (10 mM, pH 7.0) at RT; hydrogel composition: M15M'02DC05. Binding constants for MIP and NIP hydrogels were $3.9 \times 10^5 \text{ M}^{-1}$ and $7.7 \times 10^4 \text{ M}^{-1}$ , respectively.....	94
Figure 4.30	Protein binding selectivity for MIP and NIP hydrogels with total initial protein concentration of 0.5 g/l.....	94
Figure 4.31	Influence of temperature on binding for MIP and NIP hydrogels. Initial protein concentration 0.5 g/l; hydrogel composition: M15M'02DC05. ....	96
Figure 4.32	Volume shrinking for MIP and NIP hydrogels as function of lysozyme concentrations in tris-HCl buffer (10 mM, pH 7.0) at RT; hydrogel composition: M15M'02DC05. ....	97
Figure 4.33	Volume shrinking upon protein binding for MIP and NIP hydrogels with increasing template-monomer content. Initial protein concentration of 0.5 g/l lysozyme in tris-HCl buffer (10 mM, pH 7.0) at RT.....	97
Figure 4.34	Conversion from TOC to PNIPAAm-co-vCE hydrogels with various crown ether content. Hydrogels were obtained using initiator TEMED/APS 4.0 : 1. Other conditions <i>c.f.</i> Table 4.4. ....	98
Figure 4.35	Copolymerization of PNIPAAm-co-vCE hydrogels with various crown ether content <i>via</i> FTIR analysis at $1052 \text{ cm}^{-1}$ (symmetrical C-O-stretching in Ar-O-R), $1129 \text{ cm}^{-1}$ (asymmetrical C-O-stretching in R'-O-R), $1264 \text{ cm}^{-1}$ (asymmetrical C-O-stretching in Ar-O-R), $1518 \text{ cm}^{-1}$ (C=C-stretching of phenyl ring).....	99
Figure 4.36	Copolymerization of PNIPAAm-co-vCE hydrogels <i>via</i> FTIR analysis with various crosslinker content. ....	100

Figure 4.37	Influence of (a) crown ether content; and (b) crosslinker content on the onset of gelation. ....	100
Figure 4.38	Equilibrium swelling degree of PNIPAAm- <i>co</i> -vCE hydrogels as a function of temperature: (a) influence of crown ether content; (b) influence of crosslinker content on hydrogels with 5 % crown ether content; and (c) influence of crosslinker content on hydrogels with 10 % crown ether content. ....	101
Figure 4.39	Equilibrium swelling degree of PNIPAAm- <i>co</i> -vCE hydrogels with various crown ether content at 37 °C as a function of potassium ion concentration (left); size of ions (right).....	104
Figure 4.40	Equilibrium swelling degree of PNIPAAm- <i>co</i> -vCE hydrogels with various crosslinker content at 37 °C as a function of potassium ion concentration (left); size of ions (right). Hydrogels obtained with 5 % crown ether content.....	104
Figure 4.41	Equilibrium swelling degree of PNIPAAm- <i>co</i> -vCE hydrogels with various crosslinker content at 37 °C as a function of potassium ion concentration (left); size of ions (right). Hydrogels obtained with 10 % crown ether content.....	104
Figure 4.42	Pore-size distribution measurement of the unmodified PET track-etched base membrane obtained from gas flow / pore dewetting permoporometry; nominal pore diameter 1000 nm. ....	105
Figure 4.43	Pore-size distributions of various pore-sizes of unmodified base membranes (analogous to Figure 4.42) and their corresponding porosity. ....	106
Figure 4.44	Permeabilities and hydrodynamic layer thicknesses after prefunctionalization step at RT and 45 °C; base membrane: 1000 nm (left) and base membrane 5000 nm (right). ....	107
Figure 4.45	Degree of functionalization (DOF) of grafted PNIPAAm for base membranes with different nominal pore diameter (monomer concentrations [wt %] / nominal pore diameter of base membranes [nm]: 1.0 / 200; 1.5 / 400; 2.5 / 1000; 7.5 / 3000; 10 / 5000).....	109
Figure 4.46	Effective hydrodynamic layer thickness of grafted PNIPAAm at RT and 45 °C (calculated from water permeability before and after prefunctionalization using Hagen-Poiseuille equation; <i>c.f.</i> Figure 2.15) for base membranes with different nominal pore diameter. ....	110
Figure 4.47	Reversible temperature responsivity of water permeability for HPFCM prepared either with or without prefunctionalization step and their	

	corresponding recovery values; base membrane: 5000 nm (hydrostatic pressure).....	113
Figure 4.48	Water permeability for HPFCM prepared either with or without prefunctionalization step as a function of pressure (left) and their corresponding recovery values (right); base membrane: 5000 nm.....	113
Figure 4.49	SEM micrographs of the outer surface of unmodified PET membranes (left) and HPFCM after 15 min UV irradiation (hydrogel composition: M15DC05, right); nominal based membrane pore size had been 5000 nm. ....	114
Figure 4.50	SEM micrographs of the cross sectional view (above) and the outer surface (below) of unmodified membranes (left), of prefunctionalized membranes (middle), and HPFCM after 15 min UV irradiation (hydrogel composition: M15DC05, right); nominal base membrane pore size had been 1000 nm. ....	117
Figure 4.51	SEM micrographs of the outer surface of unmodified PET membranes (left) and HPFCM after 15 min UV irradiation (hydrogel composition: M15DC05, right); nominal base membrane pore size had been 400 nm (above) and 1000 nm (below).....	118
Figure 4.52	Water permeability at RT of HPFCM based on PET membranes with different nominal pore sizes as function of UV irradiation time during preparation; the dotted lines are projections to the permeabilities of the precursor membranes, i.e., PET membranes after the prefunctionalization step. ....	119
Figure 4.53	Schematic representations of microstructure of HPFCM and the influence of monomer (M10 and M15) and crosslinker content (DC02, DC05 and DC10). The less crosslinked hydrogels tend to swell in the vertical direction. ....	122
Figure 4.54	Pressure dependence of water permeability at RT for HPFCM with different base membrane pore size. Measurement has been done by step-wise increasing the pressure (40 min. at each stage) with HPFCM prepared at 15 min of UV irradiation using BM without and with prefunctionalization. ....	124
Figure 4.55	Reversible temperature responsivity of water permeability for HPFCM: (a) with different base membrane pore size (hydrogel composition: M15DC05), and (b) with different compositions (BM_1000).....	125
Figure 4.56	Reversible temperature responsivity of water permeability for HPFCM prepared with base membrane 1000 nm. ....	126
Figure 4.57	Deswelling of hydrogels: microsineresis (I) vs. macrosineresis (II) <sup>[76]</sup> .....	126

Figure 4.58	Influence of UV time on ultrafiltration selectivity of HPFCM (base membrane 1000 nm; M15DC05; TMP = 0.03 bar). .....	130
Figure 4.59	Influence of base membranes pore size on ultrafiltration selectivity of HPFCM (UV time 15 min; M15DC05; TMP = 0.03 bar). .....	131
Figure 4.60	Influence of transmembrane pressure on ultrafiltration selectivity of HPFCM (UV time 15 min; M15DC05) for base membranes with different pore size: (a) 400 nm, (b) 1000 nm. ....	132
Figure 4.61	Recovery of MWCO measured before and after ultrafiltration UV time 15 min; M15DC05; TMP = 0 bar) for base membranes with different pore size: (a) 400 nm, (b) 1000 nm. ....	133
Figure 4.62	Influence of temperature on ultrafiltration selectivity of HPFCM (UV time 15 min; base membrane 1000 nm; M15DC05, TMP = 0.03 bar). ....	134
Figure 4.63	Influence of compositions on ultrafiltration selectivity of HPFCM (UV time 15 min; base membrane 1000 nm, TMP = 0.03 bar). ....	135
Figure 4.64	Size-selective separation by hydrogel pore-filled composite membrane compared with unmodified base membrane. ....	136

## ***List of Tables***

Table 2.1	Studies on polymerization-induced phase separation mechanisms. ....	20
Table 2.2	Preparation of synthetic membranes. Adapted from <sup>[155]</sup> . ....	27
Table 3.1	List of the chemicals used and their structural formulas according to hydrogel types. ....	33
Table 3.2	Precursor compositions for classic redox hydrogels. ....	34
Table 3.3	Feed compositions for: (a) classic redox hydrogels and (b) classic photopolymerized hydrogels. ....	34
Table 3.4	Feed compositions for NIP and MIP hydrogels with ionic comonomer. ....	35
Table 3.5	Feed compositions for PNIPAAm hydrogels with macrocyclic comonomer. ....	35
Table 3.6	The nominal pore size and porosity of the base membranes. ....	36
Table 3.7	Test solutes for partition and sorption experiments of PNIPAAm hydrogels. ....	37
Table 3.8	Variation of the synthesis conditions (TEMED/APS 4.0 : 1). ....	38
Table 3.9	Variation of the TEMED to APS ratio (using recrystallized monomer and deaerated precursor solution). ....	38
Table 3.10	Classic PNIPAAm hydrogels synthesized <i>via</i> redox polymerization (TEMED/APS 4.0 : 1) at 15 °C for 24 h. ....	39
Table 3.11	Determination of concentration of species <i>x</i> and <i>y</i> from decomposition of PI at certain UV irradiation time. Molar absorptivities of species <i>x</i> and <i>y</i> are 12.4 and 3.4 l/mM.cm, respectively. ....	41
Table 3.12	Summary for reaction orders 0, 1, and 2 <sup>[179]</sup> . ....	41
Table 3.13	Classic PNIPAAm hydrogels synthesized <i>via</i> photopolymerization (2 wt % PI relative to NIPAAm, 15 min UV time). ....	42
Table 3.14	NIP and MIP of PNIPAAm- <i>co</i> -MAA hydrogels synthesized <i>via</i> photopolymerization (2 wt % PI relative to NIPAAm, 15 min UV time). ....	43
Table 3.15	PNIPAAm- <i>co</i> -vCE hydrogels synthesized <i>via</i> redox polymerization (TEMED/APS 4.0 : 1) at 15 °C for 24 h. ....	44
Table 3.16	An overview of dimension of hydrogel pieces and washing medium for various hydrogel types. ....	45
Table 4.1	Theoretical carbon content calculated from composition in Table 3.2. ....	55



Table 4.2	Conversion to PNIPAAm hydrogels in water prepared with and without PEG. The conversion was calculated from the theoretical carbon content (Table 4.1) and the residues of carbon in the washing water (TOC) from Figure 4.1.....	56
Table 4.3	Conversion (TOC) of PNIPAAm hydrogels (M15DC05) prepared under various optimization procedure. Other conditions <i>c.f.</i> Figure 4.1. ....	56
Table 4.4	Physical properties of PNIPAAm hydrogels synthesized with various crosslinker content. Hydrogels were obtained using initiator TEMED/APS 4.0 : 1. Other conditions <i>c.f.</i> Figure 4.1.....	58
Table 4.5	Physical properties of PNIPAAm hydrogels synthesized at different temperature. Hydrogels were obtained using initiator TEMED/APS 4.0 : 1. Other conditions <i>c.f.</i> Figure 4.1.....	59
Table 4.6	Physical properties of PNIPAAm hydrogels (M15DC05) synthesized with various PEG content. Hydrogels were obtained using initiator TEMED/APS 4.0 : 1. Other conditions <i>c.f.</i> Figure 4.1. ....	60
Table 4.7	Mesh sizes of all PNIPAAm hydrogels (conventional; i.e. various crosslinker content <i>vs.</i> macroporous; i.e. hydrogels prepared above LCST or using PEG as a porogen calculated from swelling at 20 and 45 °C. ....	65
Table 4.8	Conversion from TOC and physical properties of PNIPAAm hydrogels synthesized with various compositions. Hydrogels were obtained using 2 wt% of PI concentration and 15 min UV time at 4 °C. ....	69
Table 4.9	Volume expansion factor of PNIPAAm hydrogels from the synthesis state to a equilibrium degree of swelling.....	71
Table 4.10	Calculated mesh size of PNIPAAm hydrogels prepared <i>via</i> photopolymerization from two independent experiments; (a) at varied UV time (hydrogel composition: M15DC05); and (b) various compositions (obtained at 15 min UV time). ....	79
Table 4.11	Recovery of swelling of photopolymerized bulk PNIPAAm hydrogel (M15DC05).....	82
Table 4.12	Monomer to hydrogel conversion (TOC) for NIP and MIP gels with various MAA contents after washing in 0.3 M NaCl solution (M'02 and M'05 represent 2 and 5 wt% MAA relative to NIPAAm, respectively). ....	89
Table 4.13	Molar ratios between template-binding monomer MAA and lysozyme from protein binding to NIP hydrogels. ....	93

Table 4.14	Water permeabilities of unmodified base membranes (average of 5 measurements within 10 % standard deviations). .....	106
Table 4.15	Water and dextran solution permeabilities for HPFCM prepared either with or without prefunctionalization step; base membrane: 5000 nm (hydrostatic pressure).....	112
Table 4.16	Degree of functionalization for HPFCM prepared from various base membranes and using varied UV irradiation time.....	115
Table 4.17	Degree of functionalization for HPFCM based on BM_1000 prepared from various hydrogel compositions. Pore-filling conditions were as for bulk gels ( <i>c.f.</i> Table 4.8).....	116
Table 4.18	Water permeabilities for HPFCM from various compositions; base membrane: 1000 nm. Pore-filling conditions are analogous to Table 4.17.....	120
Table 4.19	Darcy mean mesh-size for HPFCM prepared from various base membranes (hydrogel composition: M15DC05) determined from Darcy model ( <i>c.f.</i> Figure 2.15).....	121
Table 4.20	Darcy mean mesh-size for HPFCM prepared from various compositions (base membranes: 1000 nm) determined from Darcy model ( <i>c.f.</i> Figure 2.15). .....	122
Table 4.21	Sieving features for unmodified PET membranes (30 nm) and HPFCM from base membranes after 24 h and 1 week diffusion time, expressed in terms of molecular weight cut off (fraction of dextran of which the concentration in the permeate had been reduced by 90 % relative to the feed), revealing their correlation with the microstructure of the hydrogel ( <i>c.f.</i> Table 4.19), and effective diffusion coefficients of the 4 kg/mol dextran fraction. HPFCM were prepared from composition M15DC05.....	128
Table 4.22	Sieving features for HPFCM from various compositions after 24 h diffusion time and at RT, revealing their correlation with the microstructure of the hydrogel ( <i>c.f.</i> Table 4.20), and effective diffusion coefficients of the 4 kg/mol dextran fraction. HPFCM were prepared from base membranes 1000 nm. ....	128

## ***List of Schemes***

Scheme 1	Synthesis scheme of the PNIPAAm hydrogels by free radical copolymerization (redox initiation) with MBAAm as the crosslinking agent. From ref. <sup>[15]</sup> .....	9
Scheme 2	Mechanism of PNIPAAm hydrogel formation <i>via</i> radical copolymerization with MBAAm (photoinitiation). .....	10
Scheme 3	Synthesis scheme of the PNIPAAm- <i>co</i> -vCE hydrogels by free radical copolymerization with MBAAm as the crosslinking agent <sup>[139]</sup> .....	44

# CHAPTER 1

## INTRODUCTION

### 1.1 Introduction

Highly hydrated polymers in their crosslinked forms, known as hydrogels are an important class of "soft matter" <sup>[1]</sup>. Hydrogels are built up of three-dimensional (3D) macromolecular network architectures and resemble elastic rubbery materials. A broad spectrum of commercially-oriented products had been established from polymer-based hydrogels. Those include wound dressings (*c.f.* <sup>[2]</sup>), implants (Vantas® and Voltaren®; *c.f.* <sup>[3]</sup>) and ion exchange resins (Ceramic HyperD®; *c.f.* <sup>[4]</sup>). Particularly, poly(2-hydroxyethyl methacrylate)-based hydrogels (PHEMA) were developed for soft contact lens materials <sup>[5]</sup>. From a technological standpoint, hydrogels are of great interest for applications ranging from cell immobilization <sup>[6]</sup> and controlled release <sup>[7, 8]</sup> to gel-electrophoresis <sup>[9]</sup> and coating <sup>[10]</sup>.

To date, research related to smart hydrogels is still very active due to their unique responsivity behaviour <sup>[11-13]</sup>. In contrast to conventional hydrogels, smart hydrogels or stimuli-responsive hydrogels (SRH) undergo a sudden change in their volume upon a small change in stimuli. The frequently used stimuli are pH and temperature (*c.f.* <sup>[13]</sup>). Temperature-responsive hydrogels have been mostly prepared on the basis of poly(N-isopropylacrylamide) (PNIPAAm) that possesses a lower critical solution temperature (LCST) of about 32 °C <sup>[14-19]</sup>. The main advantage of using SRH is that they possess reversible and tunable feedback functions similar to valve. This has made them attractive especially in the fields of drug delivery <sup>[20, 21]</sup>, and microfluidic systems <sup>[22, 23]</sup>.

Stimuli-responsivity of PNIPAAm-based gels can also be combined with protein-imprinting approach for tunable protein-recognition behaviour (*c.f.* 2.2.3). Imprinting technique introduces affinity to the systems and allows high specificity of protein re-binding after the removal of templates <sup>[24-27]</sup>. Interestingly, swelling-deswelling states in response to temperature could trigger the binding abilities of such systems.

SRH are also highly suitable for fabrication of sensing-actuating element <sup>[28, 29]</sup>. This can be realized *via* copolymerization of PNIPAAm with crown ether (CE) monomer units (*c.f.* 2.2.4). CE units have remarkable properties of selectively recognizing specific ions and forming stable "host-guest" complexes <sup>[30]</sup>.

Linear and crosslinked PNIPAAm systems are also very relevant for membrane functionalization because the swelling-deswelling process allows for a regulated pore closing-opening<sup>[31, 32]</sup> or a switchable macromolecular size-selective barrier<sup>[33]</sup>. Hydrogels intended for separation applications should be fabricated in a suited format in order to protect them from excessive swelling and/or allowing for convective flow without compression; this should be combined with ease of handling. One promising approach is *via in situ* reactive pore-filling functionalization of suited based materials, e.g., porous membranes, that leads to composite structures (*c.f.* 2.3.3). To the best of my knowledge, pore-filling with smart hydrogels using isoporous track-etched membranes has not yet been done.

Undoubtedly, SRH have a bright prospect in the recent years and also in the future as intelligent materials. This chapter starts with a brief overview on hydrogels and their impact on establishing novel functional materials. The chapter continues with problems associated to hydrogel and different fruitful strategies to overcome these problems. The aims of the work are outlined in the following subsection. The scope of the work is also reported in order to create a focus on findings.

## 1.2 Problem Statement

The promise of gels as smart or intelligent materials rests on the state-of-the-art that includes:

*Demand for intelligent materials.* Hydrogels demonstrated great potential for many applications due to their hydrophilic nature and network architecture (*c.f.* 1.1 and 2.1). Conventional hydrogels however do not have intelligent properties that limit their application. For instance, their swelling behaviour is based on continuous transition (*c.f.* <sup>[1]</sup>). In contrast, drastic and reversible transitions are observed only for SRH in response to the alteration in environmental conditions. The intelligent properties of SRH could meet a demand to perform complex functions, for instance, (i) mimicking the natural feedback-response of biological systems, (ii) regulate transport of ions and molecules, (iii) convert (bio)chemical signals into electromechanical signals and vice versa, (iv) tuning catalytic activity, and many more.

*Demand for higher molecular weight (MW) of polymer.* It is not easy to synthesize certain linear polymers with higher number average MW (> 100,000 to 1,000,000 g/mol). The 3D network architectures are having higher polymer chain density. Accordingly, the 3D architectures can satisfy the demand for higher MW.

*Demand for 3D network architectures.* Having 3D network architectures is the key of enhancing of the separation selectivity based on hydrogels (*c.f.* 2.1.3). The hydrogel network imposes a porous-like structure where the transport could occur between the void spacing of hydrophilic chains connected by crosslinking points. Due to this intrinsic sieving properties of the hydrogel network, fractionation of macromolecules based on size or charge can take place.

*Poor mechanical strength.* A major disadvantage of using hydrogels is that they have poor mechanical strength and toughness after swelling. Hence, transport *via* convective flow is only possible under the precondition that the hydrogels is stabilized within a porous support matrix in order to maintain the structure integrity of hydrogel <sup>[33-35]</sup>. This imposed a need to tailor hydrogels for which their final properties fit to the specific requirements of the application, and which can be synthesized *in situ*, also in small or confined volume.

*Demand for temporal and spatial control over polymerization.* PNIPAAm hydrogels are commonly prepared by redox initiation using typically ammonium persulfate (APS) and *N,N,N',N'*-tetramethylethylenediamine (TEMED) <sup>[14-16, 36, 37]</sup>. The initiation system using TEMED/APS is based on an autocatalytic reaction <sup>[38]</sup>. An autocatalytic reaction may accelerate the polymerization and impose the risk of spatial fluctuations, yielding regions with high and low polymer density, in the final hydrogel networks <sup>[39]</sup>. Besides, this approach cannot be used for the preparation of thin films, because patterning is not possible <sup>[40]</sup>. Recently, crosslinking reactions between polymer chains induced by photoinitiation process have attracted strong attention. Photoinitiated reaction is advantageous for several reasons. The polymerization is normally very rapid and can occur *in situ* <sup>[40, 41]</sup>. Besides, this technique is very well applicable for integration of smart matrices within membrane formats <sup>[33]</sup> or microsystems <sup>[42]</sup>.

*Demand for novel membrane separation performance.* Membrane has unique separation principle, but, the selectivity of the separation process is still often limited. Conventionally, due to their permanent pore size, micro- and ultrafiltration (MF, UF) processes separate only two components or two groups of components; one being obtained in the permeate and the other in the retentate. To overcome this limitation, membranes had been modified with stimuli-responsive polymers to enhance their separation performance (*c.f.* 2.3.2 and 2.3.3) <sup>[1]</sup>.

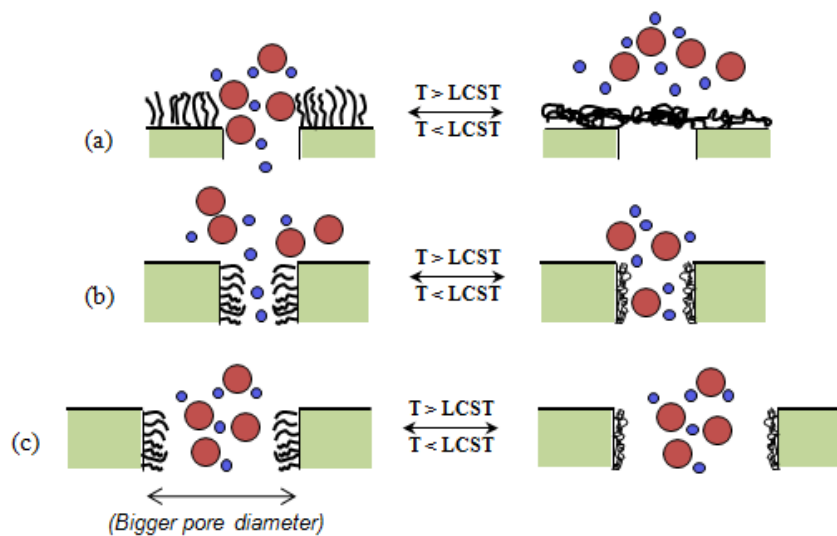


**Figure 1.1** Membrane modification (a) on the outer surface, (b) and (c) on the pore wall surface; the pore diameter does not change effectively in the case of (c).

A composite membrane for instance, can be fabricated either by coating on the outer surface of the membrane, or filling the pore of membrane or coating on the pore-wall surface of the membrane. Figure 1.1 illustrates the separation mechanisms on the outer and pore-surface with responsive linear polymer. Note that the size selectivity from hydrogel was not used. Also, these approaches are limited to modification of smaller membrane pore and do not improve the selectivity of macroporous membranes. An alternative approach towards high membrane separation performance is pore-filling functionalization of macroporous membranes with crosslinked polymer hydrogels. The smart performance of hydrogel pore-filled composite membranes (HPFCM) could be interesting for the separation of multi-component mixtures or for controlled release due to the tunability of the sieving coefficient by changing the temperature<sup>[33]</sup>.

*Characterization of hydrogels microstructure.* Despite many research works reported on bulk hydrogels or membrane functionalization, detailed studies of the interplay of a hydrogel network with a confining template such as a  $\mu\text{m}$ - or sub- $\mu\text{m}$ -size pore of a membrane are still lacking. Fundamentally, the membrane provides mechanical support and confines the hydrogel within its pores and thus allows for the convective transport. Accordingly, this provides the possibility to characterize the hydrogel network without sacrificing its functionality or structural integrity<sup>[34, 35]</sup>. Characterization of hydrogel network is important because it provides an insight into the microstructure; the mean Darcy mesh size of the hydrogel network (*c.f.* Figure 2.15 in 2.3.3.1).

### 1.3 Objective of the Research

This report revolves on the theme of stimuli-responsive PNIPAAm hydrogels and innovation of advanced functional membranes *via* pore-filling. Specifically, the aims are:

1. Synthesis of temperature-responsive PNIPAAm hydrogel; *via* redox or photopolymerization.
2. Characterization of bulk hydrogel (elasticity properties, network, swelling and etc).
3. Development and characterization of other stimuli-responsive hydrogels
  - temperature and protein-responsive molecularly imprinted polymer (MIP) hydrogel
  - temperature and ion-responsive hydrogel
4. Development of improved mechanical stability of PNIPAAm hydrogel *via* membrane reactive pore-filling leading to hydrogel pore-filled composite membranes (HPFCM).
5. Characterization of HPFCM:
  - tool for detailed characterization of hydrogel network (microstructure)
  - functional composite membrane with switchable barrier functions

## 1.4 Scope of the Research

The first task was to establish conditions for synthesis of classic bulk PNIPAAm hydrogels; i.e., *via* free radical copolymerization of *N*-isopropylacrylamide (NIPAAm) with *N,N'*-methylenebisacrylamide (MBAAm) as a crosslinker. Hydrogels were prepared under various pretreatment steps and optimization conditions. The conditions of polymerization were tuned in order to achieve high degree of monomer conversion in a kinetically controlled way. Hence, suitable synthesis conditions had to be verified, for instance by monitoring gelation in order to achieve desired microstructure.

The second task was to gain information on the gelation mechanism and kinetics by monitoring the *in situ* free radical copolymerization using rheology. The conditions of *in situ* polymerizations were further manipulated to achieve desired hydrogel properties at a desired rate of reaction. The hydrogel composition for *ex situ* and *in situ* studies were kept constant. *Via* redox-initiation, the TEMED/APS ratio was tuned to serve this purpose. An intensive study of *in situ* photopolymerization under oscillatory rheological systems was then done. The influences of UV intensity and irradiation time were closely monitored.

This was followed by characterization of physical and structural properties of resulting bulk hydrogels. Using rheology also, photopolymerized bulk PNIPAAm hydrogels were characterized to gain an insight into their microstructure and responsivity. The mesh size determined from rheological data was in a good agreement to that from swelling experiments. The study using rheology was an effort to bridge the knowledge between *ex situ* and *in situ* polymerization towards the fabrication of pore-filling hydrogels in novel temperature-responsive membranes. In the next series of study of SRH, MIP hydrogels for lysozyme recognition were prepared *via* photopolymerization. PNIPAAm hydrogel was copolymerized with methacrylic acid (MAA) as template-binding monomer in the presence of lysozyme. Tuning the ionic interactions through various MAA content could facilitate the elution of the template protein under mild conditions, so that this could be a most efficient strategy to improve imprinting efficiency and to increase recognition binding. To confirm that, a series of rheological monitoring *in situ* polymerization was carried out. As control experiment, hydrogels were also prepared in the absence of lysozyme to obtain non-imprinted polymer (NIP) hydrogels. The significant binding capacity and selectivity of MIP over NIP hydrogels were demonstrated with responsive swelling-deswelling that modulates the binding abilities. Most importantly, specific volume shrinking was observed upon rebinding with template protein.

The scope of the work also included SRH that demonstrate ion-solvating capability functions. The CE containing monomer units, 4-vinylbenzo-18-crown-6 (vCE) were incorporated into crosslinked PNIPAAm *via* redox-initiation free radical polymerization. Swelling/deswelling of these hydrogel copolymers changes in response to temperature also depends on the specific ion recognition properties



imposed by the CE pendant (sensing function). By capturing specific ion whose size fits the cavity of CE receptor, the formation of a 1 : 1 complex may increase the LCST of the copolymer. The ion-selectivity properties of these copolymers were investigated as functions of crosslinker (MBAAm) and vCE contents. Particular attention has been given on the degree of monomer conversion and copolymerization efficiency. The gelation kinetics of these copolymers were monitored rheologically. For further hydrogel characterization, swelling measurements in pure water as function of temperature were considered. The determination sensitivity of the ion was carried out based on swelling measurements of the hydrogel copolymers at the physiology temperature in sodium, potassium and barium salts solution.

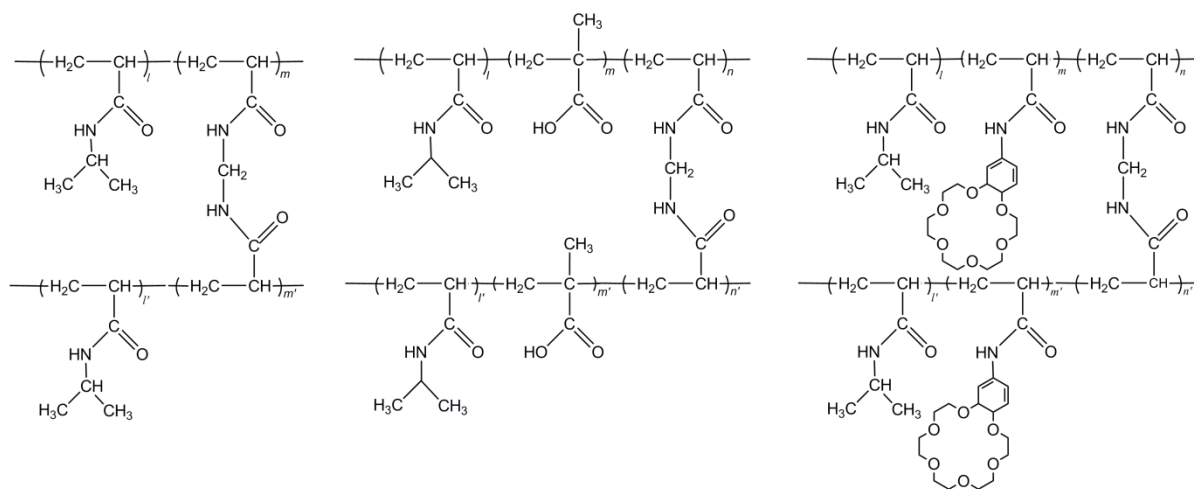


**Figure 1.2** Chemical structures of PNIPAAm, PNIPAAm-co-MAA and PNIPAAm-co-vCE hydrogels.

Furthermore, two-step pore-filling functionalizations of polyethylene terephthalate (PET) track-etched membranes (nominal pore diameters between 200 and 5000 nm) with classic PNIPAAm hydrogels were performed. Commercial PET track-etched membranes were chosen as support material due to their highly uniform pore geometry with very narrow size distribution [32, 43, 44]. Having such close to ideal structure makes PET membranes attractive because they allow accurate quantification of grafted polymer or polymer pore-filling and of the effects of the functional polymers onto barrier properties. In the first step, the linear polymer chains were grafted from the surface of membrane *via* pre-adsorption of a photoinitiator which upon UV excitation undergoes hydrogen abstraction from the base polymer ("type II" photoinitiator). Such "grafting-from" was already reported as prefunctionalization step to provide anchoring sites for further pore-filling functionalizations [45]. Conditions and details for prefunctionalization step were adopted from previous work in our group [32, 43]. In the second step, these membranes were equilibrated in a monomer solution containing "type I" photoinitiator and exposed to UV irradiation so that the same reaction conditions as for bulk photopolymerized hydrogels had been applied (Figure 1.3). This part had several aims. First aim was to find suitable conditions that lead to a

tailored composite barrier structure which is mechanically stable also for convective transport, and this should be based on suited degree of functionalization with hydrogel and its confinement in base membrane pores of suited size. Second aim was to characterize the size-selectivity under diffusion and ultrafiltration conditions as well as the responsivity to temperature changes. Final aim was to clarify the transport mechanism through the HPFCM and correlate it with the microstructure of the selective and responsive hydrogel.

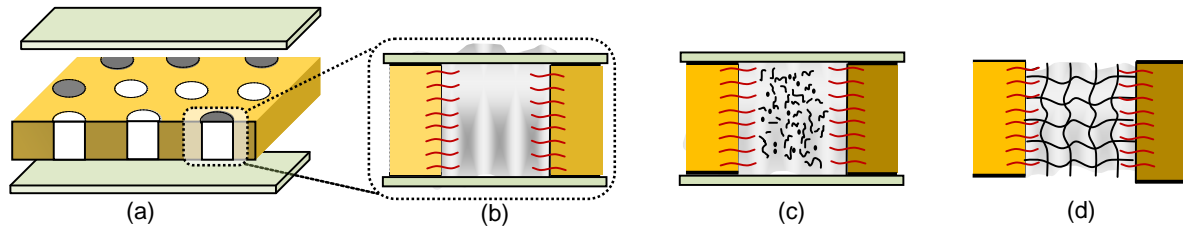


**Figure 1.3** Schematic illustration of pore-filling functionalization *via in situ* photopolymerization; (a) filling and equilibration of membrane with reaction mixture, sealing and pressing with two glass plates on top and bottom sides; (b)-(d) cross-section view of prefunctionalized membrane pore, obtained *via grafting-from* of linear functional polymer chains (*c.f.* <sup>[32, 43]</sup>), (b) during equilibration with reaction mixture, (c) during UV initiated *in situ* crosslinking polymerization, and (d) after complete reaction toward hydrogel pore-filled composite membrane (HPFCM).

## CHAPTER 2

### THEORY AND LITERATURE REVIEW

#### 2.1 Polymer-Based Hydrogels

Hydrogels are attractive soft-matter because they possess both liquid-like and solid-like properties<sup>[1]</sup>. The unique properties of hydrogels have emerged from crosslinked networks of polymer swollen in an aqueous medium. There are several evidences that considered hydrogels as highly biocompatible<sup>[46]</sup>. The biocompatibility of the hydrogels is also due to their high water content and to some extent hydrogels possess a biological tissue-like consistency. Furthermore, the soft-rubbery nature of hydrogels as well as having high degree of mobility at their surface and low interfacial tension minimize the frictional irritation to the surrounding biological tissues. Correspondingly, these properties can diminish the driving force for non-specific protein adsorption and cell adhesion due to repulsion exerted by the hydrophilic chains.

In literature, polymer gels can be classified depending on the nature of their network, whether chemical or physical means (Figure 2.1)<sup>[47, 48]</sup>. Physical gels are formed by various reversible links. These can be ionic interactions, hydrogen bonding, hydrophobic interactions, van der Waals forces, physical entanglements and so on<sup>[49]</sup>. In contrast, chemical gels are formed by irreversible covalent crosslinks. Crosslinkers are molecules with at least two reactive functional groups that allow the formation of bridges between polymeric chains. Due to presence of these crosslinks, the gel networks are no longer soluble but tend to be swellable in a good solvent.

In the following subsection, chemically crosslinked networks are reviewed and focussed on PNIPAAm hydrogels.

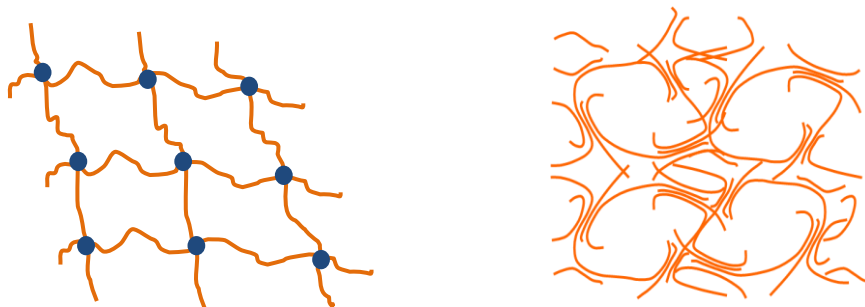
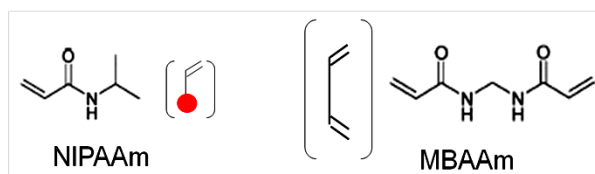
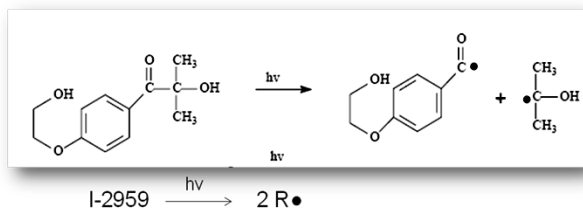


**Figure 2.1** Schematic representation of chemical and physical gels.

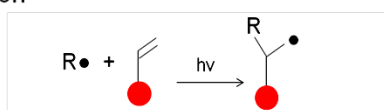




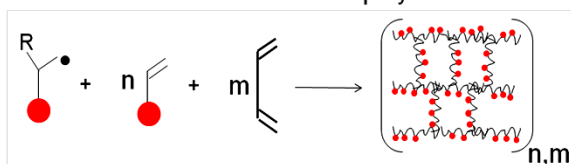
Step 1.  
Dissociation of the photoinitiator by UV-irradiation



Step 2.  
Initiation



Step 3.  
Network formation via radical copolymerization



**Scheme 2** Mechanism of PNIPAAm hydrogel formation *via* radical copolymerization with MBAAm (photoinitiation).

In general, polymerization or gelation is an exothermic process. The gelation process encompasses a transition from liquid- to solid-like matter. Thus, the straightforward approach to closely monitor the gelation process is rheological measurement<sup>[53]</sup>. The data extracted from rheology are highly reliable and reproducible. This technique is very convenient, enabling on line monitoring of gelation, during which increasing elasticity indicates the formation of interdomain hydrogel network<sup>[53, 54]</sup>. Rheological parameters, mainly elastic and viscous ( $G'$  and  $G''$ ) moduli, provide correlations between the reaction mechanism and kinetics and the resulting mechanical properties, and they also provide useful general information of the progress of the reaction.

In the past, monitoring gelation using rheology was often performed for naturally occurring polymers<sup>[55-58]</sup>. Chitosan is one of the most extensively studied biopolymers in the field of injectable drug delivery application. Rheology was used to verify the thermogelling formulation of chitosan solution at physiological pH and temperature<sup>[56-58]</sup>. The network of these hydrogels was classified as physically crosslinked. There were also several studies reporting rheological characterizations of chemically crosslinked polyacrylamide (PAAm)<sup>[38, 59-62]</sup>. Niță *et al.* performed rheological measurements to monitor the influence of heating rates and shear stress on the sol-gel transition of PAAm<sup>[38]</sup>. Okay and

Oppermann reported on improving the mechanical properties of PAAm hydrogels using Laponite (clay particles) and monitored that using rheology<sup>[59]</sup>. Calvet *et al.* applied rheological measurements for both *in situ* polymerization and viscoelastic characterization of obtained PAAm hydrogels<sup>[60]</sup>. Trompette *et al.* compared the rheological behaviour of both PAAm and poly(sodium acrylate) hydrogels<sup>[61]</sup>. They showed that the nature of the monomer determines the properties of the resulting gels. PAAm was formulated *via* photopolymerization for application in gel electrophoresis separations and the microstructure was characterized rheologically<sup>[62]</sup>. Rheological studies on hybrid gels, i.e., polymers containing both physical and chemical crosslinked networks, were also reported. Zhao *et al.* studied the sol-gel transition of chemically crosslinked PNIPAAm microgels that physically aggregated into a network<sup>[63]</sup>. Senff and Richtering used rheology to monitor the colloidal phase behaviour as a function of temperature and polymer concentration<sup>[64]</sup>. Despite many studies reported on rheology of the hydrogels during and after their gelation, only few studies had been reported on the rheology of PNIPAAm. Correspondingly, those studies had mainly been concerned with the redox-initiation polymerization<sup>[63, 64]</sup> and only one study was devoted to rheological monitoring of photo-initiated polymerization but using PAAm instead of PNIPAAm<sup>[62]</sup>.

For polymerization of other polymeric-based hydrogels *c.f.* review<sup>[65]</sup>.

### 2.1.2 Study of Hydrogel Network Structure

The study of the hydrogel network is fundamental because: (i) it reveals structure and configuration of its chains by use of appropriate theoretical models<sup>[48, 66]</sup>; and, (ii) it allows for estimation of a critical number of crosslinks per chain required to form a network<sup>[66]</sup>. In addition, the data provide information on the network structure of the hydrogel that determines their mechanical and physical properties.

The most appropriate definition of an ideal network is a collection of Gaussian chains between multifunctional junction points (crosslinking). Flory and Rehner<sup>[67]</sup> developed the most well-known theoretical model for the structure of hydrogel that do not contain ionic moieties. This model is based on two important assumptions. First, based on Gaussian distribution, the end-to-end distance between the chain ends is much smaller than the contour length of the chain. Second, the crosslinking junctions are tetrafunctional on the average.

The network structure can be represented by their intrinsic parameters such as the polymer volume fraction in the swollen state ( $v_{2,s}$ ), molecular weight (MW) between two consecutive crosslinks points ( $M_c$ ) and mesh size ( $\zeta$ )<sup>[47, 48, 68]</sup> (Figure 2.2). Then, a characteristic correlation length  $\zeta$ , serves as an indicator of the screening effect of the network on solvation or solute diffusion. The term  $\zeta$  is also known as mesh size, indicating the maximum size of solutes that can pass through the network. These

network parameters are interrelated and can be obtained theoretically or experimentally. It is important to note that, only average values for  $\zeta$  and the  $M_c$  can be calculated because of non-uniformity of the network.

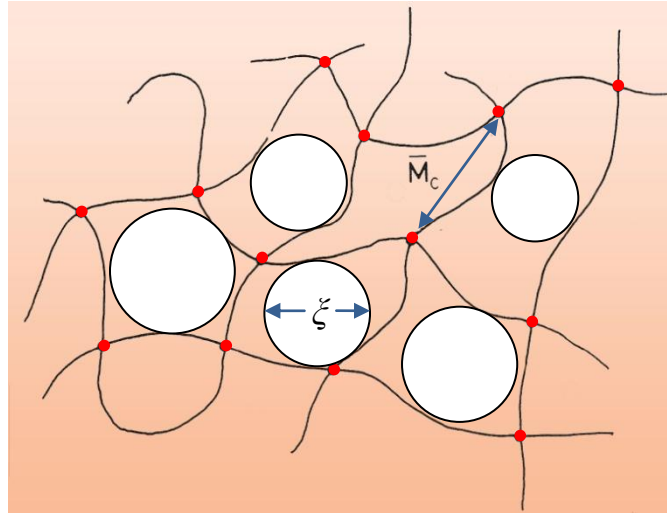


**Figure 2.2** Swollen, crosslinked structure of hydrogel by a thermodynamically compatible liquid, indicating the number average molecular weight between crosslinks,  $M_c$  and the average mesh size,  $\zeta$ . Figure adapted from <sup>[48, 68]</sup>.

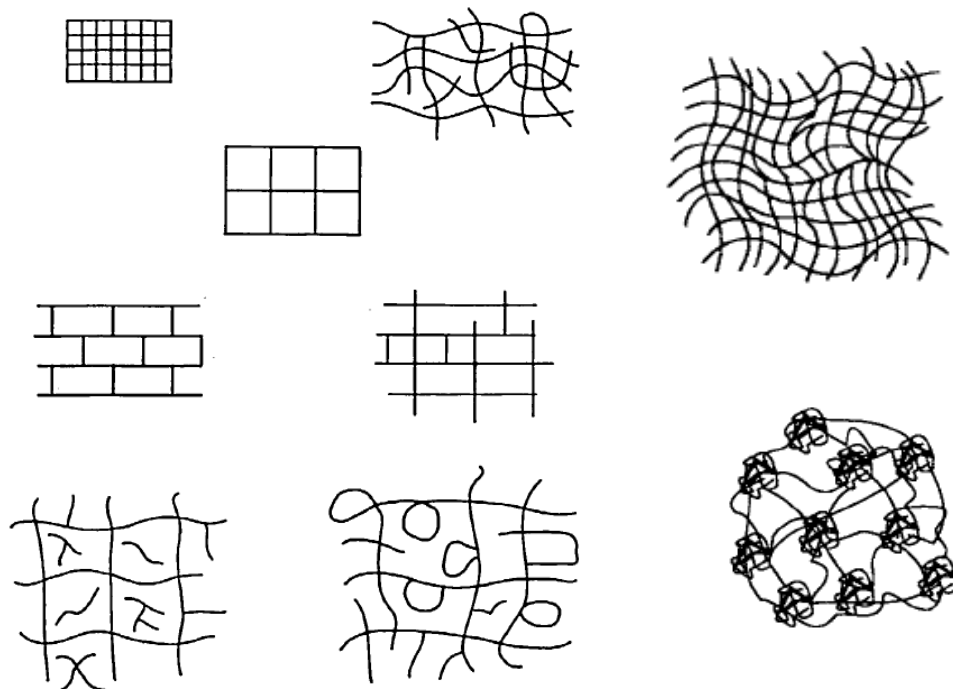


**Figure 2.3** Various types of crosslinked networks; ideal versus network imperfections (left; from ref. <sup>[66]</sup>), and conventional versus macroporous network of hydrogels (right; from ref. <sup>[17]</sup>).

However, the real hydrogel networks are rather non-ordered and irregular. The deviations from the ideal structure can be associated to acceleration of polymerization; extensive clustering and cyclization during crosslinking. As reported in the literature, the networks can exist in various configurations that include: conventional, loosely crosslinked, highly crosslinked, imperfections with loops or entanglements or unreacted functionality and heterogeneous or macroporous (Figure 2.3) <sup>[17, 48, 66, 68]</sup>. Two methods that are frequently used of studying network structures are the equilibrium swelling theory and theory of rubber elasticity.

When, the hydrogel is immersed in a water, the swelling behaviour in the polymer hydrogels is observed as a result of diffusion of water molecules ('free water') into the polymer system <sup>[48]</sup>. This process is governed by the osmotic force and polymer interaction parameter. Correspondingly, the diffusion is allowed to reach equilibrium with its surroundings, and subjected to two opposing forces, the thermodynamics force of mixing and the retractive force of the polymer chains. Together with the diffusion, the gradual water uptake of the hydrogels leads the relaxation of the hydrated polymer chains <sup>[69]</sup>. The polymer network is therefore expanded or swells into the surrounding aqueous solution. Additionally, when the porogen is introduced, the network can function like a pump, i.e. imbibed the water in or expelled the water out. The improved function of the porogen-modified network is mainly due to the heterogeneous and macroporous matrix (*c.f.* 2.2.2). The macroporous network of the gel structure is characterized by 3D sponge-like features <sup>[17, 70, 71]</sup> (Figure 2.3). The fact that the distance between the pores in a heterogeneous matrix is smaller, water molecules can diffuse in or out faster and this could increase the swelling rate. It is also easily understood that a bigger pore size of macroporous network may increase the rate of swelling rather than the conventional hydrogel with compact small pores.

The degree of swelling of the gel fraction is typically expressed either as the equilibrium volume or as the equilibrium weight swelling ratio. For highly swollen hydrogel, the gel density can be considered equal to the density of water, thus, both volume and weight swelling ratio will end up in the same value. The equilibrium volume swelling ratio is defined as the volume of the equilibrium swollen gel divided by the volume of the same gel before swelling.

Mathematically, swelling ratio,  $Q$  can be expressed as follows:

$$Q = \frac{m_s}{m_d} \text{ ..... Equation 1}$$

where  $m_s$  and  $m_d$  are mass of the swollen network and mass of the dry network respectively.

Peppas and his co-workers had established a correlation between the mesh size of a swollen crosslinked network and its equilibrium polymer volume fraction, for hydrogels in semi-dilute, dilute or concentrated conditions <sup>[47, 48, 68]</sup>. In the swollen state, the equilibrium polymer volume fraction  $v_{2,s}$  is inversely proportional to the equilibrium degree of swelling,  $Q$ . The correlation between  $\zeta$  and  $v_{2,s}$  for



hydrogels had been determined experimentally and the relationship follows the scaling law based on concentration regime of polymer solution.

Assuming the swelling is isotropic <sup>[72]</sup>, the scaling law translates into:

$$\zeta \sim \nu_{2,s}^{-1/3} \dots\dots\dots \text{Equation 2}$$

or the mesh size can be calculated using Equation 3:

$$\zeta = \frac{r}{\nu_{2,s}^{1/3}} \dots\dots\dots \text{Equation 3}$$

where  $r$  is the distance between two crosslinking points in the unswollen gel <sup>[14]</sup>. The distance  $r$  can be therefore calculated using Equation 4:

$$r = l_c \left[ \frac{2M_c}{M} \right]^{1/2} C_N^{1/2} \dots\dots\dots \text{Equation 4}$$

where  $l_c$  is the length of C-C single bond (= 0.154 nm),  $M$  is the MW of monomer; can be calculated from the MW of the two monomers and their ratio in the gel, and  $C_N$  is the characteristic ratio; a measure of the extension of polymer chain in a disordered condition (for acrylates = 6.9).

A simplified derivation of this model was introduced by taking NIPAAm and MBAAm as an example <sup>[14]</sup>. Assuming a statistical copolymerization during the gel synthesis, the  $M_c$  can be calculated using Equation 5:

$$M_c = \frac{n(NIPAAm)}{n(MBAAm)} M(NIPAAm) + M(MBAAm) \dots\dots\dots \text{Equation 5}$$

where  $M(NIPAAm)$  is the molar mass of NIPAAm (NIPAAm as monomer),  $M(MBAAm)$  is the molar mass of MBAAm (MBAAm as crosslinker),  $n(NIPAAm)$  and  $n(MBAAm)$  are the mol of NIPAAm and MBAAm incorporated in the reaction respectively.

By combining Equations 1 to 5, the mesh size of hydrogel is functions of distance and molar mass between two adjacent crosslinks in the swollen network is summarized in Equation 6:

$$\zeta = Q^{1/3} \left( \frac{2M_c}{M} \right)^{1/2} C_N^{1/2} l_c \dots\dots\dots \text{Equation 6}$$

The dynamic mechanical behaviour of crosslinked polymers can be used as a model to explore viscoelasticity properties of hydrogels at various time scales (Figure 2.4). This can be done by recording the moduli  $G'$  and  $G''$  in rheology oscillation experiments within a defined frequency range. Correlation between  $G'$  and frequency is associated with the underlying polymer relaxation that describes their conformational changes or their distinct physical states. At a lower frequency, the matter

exists as viscous liquid ( $G' < G''$ ). Once the  $G'$  is predominant, the so-called rubber plateau is reached, which describes the extent of hydrogel network formation. At a higher frequency, above the glass transition temperature the glassy or solid-like behaviour is present.

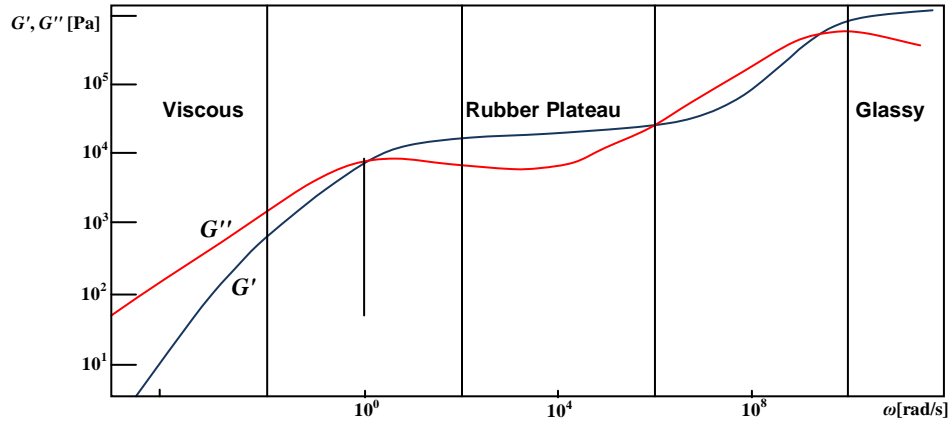


**Figure 2.4** Dynamic mechanical behaviour of polybutadiene samples <sup>[73]</sup>

From these experiments, one can elucidate the underlying hydrogel microstructure based on the theory of rubber elasticity <sup>[68]</sup>. This theory is only valid for perfect gel; the plateau  $G'$  is independent of the angular frequency. Classical rubber elasticity theory suggests the following relationship:

$$G' = n_{cl}RT \quad \text{Equation 7}$$

where  $G'$  is the modulus of elasticity or storage modulus and can be determined experimentally,  $n_{cl}$  is the number of elastically effective crosslinking points,  $R$  is the universal gas constant and  $T$  is the absolute experimental temperature. The elastic term obtained from rheological measurement is associated to the mesh size of the network from the following relationship <sup>[62]</sup>:

$$\zeta = \left( \frac{RT}{G' N_A} \right)^{1/3} \quad \text{Equation 8}$$

where  $N_A$  is Avogadro's number.

### 2.1.3 Separation Functions of Hydrogels

The separation functions of hydrogels originate from their two important features. First, the three-dimensional network of hydrogels can microscopically be envisioned as "porous" structure, having a tunable mesh-size in the nm range and thus imposing exclusion of molecules based on size or charge <sup>[1, 19, 33-35, 74-78]</sup>. Second, stimuli-responsive hydrogels (*c.f.* 2.2) can have an additional impact on the separation because the sieving coefficient may be adjusted using external stimuli, typically pH or temperature.

The selectivity of hydrogels in separation process depends on two modes; either exclusion based on size and/or charge or sorption mechanism. The size-exclusion effect can be best envisioned by imagining the gel as an expanded mesh. Small molecules can easily be transported through the pores in the mesh, but large solutes cannot enter. On the other hand, Donnan-exclusion mechanism governs the separation based on charge. The closest example of application based on size-exclusion separation principle is the use of hydrogels as electrophoretic media (for review, *c.f.* <sup>[79]</sup>). PAAm is one of the most studied and used polymer for the development of gel-electrophoresis.

The size-exclusion can be assessed based on partitioning of solutes in terms of intrinsic properties of hydrogels. Although there are different water structures in hydrogel; i.e. 'free-water', 'freezing bound water', and 'non-freezing bound water', only free water is available for solute partitioning and diffusion within the swollen mesh <sup>[19]</sup>. The partition coefficient of a solute molecule ( $K$ ) is defined as:

$$K = \frac{c^{gel}}{c^{sol}} \dots\dots\dots \text{Equation 9}$$

where  $c^{gel}$  and  $c^{sol}$  are the equilibrium concentration in the gel (based on total gel volume) and the solution concentration, respectively.

In the absence of attractive interactions between the solute and gel networks,  $K < 1$ ; because the volume occupied by the network excludes the solute based on the solute's size <sup>[75]</sup>. Thus, reflection or retention coefficient ( $\sigma$ , valid for capillary pores) can be calculated based on the following equation <sup>[80]</sup>:

$$\sigma = (1 - K)^2 \dots\dots\dots \text{Equation 10}$$

A wide variety of functional groups can be attached to a polymer network to impart ionic properties. In the presence of attractive interactions between the solute and gel networks,  $K > 1$ ; the oppositely charged macromolecules such as proteins are very favourably adsorbed in the gels at low ionic strengths <sup>[81, 82]</sup>. Thus, such interactions are favourable for hydrogels to function as extraction media, ion-exchanger or adsorber. The matrix of hydrogels intended for extraction application does not have a defined pore size. Here the pores are usually bigger in order to avoid any possible molecular sieving effects during separation <sup>[82]</sup>.

$K$  is also correlated to the polymer volume fraction of swollen gel,  $v_{2,s}$ , as well as the radius of the solute  $r_s$ , and the radius of the polymer fiber  $r_f$  (Ogston model) <sup>[83]</sup>. Theoretically,  $K$  can be obtained through a series of calculation from Equations 11 to 15 as the following:

$$K = \exp\left[-v_{2,s}\left(1 + \frac{r_s}{r_f}\right)^2\right] \dots\dots\dots \text{Equation 11}$$

$r_f$  is associated with the microstructure of the gel and can be calculated by fitting to the empirical Darcy permeability of the gel ( $k_{gel}$ ) as a function of volume fraction  $f(v_{2,s})$  <sup>[35]</sup>.

$$k_{gel} = r_f^2 f(v_{2,s}) \dots\dots\dots \text{Equation 12}$$

Re-arranged Equation 12 gives

$$r_f = \sqrt{\frac{k_{gel}}{f(v_{2,s})}} \dots\dots\dots \text{Equation 13}$$

$k_{gel}$  can be calculated based on relationship obtained from experimental values for neutral PAAm gel <sup>[35]</sup>

$$k_{gel} = 4.35 \cdot 10^{-4} v_{2,s}^{-3.34} \dots\dots\dots \text{Equation 14}$$

this equation is only valid for.  $v_{2,s} > 0.04$

the best fit of  $f(v_{2,s})$  to obtain  $r_f$  was derived by Jackson and James <sup>[84]</sup>

$$f(v_{2,s}) = \frac{-3}{20v_{2,s}} [\ln(v_{2,s}) + 0.93] \dots\dots\dots \text{Equation 15}$$

## 2.2 Stimuli-Responsive Polymer Hydrogel Systems

The stimuli-responsive polymer-based hydrogels (SRH) possess few intelligent properties that make them demandable and they have different characteristics from conventional materials. In the literature, they are also known as smart or intelligent hydrogels. This section focuses on the state-of-the-art of stimuli-responsive and intelligent properties of hydrogels.

### 2.2.1 General Properties and Classification

SRH are the basis of designing intelligent materials, they are multifunctional and possess a memory effect. Therefore, SRH are capable of mimicking the biological functions, actuating the action of muscles, sensing specific analytes and many more <sup>[13]</sup>. The attractiveness of the SRH is predominantly determined by their swelling behaviour. SRH demonstrate discontinuous transition; a rather spontaneous swelling phenomenon in different moieties. There are four fundamental interactions that control the swelling behaviour of responsive gels; ionic, hydrophobic, hydrogen bond, Van der Waals <sup>[49, 85]</sup>. An infinitesimal change of the balance between these interactions is responsible for the gel to interconvert between two distinct phases. The dominating repulsive force can cause the solvent uptake into the gel network. However, if attractive force between the gel networks is dominating, the gel collapses due to expulsion of the solvent.

Physicochemical stimuli, such as ionic strength <sup>[86]</sup>, pH <sup>[86]</sup>, temperature <sup>[14-17, 87-93]</sup> or electrical potential <sup>[94]</sup> may provide various energy sources for altering molecular interactions <sup>[91, 92]</sup> that are responsible to change the properties of polymeric materials (Figure 2.5). Besides swelling, other bulk and surface properties of SRH are also tunable upon application of an external stimulus. Those include their sorption capacities, swelling behaviour, permeability, surface active or selective properties and also optical properties <sup>[48, 95]</sup>.

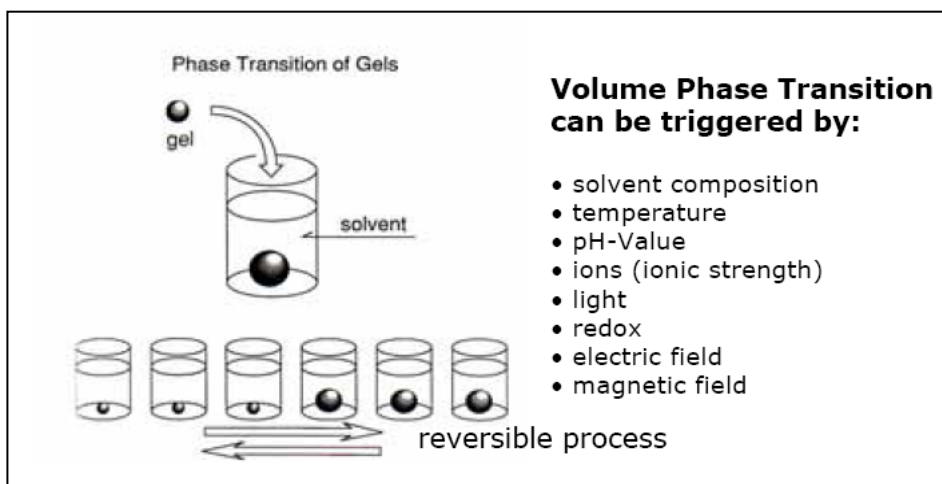


Figure 2.5 Reversible volume phase transition of stimuli-responsive gels. From ref. <sup>[49]</sup>.

## 2.2.2 Classical Temperature-Responsive Hydrogels

Hydrogels that show phase separation upon temperature increase are considered to exhibit LCST. [93]. From a thermodynamic point of view, the temperature-induced phase separation (TIPS) is principally an entropic occurrence [90, 93]. PNIPAAm is one of the best known temperature-responsive polymers [14-19, 40, 87-92, 96]. When the external temperature exceeds the LCST, PNIPAAm chains adopt coil-globule conformation [97-99]. To date, the phase separation phenomenon of PNIPAAm was investigated using small-angle neutron scattering [100], atomic force microscopy [98], high sensitivity differential scanning microcalorimetry [85] and laser light scattering [99].

Understanding the concept of phase separation in temperature-responsive polymer is fundamental. A number of studies have reported the possible mechanisms of SRH. During the phase separation, hydration-dehydration of PNIPAAm chains take place and the SRH change its appearance from transparent to opaque [40]. Zhang *et al.* [15] reported that, the phase separation behaviour of PNIPAAm across its LCST is attributed to the reversible formation and breakage of the hydrogen bonding between the water and hydrophilic groups of PNIPAAm. Moreover, this behaviour is also governed by hydrophilic/hydrophobic balance between hydrophilic and hydrophobic groups within PNIPAAm polymer chains [87, 93]. Therefore, the phase separation of the PNIPAAm hydrogel is the result of a balance between polymer-solvent interactions in the hydrophilic amide group of the PNIPAAm macromolecule and its hydrophobic isopropyl pendant group. As the temperature increases, the pendant groups become more mobile, and the hydrophobic isopropyl groups also become more active, causing phase separation at temperatures greater than LCST [90-92]. Otake *et al.* [87] and others [90, 93] also suggested that this phase separation is attributable to the hydrophobic interactions. They proposed that the good solubility of the polymer at a lower temperature is due to the hydration and water molecules forming cage-like structures around the hydrophobic solutes. As the temperature ( $T$ ) increases, the structured water molecules around the hydrophobic groups are destroyed, and the hydrophobic groups of polymer chains start to associate. The LCST phase separation occurs when the entropy contribution ( $T\Delta S$ ) to the Gibbs free energy ( $\Delta G$ ) exceeds the enthalpy term ( $\Delta H$ ). The phase separation mechanisms of PNIPAAm below and above its LCST can be best visualized from Figure 2.6.

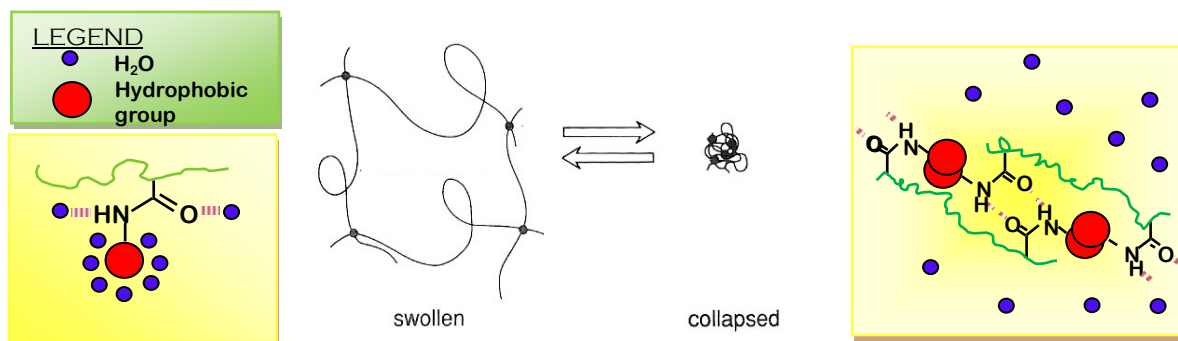


Figure 2.6 Phase separation mechanisms of PNIPAAm below and above its LCST [101].

In general, phase separation can be divided into two categories, i.e., phase separation which is attributed to external temperature cycle across the LCST (TIPS) <sup>[15, 87, 88, 90-93]</sup> and also polymerization-induced phase separation (PIPS) <sup>[14, 16-18, 40]</sup>. TIPS is a reversible process and can be externally controlled by the temperature, but this is not the case for PIPS. This is because PIPS is a process by which the initially homogeneous gel solution becomes phase separated during the course of its polymerization. Therefore network formation *via* PIPS is fixed by the irreversible nature of chemical bond.

PIPS can be induced by a number of factors; polymerization above LCST <sup>[40]</sup> (*c.f.* 4.1.1.3.2), continuous increase in the fraction of molecules with high molecular weight <sup>[18]</sup> or the unfavourable interactions between the polymer and non-reacting, inert species in the reaction mixture <sup>[14, 16-18]</sup>. The addition of inert species could act as chain transfer agents or inhibitors in the polymerization in the reaction mixtures lead generally to a dramatic decrease in the overall monomer conversion <sup>[16]</sup>. The extensive amount of literatures has reported on the utilization of PIPS to produce macroporous polymeric network (Table 2.1).

**Table 2.1 Studies on polymerization-induced phase separation mechanisms.**

Polymers	Additive(s)	Remarks
PNIPAAm	---	PIPS as a result of polymerization above LCST of PNIPAAm <sup>[40]</sup>
	Solvent [ethanol, tetrahydrofuran (THF)]	PIPS as a result of co-nonsolvency phenomenon in PNIPAAm chains <sup>[16, 40]</sup>
	Polyethylene glycol (PEG)	PIPS as a result of volume exclusion of PEG molecules <sup>[14, 18]</sup> PEG as a pore-forming agent. The phase separation occurs when certain critical concentration of PEG is reached <sup>[14]</sup>
	Ionic species	PIPS is realized by introducing a small amount of ionic species into the gel network, because the ionic osmotic pressure generally makes the transition a discontinuous one <sup>[102]</sup>
	hydroxypropyl cellulose (HPC)	PIPS as a result of precipitation of PNIPAAm chains around the HPC "seed" particles. The addition of HPC is not active, but may act as a nucleating agent <sup>[17]</sup>
PAAm	PEG	PIPS as a result of competition between the gelation process and segregation in two-polymer solution. The phase separation process exhibit spinodal decomposition and is responsible for the formation larger pores <sup>[103]</sup>
	PEG, polypropylene glycol (PPG)	PIPS as a result of immiscibility of PEG and PPG that induced formation of looser and more heterogeneous structure of gels <sup>[104]</sup>
PHEMA	Sucrose, glucose and ice crystals	The additives as void fillers to create macroporous network <sup>[105, 106]</sup>

### 2.2.3 Temperature-Responsive and Protein-Selective Hydrogels

In fact, most of the unique property of SRH have emerge from their swelling behaviour <sup>[13]</sup>. These hydrogels can respond to external stimuli and undergo a sudden change in their volume reversibly (*c.f.* 2.2.1). Inspired by the natural feedback-response of biological systems, hydrogels are designed to function as artificial recognition elements <sup>[13]</sup>. Molecular imprinting has unveiled the path for designing tailor made hydrogels with high specificity of molecular recognition properties <sup>[24]</sup>.

Fabrication of molecularly imprinted polymers (MIP) has gained considerable attention in recent years <sup>[24, 107, 108]</sup>, and MIPs are commonly prepared by means of non-covalent approach <sup>[24, 109]</sup>. Due to their interesting features, molecular imprinting was investigated for various applications including antibody mimics <sup>[110, 111]</sup>, ultrasensitive sensors <sup>[112]</sup>, biomimetic immunoassays <sup>[113]</sup> and complex separations <sup>[114]</sup>. As shown in Figure 2.7, molecular imprinting proceeds through crosslinking copolymerization of functional monomers having template-binding groups in the presence of template molecules followed by their removal for creation of complementary recognition sites.

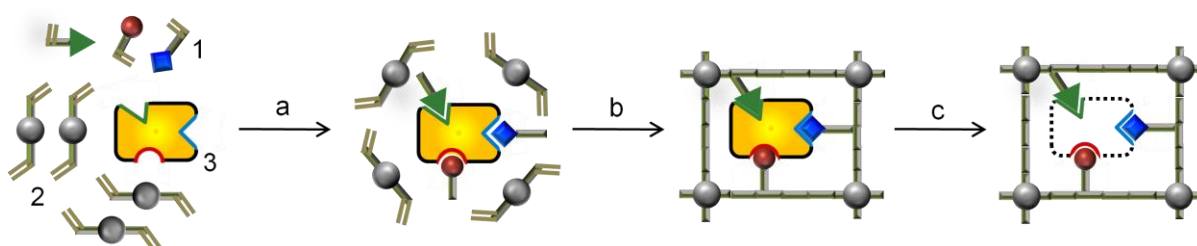


**Figure 2.7** Principles of molecular imprinting (1 = functional monomers, 2 = crosslinker monomer, 3 = template molecule; a = self-assembly, b = polymerization, c = removal of template molecule). Adapted from ref. <sup>[115]</sup>.

The imprinting of low molecular weight compounds had been successfully established <sup>[116-118]</sup>. On the contrary, imprinting of relatively larger biomolecules, for instance proteins, remained a challenging task and has been investigated in less detail. Bergmann and Peppas reported that protein-imprinting requires 3D spatial orientation to accommodate large and complex dimensions of protein <sup>[119]</sup>. Correspondingly, designing an appropriate crosslinker to functional monomer ratio is important to ensure the accessibility of binding sites while retaining the recognition specificity of the network <sup>[120, 121]</sup>. In the previous studies, various molecular imprinting protocols with stronger or weaker interactions have been developed for protein recognition, for instance *via* metal coordination <sup>[26]</sup> or hydrophobic interactions and hydrogen bonding, respectively <sup>[122, 123]</sup>. Recent studies by Janiak *et al.* dealt with the effect of hydrogel charge of the MIP in terms of affinity towards bovine hemoglobin or cytochrome C <sup>[124, 125]</sup>. Protein imprinting relying on moderately interactions between functional monomers and template



assures the ease of the template removal under mild conditions as well as the reversibility of binding and repeatability of use <sup>[24]</sup>.

The use of PAAm for gel-electrophoresis has been also extended for imprinting approach. Copolymerization of PAAm with methacrylic acid (MAA) had been reported for affinity towards lysozyme <sup>[126]</sup>. The complexation of MAA and lysozyme had prevented it from free radical attack and thus facilitated the removal of template protein after polymerization. Hirayama *et al.* copolymerized either PAAm with acrylic acid or PAAm with *N,N*-dimethylaminopropylacrylamide on a silica bead surface for lysozyme recognition, and high sensitivity for lysozyme was observed with a quartz crystal microbalance sensor <sup>[127]</sup>. Other studies using PAAm as macromolecular matrix for fabrication of MIP materials were reported by Bergmann and Peppas <sup>[119]</sup>, Xia *et al.* <sup>[128]</sup> and Hjertén *et al.* <sup>[123, 129]</sup>. In the view of stimuli-responsivity, PNIPAAm-based hydrogels were used as the main component in the imprinting matrix that showed both temperature-responsive swelling and recognition. Few related examples were provided by the work of Turan *et al.* for recognition of myoglobin <sup>[130]</sup>, by Chen *et al.* for recognition of lysozyme or cytochrome C <sup>[131]</sup> and by Hua *et al.* for recognition of bovine serum albumin <sup>[27]</sup>. Similarly, pH <sup>[132]</sup> and magnetic-responsive recognition <sup>[133]</sup> were also reported. It was also noticeable that interactions between imprint molecules and imprinted binding sites could induce signals and the amplification of these signals, because the responsivity has led to specific swelling <sup>[134]</sup> or shrinking <sup>[25, 131, 135, 136]</sup>. In those studies, the preparation of MIP was typically done *via* chemically initiated free radical copolymerization since it can be performed under mild condition and prevents denaturation of protein.

A crucial step in the preparation of MIP hydrogels is template-protein removal because the counter salt ions compete with the protein molecules and occupy the binding sites <sup>[137]</sup>. The efficiency of template protein removal depends of several factors such as washing medium and conditions, composition of the hydrogels, in particular the choice of comonomer, kinetics of a polymerization and many more.

#### 2.2.4 Temperature-Responsive and Ion-Selective Hydrogels

Smart hydrogels that can respond to multiple stimuli have received considerable attentions due to their increasing level of functionality. In the previous research, the most investigated multi stimuli responsive hydrogels (multi-SRH) are based on dual temperature- and pH-responsive hydrogels. To date, only few publications dealt with the phase-transition behaviours of these polymers induced by specific ion interactions <sup>[28, 29, 138, 139]</sup>. PNIPAAm containing crown ether (CE) in their side chain is reported to possess both temperature and ion-responsive behaviour <sup>[28, 29, 138-141]</sup>.

CE compound was discovered in 1967 by Charles Pedersen; who later received Nobel Prize for his discovery <sup>[142, 143]</sup>. After the birth of this compound, the family of macrocyclic polyethers has grown

rapidly. Most common CEs are 12-crown-4 (CE-12,4), 15-crown-5 (CE-15,5) and 18-crown-6 (CE-18,6) (Figure 2.8). In general, CEs are macrocyclic compounds of several ether groups and contain donor groups such as oxygen. Substitution of oxygen by nitrogen or other heteroatoms has led to aza and other CE derivatives.

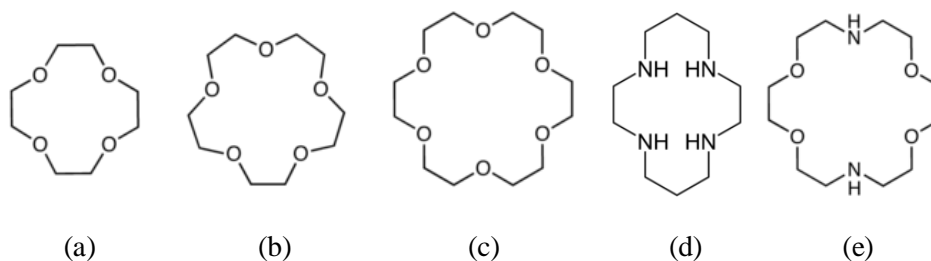


**Figure 2.8** Chemical structures of common crown ethers: (a) 12-crown-4 (CE-12,4), (b) 15-crown-5 (CE-15,5) and (c) 18-crown-6 (CE-18,6). (d) and (e) are nitrogen-substituted aza crown ether of CE-18,6 family members.

The principle of phase separation induced by ion-recognition can be explained as the following. PNIPAAm demonstrates actuating function by its volume change and it possess single LCST. This property is based on the coexistence of hydrophilic (amide) and hydrophobic (isopropyl) groups attached to the PNIPAAm chains (*c.f.* Figure 2.6 in 2.2.2). Copolymers of PNIPAAm and CE are reported to exhibit LCST shift when CE receptor selectively recognizes specific ion and forms "host-guest" complex. In other word, CE copolymer acts as an ion-sensor. Such behaviour is attributed to the incorporation of comonomers that alters the hydrophilic-hydrophobic balance of the polymer chains; involving either positive<sup>[144]</sup> or negative<sup>[138]</sup> LCST shift (Figure 2.9). Interactions of potassium ion with copolymers containing either CE-15,5 or CE-18,6 in the side chains form stable complexes at a ratio of 2 : 1 or 1 : 1 (ligand/cation) respectively. Two major parameters that governed the complex formation; (i) nature of the ion such as size of fitting of ion to the CE receptor, and (ii) complex stability constant. The complex stability constant of some ions is in the following order:  $\text{Ba}^{2+} > \text{K}^+ > \text{Na}^+ > \text{Li}^+$  [140, 144]. The order of the constant is preserved for CE-15,5 or CE-18,6 but in some cases the magnitude of the constant is several magnitudes higher. The 2 : 1 complex formation disrupts the hydrogen bonding between the oxygen atoms in the CE and the hydrogen atoms of water. As a result, the hydrophobicity of the polymer is enhanced, and the LCST for phase transition shifts negatively to a lower value. On the other hand, the 1 : 1 complex formation results in overall hydrophilic enhancement of the network as a result of extended hydrogen bonding. Increasing hydrophilicity in the PNIPAAm-CE copolymer can be obtained by using a more hydrophilic aza substituted CE such as cyclam<sup>[145]</sup>. Therefore, the LCST is raised. The shift to higher temperatures; i.e. to 37 °C is particular of interest. This is because the LCST shift to a physiological temperature can be used to monitor biologically relevant activity. On the other hand, Mi *et al.* reported that negative LCST shift could also be beneficial<sup>[138]</sup>. The drug-release to the

target takes place upon collapsing of the functional polymer gates of a microcapsule. The collapsing of the polymer gates is triggered upon recognizing specific metal ions; recognizing an abnormal increase of  $K^+$  concentration at some pathological sites in the body.

An interesting aspect of this study is because the ion sensitivity has an influence to the biological activity. In 1993; Irie *et al.* first reported the synthesis of linear copolymer PNIPAAm-*co*-4-acrylamidobenzo-18-crown-6), which can selectively recognize  $K^+$  [146]. Potassium ion regulates the concentration of other ions in the living cell and therefore plays an important role in biological systems [138, 139, 141]. Potassium ions also involve in the maintenance of extracellular osmolarity. There are also several other studies reporting on potassium ion recognition [28, 29, 138, 139]. In those studies, the temperature and ion-responsive copolymers can regulate chemical signal transduction in biological systems through monitoring the potassium ion concentration. Luo *et al.* investigated on multi-stimuli microgels for fabrication of lead sensor using the same sensing principle [147]. They had observed that the swelling was induced by the formation of host-guest complex between  $Pb^{2+}$  and the pendant crown ether groups, as a result of hydrophilicity enhancement of the copolymer. The lead sensitivity of the microgels increases with increasing crown ether content. Kuckling *et al.* incorporated cyclam; an aza analogue CE monomer (*c.f.* Figure 2.8), into PNIPAAm chains [145]. The incorporation of cyclam increased the hydrophilicity of the copolymer. In the presence of  $Cu^{2+}$  or  $Ni^{2+}$ , the LCST of PNIPAAm/cyclam was raised by 12 K. Yamaguchi and co-workers contributed major investigations of ion-gating membranes [140, 144, 148-150]. The copolymer of PNIPAAm and CE was grafted onto porous polyethylene supports *via* plasma treatment. The grafted copolymer swells when the CE receptor captures specific ions and closes the membrane pores. Such response mechanism was studied for osmotic pressure control, control release and self-oscillation membranes.

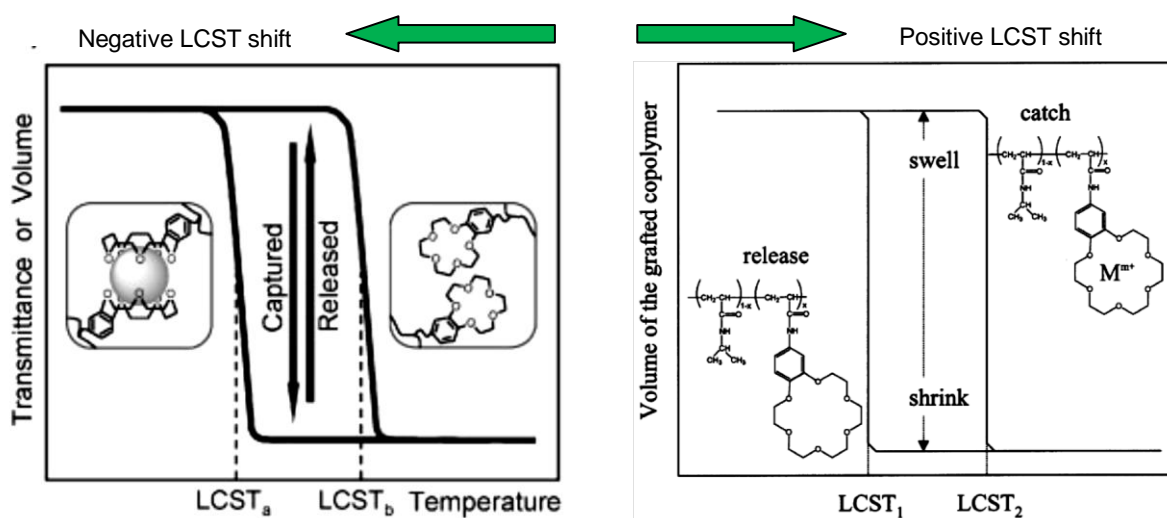


**Figure 2.9** Formation of 2 : 1 (left [138]) and 1 : 1 (right [144]) stable complexes of PNIPAAm copolymerized either with CE-15,5 (left) or CE-18,6 (right) in the presence of potassium ion that induced negatively or positively LCST shift, respectively.

## 2.3 Membranes and their Functionalization

In the most general sense, a membrane is an interphase between two adjacent phases acting as a selective barrier, regulating the transport of substances between the two compartments [44, 151-154]. Separations in membrane processes are unique and driven by the differences in chemical concentration, temperature, pressure or the transport rates of chemical species through the membrane interphase as being selective to one substance while retaining others.

Membrane can be classified based on types of their matrix; i.e., isotropic, asymmetric, mixed matrix and composite-type. Isotropic membranes have a uniform composition and structure (porous or dense) while anisotropic (or asymmetric) membranes have a thin selective layer supported on a much thicker, highly permeable microporous substrate. Mixed-matrix membranes are membranes prepared from materials that consist of inorganic particles dispersed in the polymer matrix. Composite-type membranes differ from mixed-matrix membranes and obtain from membrane post-modification process. A composite membrane is a membrane having chemically or structurally distinct layers [155]. In a composite membrane, different polymers are mainly fabricated *in situ* as a selective layer or barrier onto/within the pores of microporous support. As shown in Figure 2.10, there are three different composite membranes; thin-film, pore-surface functionalized and pore-filled composite membranes.

Nowadays, the technical membranes and membrane separation processes have been established from a simple laboratory scale to a commercial industrial process [44]. The industrial established application of membranes is a great of interest ranging from producing potable water from sea by reverse osmosis to remove urea and other toxins from the blood stream by dialysis in an artificial kidney [151-154]. Conventional membranes, however, have fixed size selectivity. When it comes to complex technical separation tasks that require advanced specialized membranes, the state-of-the-art of conventional membranes are facing limitations. This has imposed the needs to modify the membranes (flexible and tailor-made) in order to overcome their limitations [1, 33, 44].

Due to the relevance of the work, the next subsection will focus only on the principle of MF and UF membranes. Several strategies of membrane functionalization of UF or MF membranes based on hydrogel composite approach are also reviewed.

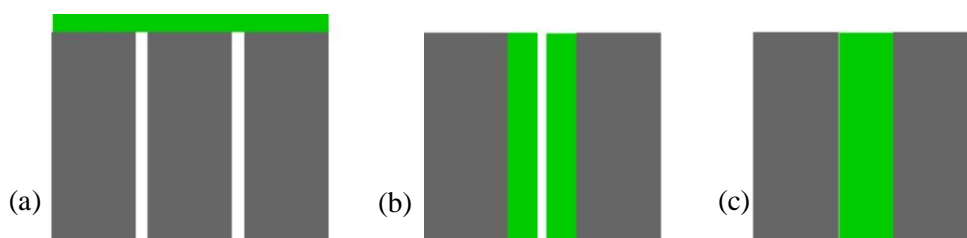


**Figure 2.10** Schematic depiction of three main composite membrane types: (a) thin-film, (b) pore-filling and (c) pore-surface functionalization [1].

### 2.3.1 Basic Principles of Conventional Ultrafiltration and Microfiltration Membranes

Microfiltration (MF) is a low-pressure, size-based membrane filtration process that retains suspended particles with diameter from 0.1 to 10  $\mu\text{m}$ . Ultrafiltration (UF) is also a technical size-based separation process similar to MF. However, the pore sizes of UF membranes are smaller (2 nm to 0.1  $\mu\text{m}$ ) and the separation process take place at slightly higher pressure (up to 10 bar) as compared to MF membranes. As shown in Figure 2.11, MF closely resembles conventional coarse filtration while UF fall between nanofiltration (NF) and MF membranes. UF membranes can discriminate fine particle suspensions or fractionate macromolecules. Membranes with macroporous structure (usually with an isotropic cross-section) are typical for MF membranes. UF membrane are usually more asymmetric <sup>[153-155]</sup>. MF membranes are typically characterized by the size of particles that they retained (in microns). On the other hand, UF is distinguished in terms of the molecular weight cut-off (MWCO) at 90 % rejection.

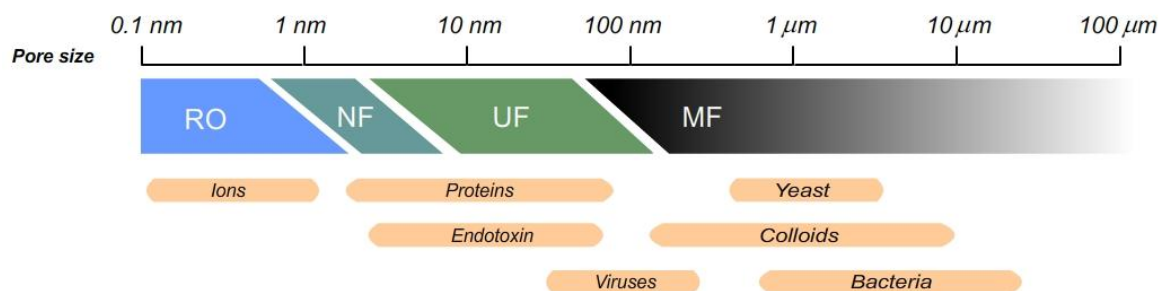


**Figure 2.11** Schematic illustration of different pressure-driven membrane processes according to size of pores in the selective barrier and size of exemplaric targets for separation <sup>[1]</sup>.

Synthetic membranes are mainly made from organic polymers. Both MF and UF membranes are developed from cellulosic polymers and other noncellulosic polymers, including poly(vinylidene fluoride) (PVDF), polyamides (PAm), and polyethersulfone (PES). However, only certain polymers are developed for certain membranes. For instance, polyacrylonitrile (PAN), polysulfone (PSu), polyetherimides were employed as materials for UF membranes. On the other hand, poly(tetrafluoroethylene) (PTFE), PET, polycarbonate (PC), polypropylene (PP) and polyethylene (PE) were employed as materials for MF membranes (for review *c.f.* <sup>[44]</sup>).

There exist several methods to prepare polymeric membranes (for ref. *c.f.* <sup>[153-155]</sup>). Some of these methods are applicable to a variety of polymers, others are material-specific, for instance the stretching method is usually used to make pores in microporous polyolefins membranes, whereas track-etched membranes are prepared from PC (e.g. Nuclepore) or PET (e.g. RoTrac®) films (Table 2.2).

**Table 2.2 Preparation of synthetic membranes. Adapted from <sup>[155]</sup>.**

Method	Polymer Materials
Phase inversion by: i) solvent evaporation ii) temperature change iii) precipitation	Cellulose acetate, PAm PP, PAm PSu, PES
Stretching sheets of partially crystalline polymers	PTFE, PP
Track-etching	PC, PET

The technically commercial membranes are normally prepared *via* phase inversion methods (Figure 2.12a). The phase inversion process involves a phase separation induced by a change either in temperature, solvent evaporation, vapour or by immersion precipitation in a non-solvent bath. In general, the method includes casting of polymer solution on a suitable support. The pores are formed as a result of demixing process; a precipitation of polymer from non-solvent. This is controlled by various parameters such as polymer concentration, residence-time during precipitation, humidity, and the composition of the casting solution (e.g. additives).

The next method is so-called stretching. Small ruptures occur upon stretching of an extruded film or foil that creates a porous structure with dimensions from 0.1 to 3  $\mu\text{m}$  (Figure 2.12b). The porosity of stretched membranes is usually high, up to 90 %.

The method to produce a close-to-ideal structure of porous membrane is established *via* track-etching (Figure 2.12c). The track-etching process involves bombarding the film with accelerated heavy ions and then plunging the membrane into an acidic or basic bath that etches pathways along where the ions passed through the membrane. These membranes have a narrow pore size distribution and minimal tortuosity (straight, aligned iso-cylindrical pores) with a pore size between 0.02 to 10  $\mu\text{m}$ . The porosity of track-etched membranes is usually low (up to 15 %) and mainly governed by the irradiation time. Such ‘isoporous’ membranes have become favourite support materials for the investigation of novel (polymeric) barrier membranes as well as for exploring completely novel separation principles based on functional polymers <sup>[155]</sup>.

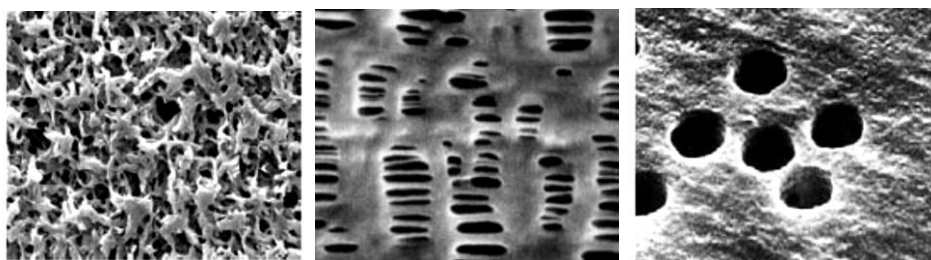


**Figure 2.12 Morphology of MF membrane prepared by phase inversion (left) <sup>[156]</sup>, stretching (middle) <sup>[157]</sup>, and track-etching (right) <sup>[32]</sup>.**

### 2.3.2 Surface Functionalization via Grafting-From

According to Ulbricht<sup>[44]</sup> and Yang *et al.*<sup>[1]</sup>, the membrane surface functionalization is a technique to modify membranes (mostly post-modification process) that has successfully been able to reduce membrane fouling, or to impart additional functionalities such as affinity, responsive or catalytic properties. Recently, this technique is reported to produce an anchoring layer for hydrogels prepared *via* membrane reactive pore-filling<sup>[33, 45]</sup>.

Surface functionalization involves the attachment of small moieties or polymers to the surfaces of porous membranes *via grafting-to* or *grafting-from* reactions<sup>[32, 43, 44]</sup>. Among these techniques, *grafting-from* offers the flexibility of the grafted polymer layer and variations of layer functionality and base polymer surface coverage are much larger<sup>[43]</sup>. The mechanism of UV-activated heterogeneous graft copolymerization is shown in Figure 2.13. This approach can be done in two steps. First, adsorption of type II photoinitiator, e.g. benzophenone on the membrane surface takes place. And second, upon UV irradiation, starter radicals on the base polymer are formed from hydrogen abstraction on the membrane surface in the presence of monomer.

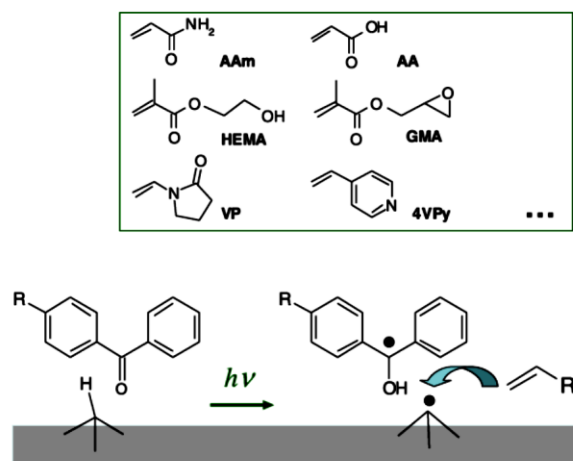


**Figure 2.13** A two-step UV-assisted graft copolymerization (*grafting-from*) applicable to various functional monomers according to Ulbricht<sup>[44]</sup>.

This method had been used for the surface functionalization of UF or MF membranes from PET, PES, PAm, PAN, PVDF or PSu with various functional monomers to prepare anti-fouling membranes, pH or temperature-responsive membranes and etc<sup>[31, 32, 158-162]</sup>. In those studies, the photo-grafted membranes reveal no degradation on their entire morphology since the functionalization can be done under mild conditions. Interestingly modification of membranes with ideal property, e.g. track-etched membranes under suited functionalizations enabled the accurate quantification about the grafted layer thickness based on Hagen-Poiseuille model and etc (*c.f.* Figure 2.15 in 2.3.3.1).

### 2.3.3 Pore-Filling Functionalization

An alternative approach towards high membrane separation performance is pore-filling functionalization of macroporous membranes using suitable polymers. Layers of grafted linear hydrophilic polymers also considered as hydrogels because the confinement on the substrate and/or the chain density can be analogous to bulk hydrogels structure. An overview and also underlying principle on this topic can be found in 2.3.3.1 to 2.3.3.3.

#### 2.3.3.1 Concept and overview

The concept of the pore-filling functionalization is schematically shown in Figure 2.14. The membrane is a composite-type and composed of the porous substrate film and the filling-polymer material. The underlying principle of such composite membrane lies on two factors; (i) space-filling capability of the filling-material to be fabricated *in situ* covalently or non-covalently, and (ii) confinement effect by the membrane pore in order to impose swelling restriction towards the filling-polymer. The basic engineering problem is to protect the filling material against the mechanical and osmotic forces <sup>[34, 35]</sup>. Pore-filling alters the entire pore-volume, reduces the membrane porosity, but the overall membrane thickness remains unchanged <sup>[1]</sup>.

Porous supports having highly uniform pore geometry with very narrow size distribution allow accurate quantification of polymer pore-filling and the effects of the functional polymers onto barrier properties. Polymer-based hydrogels are suitable filling materials because their networks impose a sieving structure and may be used to enhance size selectivity processes. The transport of water and dissolved substances through the completely filled composite membranes will be controlled by the hydrogel. And this also means that hydrogel controlled the desired selectivity for a certain separation. A more promising approach towards novel separation membranes can be achieved by tailoring the barrier properties of these membranes with SRH because it allows for tunable and switchable barrier functions <sup>[33]</sup>.

With respect to the stability of pore-filling, the pore wall of support membranes is subjected to pre-functionalization (*c.f.* 2.3.2). The linear grafted polymer layers to the pore-wall provide anchoring sites to the hydrogel matrix in the membrane pore. In addition, this technique in which the filling polymer is combined with the porous substrate by chemical bonds can prevent leakage at interface between the pore wall and the filling polymer <sup>[45]</sup>.

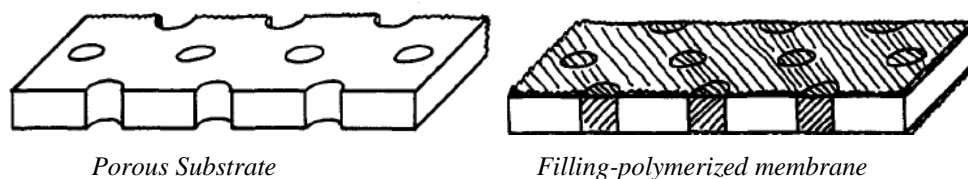


**Figure 2.14** The pore-filling concept according to Yamaguchi *et al.* <sup>[163]</sup>.



Measurement of hydrodynamic permeability of a bulk gel is often very difficult because of its intrinsic soft nature and the ease of gel compression under the test conditions <sup>[164]</sup>. The concept of confinement of the filling material in the pore could in principle be applied for detailed characterization of the pore-filled hydrogel network <sup>[35]</sup>. Using the Darcy model, this concept can be used to characterize one of the fundamental properties of hydrogels; hydrodynamic permeability,  $k_{mem}$  (Figure 2.15). Hydrodynamic permeability is closely related to the microstructure of the gel network, with the square root of  $k_{mem}$ , being regarded as a measure of the mean spacing or mesh size between the gel network <sup>[35]</sup>. The hydrodynamic screening length is an important parameter and used in modelling molecular transport within gels <sup>[34, 35, 75, 165]</sup>.

### Hagen-Poiseuille equation

(Membrane pore size)

$$J = \frac{V}{A \cdot \Delta t} = r^2 \cdot \frac{\varepsilon_{mem}}{8\eta} \cdot \frac{\Delta P}{\Delta x}$$

### Darcy permeability

(Mesh size)

$$J = \frac{V}{A \cdot \Delta t} = k_{mem} \cdot \frac{\varepsilon_{mem}}{\eta} \cdot \frac{\Delta P}{\Delta x}$$

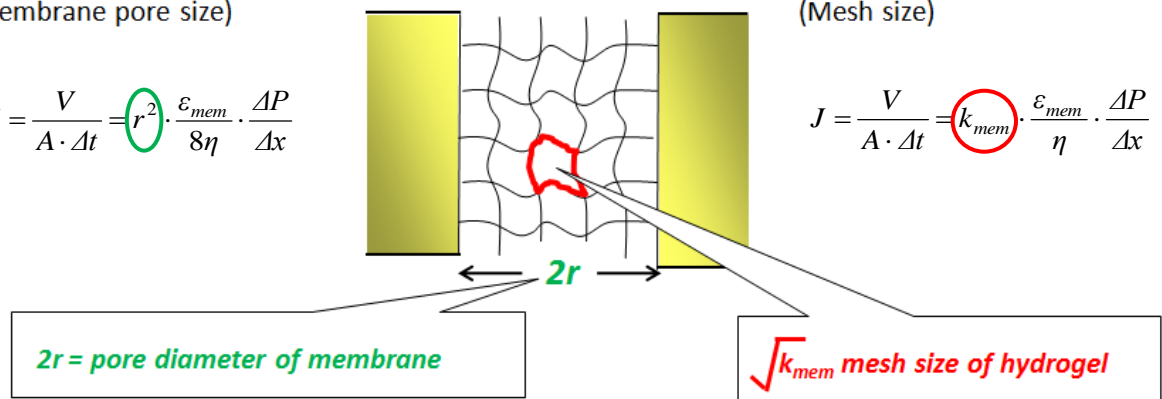


**Figure 2.15** Using water permeabilities in combination with Hagen-Poiseuille and Darcy models to characterize the unmodified, prefunctionalized and hydrogel pore-filled composite membrane.  $J$  is water flux through the membrane [ $\text{l/m}^2\text{h}$ ],  $V$  is volume of permeate [ $\text{l}$ ],  $A$  is membrane outer surface area [ $\text{m}^2$ ],  $\varepsilon_{mem}$  is membrane porosity [%],  $\eta$  is viscosity of water [ $\text{Pa}\cdot\text{s}$ ],  $\Delta P$  is transmembrane pressure [ $\text{bar}$ ],  $\Delta t$  is time [ $\text{s}$ ] and  $\Delta x$  is membrane thickness [ $\text{m}$ ].

The permeation experiment can be constructed to characterize both MF and UF membranes <sup>[155, 166]</sup>. From this experiment, the (hydrodynamic) pore size could be determined using the relationship between the flux through the effective membrane surface area in the time period (Figure 2.15). The permeability method is direct characterization method for determination of the actual separation parameters. Nevertheless, calculation of pore size is difficult because the pore size and shape are not well defined. Indeed, several assumptions have to be made in order to fit the pore parameters (especially pore geometry) to models and equations. If the capillary pores are assumed to be presented, the pore size can be calculated using Hagen-Poiseuille model, whereas in the Kozeny-Carman model (will not be discussed here), the pores are the voids between closed-packed spheres of equal diameter <sup>[155, 166]</sup>.

### 2.3.3.2 Preparation of composite membranes

A limited amount of research on membrane-supported hydrogels has been reported so far since most membrane functionalizations are focused on either their outer or their pore surface<sup>[1]</sup>.

The early work on pore-filling of porous membranes with hydrogels was inspired by the concept of the "gel in a shell" as chromatographic medium. Anderson *et al.* had fabricated crosslinked polyacrylamide (neutral and charged) within PVDF MF membrane support (average pore diameter of 0.5  $\mu\text{m}$ ) *via in situ* free radical photopolymerization<sup>[34, 35, 76]</sup>. The pore-filling was performed without covalent bonding of the functional hydrogel to the inner pore wall.

Childs *et al.* had prepared composite membranes *via in situ* crosslinking of polyelectrolytes within PP MF membranes (average pore diameters of 0.2, 0.5 and 0.8  $\mu\text{m}$ )<sup>[167, 168]</sup>. It has been demonstrated that the separation performance could be tuned from adaptation of synthesis conditions. In addition, they were able to adjust the charge density within the pore-filling hydrogel. They also comprehensively investigated the pore-filling for obtaining NF membranes. The strategy to produce such composite membranes was reported in detail.

Pore-filling can also be achieved by grafting techniques. Yamaguchi *et al.* had investigated so called filling-polymerized membranes for enhancement of selectivity in pervaporation process<sup>[163, 169]</sup>. In their work, PE support membranes (0.02 or 0.05  $\mu\text{m}$ ) were first plasma activated and subsequently graft copolymerized with acrylate-based monomers.

Large scale versions of the pore-filling concept were also adopted for fabrication of other composite materials such as stimuli-responsive polymers embedded within capillaries or channels of microfluidic devices<sup>[22, 170]</sup> or for microfabrication of porous polymeric monoliths within a chromatographic column acting as a mould<sup>[42, 171, 172]</sup>. Composite materials for protein purification *via* gel electrophoresis were industrially developed<sup>[173]</sup>. However, in all these cases, the channel dimension was in the 10 to 100  $\mu\text{m}$  range.

### 2.3.3.3 Performance and function

The "gel in a shell" chromatographic medium prepared by Anderson and co-workers shows excellent promise in the separation of proteins by their charge and also sieving properties of hydrogel *via* size-exclusion mechanism<sup>[34]</sup>. The feasibility of convective transport through such composite membranes was due to enhanced mechanical stability of the gel interpenetrated with the pore structure of the membrane. The permeability of the membrane-supported gels was comparable to measurements made with bulk PAAm gels<sup>[174]</sup> when the polymer network had a volume fraction of 8 % or greater. Pressure differences as great as 3 bar over membranes  $\sim$  125  $\mu\text{m}$  thick were applied without any

apparent damage to the gel and negligible compression (i.e., water flow was proportional to pressure over the pressure range). These results indicate the feasibility of convective transport through such composite membranes due to enhancement of mechanical stability. This means that the gel interpenetrated with the pore structure of the membrane is resistant towards mechanical and osmotic forces.

Pore-filled polyelectrolyte hydrogels prepared by Childs *et al.* demonstrated outstanding performance for NF separation of ions and molecules: For instance, poly(4-vinylpyridine)-based pore-filled gel exhibited under filtration conditions pH-responsive behaviour similar to a "chemical valve", and it rejected molecules and ions based on a combined size and Donnan exclusion mechanism. In their recent publication, asymmetric composite membranes, either due to asymmetric pore geometry of the base membrane or the asymmetric hydrogel structure within the pores, possessed higher performance compared to the symmetric ones. Higher flux was achieved by keeping high rejection rates (for Na<sup>+</sup>, Ca<sup>2+</sup>, Mg<sup>2+</sup>), also in comparison to commercial NF membranes.

There also exist other composite membranes prepared using hydrogels as filling materials. In those cases, the composite membranes have a relatively dense barrier and as a result, convective flow is strongly reduced or impossible. For instance, the pore-filling approach has been reported to improve the permselectivity of organic liquid mixture in pervaporation process <sup>[163, 169, 175, 176]</sup>. The incorporation of PEG-derivative hydrogels into UF membranes contributed to the high permselectivity of CO<sub>2</sub> over N<sub>2</sub> in gas separation. Pore-filling was also employed improve the performance of fuel cells by controlling the methanol crossover to the cathode during the operation. The hydrogels prepared within battery separator matrix not only improve the overall battery performance; i.e., improved high liquid electrolyte at high temperature, but also their shutdown capability may fulfil some safety requirements.

Finally, when the pore-filling concept is combines with SRH, not only the separation function of pore-filled composite membrane is further improved but also the membrane can be used as a tool for detailed characterization of the gel network. Such novel approach is of course very important since it could overcome the single size limitation with respect to retention of components by conventional MF or UF processes.

## CHAPTER 3

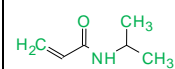
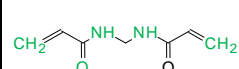
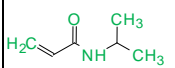
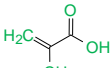
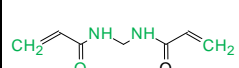
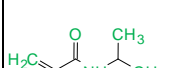
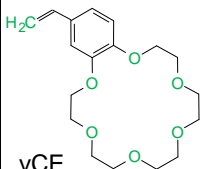
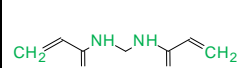
### EXPERIMENTAL

#### 3.1 Chemicals and Materials

##### 3.1.1 Hydrogel Compositions

All chemicals used for hydrogel preparations were at least analytical grades. NIPAAm, vCE, APS, TEMED and tris(hydroxymethyl)aminomethane (Tris) (base) were purchased from Acros (Geel, Belgium). MBAAm, MAA and HCl were purchased from Sigma-Aldrich (Steinheim, Germany). “Type I” photoinitiator (PI); 1-[4-(2-hydroxyethoxy)-phenyl]-2-hydroxy-2-methyl-1-propane-1-one with the trade name Irgacure 2959<sup>®</sup> was supplied by BASF-Ciba Chemicals (Basel, Switzerland). Polyethylene glycol (PEG, MW = 400 g/mol) and THF were obtained from Fluka (Buchs, Switzerland). The NIPAAm was recrystallized from *n*-hexane (unless specified), and all other chemicals were used as received without a purification. Water purified with a Milli-Q system from Millipore (USA) was used for all experiments. The summary of chemicals used is shown in Table 3.1.

**Table 3.1** List of the chemicals used and their structural formulas according to hydrogel types.

	Main Monomer	Second Monomer	Crosslinker Monomer	Initiator	Solvent
(a) classic		---		<ul style="list-style-type: none"> <li>• TEMED/APS</li> <li>• Irgacure 2959</li> </ul>	<ul style="list-style-type: none"> <li>• Water</li> <li>• Water/PEG</li> </ul>
*(b) with ionic comonomer		MAA 		Irgacure 2959	Tris-HCl, buffer, pH 7 10 mM
(c) with macrocyclic comonomer				TEMED/APS	Water/THF

\*with or without template protein; c.f. Table 3.4.

## 3.1.1.1 Hydrogel compositions for classic hydrogels

The nomenclature of the hydrogels was given based on the content of the main monomer relative to the solvent and the content of other components relative to in the main monomer. In general, the reaction mixtures contained NIPAAm as a main monomer (10 to 15 wt % → M10, M15) and MBAAm as a crosslinker (2 to 10 wt % relative to NIPAAm → DC02, DC05, DC10). The reaction mixture containing 15 wt% NIPAAm and 5 wt% MBAAm relative to NIPAAm was chosen as standard composition for classic hydrogels. The reaction mixtures for classic PNIPAAm hydrogels were prepared either in water or a mixture of water/PEG (10 to 40 wt% of PEG in the solvent mixture → PEG10, PEG20, PEG40) as solvents. The preliminary precursor solutions in Table 3.2 were prepared in 50 g solvent and used to study the effect of various polymerization conditions (*c.f.* 3.2.1.1, 3.2.2.1 and 3.2.2.2). The feed compositions for classic redox and photopolymerized hydrogels were obtained in 25 g solvent (Table 3.3).

**Table 3.2 Precursor compositions for classic redox hydrogels.**

Hydrogel	Mass of NIPAAm [g]	Mass of MBAAm [g]	Mass of Water [g]	Mass of PEG 400 [g]
M15DC05	7.5	0.375	50	0
M15DC05PEG40	7.5	0.375	30	20

**Table 3.3 Feed compositions for: (a) classic redox hydrogels and (b) classic photopolymerized hydrogels.**

(a) Hydrogel	Mass of NIPAAm [g]	Mass of MBAAm [g]	Mass of Water [g]	Mass of PEG 400 [g]
M15DC02	3.75	0.0750	25	0
M15DC05	3.75	0.1875	25	0
M15DC10	3.75	0.3750	25	0
M15DC05PEG10	3.75	0.1875	22.5	2.5
M15DC05PEG20	3.75	0.1875	20.0	5.0
M15DC05PEG40	3.75	0.1875	15.0	10.0

(b) Hydrogel	Mass of NIPAAm [g]	Mass of MBAAm [g]	Mass of Water [g]	Mass of PEG 400 [g]
M7.5DC05	1.875	0.0938	25	0
M10DC05	2.50	0.1250	25	0
M15DC02	3.75	0.0750	25	0
M15DC05	3.75	0.1875	25	0
M15DC10	3.75	0.3750	25	0
M15DC05PEG40	3.75	0.1875	15.0	10.0

## 3.1.1.2 Hydrogel compositions with ionic comonomer

For preparation of reaction mixtures with ionic comonomer, MAA was incorporated as a template-binding monomer at four different levels (1 to 10 wt % relative to NIPAAm → M'01, M'02, M'05, M'10). The MIP and NIP hydrogels were prepared with and without lysozyme (10 wt% relative to NIPAAm → L10), respectively. Lysozyme (chicken egg white, MW 14.6 kDa, isoelectric point (IEP) 10.8) was obtained from Fluka (Belgium). All solutions were prepared in 0.01 M tris-HCl buffer, pH 7.0.

**Table 3.4 Feed compositions for NIP and MIP hydrogels with ionic comonomer.**

Hydrogel		Mass of NIPAAm [g]	Mass of MAA [g]	Mass of MBAAm [g]	Mass of Lysozyme [g]	Mass of buffer [ml]
NIP	M15M'01DC05	3.75	0.0375	0.1875	0	25
	M15M'02DC05	3.75	0.0750	0.1875	0	25
	M15M'05DC05	3.75	0.1875	0.1875	0	25
	M15M'10DC05	3.75	0.3750	0.1875	0	25
MIP	M15M'01DC05L10	3.75	0.0375	0.1875	0.3750	25
	M15M'02DC05L10	3.75	0.0750	0.1875	0.3750	25
	M15M'05DC05L10	3.75	0.1875	0.1875	0.3750	25
	M15M'10DC05L10	3.75	0.3750	0.1875	0.3750	25

## 3.1.1.3 Hydrogel compositions with macrocyclic comonomer

For preparation of reaction mixtures with macrocyclic comonomer, vCE was incorporated as a second monomer at four different levels (0 to 10 wt % relative to NIPAAm → CE00, CE02, CE05, CE10). Besides, the crosslinker content was also varied at two levels. All solutions were prepared in water/THF with volume ratio of 4 : 1.

**Table 3.5 Feed compositions for PNIPAAm hydrogels with macrocyclic comonomer.**

Hydrogel	Mass of NIPAAm [g]	Mass of vCE [g]	Mass of MBAAm [g]	Mass of Water/THF solvent mixture [g]
M10DC02CE00	0.5	0	0.01	5
M10DC02CE02	0.5	0.010	0.01	5
M10DC02CE05	0.5	0.025	0.01	5
M10DC02CE10	0.5	0.050	0.01	5
M10DC05CE05	0.5	0.025	0.025	5
M10DC05CE10	0.5	0.050	0.025	5

### 3.1.2 Membranes

Commercial PET track-etched membranes (RoTrac<sup>®</sup>– hydrophilic capillary pore membranes) were purchased from Oxyphen, Switzerland. The molecular structure of PET is shown in Figure 3.1.

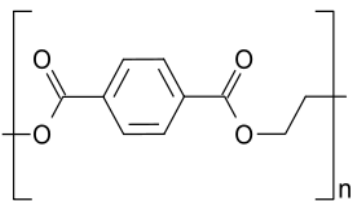


**Figure 3.1** The chemical structure of PET.

Membranes with nominal pore diameters from 200 to 5000 nm and 21 to 23  $\mu\text{m}$  thick were employed as base membranes (BM) for functionalization. The porosity of BM was given from supplier as shown in Table 3.6. The nominal pore diameter of the reference membrane was 30 nm and it was 8  $\mu\text{m}$  thick with 4.9 % porosity. Prior to functionalization, all membranes (cut in circular samples with diameter of 25 or 44 mm) were washed in ethanol and dried for one hour.

**Table 3.6** The nominal pore size and porosity of the base membranes.

Nominal pore size [nm]	200	400	1000	3000	5000
Porosity [%]	10.1	12.6	17.3	14.1	11.8

### 3.1.3 Information on Test Solutes

For partitioning experiments of classic bulk PNIPAAm hydrogels, 1 g/l of aqueous dextrans solution from various MW containing 0.01 M  $\text{NaN}_3$  (Sigma-Aldrich, Steinheim, Germany) and 0.5 g/l lysozyme in 0.01 M tris-HCl buffer, pH 7.0 were used as test solutes.

Sorption experiments of PNIPAAm-*co*-MAA hydrogels were performed with either lysozyme (0.5-5 g/l) solutions or solutions containing equimass mixture of lysozyme and cytochrome C at a total concentration of 0.5 g/l in the same tris-HCl buffer as above. The dimensions of the test solutes are listed in Table 3.7.

$$r_s = 0.033 \cdot \text{MW}^{0.46} \dots \dots \dots \text{Equation 16}$$

where  $r_s$  = Stokes radius [nm] and MW = molecular weight [g/mol].

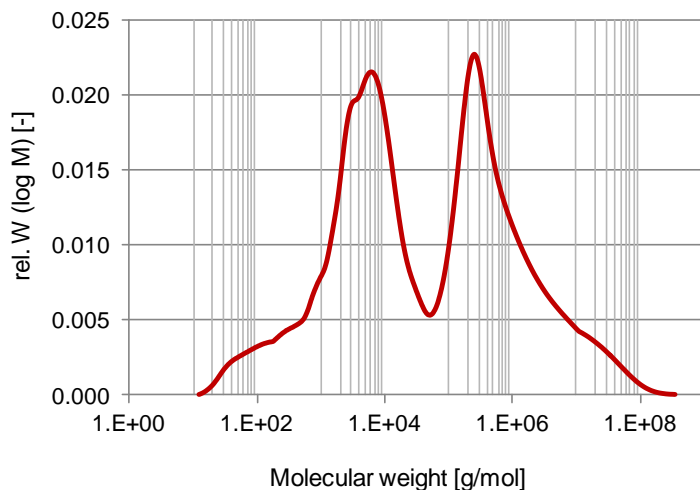
**Table 3.7 Test solutes for partition and sorption experiments of PNIPAAm hydrogels.**

Experiments	Test Solutes	Molecular weight [kg/mol]	IEP	Diameter [nm]	Manufacturer
Partitioning (classic hydrogels)	Dextran	4	--	*3	Serva, Heidelberg, Germany
		10	--	*4.6	
		500	--	*27.6	
		2000	--	*54	
	Lysozyme	14.6	10.8	**4	Sigma-Aldrich, Germany
Sorption (ionic hydrogels)	Lysozyme	14.6	10.8	**4	Sigma-Aldrich, Germany
	Cytochrome C	12.4	9.8	**3.4 - 3.8	Sigma-Aldrich, Germany

\*from the Stokes radius according to Equation 16

\*\*from hydrodynamic radius (c.f.<sup>[177, 178]</sup>).

1 or 10 g/l equimass mixture of two dextrans with average MWs of 4 and 2000 kg/mol in 0.01M  $\text{NaN}_3$  were used to perform diffusion and filtration experiments. MW distribution (MWD) of feeds was determined with high performance gel permeation chromatography (HP-GPC, PSS WinGPC Unity, Germany; the GPC column SUPREMA calibrated from 100 to 100,000,000 g/mol). Figure 3.2 shows MWD of feed used for UF test.

**Figure 3.2 Molecular weight distribution of feed used for diffusion and filtration experiment.**

### 3.1.4 Others

Benzophenone (“type II” photoinitiator) was purchased from Acros, Geel, Belgium. Ethanol p.a. and NaCl were obtained from VWR, Germany.  $\text{NaNO}_3$  and  $\text{Ba}(\text{NO}_3)_2$  were supplied from Sigma-Aldrich, Steinheim, Germany.  $\text{KNO}_3$  was the product from Fluka Buchs, Switzerland. Nitrogen pure gas was from Messer Griesheim GmbH, Germany.



## 3.2 Synthesis of Stimuli-Responsive Bulk Hydrogels

### 3.2.1 Redox-Polymerization of Poly(N-Isopropylacrylamide) Hydrogels

#### 3.2.1.1 Preliminary experiments

The homogeneous precursor solutions in Table 3.2 were transferred into glass vessels (diameter ~ 25 mm) and pre-cooled in an ice bath (~ 4 °C) for 10 min. Thereafter, 43.29 mg of APS and 173.2 mg of TEMED (mass ratio of TEMED to APS; 4.0 : 1) were added in order to initiate the polymerization under various conditions given in Table 3.8. The vessel was sealed, and the solution was kept at 15 °C for 24 h (for simple polymerization mechanism *c.f.* Scheme 1 in 2.1.1). After the polymerization, hydrogels were removed from the reaction vessel and washed. The conversion of hydrogels was determined (*c.f.* 3.3.1) prior to other characterization.

**Table 3.8** Variation of the synthesis conditions (TEMED/APS 4.0 : 1).

Hydrogel	Conditions	
	Using recrystallized monomer	Deaeration of precursor solution with argon
M15DC05_ 1	No	No
2	No	Yes
3	Yes	No
4	Yes	Yes
M15DC05PEG40	No	No

The standard compositions for classic hydrogels (M15DC05) were prepared using recrystallized NIPAAm and by stirring under argon for the next preliminary experiments. Then, initiators were added to the pre-cooled precursor solutions (pre-cooling conditions; *c.f.* above) with various ratios as shown in Table 3.9 in order to be polymerized at 15 °C. The time when the reaction mixtures became turbid was recorded as a gelation point and the conversion of these hydrogels was determined according to 3.3.1.

**Table 3.9** Variation of the TEMED to APS ratio (using recrystallized monomer and deaerated precursor solution).

Hydrogel	TEMED	APS
M15DC05_ 1	4.0	1
2	2.0	1
3	1.0	1
4	0.5	1
5	0.1	1
6	0	1

### 3.2.1.2 Synthesis of conventional and phase-separated hydrogel

There were six different compositions of *ex situ* classic PNIPAAm hydrogels synthesized using redox initiators with mass ratio of 4.0 : 1 (Table 3.10). These hydrogels were prepared from the 'pre-treated' homogeneous reaction mixtures in Table 3.3a. The pre-treated reaction mixtures simply implied that the solutions were degassed and using recrystallized NIPAAm. The crosslinker content was varied at three levels. The content of PEG in water was also varied at three levels. The synthesis of these hydrogels was carried out at 15 °C for 24 h in glass vessels (diameter ~ 25 mm). Conversion and characterization of hydrogels can be referred to 3.3.

**Table 3.10** Classic PNIPAAm hydrogels synthesized *via* redox polymerization (TEMED/APS 4.0 : 1) at 15 °C for 24 h.

Content of crosslinker relative to NIPAAm (DC)	Conventional redox hydrogels	PEG-modified hydrogels
02	M15DC02	--
05	*M15DC05	M15DC05PEG10 M15DC05PEG20 M15DC05PEG40
10	M15DC10	--

### 3.2.1.3 Rheology monitoring *in situ* redox-polymerization

*In situ* polymerization were carried out using a 25 mm cone-plate geometry of a rheometer (model MCR-300, Anton Paar, Graz, Austria). A Peltier device was used to control the temperature of the measuring cell; i.e., at 15 °C.

Analogous pre-cooled hydrogel precursor solution as for bulk syntheses was prepared (M15DC05). TEMED/APS with various ratios (0.1 : 1 to 4.0 : 1) were added to the solution which was then immediately poured onto the lower plate (sample volume = 150 µL). The gap setting was fixed by the measuring system (0.1 mm). The measurement was done under oscillating conditions with an angular frequency,  $\omega = 10$  rad/s, and small strain amplitude,  $\gamma = 0.01$  %, to ensure a linear regime of oscillatory deformation. Argon gas was supplied throughout the measurements. During all rheological measurements, a solvent trap was used to minimize evaporation. The measurement time was not fixed but it was carried out until either onset of gelation was observed or until the moduli became constant (in the oscillating mode described above). All measurements were repeated at least three times.

### 3.2.2 Photopolymerization of Poly(*N*-Isopropylacrylamide) Hydrogels

#### 3.2.2.1 Preliminary experiments: efficiency of photoinitiator

The PI was dissolved in methanol with the initial concentration  $c_{x,0} = 0.15$  mM. The PI solution was exposed to UV using UVA system (Hönle AG, Germany) with  $\lambda > 300$  nm and UV intensity  $\sim 30$  mW/cm<sup>2</sup> at pre-determined irradiation times until it reached complete conversion (no further changes in absorbance was observed). The UV absorbance was measured immediately after each irradiation at characteristic wavelength  $\lambda = 276$  nm using UV-Visible Spectrophotometer (Varian Cary 50 Probe, Santa Clara, USA; Table 3.11).

The decomposition of PI was assumed to undergo pseudo reaction of species  $x$  reacted to produce species  $y$  (Equation 17):



where  $x$  and  $y$  are reactant and product species, respectively.

The Beer-Lambert law ( $Abs = \text{absorbance}$ ,  $\varepsilon = \text{the molar absorptivity}$ ,  $l = \text{the path length}$ , and  $c = \text{the concentration}$ ; Equation 18) was employed to determined the molar absorptivity (Equation 19) of a single absorbing species.

$$Abs = \varepsilon \cdot c \cdot l \quad \text{Equation 18}$$

$$\varepsilon = \frac{Abs}{c \cdot l} \quad \text{Equation 19}$$

The measured absorbance at any reaction time is the sum of the absorbance for each individual species:

$$Abs = (\varepsilon_x \cdot c_x + \varepsilon_y \cdot c_y) \cdot l \quad \text{Equation 20}$$

where  $\varepsilon_x$  and  $\varepsilon_y$  are the molar absorptivity (*c.f.* Equation 19),  $c_x$  and  $c_y$  are concentrations of species  $x$  and  $y$ , respectively.

At time  $t = 0$  s, only species  $x$  was existing. With increasing reaction time, the concentration of species  $x$  decreased  $\rightarrow 0$ , while the concentration of species  $y$  increased  $\rightarrow 100\%$  (0.15 mM; assuming 100% conversion). Thus, at any reaction time, the concentration of both species can be calculated using Equation 21. These values are given in Table 3.11.

$$c_x = c_{x,0} - c_y \quad \text{Equation 21}$$

**Table 3.11 Determination of concentration of species *x* and *y* from decomposition of PI at certain UV irradiation time. Molar absorptivities of species *x* and *y* are 12.4 and 3.4 l/mM.cm, respectively.**

UV-irradiation time [s]	Absorbance (at 276 nm)	Concentration	
		Species <i>y</i> [mM]	Species <i>x</i> [mM]
0	1.8582	0	0.15
10	1.0878	0.0859	0.0641
60	0.8211	0.1157	0.0343
120	0.7272	0.1261	0.0239
180	0.6682	0.1327	0.0173
240	0.6267	0.1374	0.0126
300	0.5895	0.1415	0.0085
600	0.5327	0.1478	0.0022
900	0.5138	0.1497	0.0003
1200	0.5131	0.15	0

From here, the calculated concentration of the reacting species was used to construct kinetic plots based on integrated rate equation (Table 3.12). Thereafter, the reaction order, reaction-rate constant (*k*), and half-life ( $t_{1/2}$ ) was determined (*c.f.* 4.1.2.1).

**Table 3.12 Summary for reaction orders 0, 1, and 2 [179].**

	Zero-order	First order	Second-order
Rate Law	$-\frac{d[x]}{dt} = k$	$-\frac{d[x]}{dt} = k[x]$	$-\frac{d[x]}{dt} = k[x]^2$
Integrated Rate Law	$[x] = [x]_0 - kt$	$[x] = [x]_0 e^{-kt}$	$\frac{1}{[x]} = \frac{1}{[x]_0} + kt$
Units of Rate Constant ( <i>k</i> )	$\frac{\text{M}}{\text{s}}$	$\frac{1}{\text{s}}$	$\frac{1}{\text{M} \cdot \text{s}}$
Linear Plot to determine <i>k</i>	$[x]$ vs. $t$	$\ln([x])$ vs. $t$	$\frac{1}{[x]}$ vs. $t$
Half-life	$t_{1/2} = \frac{[x]_0}{2k}$	$t_{1/2} = \frac{\ln(2)}{k}$	$t_{1/2} = \frac{1}{k[x]_0}$

### 3.2.2.2 Optimization of photopolymerization conditions

The optimization of photopolymerization conditions was carried out in a glass vessel (diameter ~ 25 mm) using standard pre-treated precursor solution (M15DC05). Various amounts of PI were added to the precursor solution (1 to 5 wt% relative to NIPAAm). The mixture was further stirred under argon until completely dissolved (~ 30 min) and then pre-cooled in the ice bath (~ 4 °C) for 10 min. The mixture was then exposed to UV light (UVA system, with  $\lambda > 300$  nm and intensity ~30 mW/cm<sup>2</sup>) between 2.5 to 20 min at 4 °C (for simple polymerization mechanism *c.f.* Scheme 2 in 2.1.1). Further characterization (*c.f.* 3.3), including determination of conversion, was the same way as for redox-initiated polymerization.

### 3.2.2.3 Synthesis of hydrogels various compositions

PNIPAAm hydrogels were synthesized with the same procedure as in 3.2.2.2 using the constant proportion of PI to NIPAAm (2 wt%) and also UV-irradiation times (15 min). The system was homogeneous when water was used as solvent; whereas the system was heterogeneous in a mixture of water/PEG. These reaction mixtures were polymerized in the ice-water bath (~ 4 °C). The feed compositions and hydrogels nomenclature for the reaction mixtures are summarized in Table 3.3b and Table 3.13 respectively. The NIPAAm content was varied at three levels. The crosslinker content was also varied at three levels.

**Table 3.13 Classic PNIPAAm hydrogels synthesized *via* photopolymerization (2 wt % PI relative to NIPAAm, 15 min UV time).**

Content of crosslinker relative to NIPAAm (DC)	Content of NIPAAm relative to solvent (M)		
	7.5	10	15
02		--	M15DC02
05	M7.5DC05	M10DC05	M15DC05 M15DC05PEG40
10		--	M15DC10

### 3.2.2.4 Rheology monitoring *in situ* photo-polymerization

The temperature of the measuring cell was kept constant at 4 °C. The standard hydrogel precursor solution (M15DC05) was mixed with 2 wt% of PI relative to NIPAAm. After that this solution was loaded onto the lower plate (optically transparent base plate) and allowed to equilibrate prior to UV irradiation. The UV source (EXFO Omnicure Series 1000, EXFO, Quebec, Canada) was switched on 10 s later (the measurement was again performed under oscillating mode as described in

3.2.1.3). Since the gap setting was fixed by the measuring system (0.1 mm), only UV intensity could be adjusted in order to reproduce similar illumination intensity as under bulk conditions (intensity 30 mW/cm<sup>2</sup>, path length = 25 mm). Therefore, the *in situ* photopolymerization was performed with various intensities (30, 5, 1 mW/cm<sup>2</sup>) for up to 15 min of irradiation time or with various irradiation times (5, 10, 15 and 20 min) at 1 mW/cm<sup>2</sup>. The measurements were also done with the total exposure time of 15 min at 1 mW/cm<sup>2</sup> and accompanied with an interval of at least 10 min without UV light. The desired reaction time as well as moments for switching UV on or off were set and controlled by the rheometer program.

Additionally, the compositions for *in situ* gelation were varied (*c.f.* Table 3.13) under constant UV irradiation time and intensity; i.e. 15 min at 1 mW/cm<sup>2</sup>.

### 3.2.3 Synthesis of Molecularly Imprinted and Non-Imprinted Poly(*N*-Isopropylacrylamide-*co*-Methacrylic Acid) Hydrogels *via* Photopolymerization

NIP and MIP hydrogels were synthesized in the absence or in the presence of lysozyme (10 wt% relative to NIPAAm) as template-protein *via* photopolymerization. The principles of molecular imprinting are shown in Figure 2.7 (*c.f.* 2.2.3). There were nine different compositions of NIP and MIP hydrogels synthesized with various ratios of ionic comonomers (Table 3.14). The feed compositions of these hydrogels (*c.f.* Table 3.4) were developed from the standard precursor solution (M15DC05).

**Table 3.14** NIP and MIP of PNIPAAm-*co*-MAA hydrogels synthesized *via* photopolymerization (2 wt % PI relative to NIPAAm, 15 min UV time).

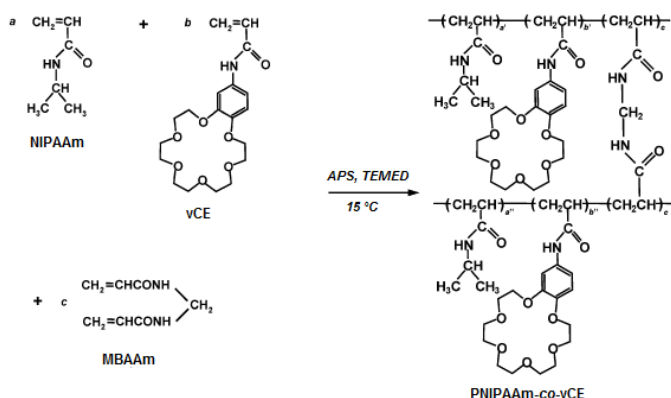
Gel	Content of MAA relative to NIPAAm (M')				
	00	01	02	05	10
NIP	M15M'00DC05	M15M'01DC05	M15M'02DC05	M15M'05DC05	M15M'10DC05
MIP	--	M15M'01DC05L10	M15M'02DC05L10	M15M'05DC05L10	M15M'10DC05L10

*Ex situ* hydrogels were synthesized with the same procedure in 3.2.2.2 using the constant proportion of PI to NIPAAm (2 wt%) and also UV irradiation time (15 min). After the polymerization, extraction of the unreacted monomer and lysozyme were performed according to 3.3.

*In situ* polymerizations were carried out analogous to *ex situ* conditions and were monitored by online rheometry according to 3.2.2.4.

### 3.2.4 Synthesis of Poly(*N*-Isopropylacrylamide-*co*-4-vinylbenzo-18-crown-6) Hydrogels via Redox-Polymerization

PNIPAAm-*co*-vCE hydrogels were prepared by redox-initiation free radical copolymerization. The synthesis scheme is shown in Scheme 3.



**Scheme 3** Synthesis scheme of the PNIPAAm-*co*-vCE hydrogels by free radical copolymerization with MBAAm as the crosslinking agent <sup>[139]</sup>.

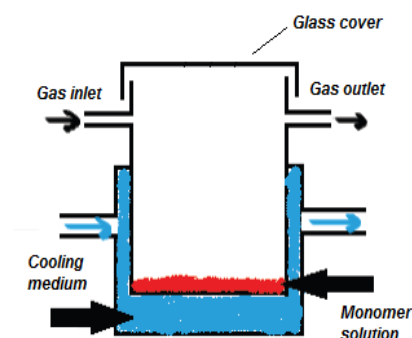


**Figure 3.3** Reaction vessel for synthesis of PNIPAAm-*co*-vCE hydrogels.

The *ex situ* gelation was performed in a reaction vessel (diameter ~ 70 mm) connected with gas tubes and thermostat (Julabo, Seelbach, Germany) as shown in Figure 3.3. The reaction mixture obtained from Table 3.5 was homogeneously mixed with redox initiators (TEMED/APS 4.0 : 1), and then quickly transferred into the reaction vessel (sample volume 5 ml). The polymerization was continued under sealed argon atmosphere at 15 °C for 24 h. Other synthesis conditions were adopted from the procedure in 3.2.1.2. In total, PNIPAAm-*co*-vCE hydrogels were synthesized from eight different compositions as shown in Table 3.15.

*In situ* polymerizations were carried out analogous to *ex situ* conditions and were monitored by online rheometry according to 3.2.1.3.

**Table 3.15** PNIPAAm-*co*-vCE hydrogels synthesized *via* redox polymerization (TEMED/APS 4.0 : 1) at 15 °C for 24 h.

Content of crosslinker relative to NIPAAm (DC)	Content of vCE relative to NIPAAm (CE)			
	00	02	05	10
02	M15DC02CE00	M15DC02CE02	M15DC02CE05	M15DC02CE10
05	M15DC02CE00	M15DC02CE02	M15DC05CE05	M15DC05CE10

### 3.3 General Characterization of Hydrogels

#### 3.3.1 Washing and Conversion

After the polymerization, the hydrogel was cut with scalpel or punched out with hollow puncher (diameter ~1.3 cm) into small pieces with the dimension that were suited for the subsequent characterization (Table 3.16). The hydrogel pieces were immersed in the washing medium which was refreshed several times every 24 h. Complete extraction of the unreacted monomer, oligomer or other unbound components from the obtained hydrogel was monitored using total organic carbon analyzer (TOC-Vcpn system, Shimadzu, Japan); the obtained data were used to calculate the monomer to gel conversion on the basis of mass balance from the following series of equations:

$$m_{c,gel} = m_{c,mon} + m_{c,co-mon} + m_{c,cl} \quad \text{Equation 22}$$

$$m_{res,tot} = \sum_1^n (TOC \cdot V_{wash})_1 + (TOC \cdot V_{wash})_2 \dots + (TOC \cdot V_{wash})_n \quad \text{Equation 23}$$

$$m_{res,net} = m_{res,tot} - m_{c,inert} \quad \text{Equation 24}$$

$$\text{Conversion} = \frac{m_{c,gel} - m_{res,net}}{m_{c,gel}} \cdot 100 [\%] \quad \text{Equation 25}$$

where  $m_{c,gel}$  is the mass of carbon in gel.  $m_{c,mon}$ ,  $m_{c,co-mon}$ ,  $m_{c,cl}$  are mass of carbon in monomer, comonomer and crosslinker, respectively.  $m_{res,tot}$  is the summation mass residues of carbon (TOC content in the volume of washing medium ( $V_{wash}$ ) for  $n$  number of washing). The net mass residues of carbon in the washing water ( $m_{res,net}$ ) is equivalent to the difference between the  $m_{res,tot}$  and the mass of carbon in inert material;  $m_{c,inert}$  i.e., co-solvent.

**Table 3.16** An overview of dimension of hydrogel pieces and washing medium for various hydrogel types.

Hydrogel types	Washing medium	Hydrogel pieces	Characterization
Classic redox	distilled water	*square-like ~ 1cm <sup>3</sup>	conversion, swelling
Classic photo	distilled water	*square-like ~ 1cm <sup>3</sup> *disc-like ~ 1 to 2 mm thick	conversion, swelling volume expansion, rheology, morphology, partitioning
NIP / MIP gel	0.03 M NaCl	*disc-like ~ 1 to 2 mm thick	conversion, swelling, protein sorption.
PNIPAAm-co-vCE	distilled water	**disc-like ~ 1 to 2 mm thick	conversion, copolymerization efficiency, swelling, ion-responsivity

\*from cutting  
\*\* from hollow punching



### 3.3.2 Evidence of Copolymerization

The chemical structures of PNIPAAm and PNIPAAm-*co*-vCE hydrogel disks were recorded with a Fourier transform infrared spectroscopy (FTIR: Varian 3100, Excalibur Series, Santa Clara, USA). A nominal resolution of  $4\text{ cm}^{-1}$  and 64 scans were used. Hydrogel samples for FTIR analysis were pre-freeze-dried at  $-18\text{ }^{\circ}\text{C}$  and subsequently freeze-dried at  $-53\text{ }^{\circ}\text{C}$  for 72 h.

### 3.3.3 Swelling Experiments

The hydrogel pieces were incubated in water (or in tris-HCl buffer, 10 mM, pH 7.0 for NIP/MIP hydrogels) within the temperature range from 15 to  $45\text{ }^{\circ}\text{C}$  for 24 h at each individual temperature. Then, the mass of these samples were determined ( $m_s$ ). After this equilibration, the samples were dried for another 24 h in a vacuum oven at  $60\text{ }^{\circ}\text{C}$  and the dried mass of was determined ( $m_d$ ). The degree of swelling ( $Q$ ) was calculated using Equation 1 (an average of triplicate measurements).

### 3.3.4 Rheology and Viscoelasticity of Hydrogels

For characterization of bulk hydrogels, a plate-plate geometry with a 25 mm diameter upper plate was used. The sample was 25 mm in diameter and  $\sim 2$  mm thick. The upper plate was set at the desired separation distance that was equivalent to a normal force of 5 N (within a linear range; the moduli are independent of the magnitude of imposed force) corrected with a “true gap” function of the instrument. The bulk hydrogels were characterized under frequency sweep ( $\omega = 0.1$  to  $100\text{ rad/s}$ ,  $20\text{ }^{\circ}\text{C}$ ) or at various heating rates (5, 0.05 and  $0.005\text{ }^{\circ}\text{C/min}$ ,  $25$  to  $50\text{ }^{\circ}\text{C}$ ,  $\omega = 1\text{ rad/s}$ ). The strain amplitude,  $\gamma = 1\%$ , was kept constant throughout the experiments.

### 3.3.5 Determination of the Mesh Size

The mesh size ( $\xi$ ) from the swelling experiments was calculated using Equations 5 and 6. The mesh size was also calculated from the rheology data using Equation 8.

### 3.3.6 Morphology Investigation of Hydrogels

Scanning electron microscopy (SEM) and environmental SEM (ESEM) measurements (Quanta FEG 400, FEI, USA) were performed to characterize the morphology of PNIPAAm hydrogel in the dried and wet states respectively. The hydrogel disks (*c.f.* Table 3.16) were fractured in liquid nitrogen ( $-196\text{ }^{\circ}\text{C}$ ). For SEM characterization, swollen hydrogels were freeze-dried (*c.f.* 3.3.2) and then sputtered with gold/palladium (Sputter Coater, Emitech, UK). The hydrogel cross-section was observed under standard SEM vacuum conditions. For ESEM measurement, the fractured swollen hydrogels were characterized without further preparation. The ESEM chamber was pre-set at  $2\text{ }^{\circ}\text{C}$  with a vapour pressure 4.0 Torr and relative humidity at 85 %.

## 3.4 Functional Characterization of Hydrogels

### 3.4.1 Partitioning Test for Non-ionic Hydrogels

A swollen hydrogel disk of 100-200 mg was incubated in 10 ml test solution (Table 3.7) for 3 days on a shaker at 20 °C. The concentrations of test solutes in the solution and in the gel after equilibration were measured using TOC analyzer or using a UV-VIS spectrometer. The partitioning coefficient was determined from Equation 9. The data was an average of three measurements.

### 3.4.2 Sorption Experiments for Molecular-Imprinted and Non-Imprinted Hydrogels

#### 3.4.2.1 Rebinding Tests with Template-Protein

All rebinding tests were performed for fully swollen hydrogels (mass of dried gels ~ 10 mg) and repeated for three times. For obtaining an equilibrated sorption, the experiment was done for at least 3 days.

*Effect of template-binding monomer content.* The rebinding test was performed at constant lysozyme concentration (10 ml, 0.5 g/l in tris-HCl buffer). The MIP and NIP hydrogels with various MAA content were incubated in the template protein solution at room temperature (RT,  $23 \pm 2$  °C) and placed on a shaker. The binding was monitored from the decrease of lysozyme UV absorbance signal at 280 nm using a UV-VIS spectrometer.

*Sorption isotherm.* For sorption isotherm test, hydrogels with 2 wt% MAA content (M'02) were equilibrated in various lysozyme concentrations (initial concentration range 0 to 5 g/l) on a shaker at RT. Analogous protocol as above to determine the amount of lysozyme bound to the samples was employed.

*Effect of temperature.* The hydrogel samples (M'02) were equilibrated in a solution of 0.5 g/l lysozyme in tris-HCl buffer. The experiments were performed on a shaker at temperatures below or above or in the vicinity of the LCST of PNIPAAm. Analysis of the amount of bound protein was done as described above.

#### 3.4.2.2 Rebinding Tests with Competitive-Protein

To determine the selectivity of MIP hydrogel to lysozyme, experiments were carried out for the samples (M'02) in 10 ml of a protein mixture at RT under shaking condition. This protein solution consisted of equimass amounts of lysozyme and cytochrome C (total concentration 0.5 g /l). After the equilibrium sorption was reached, the remaining protein in the solution were measured using UV-VIS spectrometry at 280 nm and 408 nm, corresponding to the absorbance of total protein (considering their individual absorbance coefficients) and cytochrome C, respectively.

### 3.4.3 Ion-Sensitivity Test for Poly(*N*-Isopropylacrylamide-*co*-4-vinylbenzo-18-crown-6) Hydrogels

The ion-containing solutions were prepared by dissolving nitrate salts; either  $\text{NaNO}_3$ ,  $\text{KNO}_3$  or  $\text{Ba}(\text{NO}_3)_2$  (0.002 or 0.02 M) in deionized water. The hydrogel disks were placed in the corresponding salt solution at 37 °C for 24 h. After this incubation, the samples were dried for another 24 h in a vacuum oven at 60 °C. Ion-sensitivity test was analyzed gravimetrically analogous to swelling experiment in 3.3.3. The measurement was repeated for three times.

## 3.5 Functionalization of Membranes

Membrane functionalizations was performed using an UVA print system, equipped with a UVA print lamp to realize illumination wavelengths  $> 300$  nm. By using either a glass petri dish (60 x 15 mm<sup>2</sup>) and a filter paper (for prefunctionalization step; *c.f.* Figure 3.4) or a glass plate (50 x 70 mm<sup>2</sup>) and the plastic bag (for pore-filling step) on top of the membranes (*c.f.* Figures 3.5 and 3.6), the UV intensity had been reduced to 8-15 mW/cm<sup>2</sup> (measured with a UVA meter, Hoenle AG, Germany).

### 3.5.1 Prefunctionalization via Grafting-From Photoinitiator Adsorption Method

The PET membranes were first soaked in 50 mM benzophenone in ethanol/water (10:1) as a base solvent for 60 min. After this pre-adsorption of photoinitiator, membranes were rinsed with base solvent and immersed in solutions with various concentrations of NIPAAm in water (5 ml; 1 to 10 wt %) up to 2 min. Thereafter, UV irradiation took place for 15 min. Conditions and details for this step were adopted from previous work in our group<sup>[32, 43]</sup>. The prefunctionalized membranes were washed and characterized before further pore-filling functionalization. The prefunctionalization step is illustrated in Figure 3.4.

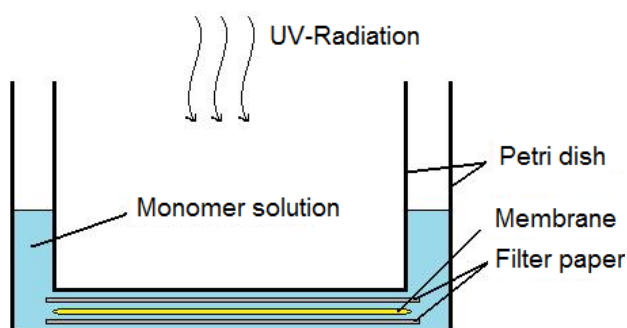
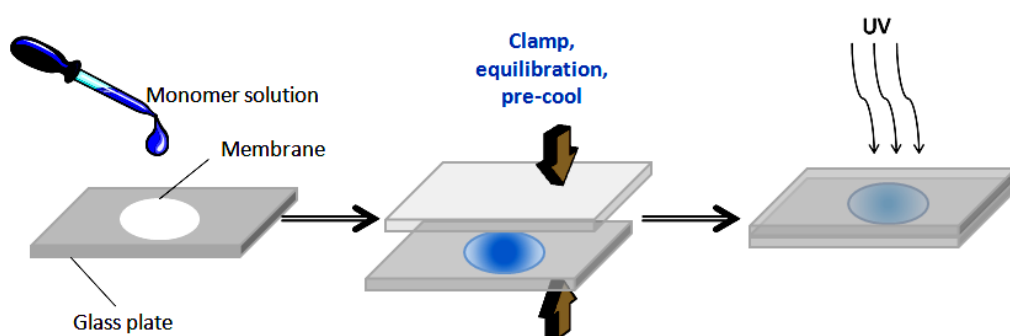


Figure 3.4 Illustration of prefunctionalization experimental set-up via *grafting-from*.

### 3.5.2 Pore-Filling Functionalization

*'Open' pore-filling.* An aqueous reaction mixture of the same composition as used in the bulk gel preparation (M15DC05; PI 2 wt% relative to NIPAAm) was prepared. A non-prefunctionalized PET membrane was laid down on a glass plate and the monomer solution was dropped with an excess onto it (Figure 3.5). Another similar glass plate was placed on top of the wetted membrane, tightly clamped from four corners and allowed to equilibrate for 10 min at 4 °C. The membrane samples were then subjected to UV irradiation for 15 min. The membranes were removed from the glass plates and washed in Milli-Q water for several hours and then stored in an aqueous  $\text{NaN}_3$  solution.



**Figure 3.5** Illustration of 'open' pore-filling functionalization steps. The membrane was equilibrated with the monomer solution between 2 glass plates and then subjected to UV irradiation.

*'Closed' pore-filling.* The non-prefunctionalized or prefunctionalized PET membranes were equilibrated in an excess of standard precursor solution (M15DC05; PI 2 wt% relative to NIPAAm) in a plastic bag (50 x 70 mm<sup>2</sup>, polyethylene) for 5 min at 4 °C (Figure 3.6). Then, the extra solution (or air bubbles) was squeezed from the bag before it was sealed and clamped between two glass plates and placed for another 10 minutes equilibration time at 4 °C. Thereafter, the samples were irradiated for various times (5-20 min). Pore-filling in a closed equilibration scheme was also carried out for various reaction mixtures (*c.f.* Table 3.3b) and UV irradiation for 15 min. The membranes were removed from the plastic bag and washed and stored similar to above conditions.

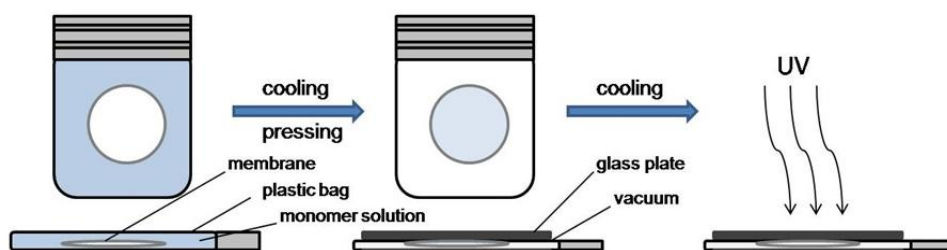


**Figure 3.6** Illustration of 'closed' pore-filling functionalization steps. The membrane equilibrated with the monomer solution was sealed in a plastic bag, pressed between 2 glass plates and then subjected to UV irradiation.

### 3.5.3 Degree of Functionalization

The degree of functionalization (DOF) for the composite membranes (after prefunctionalization and after pore-filling) was determined gravimetrically and calculated based on the mass difference before and after the respective functionalization per outer surface area of the membrane [ $\mu\text{g}/\text{cm}^2$ ].

### 3.5.4 Scanning Electron Microscopy

The membranes were freeze-dried and sputtered with gold/palladium using a K 550 sputter coater (Emitech, U.K.). The surface morphology was then observed using SEM (Quanta 400 FEG, FEI, USA) at standard vacuum conditions.

## 3.6 Functional Characterization of Base, Prefunctionalized and Pore-Filled Composite Membranes

### 3.6.1 Water Permeability

The volumetric flow through the base, prefunctionalized and pore-filled composite membranes were measured using Amicon filtration cells with 1.77 or 12.6  $\text{cm}^2$  effective membrane area (model 8003 or 8050, Millipore, USA). The data for base and prefunctionalized membranes were collected by adjusting the height of the connected reservoir (hydrostatic pressure; 0.03 bar). For HPFCM, pressure from a nitrogen tank was used (0.5 - 1 bar). The measurements were carried out at RT. The permeabilities,  $L_p$  were calculated by dividing the water flux to the transmembrane pressure (TMP, for water flux; *c.f.* Figure 2.15).

$$L_p = \frac{J}{\Delta P} \text{ ..... Equation 26}$$

The resulting permeability data was used to study (i) the pore characteristics of the membranes, and (ii) the properties of grafted polymer chains, for both using the Hagen-Poiseuille equation <sup>[32, 43]</sup>, or (iii) to estimate the microstructure of gels in HPFCM using the Darcy model (Figure 2.15).

### 3.6.1.1 Determination of Hydrodynamic Layer Thickness

The hydrodynamic layer thickness is corresponding to the thickness of the grafted polymer layer on the pore walls,  $l_h$ . Assuming a uniform prefunctionalization has taken place, the layer was determined from the Equation 27:

$$l_h = \frac{d_{p,0} - d_{pref}}{2} \quad \text{Equation 27}$$

where  $d_{p,0}$  and  $d_{pref}$  are the pore diameters of the unmodified and the prefunctionalized membranes respectively. The pore radius was calculated using the formula deduced from the Hagen-Poiseuille equation in Figure 2.15.

### 3.6.1.2 Determination of Darcy Void-Spacing

Darcy void-spacing,  $\sqrt{k_{mem}}$ , is a measure of hydrodynamic screening length between the polymer chains forming the gel network [34, 35]. By definition, the Darcy void-spacing and the mesh size of a gel are equal. This parameter was determined from the square root of Darcy permeability;  $k_{mem}$ , that described the flow through a porous membrane whose pores were filled with polymer network as shown in Figure 2.15. The model is only valid on the condition that the gel is isotropic and the mesh size is significantly smaller than the membrane pore diameter.

### 3.6.1.3 Permporometry

The pore size distributions were analyzed using gas flow / liquid displacement permporometry with a capillary flow porometer (Porous Materials, Inc., NY, USA) *via* the “Dry up / Wet up” method [32, 43]. The membrane samples were 25 mm in diameter. Data in the first step was related to the gas flow through the dry membrane. In the second step, the instrument recorded data for wetted membrane (wetting liquid; 1,1,2,3,3,3-hexafluoropropene, “Galwick”, PMI, surface tension of 16 dyn.cm<sup>-1</sup>). The software deduced the pore size distribution from the comparison between the dried and wetted membrane data. The membrane pore diameter was determined from pore distribution with the maximum number pore count. The maximum TMP for the air flow measurements was 5 bar.

### 3.6.2 Stability Tests

The stability of PNIPAAm hydrogels within the PET porous support was investigated as a function of TMP at RT. The tested membrane was mounted on a stirred Amicon 8003 or 8050 cell. The water permeability was measured by increasing pressure from a nitrogen tank stepwise; 40 min at each stage up to 4 bar (*c.f.* Equation 26). The measurement at low pressure (0.05 bar) was repeated to determine the flux recovery as well as to deduce whether the hydrogel remained in the membrane after high pressure evaluation. The measurement was carried out in the Amicon cell (model 8003 or 8050).

### 3.6.3 Switchability Tests

Permeation experiments were performed at RT and 45 °C; the latter adjusted with a thermostat (Julabo, Seelbach, Germany) to study the switching effect of the composite membranes. The data was collected under a pressure of 0.5 bar; pressurized using pure nitrogen. The membrane temperature was changed stepwise, and each step was maintained for 20 min. The filtration was started at least 5 min after the temperature of the feed solution reached the target temperature and the permeability was calculated using Equation 26. During the measurement, the cell and permeating solution were kept in a thermostat water bath, to maintain the temperature. To determine the reversibility of the switching, the measurement was conducted for several cycles. The degree of switching for HPFCM was investigated as function of compositions. The switchability tests were also carried out in the Amicon cell (model 8003 or 8050).

### 3.6.4 Size-Selectivity Tests *via* Convective Fractionation of Solute

The same filtration setup and conditions in as in 3.6.1 were also used to carry out UF measurements. This was done using an equimass mixture of two dextrans with average molecular weights of 4 and 2000 kg/mol at a total concentration of 1 g/l (*c.f.* Figure 3.2 in 3.1.3). The compositions of the feed ( $c_F$ ) and the permeate ( $c_P$ ) were analyzed using HP-GPC and TOC. The rejection; either for overall rejection (from TOC) or for construction of sieving curves (from GPC) was calculated using Equation 28.

$$Rejection = (1 - c_P/c_F) \cdot 100 [\%] \dots \dots \dots \text{Equation 28}$$

The measurements were carried out at RT and 45 °C.

### 3.6.5 Size-Selectivity Tests *via* Solute Diffusion

Diffusion measurements were performed to determine the rate of diffusion through the corresponding membranes (effective diffusion coefficient) and the solute fractionation under these conditions. This measurement was carried out using a diffusion cell which was composed of two half-cells. The membrane was fixed between these half-cells with the membrane side which had been exposed to UV light in the feed direction. The two half cells were filled at the same time to the same height level with receiving solution (0.01 M NaN<sub>3</sub>; 127 ml) and feed solution (10 g/l equimass mixture of dextrans with average molecular weight of 4 and 2000 kg/mol in 0.01 M NaN<sub>3</sub>; 135 ml) and stirred at the same stirring rate. The diffusion of dextran through the membrane was monitored by measuring the concentrations using TOC in both half-cells at certain times for up to 24 hours (control experiments were also done for up to a week). Based on the HP-GPC analysis, the amounts of diffused or not diffused solute through membrane could be determined as function of their molecular weight. The effective diffusion coefficient,  $D$ , was calculated from the amount of material,  $\Delta N$ , transported across the effective membrane area,  $A_{eff}$ , and its thickness,  $\Delta x$ , in various time intervals for diffusion,  $\Delta t$  and considering the actual concentration difference,  $\Delta c$ , between the two half-cells using Equation 29.

$$D = \frac{\Delta N \cdot \Delta x}{\Delta t \cdot A_{eff} \cdot \Delta c} \text{ ..... Equation 29}$$

$D$  was calculated from the average of the data collected over up to 24 h.



## CHAPTER 4

### RESULTS AND DISCUSSION

#### 4.1 Poly(*N*-isopropylacrylamide) Bulk Hydrogels

PNIPAAm hydrogels were synthesized by copolymerizing NIPAAm and MBAAm. The polymerization proceeds through polyaddition reaction initiated either *via* redox- (*c.f.* 4.1.1) or photopolymerization (*c.f.* 4.1.2).

##### 4.1.1 Redox-Polymerization

A simplified mechanism of redox-initiation polymerization is given in Scheme 1 (*c.f.* 2.1.1). The polymerization involves free radical-generating system using APS and TEMED. The preliminary studies were firstly carried out in order to optimize the synthesis conditions. This was followed by rheological online of monitoring polymerization and characterization of resulting hydrogels based on established conditions.

##### 4.1.1.1 Hydrogel washing and calculation of conversion

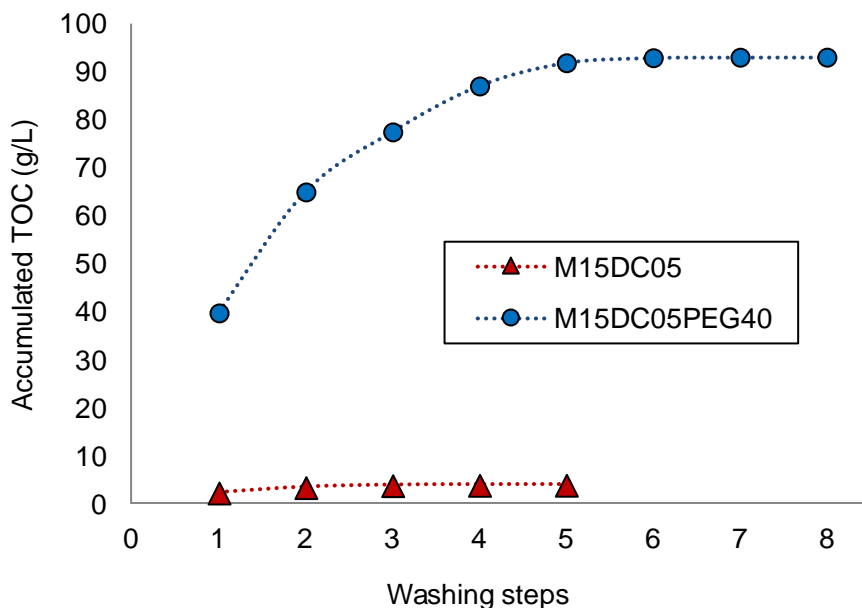
After the synthesis, all hydrogels were washed (for every 24 h in each washing step; *c.f.* 3.3.1) in order to elute unreacted monomers (as well as porogen). The mass of leached carbon into the washing water were monitored from TOC measurement. From this measurement, not only the number of washing step can be estimated, but most importantly the degree of monomer conversion can be determined from the mass balance. The degree of monomer conversion was calculated based on the fraction of leached carbon using Equations 22 to 25.

Figure 4.1 shows accumulated mass of leached carbon (TOC) from washing of two hydrogels; i.e. conventional hydrogel (M15DC05) and PEG-modified hydrogel (M15DC05PEG40). These hydrogels were obtained prior to optimization procedure. The washing steps were regarded as completed when no significant changes of the TOC values between two consecutive washings can be detectable (< 2.0 %). From Figure 4.1, it can be seen that the extraction of these residues had been completed after 5 to 8 washing steps. 0.386 g of carbon were washed out from the conventional hydrogel. The theoretical carbon content of this hydrogel were 4.979 g (*c.f.* Table 4.1). This gave rise to a conversion of 92.2 % (Table 4.2).

PEG-modified hydrogel (M15DC05PEG40) contained very high residues of carbon (9.311 g) compared to conventional hydrogel (Figure 4.1). The fact that PEG was not consumed during reaction (*c.f.* 2.2.2)<sup>[18]</sup>, two assumptions can be made. First, the theoretical carbon content of PEG-modified hydrogel is analogous to that of conventional hydrogel (*c.f.* Table 4.1). And second, it can therefore be claimed that the PEG had been completely leached from the hydrogel since their corresponding mass of carbon (7.74 g) was smaller than the total mass of carbon leached (9.311 g). The remaining 1.571 g carbon residual of the unreacted monomers gave rise to a conversion of 68.4 % (Table 4.2). Both conventional and PEG-modified PNIPAAm hydrogels can be easily synthesized. However, the existence of PEG influences the conversion of PNIPAAm hydrogel (*c.f.* 4.1.1.3.3).

**Table 4.1** Theoretical carbon content calculated from composition in Table 3.2.

Hydrogel	Mass of C in NIPAAm [g]	Mass of C in MBAAm [g]	Mass of C in PEG 400 [g]	Total C in hydrogel [g]
M15DC05	4.775	0.204	0	4.979
M15DC05PEG40	4.775	0.204	7.74	4.979



**Figure 4.1** Sum of the washed carbon per washing step in PNIPAAm hydrogels with and without PEG as a porogen. The monomer was not recrystallized prior to the synthesis. The argon deaeration step was omitted during the preparation of hydrogels. The polymerization was performed for 24 h, at 15 °C using TEMED/APS 4.0 : 1.

**Table 4.2 Conversion to PNIPAAm hydrogels in water prepared with and without PEG. The conversion was calculated from the theoretical carbon content (Table 4.1) and the residues of carbon in the washing water (TOC) from Figure 4.1.**

Hydrogels	Conversion [%]
M15DC05	92.2
M15DC05PEG40	68.4

In order to increase the degree of monomer conversion, hydrogels were prepared under various optimization procedures. High degree of monomer conversion is very important due to several factors. Theoretically, the accuracy of network quantification depends on the high monomer conversion. Secondly, high conversion will ensure the mechanical stability of hydrogels for certain application (i.e., separation media; *c.f.* [33, 62]). As shown in Table 4.3, hydrogels obtained under argon condition and using recrystallized monomer have improved the overall conversion.

It can be seen that monomer purification alone has a significant influence on the conversion. NIPAAm monomer from the manufacturer is typically stabilized from self-polymerization. Therefore, elimination of the stabilizing agent through recrystallization of the monomer results in an increase of conversion. The data in Table 4.3 also suggested that it is necessary to perform the polymerization under argon condition. Without deaeration step, a certain amount of oxygen may be presented in the reaction solution that can inhibit polymerization and influence the degree of monomer conversion.

**Table 4.3 Conversion (TOC) of PNIPAAm hydrogels (M15DC05) prepared under various optimization procedure. Other conditions *c.f.* Figure 4.1.**

Samples	Conversion [%]
Preparation without argon deaeration step using not recrystallized monomer	92.2
Preparation with argon deaeration step using not recrystallized monomer	94.6
Preparation without argon deaeration step using recrystallized monomer	95.3
Preparation with argon deaeration step using recrystallized monomer	96.3

## 4.1.1.2 Optimization of accelerator to initiator ratio

The final properties of hydrogels can be greatly influenced by the way their initiation triggers the polymerization. First, it was investigated whether the initiator ratio TEMED/APS can be manipulated to achieve desired hydrogel properties in a kinetically-controlled manner. This would mean that polymerization should be accompanied with some lag period (time before onset of gelation) allowing equilibration to take place before reaction will occur *in situ*. The standard ratio of TEMED to APS reported in the literature was 4.0 : 1 [14, 15, 180, 181]. The ratio of TEMED to APS should be reduced and their influence towards gelation of PNIPAAm should be investigated.

As shown in Figure 4.2, the gelation occurred almost instantaneously (< 1 min) with the highest TEMED/APS ratio (4.0 : 1). Here, the gelation time was recorded as the reaction mixture became turbid by visual inspection (the conversion was determined after 24 h of total polymerization time). Increasing TEMED/APS ratio decreased the gelation time. Indeed it has already been reported in the literature that TEMED promoted decomposition of APS into free radicals, and hence accelerated the polymerization and crosslinking reaction. NIPAAm and MBAAm with -C=C- bond are susceptible towards free radical attacks. Controlling the formation of starter radicals therefore delayed the onset of the polymerization and decelerated their overall rate. Interestingly, reducing the TEMED/APS ratio from 4.0 : 1 to 0.1 : 1 did not affect the monomer conversion significantly. Nevertheless, without TEMED, only a very slow gelation was observed (after 17 h) with relatively very low conversion (~ 70 %). These data suggested that proper tuning of TEMED/APS ratio away from extreme values offers the possibility to fabricate the hydrogels *in situ* in a controllable manner.

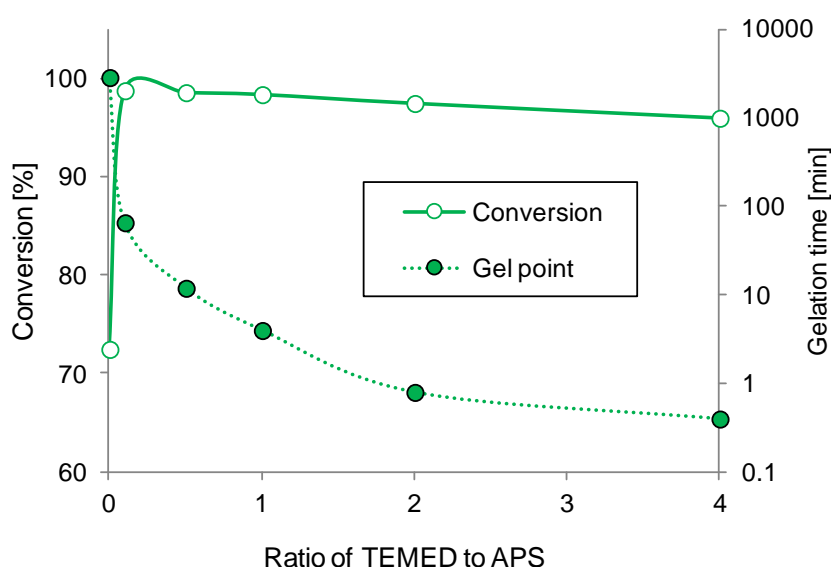


**Figure 4.2** Influence of TEMED to APS ratio towards gelation of hydrogels with 15 wt% NIPAAm and 5 wt% MBAAm (M15DC05). From here the polymerization was performed under Argon conditions and using recrystallized monomer. Other conditions *c.f.* Figure 4.1.

### 4.1.1.3 Physical properties of redox hydrogels

Hydrogels synthesized with various parameters affected the resulting properties. Physical properties of these hydrogels are summarized in Tables 4.4 to 4.6.

#### 4.1.1.3.1 Effect of crosslinker

Regardless of their degree of crosslinking, hydrogels were obtained with sufficiently high conversion (Table 4.4). These hydrogels are typically transparent associated to the homogeneity of the hydrogel network. However, an increase in turbidity was observed for the hydrogel with the highest content of crosslinker (M15DC10). The slightly turbidity may indicate that the level of network heterogeneity increased. These heterogeneities have been associated to the microphase separation arisen from concentration fluctuations during the course of reaction that are “frozen” in the final network [59, 182].

A strong scattering at small angle from highly crosslinked PAAm and PNIPAAm gels was already observed by Hecht et al.<sup>[182]</sup> and Suzuki et al.<sup>[183]</sup> respectively. It had been explained by considering large clusters of crosslinks which are randomly distributed over the network<sup>[184]</sup>. The heterogeneity can also be induced by the fact that crosslinkers are more reactive than NIPAAm monomers. Thus for highly crosslinked hydrogel system, formation of MBAAm (crosslinker) aggregates are more favoured. Due to aggregation of crosslinkers, the extensive cyclization and branching took place leading to rather compact clusters connected with shorter polymer chains. The formation of compact clusters causes a decrease in polymer-solvent compatibility. All these effects are known to give rise to microphase separation during crosslinking copolymerization.

**Table 4.4 Physical properties of PNIPAAm hydrogels synthesized with various crosslinker content. Hydrogels were obtained using initiator TEMED/APS 4.0 : 1. Other conditions *c.f.* Figure 4.1.**

Hydrogel Composition	Conversion [%]	Appearance	Designation
M15DC02	96.4	Transparent	Conventional
M15DC05	96.3	Transparent	Conventional
M15DC10	94.1	Cloudy	Conventional

#### 4.1.1.3.2 Effect of synthesis temperature

In order to investigate the effect of synthesis temperature on physical properties of PNIPAAm hydrogels, gels were prepared below and above the LCST of PNIPAAm from the same composition mixture. As shown in Table 4.5, hydrogels changed its appearance from transparent to opaque upon polymerization above its LCST. Analogously, this observation can be associated to heterogeneity of the network.

On one hand, increasing temperature increased the rate of transfer reaction during polymerization. Since the rate of the transfer reaction increased, additional crosslinking may occur during polymerization that induced the phase separation<sup>[40]</sup>. Gelation process is highly exothermic. On the other hand, with increasing temperature, the solubility of the propagating PNIPAAm chains is reduced as a result of increasing hydrophobicity<sup>[87, 93]</sup>.

In comparison, the hydrogel obtained above LCST has only slightly lower conversion. Note that the synthesis temperature has almost no significant effect on the degree of monomer conversion.

**Table 4.5 Physical properties of PNIPAAm hydrogels synthesized at different temperature. Hydrogels were obtained using initiator TEMED/APS 4.0 : 1. Other conditions *c.f.* Figure 4.1.**

Hydrogel Composition	Reaction Temperature [°C]	Conversion [%]	Appearance	Designation
M15DC05	15	96.3	Transparent	Conventional
M15DC05	40	95.6	Opaque	Macroporous

#### 4.1.1.3.3 Effect of solvent/porogen

Some physical properties of conventional and PEG-modified PNIPAAm hydrogels synthesized in this study are summarized in Table 4.6. First, it can be seen that increasing content of PEG had resulting to a decrease in the overall monomer conversion. Correspondingly, a continuous increase in the fraction of molecules with high molecular weight has imposed unfavourable interactions (co-nonsolvency; *c.f.*<sup>[16]</sup>) between polymer chains and other species in the reaction mixture<sup>[14, 16-18]</sup>. This has therefore created the competition between the gelation and the segregation of polymer chains in the length scale of developed two-phase domains<sup>[103]</sup>.

Hydrogels prepared with PEG content < 20 wt% were transparent, whereas those prepared with PEG content > 20 wt% were opaque (Table 4.6 and Figure 4.3)<sup>[18]</sup>. At a very low PEG content (< 20 wt%), a phase separation occurred at local neighbouring chains only, therefore the macroscopic appearance of the hydrogel would still be unaffected (Table 4.6). A further increase of PEG content (> 20 wt%)

imposed inhomogeneities which are fixed in the entire macromolecular network. Analogous to the degree of monomer conversion, this observation indicates that a phase separation had taken place for higher porogen threshold content. The threshold content of porogen depended on the molecular weight; being lower for higher molecular weight <sup>[18]</sup>. Note that heterogeneous hydrogels can also be obtained *via* thermally induced phase separation (*c.f.* 4.1.1.3.2). However PEG-modified hydrogels in this study were synthesized below the LCST (15 °C). Thus it was unlikely that the phase separation observed within these hydrogels was induced thermally.

It is also known that PNIPAAm chains dissolve well in water. However, PNIPAAm chains may collapse and precipitate from the water/PEG polymerization mixture. This was due to: i) hydration of PEG molecules; and ii) volume exclusion of PEG molecules that lead to polymer-polymer poor domains. The addition of PEG could act as porogens <sup>[14, 18]</sup>; pore-forming or space filling agents that prevent polymerization in specific locations through physical hindrances <sup>[185]</sup>. Thus, hydrogels with larger pores were formed and they were opaque due to scattering of lights from its separated phase <sup>[104]</sup>. These hydrogels had been regarded as macroporous gels.

**Table 4.6** Physical properties of PNIPAAm hydrogels (M15DC05) synthesized with various PEG content. Hydrogels were obtained using initiator TEMED/APS 4.0 : 1. Other conditions *c.f.* Figure 4.1.

Hydrogel Composition	Conversion [%]	Appearance	Designation
PEG0	96.3	Transparent	Conventional
PEG10	83.4	Transparent	Conventional
PEG20	75.9	Opaque	Macroporous
PEG40	72.4	Opaque	Macroporous

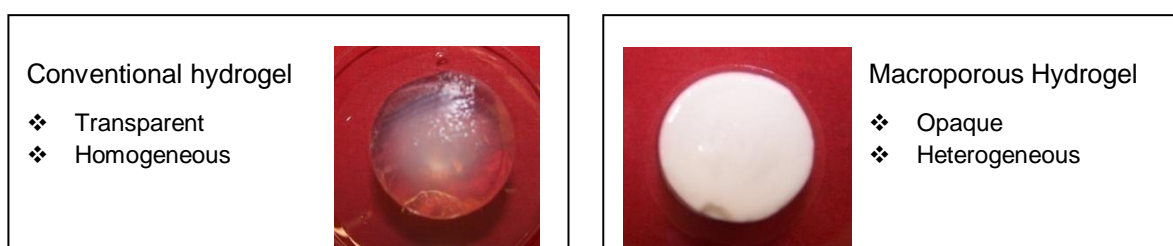


**Figure 4.3** Photograph showing the appearance of hydrogels obtained without PEG (PEG0, left-hand side) or with PEG (PEG40, right-hand side)

## 4.1.1.4 Rheology

For on line rheological study of *in situ* polymerization the same reaction mixture as in bulk (M15DC05) was used. Both viscous ( $G''$ , liquid-like) and elastic ( $G'$ , solid-like) responses were recorded at 15 °C under oscillating mode ( $\omega = 10$  rad/s,  $\gamma = 0.01$  %).

## 4.1.1.4.1 Gelation point and reproducibility of gelation

Figure 4.4 reveals a typical evolution of gelation (example with TEMED/APS 0.5 : 1) plotted in semi-logarithmic scale, revealing a polymerization process for which three different phases can be identified. Those phases are representing the lag period where the system responded as viscous liquid ( $G' < G''$ ), followed by the onset of gelation ( $G' = G''$ , at ca. 400 min) and a sudden rise of modulus attributed to the transformation from liquid- into a solid-like gel ( $G' > G''$ ) and a period where this increase levelled off with further increasing polymerization time. The curves from triplicate measurements could be very well reproduced under the same conditions.

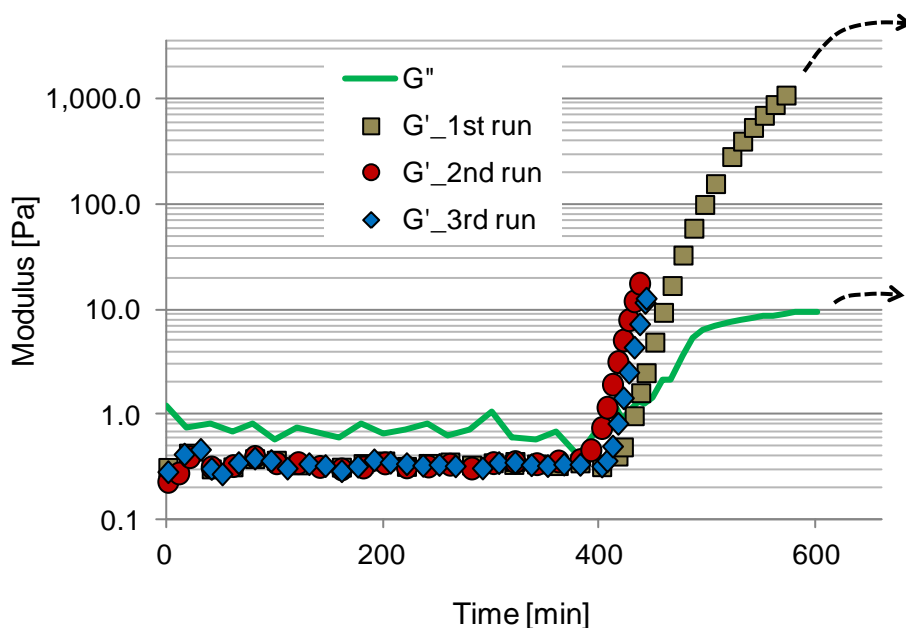


**Figure 4.4** Gelation point (cross-over between  $G'$  and  $G''$ ) and reproducibility of the online rheological monitoring. *In situ* polymerization toward PNIPAAm hydrogels was performed using initiator TEMED/APS 0.5 : 1. Other conditions were as for bulk gels (*c.f.* Figure 4.1). Arrows indicate the further development of storage and loss moduli (in first run).



#### 4.1.1.4.2 Influence of accelerator to initiator ratio

The redox polymerization of NIPAAm was further monitored with respect to oscillating rheometry response at a longer reaction time as shown in Figure 4.5. As can be seen, the kinetics of the gelation process was significantly affected by varying the TEMED/APS ratio. At a higher initiator ratio, onset of gelation occurred almost without any delay followed by relatively steep evolution of the storage modulus  $G'$ . In contrast, at a lower ratio, a relatively slow increase of  $G'$  after a longer lag period was observed. This was obviously due to slower polymerization, i.e., the influence of TEMED/APS ratio visually observed for the polymerization in bulk (*c.f.* Figure 4.2) affected the *in situ* rheometry data in a similar way.

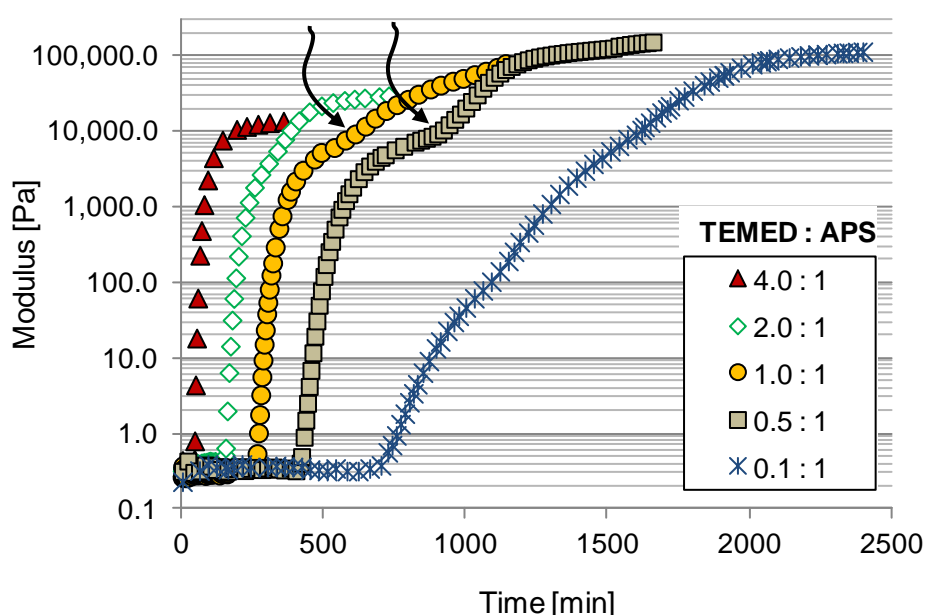


**Figure 4.5** *In situ* polymerization toward PNIPAAm hydrogels with variation in TEMED/APS ratio (arrows indicate acceleration of  $G'$  due to "gel-effect"). Other conditions were as for bulk gels (*c.f.* Figure 4.1)

These results were again associated with faster decomposition rate of initiator into starter radicals caused by increasing fraction of TEMED, and that ultimately increased overall rate of gelation. One consequence of too fast (uncontrolled) gelation is the so called "gel-effect" or "Tromsdorff effect", represented by an acceleration of the  $G'$  vs. time curve (*c.f.* Figure 4.5). With increasing degree of monomer conversion, an increase in viscosity imposed hindrance to the further growth of polymer chains. This effect can yield inhomogeneous distribution of polymer fraction in hydrogels. In addition, the polymerization *via* redox initiation is "auto-triggered"; variation of TEMED/APS ratio can only lag the gelation but full control on the entire polymerization cannot be exerted (*c.f.* <sup>[186]</sup>).

## 4.1.1.5 Equilibrium swelling degree and mesh size

The swelling degree was determined in a range of 15 to 45 °C based on the average value of three measurements using Equation 1.

In all cases, the swelling degree of all PNIPAAm hydrogels decreased as the temperature increases (Figure 4.6). A sharp transition in the swelling degree between 30 and 35 °C was seen. This is a classical swelling behaviour of PNIPAAm hydrogels. At temperatures below LCST, the PNIPAAm hydrogels showed the water-swollen property because of the hydrogen-bonding interactions between the water and hydrophilic amide groups of the polymer. At a temperature near or greater than LCST, the intrinsic affinity of PNIPAAm polymer chains for themselves was enhanced because of the thermal dissociation of hydrating water molecules from the polymer chains<sup>[15]</sup>. Hydrophobic interactions between the isopropyl pendant groups increased, and the water is pushed out from the network. As a result, the PNIPAAm chains collapsed above its LCST. Data also shows that the PNIPAAm hydrogels in this case exhibited LCST in the range which is in agreement with findings of others<sup>[14-16, 18, 40, 41]</sup>.

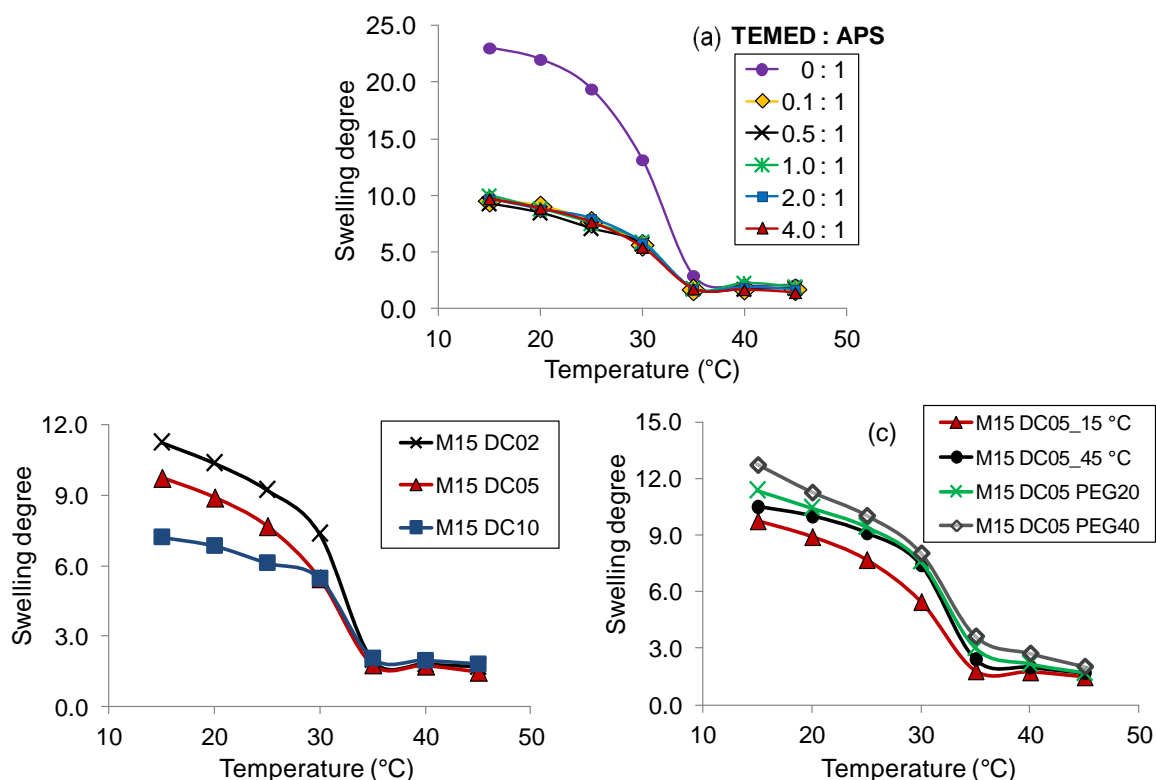


**Figure 4.6** Equilibrium swelling degree of PNIPAAm hydrogels as a function of temperature: (a) influence of TEMED/APS ratio (M15DC05); (b) influence of crosslinker content (TEMED/APS 4.0 : 1); and (c) conventional vs. macroporous PNIPAAm hydrogels (macroporous hydrogels were prepared either above LCST or using PEG as a porogen, TEMED/APS 4.0 : 1).

The swelling degree was firstly studied for hydrogels prepared with various TEMED/APS ratios (Figure 4.6a). The temperature-responsive behaviour of hydrogels could therefore be confirmed from the swelling experiment. Apart from the preparation without TEMED, all other hydrogels from similar compositions had similar swelling degree. Obviously, this deviation emerged from the fraction of unpolymerized monomer; a hydrogel obtained with lower polymer fraction would swell to a greater extent. It is therefore clear that the reduced TEMED/APS ratio (but not to zero) did not compromise the swelling properties, i.e., the microstructure of the hydrogel, but only lengthened the lag period of gelation (*c.f.* 4.1.1.2).

The influence of varying crosslinker content on the swelling degree of PNIPAAm hydrogels is shown in Figure 4.6b. These hydrogels were obtained using initiator TEMED/APS 4.0 : 1. Note that the LCST of PNIPAAm was virtually not affected by the degree of crosslinking. Nevertheless, the swelling degree decreased as the crosslinker content was increased. This is due to the fact that an increase in degree of crosslinking results in formation of hydrogels with denser network. Analogously, this has led to the reduction of mesh size, which in turn, reduced the water holding capacity and thus lowered the swelling degree <sup>[16]</sup>. There was no noticeable influence of crosslinker content on the swelling degree of PNIPAAm hydrogels at a temperature above their LCST. This could imply that regardless the degree of crosslinking, all PNIPAAm hydrogels collapsed into a similar degree of deswelling.

The swelling behaviour of conventional and macroporous or phase-separated hydrogels are given in Figure 4.6c. Below the LCST, macroporous hydrogels swelled to the larger extent than their conventional counterpart. Macroporous hydrogels are heterogeneous; they contain permanent macropores and numerous number of small channels; thus more water would reside <sup>[16]</sup>. Even at temperatures above LCST, the deswelling states of macroporous hydrogels were considerably different than the conventional hydrogel (Figure 4.6c). This could be a fraction of pores filled with water may still exist within macroporous hydrogels. It was also discovered from Figure 4.6c that the hydrogel prepared above LCST (M15DC05\_40°C) and PEG-modified hydrogel (M15DC05PEG20) revealed similar swelling degree. This could indicate that these hydrogels were obtained with the same level of heterogeneity. It is most likely the macroporous network generated either *via* PIPS or TIPS under those specified conditions could lead into a similar macroporous structure. The precipitation of PNIPAAm chains might be similar to the extent that the unfavourable interactions of PEG in the reaction mixture during PIPS increasing hydrophobicity at an increased reaction temperature during TIPS. Analogous to the previous work, the addition of PEG to the reaction mixture had no significant influence on LCST <sup>[14]</sup>.

From the swelling experiment, the mesh sizes were calculated based on Peppas et al. <sup>[68]</sup> and Fänger et al. <sup>[14]</sup> using Equations 5 and 6. The calculations were done for all hydrogel samples at 20 and 45 °C and given in Table 4.7. In all cases, the mesh size of a given hydrogel which essentially depends on the swelling behaviour is larger at 20 °C (swollen state) than that at 45 °C (collapsed state).

It was observed that the degree of crosslinking had a significant influence on the mesh size. Hydrogel with higher degree of crosslinking has relatively shorter distance between two crosslinking points ( $r$ )<sup>[16]</sup>; i.e. 3.4, 3.0 and 1.5 nm for hydrogels M15DC02, M15DC05 and M15DC10 respectively. Accordingly, mesh sizes of these hydrogels in their swollen state decreased strongly; from about 7 nm to almost 3 nm with increasing crosslinker content from 2 to 10 wt% (Table 4.7). Even though these hydrogels revealed a similar degree of deswelling above LCST (Figure 4.6b), a significant difference in their corresponding mesh sizes can still be observed (Table 4.7). Besides swelling degree, the  $r$  value was one of the basic parameter for the estimation of the mesh size (*c.f.* Equation 3). Hence, the variation in mesh sizes was attributed to the difference in  $r$  values.

The effect of PEG content onto mesh size was also pronounced. The mesh size was found to be apparently higher for the series of heterogeneous hydrogel as compared to conventional hydrogel from the same composition (M15DC05). Indeed, the heterogeneous and macroporous morphology of these hydrogels were attributed to the phase separation induced during polymerization (*c.f.* 4.1.1.3.3).

Moreover, the mesh size of conventional hydrogel (M15DC05) obtained from polymerization using initiators with mass ratio 0 : 1 was significantly larger than that with mass ratio 4 : 1. The initiation system without TEMED resulted in an extremely slow reaction and thus may impose higher rate of termination reaction than the rate of growing polymer chains (*c.f.* 4.1.1.2) that reduced the degree of crosslinking.

**Table 4.7** Mesh sizes of all PNIPAAm hydrogels (conventional; i.e. various crosslinker content vs. macroporous; i.e. hydrogels prepared above LCST or using PEG as a porogen calculated from swelling at 20 and 45 °C.

Hydrogel Composition	$\xi$ (20 °C) [nm]	$\xi$ (45 °C) [nm]
<b>TEMED/APS 0 : 1</b>		
<u>Conventional</u>		
M15DC05	8.5	3.9
<b>TEMED/APS 4.0 : 1</b>		
<u>Conventional</u>		
M15DC02	7.3	4.1
M15DC05	6.0	3.4
M15DC10	2.9	2.0
<u>Macroporous</u>		
M15DC05_40 °C	6.5	3.6
M15DC05PEG20	6.6	3.6
M15DC05PEG40	6.7	3.8

### 4.1.2 Photopolymerization

In this section, PNIPAAm hydrogels were obtained *via* photopolymerization as an alternative to chemically-initiated polymerization. The photopolymerization was performed far below the LCST; i.e. at 4 °C. The NIPAAm monomers were photocrosslinked with MBAAm *via* free radical copolymerization using Irgacure-2959® as a PI (photopolymerization mechanism; *c.f.* Scheme 2). First, a systematic investigation on kinetics and optimization of photopolymerization was established (*c.f.* 3.2.2.1, 3.2.2.2 and 4.1.2.2). These data were utilized to synthesize various compositions of bulk PNIPAAm hydrogels (*c.f.* 4.1.2.3) as well as for *in situ* fabrication of PNIPAAm hydrogel within membrane support (*c.f.* 4.6).

#### 4.1.2.1 Kinetics of photoinitiator

Preliminary experiments were performed in order to get information on the kinetics of PI. A solution containing only PI was exposed to UV light at various predetermined time until no observable changes in the UV absorbance can be detectable. The UV absorbance after each irradiation is given in Table 3.11.

As seen from this table, there are two main observations that should be emphasized. First, the absorbance of reactant species decreases with increasing irradiation time. Irgacure-2959® is a benzoin derivative PI. Benzoin derivatives undergo photochemical  $\alpha$  cleavage (Norrish type I photolysis) to form an  $\alpha$ -substituted benzoyl radical pair (*c.f.* Step 1 in Scheme 2) <sup>[187]</sup>. When the PI solution is exposed to UV, the number of radicals formed is consistent with the decomposition of the initiator itself. The decay of these radicals is often the major pathway for the direct conversion of starter radicals to non-radical products in the PI solution and therefore reduced the UV absorbance. The determination of PI concentration from 3.2.2.1 implied that the concentration of PI decayed with time (Table 3.11).

Secondly, it was observed that a further irradiation than 900 s imposed no significant change in UV absorbance of the PI. This could indicate that the PI had been fully decomposed. Since PI is a small chromophore-containing compound, the threshold absorbance can still be observed (Table 3.11). Hence, correction in concentration of PI must be made by assuming the concentration of reactant species corresponding to the threshold absorbance is zero.

The order of reaction can be determined from the kinetic plot. Thus, based on integrated rate equations (*c.f.* Table 3.12) the kinetic plots were constructed for zero-, first- and second-order, respectively (Figure 4.7). The overall first order of reaction was observed after taking into account the corrected value of concentration (Figure 4.7). The first order reaction is also typical for PI which undergoes unimolecular decomposition <sup>[173]</sup>. The reaction-rate constant can be straightforwardly determined from the slope;  $0.006 \text{ s}^{-1}$ . The half-life ( $t_{1/2}$ ; *c.f.* Table 3.12) is related to the decomposition rate constant by  $\ln(2)/k$

(115 s). The results from this preliminary experiment were used as guideline for choosing the photopolymerization conditions of PNIPAAm hydrogel.

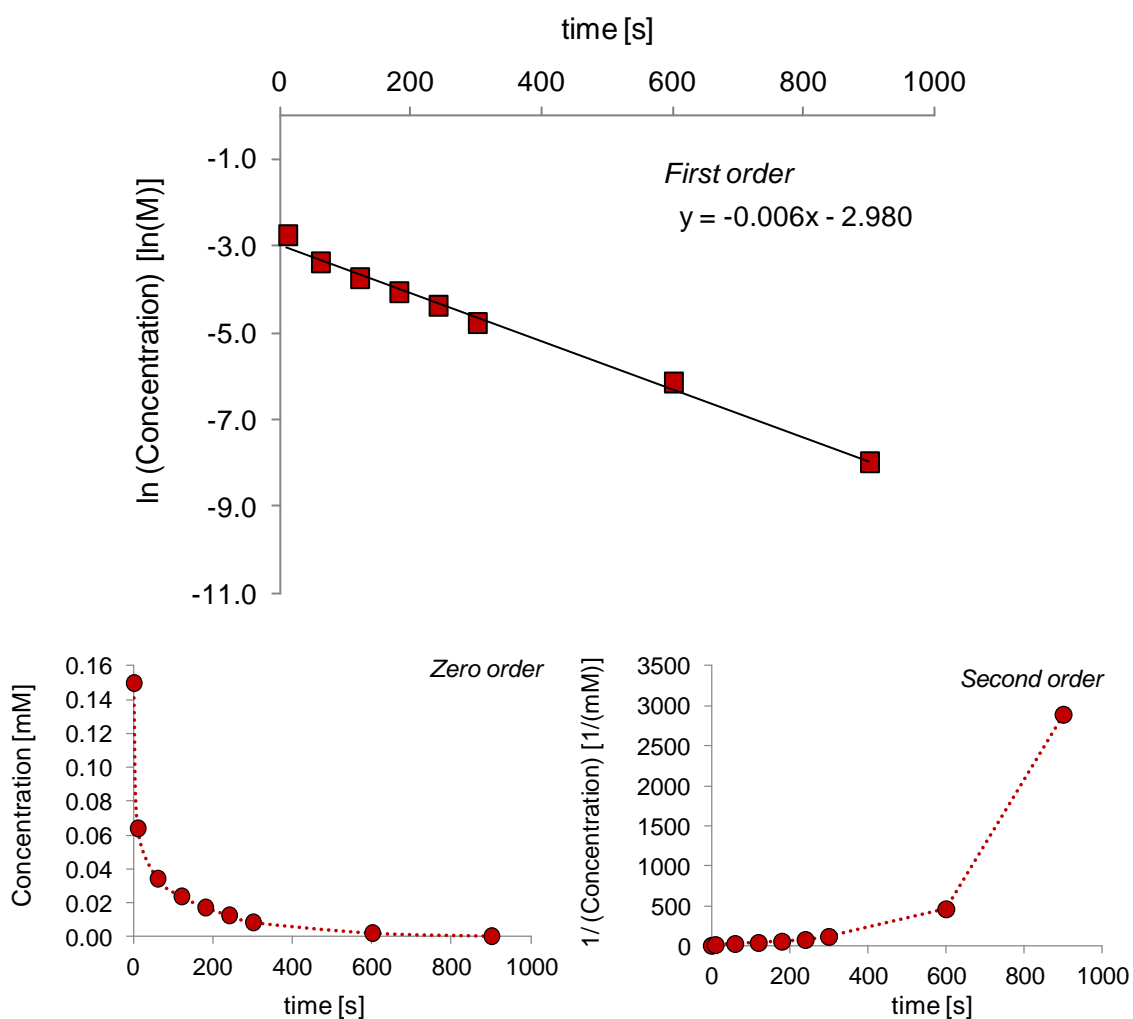


**Figure 4.7** The kinetic plots of photoinitiator Irgacure-2959® fit the first reaction order.

#### 4.1.2.2 Optimization of photopolymerization conditions

With regard to successful photopolymerization of hydrogels, two important parameters are of most concern, irradiation time and PI concentration. In that respect, an adequate amount of PI concentration to form starter radicals at appropriate rate throughout the complete volume of gel precursor is desired.

##### 4.1.2.2.1 Effect of photoinitiator concentration

Preliminarily, the PNIPAAm hydrogels were prepared using the PI concentration from 1 to 5 wt %. This was the recommended range of use from the manufacturer (*c.f.* <sup>[188]</sup>).

As shown in Figure 4.8, a very high and almost complete conversion of monomer to hydrogel was achieved with PI concentration of 2 wt%. Polymerization with too low concentration of PI (1 wt %) imposed the risk of incomplete conversion; there was much non-reacted monomer, and the polymerization was slowed down. Increasing the concentration of PI too much resulted apparently in a decrease of average polymer chain length and even reduced the degree of monomer conversion (PI concentration > 2 wt %) since the probability for termination *via* recombination was significantly increased. In addition, too much radicals end up in the gels, reduced the gels purity and apparent decrease in gel elasticity was observed. As PI decreases less light is absorbed in unit volumes within the film, resulting in slower curing rates. These opposing factors generally result in an optimum PI concentration in through-curing process<sup>[173]</sup>.

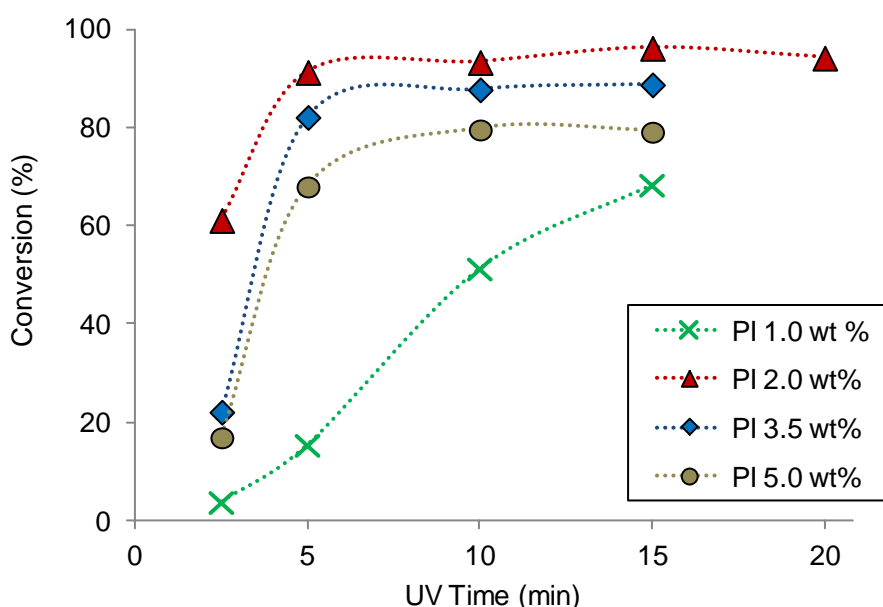


**Figure 4.8** Influence of PI concentration and UV time toward conversion (TOC) of PNIPAAm hydrogels (M15DC05). The polymerization was performed at 4 °C.

#### 4.1.2.2.2 Effect of UV irradiation time

The data from the kinetics of PI was employed to obtain the conditions of photopolymerization; i.e., the necessary irradiation time. Since the  $t_{1/2}$  was 1.9 min, the precursor monomer solutions were irradiated from 2.5 to 20 min.

From Figure 4.8, degree of monomer conversion increased with increasing UV time, until a plateau value was reached. It can also be seen that the plateau could be reached in a shorter or much delayed time depending on PI concentration (*c.f.* 4.1.2.2.1). Incomplete conversion may result from too short irradiation time (Figure 4.8); more than 60 % of the sample remains as solution when irradiated less

than 5 min. Regardless of given PI concentration range, the UV irradiation at 20 min resulted in yellowing of the hydrogel (Figure 4.9) and the hydrogel became more brittle. These data also suggest that the risk of over-curing may increase if the irradiation will be performed longer than 15 min.



**Figure 4.9** Photograph showing the appearance of hydrogels (M15DC05) obtained with 2 wt% of PI, irradiated 15.0 (left) and 20 min (right).

#### 4.1.2.3 Conversion and physical properties of various compositions of photopolymerized hydrogels

After the optimization step, the photopolymerization parameters were set. The bulk PNIPAAm hydrogels were photopolymerized using 2 wt% PI and 15 min irradiation at 4 °C. Physical properties as a function of composition are listed in Table 4.8.

**Table 4.8** Conversion from TOC and physical properties of PNIPAAm hydrogels synthesized with various compositions. Hydrogels were obtained using 2 wt% of PI concentration and 15 min UV time at 4 °C.

Hydrogel Composition	Conversion [%]	Appearance	Designation	Shape Features
<b>M7.5DC05</b>	94.5	Transparent	Conventional	Rather weak
<b>M10DC05</b>	94.9	Transparent	Conventional	Elastic
M15 <b>DC02</b>	96.3	Transparent	Conventional	Elastic
M15 <b>DC05</b>	96.3	Transparent	Conventional	Elastic
M15 <b>DC10</b>	94.3	Cloudy	Conventional	Rigid
M15DC05 <b>PEG40</b>	76.0	Opaque	Macroporous	Sponge-like



Synthesis conditions had been established so that for all compositions in water almost complete monomer conversion (> 94 %) was achieved. The conversion was evaluated by means of TOC analysis of washing water similar to 4.1.1.1. Here, also five washing steps were necessary to completely leach out the residual monomer. It can be seen from Table 4.8 that no clear trend can be deduced whether the conversion depended from the monomer or crosslinker content.

Furthermore, the mechanical properties of these hydrogels also depend on their compositions (Table 4.8). Hydrogels are known to have soft-rubbery elastic behaviour <sup>[1, 60, 189]</sup>. On one hand, due to high crosslinking content, it can therefore be expected an increase in mechanical stability, which is reflected in the form of a rigid gel. On the other hand, reducing the monomer content; i.e., to 7.5 %, contributes to a slight weakening of the stability.

The physical appearance of synthesized hydrogel as a function of its compositions is shown in Figure 4.10. Conventional hydrogels have typically a transparent appearance that is closely related to the homogeneity of the network. In case of hydrogel with high crosslinker content, it appeared to be cloudy. Since the heterogeneity increases with a high crosslinking, this will cause turbidity through light scattering (please see the details discussion in 4.1.1.3.1).



**Figure 4.10** Photograph showing the conventional hydrogel (left; M15DC05) as well as the influence of crosslinker (middle; M15DC10) and porogen content (right; M15DC05PEG40) on the appearance of hydrogels.

As can be seen from Figure 4.10, the physical properties of macroporous hydrogel with a PEG ratio of 40 % differ significantly from those of conventional gels. Similar to macroporous hydrogels obtained *via* redox polymerization, the conversion was determined after seven washing step (*c.f.* 4.1.1.1). This was corresponded to a conversion of 76.0 %, which was lower than in the conventional case. Regardless redox or photopolymerization of PNIPAAm hydrogel, the addition of PEG imposed unfavourable interactions in the polymerization mixture. As a result, significant decrease in solubility has led into polymerization in two coexisting phases. The soluble compound was then removed from the phase-separated network and this gave rise to a much lower conversion. This was already comprehensively explained in 4.1.1.3.3. The resulting heterogeneous network is opaque in appearance (Figure 4.10) and has a very soft sponge-like feature (Table 4.8).

It should be noted that the synthesis of a hydrogel in a limited volume leads typically to a not equilibrated structure; only upon immersion into an excess of water the free swelling equilibrium will be reached. As shown in Table 4.9, the volume expansion factor of PNIPAAm hydrogel from the synthesis to equilibrium state was a function of its compositions. The influence of crosslinker was found to be greater than the monomer content. In this case, an increase in volume was observed; from about 33 to 76 % with decreasing crosslinker content from 2 to 5 wt%. The volume expansion was originated from the ability of a gel to swell in a thermodynamically compatible solvent; i.e. water. The difference in chemical potential is the main driving force for water uptake. Thus, when a hydrogel in its initial state is in contact with solvent molecules, it absorbs solvent until the solvent chemical potentials in the polymer phase are equivalent to that in the free solution phase. The resulting expansion of the hydrogel network therefore contributed to the overall volume expansion behaviour of the hydrogel. Since macroporous hydrogel (M15DC05PEG40) contains more water channels (*c.f.* 4.1.1.5), the penetration of water molecules has resulted into almost double of the volume. In contrast, almost no volume expansion was observed for hydrogels synthesized with the highest crosslinker content 10 wt%. For this particular hydrogel, presumably it was obtained from the condition that was not far away from its equilibrated structure; the rigidity imposed by the network was the reason of lower water uptake and the volume expansion had been much hindered.

**Table 4.9** Volume expansion factor of PNIPAAm hydrogels from the synthesis state to a equilibrium degree of swelling.

Hydrogel Composition	Volume expansion factor
<b>M10DC05</b>	1.38
M15 <u>DC02</u>	1.76
M15 <u>DC05</u>	1.33
M15 <u>DC10</u>	1.01
M15DC05 <u>PEG40</u>	2.05

#### 4.1.2.4 Rheology

A series of *in situ* rheology photopolymerizations at 4 °C was performed as shown in Figures 4.11 - 4.15. Oscillatory parameters were kept the same as for *in situ* redox polymerizations. Systematic rheological investigations also allowed for the characterization of the viscoelastic properties of the hydrogels. The measurements were made under dynamic conditions ( $\gamma = 1\%$ ). A normal force ( $F_N = 5$  N, within linear range) was exerted in order to maintain the contact between the fully swollen hydrogel piece and the upper plate of the measuring system without squeezing it out, regardless whether the material was in its swollen or collapsed state.

##### 4.1.2.4.1 Influence of UV intensity

As the gel precursor solution was irradiated with UV, the course of reaction could be monitored from the evolution of  $G'$  ( $G''$  remained small during the entire polymerization process and is not shown). The effect of UV intensity on *in situ* gelation is shown in Figure 4.11. The UV intensities were varied between 30, 5 and 1 mW/cm<sup>2</sup>. At the highest intensity, gelation took place immediately corresponding to a very steep increase of  $G'$  until a plateau was reached within the first 2 min of irradiation. The onset of gelation was delayed at a lower UV intensity and  $G'$  gradually increased with time leading to a slightly larger end value of  $G'$ . All these observations were governed by the kinetics of gelation and a better balance between decomposition rate of PI and crosslinking reaction associated with the number of growing polymer chains; that leads to higher mechanical strength.

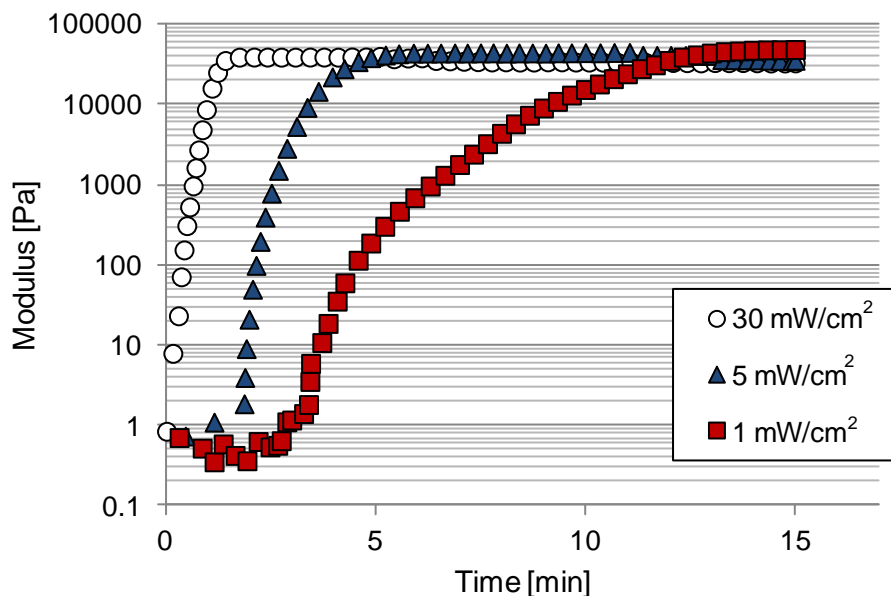


**Figure 4.11** *In situ* photopolymerization towards PNIPAAm hydrogels (UV time 15 min; hydrogel composition: M15DC05, 2 wt% PI) performed at different UV intensities. Other conditions were as for bulk gels (*c.f.* Table 4.8).

It should be noted that even though the polymerization of the bulk hydrogels had been established with an intensity of  $30 \text{ mW/cm}^2$ , it cannot be directly compared with the *in situ* measurement at the same intensity due to difference in path length of gel precursor solution. By comparing data with the reduced intensity,  $\sim 1 \text{ mW/cm}^2$ , more appropriate interpretation of the degree of monomer conversion can be inferred (here initiation had been done using  $1/30$  UV intensity in a volume with  $1/25$  UV path length, both relative to bulk conditions).

#### 4.1.2.4.2 Influence of UV irradiation time

*In situ* photopolymerization within rheometer has been done in two intervals. In the first interval (represented by filled symbols; Figure 4.12) the gel precursor solutions have been irradiated for 5, 10, 15 and 20 min at  $1 \text{ mW/cm}^2$ . In all cases, same onset of gelation was observed and overlapping progression of  $G'$  with time indicated the reproducibility of experiments under same conditions. The UV light was switched off in the second interval and  $G'$  evolution profiles were further recorded under oscillatory mode up to a total time of 20 min (represented by open symbols; Figure 4.12). Immediately after switching off UV light,  $G'$  started to level off, but with slight differences for different irradiation times.

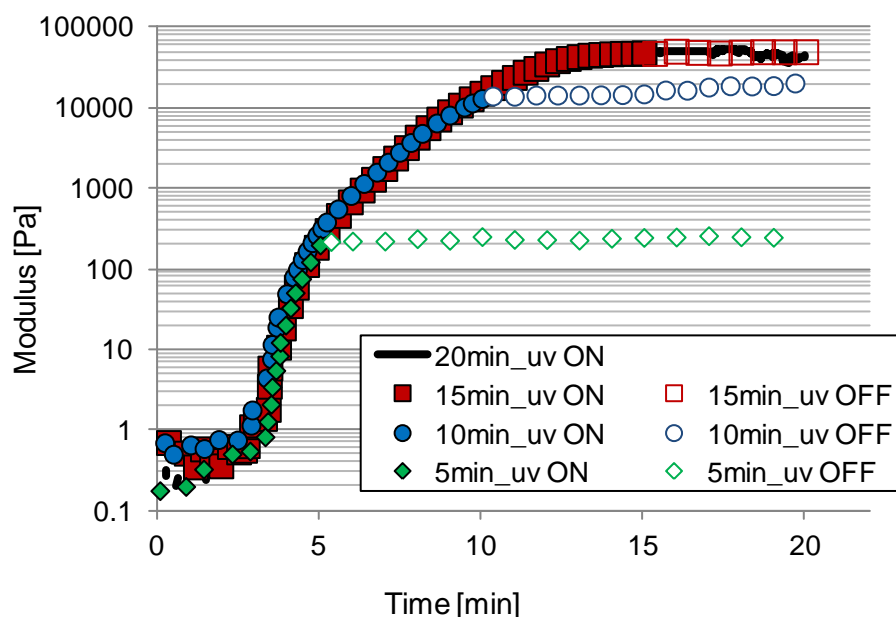


**Figure 4.12** Investigation of UV irradiation time to achieve complete reaction to crosslinked PNIPAAm hydrogel (UV time 15 min; hydrogel composition: M15DC05, 2 wt% PI). Measurement was performed at constant UV intensity of  $1 \text{ mW/cm}^2$ , and UV irradiation was kept “on” for the described time followed by another period with UV “off”.

The modulus after 5 min irradiation remained almost constant, with a very minor increase, at a corresponding low  $G'$  value. However, after 10 min irradiation, within the next minutes the modulus increased almost twofold. This can be attributed to radicals present after the switching off the UV as they may require longer time to be consumed by polymerization. On the other hand, after 15 min irradiation, as the gelation had already reached their final stage, no more changes of modulus were observed. Both evolution profiles of  $G'$ , for 15 min and 20 min irradiation, were identical. Hence, after 15 min the hydrogel had reached its ultimate microstructure. These studies demonstrate the ability to identify the optimum photopolymerization conditions and are in good agreement with data obtained from conversion of bulk gels.

#### 4.1.2.4.3 Influence of UV as a trigger of photopolymerization

The next investigation was to elucidate reactivity of the free radicals after some time intervals. The measurements consisted of two cycles of switching UV on and off that yielded four intervals in total (Figure 4.13). The first measurement; exp(1) had already been shown in Figure 4.12 and was used as reference.

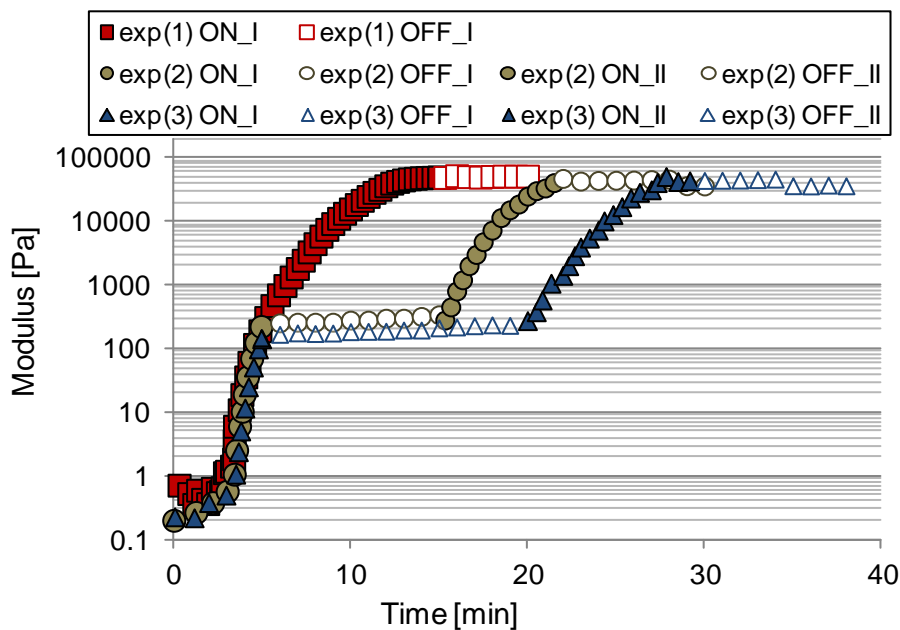


**Figure 4.13** Investigation of photopolymerization toward PNIPAAm hydrogels using interrupted UV irradiation at constant intensity of  $1 \text{ mW/cm}^2$ . Experiment 1 is a control experiment (analogous to Figure 4.12).

The reaction mixtures were irradiated for 5 min in the second and third experiments, and then measured in dark for 10 or 15 min, respectively. Slightly increased moduli ( $G' \sim 100$  to 300 Pa), similar to the effect observed in Figure 4.12, indicated the existence of left over radicals. Within the third interval where UV was on again, a further increase in  $G'$  was observed. This implied that the reaction can be re-activated upon UV irradiation as a trigger of photopolymerization since not all PI had been decomposed in the first UV interval. Because a fraction of non reacted monomer had still been present, a further increase in  $G'$  until a plateau could be well explained. And after the total net exposure time of 15 min complete conversion had been reached. That about the same level of  $G'$  had been obtained in all cases indicates that the interruption periods did not cause major changes of the hydrogel microstructure.

#### 4.1.2.4.4 Influence of monomer content

The relationship between monomer content and gelation point is shown in Figure 4.14. These data were extracted from the *in situ* rheology photopolymerization of  $G'$  and  $G''$  plot versus time analogous to Figure 4.11. The gelation time was taken as the point where  $\tan \delta = G''/G' = 1$ .

Before the onset of gelation, the period of incubation was observed. This observation is common for radical polymerization process<sup>[190-192]</sup>. Here, a high proportion of monomer has shortened the incubation period resulting for an earlier start of the reaction (< 200 s). This is due to the fact that high content of monomer increases the probability of radical attacks with monomer units directly after the initiation. Clearly, monomer content has greater influence on polymerization kinetics since the first step towards growing polymer chains involved incorporation of monomer molecules as units containing double bonds<sup>[193]</sup>. High monomer content can contribute to faster gelation kinetics *via* increasing number of active points available for crosslinking process<sup>[62]</sup>.

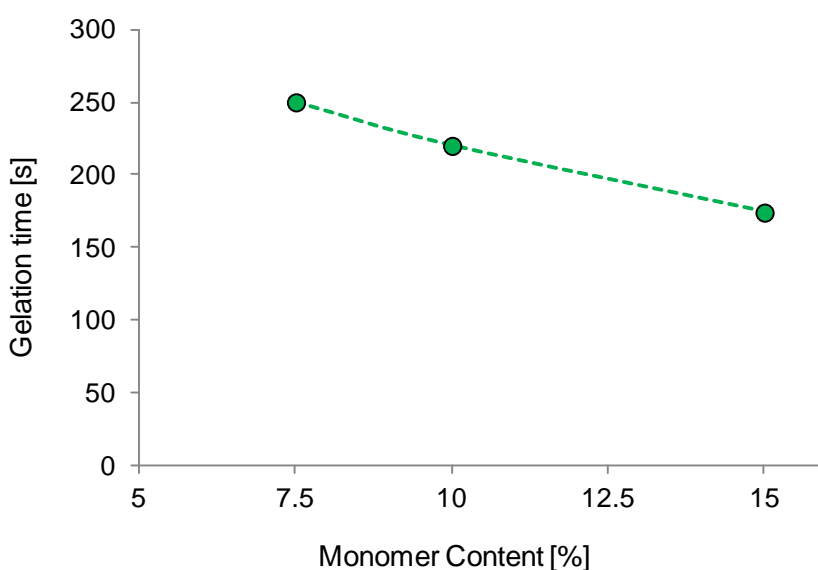


**Figure 4.14** Influence of monomer content (M\_DC05) on the onset of gelation. Measurement was performed at constant UV intensity of 1 mW/cm<sup>2</sup> (analogous to Figure 4.12).

#### 4.1.2.4.5 Influence of crosslinker content

In order to investigate the influence of crosslinker concentration, a series of experiments was performed using constant monomer composition; 15 wt% of NIPAAm and the crosslinker content had been varied from 2 to 10 wt% relative to NIPAAm.

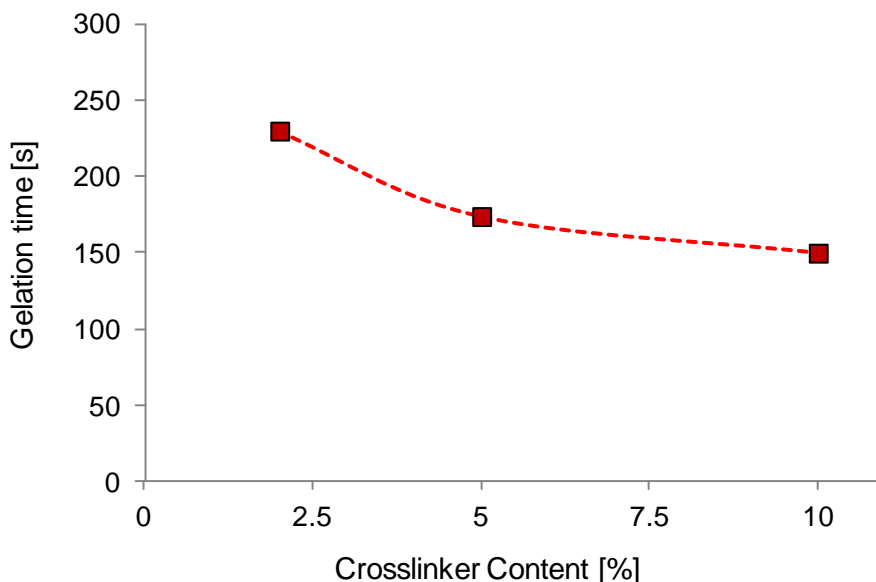


**Figure 4.15 Influence of crosslinker content (M15DC<sub>\_\_</sub>) on the onset of gelation. Measurement was performed at constant UV intensity of 1 mW/cm<sup>2</sup> (analogous to Figure 4.12).**

With respect to gelation point, similar trend was observed in Figure 4.15 as compared to Figure 4.14; earlier onset of gelation with a higher crosslinker content. This is anticipated based on the enhanced capability to form elastic junctions when additional crosslinker molecules are available for incorporation into network formation <sup>[39, 193]</sup>. A MBAAm crosslinker has two double bonds per molecule as compared to NIPAAm monomer. Thus, it was established that higher degree of functionality has led into more rapid onset of gelation. The increasing amount of monomer content can only affect their neighbouring chains *via* cyclization (intramolecular). On the other hand, high crosslinker content can impose fast kinetics on the higher level since it involved intermolecular attacks of the radical site on the pendant double bond to form a network. This could imply that a crosslinker has a more pronounced influence on the gelation kinetics than the monomer.

## 4.1.2.4.6 Temperature-responsivity

Characterization of temperature dependence of swelling and of the volume phase transition of PNIPAAm hydrogels was also attempted, using the rheometer system equipped with a temperature controlling unit. The measurement has been done under constant oscillating parameters and load from 25 to 50 °C, the range of interest to observe the LCST of the hydrogel (Figure 4.16). Three different heating rates were applied. All measurements revealed two distinct regions of  $G'$  with the lower and higher  $G'$  corresponding to hydrogel in their swollen and collapsed state, respectively. The onset of the transition between the two regions could be observed clearly in the vicinity of 33-36 °C, linked to the LCST of PNIPAAm consistent to that reported in the literature. A very pronounced increase of  $G'$  ( $\sim 1$  order of magnitude) implied that the collapse of the hydrogel networks took place and this volume reduction led into an increase in rigidity. Thus, only infinitesimal change of hydration at the molecular scale can induce a large mechanical response.

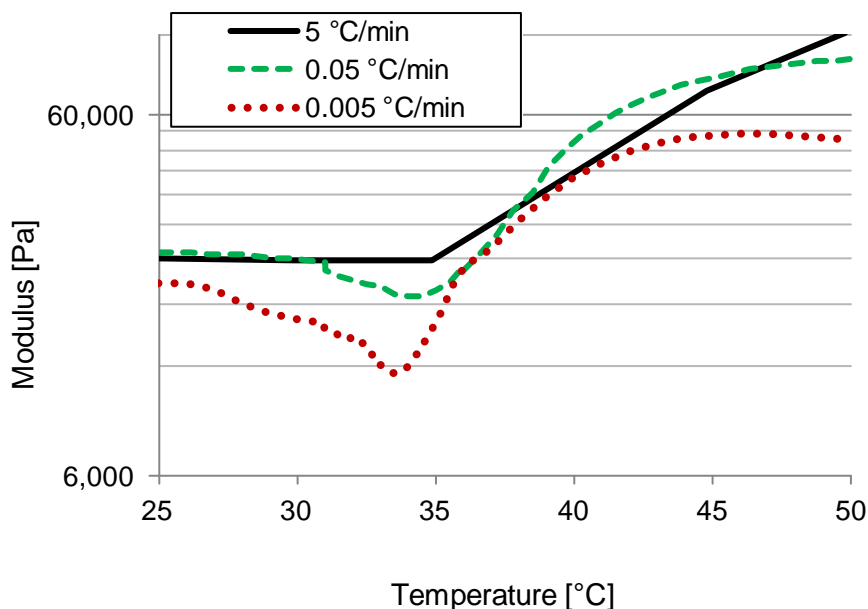


**Figure 4.16** Monitoring temperature-responsivity of PNIPAAm hydrogels (bulk gels prepared with 15 min photopolymerization,  $\omega = 1$  rad/s,  $\gamma = 1$  %,  $F_N = 5$  N) using different heating rates.

It is also observed in Figure 4.16, that apparent LCST depended on the heating rate. Fast heating rate (5 °C/min. corresponds to 5 min of measuring time) shifted apparent LCST towards higher temperature (35 °C). This heating rate was much faster than the timescales for conformational changes in and water release from the hydrogel network. This study revealed that it is also possible to characterize the temperature-responsivity of PNIPAAm hydrogels by their rheological behaviour.



#### 4.1.2.4.7 Viscoelasticity of hydrogels and their mesh sizes

A key parameter describing the hydrogel microstructure is the mesh size which could be determined from the rheological measurements. The requirement is that the hydrogels behave “ideally”. For this purpose the frequency dependence of elastic responses (represented by  $G'$ ) was recorded as shown in Figure 4.17. Note that hydrogels photopolymerized directly in the rheometer (Figures 4. 11 - 4. 15) yielded higher moduli compared to the values obtained for bulk hydrogels (Figure 4.17). This can be explained easily because the equilibrium degree of swelling cannot be achieved directly under synthesis conditions; it is only reached upon immersion into an excess of swelling agent (here water). Therefore the quantification of the microstructure was done with fully swollen bulk gels (i.e., the materials obtained from *ex situ* photopolymerization and after their swelling characterization).

In general, correlation between  $G'$  and frequency is associated with the underlying polymer relaxation that describes their conformational changes or their distinct physical states. Figure 4.17 indicates a nearly frequency independent response of  $G'$  within the frequency window from 0.1 to 100 rad/s; a range that corresponds to the rubber plateau. Hydrogels showing this behaviour can be classified as “perfect gel” enabling the estimation of their microstructure based on the theory of rubber elasticity. The gels had indeed soft rubbery-like properties ( $G' \sim 10^4$  Pa).<sup>[60, 189]</sup>

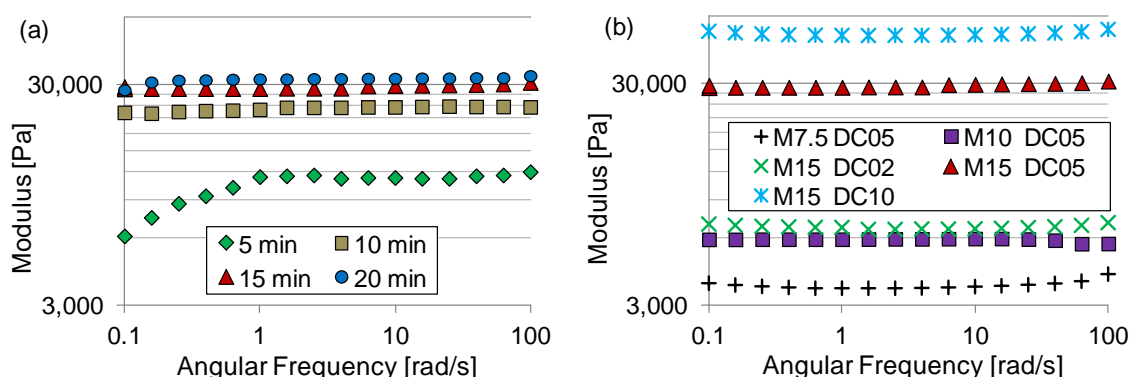


**Figure 4.17** Storage modulus at 20 °C as a function of shear frequency for PNIPAAm hydrogels (a) prepared at different UV irradiation times (hydrogel composition: M15DC05); and (b) various compositions (obtained at 15 min UV time).

The storage modulus can also be considered as a measure of the extent of hydrogel network formation. As shown in Figure 4.17a, the effect of UV time on viscoelasticity of M15DC05 PNIPAAm hydrogels was first investigated. Hydrogels obtained after 5 min UV irradiation possessed the lowest  $G'$ , and the plateau  $G'$  value increased systematically from 6000 to 35000 Pa with increasing reaction time. This can be related to the densification of the hydrogel network with increasing degree of conversion during the course of the polymerization. The further increase of  $G'$  for hydrogels obtained between 15 and 20

min was almost insignificant. This is agreement with the fact that 15 UV irradiation lead to maximum monomer conversion around 95% for such bulk hydrogels (*c.f.* Figure 4.8).

The influence of composition on the rheological properties of PNIPAAm hydrogels obtained at 15 min UV time was also explored (Figure 4.17b). The plateau value of  $G'$  increased remarkably; by one order of magnitude with increasing monomer content from 7.5 to 15 wt%. Similar trend was also observed for increasing crosslinker concentration from 2 to 10 wt% relative to NIPAAm. Obviously, an increase in monomer or crosslinker content results in formation of hydrogels with denser network<sup>[66]</sup>. From the rubber elasticity theory, the modulus in the rubbery range is related to the change in entropy. The increasing monomer and/or crosslinker contents will therefore have the same effects as an increase in stiffness or toughness of the network as a result of decrease in chain mobility. This also suggested an enhancement of mechanical properties of such hydrogels. On the other hand, the lowest  $G'$  was observed for the lowest polymer content (M7.5D05). This hydrogel is mechanically less stable and therefore less suited for sieving matrix formulations.

**Table 4.10** Calculated mesh size of PNIPAAm hydrogels prepared *via* photopolymerization from two independent experiments; (a) at varied UV time (hydrogel composition: M15DC05); and (b) various compositions (obtained at 15 min UV time).

(a)	Hydrogels	Average mesh size [nm]	
		From rheology	From swelling
	5 min	n.d.	7.2
	10 min	5.6	6.6
	15 min	5.2	6.0
	20 min	5.0	5.6

(b)	Hydrogels	Average mesh size [nm]	
		From rheology	From swelling
	M7.5DC05	10.3	11.2
	M10DC05	8.8	6.6
	M15DC02	8.5	10.9
	M15DC05	5.2	6.0
	M15DC10	4.3	4.0

The respective mesh sizes calculated from the average of  $G'$  over the frequency range using Equation 8 are listed in Table 4.10. The calculation was not performed for hydrogels after 5 min UV time since

they do not fulfil the criteria of “perfect” gels (Figure 4.17a). Otherwise mesh sizes decreased with the degree of monomer conversion. The greater  $G'$  value implied that the gel is built from shorter interconnected polymer chains, equivalent to reduced mesh size. The mesh size obtained in this work was slightly larger than that reported for PAAm gels.<sup>[62]</sup> This small deviation can be explained by the difference in the segment structure and synthesis conditions. For calculation of mesh size of various hydrogel compositions, Equation 8 may fairly be fitted for hydrogels with low monomer or crosslinker content since the plateau  $G' < 10^4$  Pa (Figure 4.17b)<sup>[66]</sup>. However, the almost independent plateau  $G'$  in the respective rubbery frequency windows has enabled the estimation of mesh size of these hydrogels in the range of about 4 to 10 nm (Table 4.10b). The bigger mesh size was obtained for relatively less dense hydrogel and vice versa. The structure-properties relationship therefore might be explained by the aforementioned microscopic properties of hydrogels.

For further verification, comparison was made with the mesh size estimated from the swelling measurements (*c.f.* 4.1.2.5) using Equation 6 (Table 4.10). The results from two independent experiments revealed a slight deviation which can be considered negligible because both estimations are based on models. Also the mode of the measurements itself, static (swelling) versus dynamic (rheology) may have an influence. Therefore, it is even more remarkable that the results including the trends as function of reaction time are very similar (Table 4.10a). This indicates that the gels are homogeneous. Analogously, the same trends were also observed as function of compositions except for M10DC05 (Table 4.10b). This discrepancy may be attributed to the nature of less dense network structure ( $G' < 10^4$  Pa) since it resembles that of a non-crosslinked polymer. It was also found that the estimation of mesh size revealed a more close approximation between the measurement from rheology and swelling for highly crosslinked hydrogels (Table 4.10b). This may indicate that the measurement is a more sensitive to characterize a perfectly elastic system<sup>[66]</sup>. Furthermore, the range of mesh size obtained suggested that this type of hydrogel can be potentially employed as a material for the fractionation of macromolecules based on their size<sup>[33, 62]</sup>.

#### 4.1.2.5 Equilibrium swelling degree as function of temperature and recovery of swelling

The temperature dependent swelling measurement of photopolymerized hydrogels was carried out based on gravimetric analysis analogous to redox hydrogels in 4.1.1.5. The data in Figure 4.18 represent the swelling behaviour of PNIPAAm hydrogels over a temperature range of 10 to 45 °C; a range which entails the expected LCST transition.

Figure 4.18 (a and b) revealed the influence of PI concentration and irradiation time on swelling degree of constant PNIPAAm hydrogels composition (M15DC05). Here, it can be seen that the swelling degree of hydrogels prepared with 2 wt % PI was higher than that prepared with 3.5 wt %. This can be simply explained in following manner; higher PI concentration will lead to more starter radical species

per mol of monomer solution. As a result, this will lead higher tendency towards photocrosslinking, and thus reduced swelling. Regardless of PI content, longer UV time imposed densification of hydrogel network and again reduced swelling. Thus, the LCST was more sharp for hydrogel after 15 min which can be associated with a higher degree of monomer conversion (Figure 4.18a). On the other hand, the influence of UV time for hydrogels prepared with 3.5 wt% PI was less pronounced (Figure 4.18b). Presumably, those influences were already compensated by the higher rigidity of hydrogel network obtained with higher amount of PI.

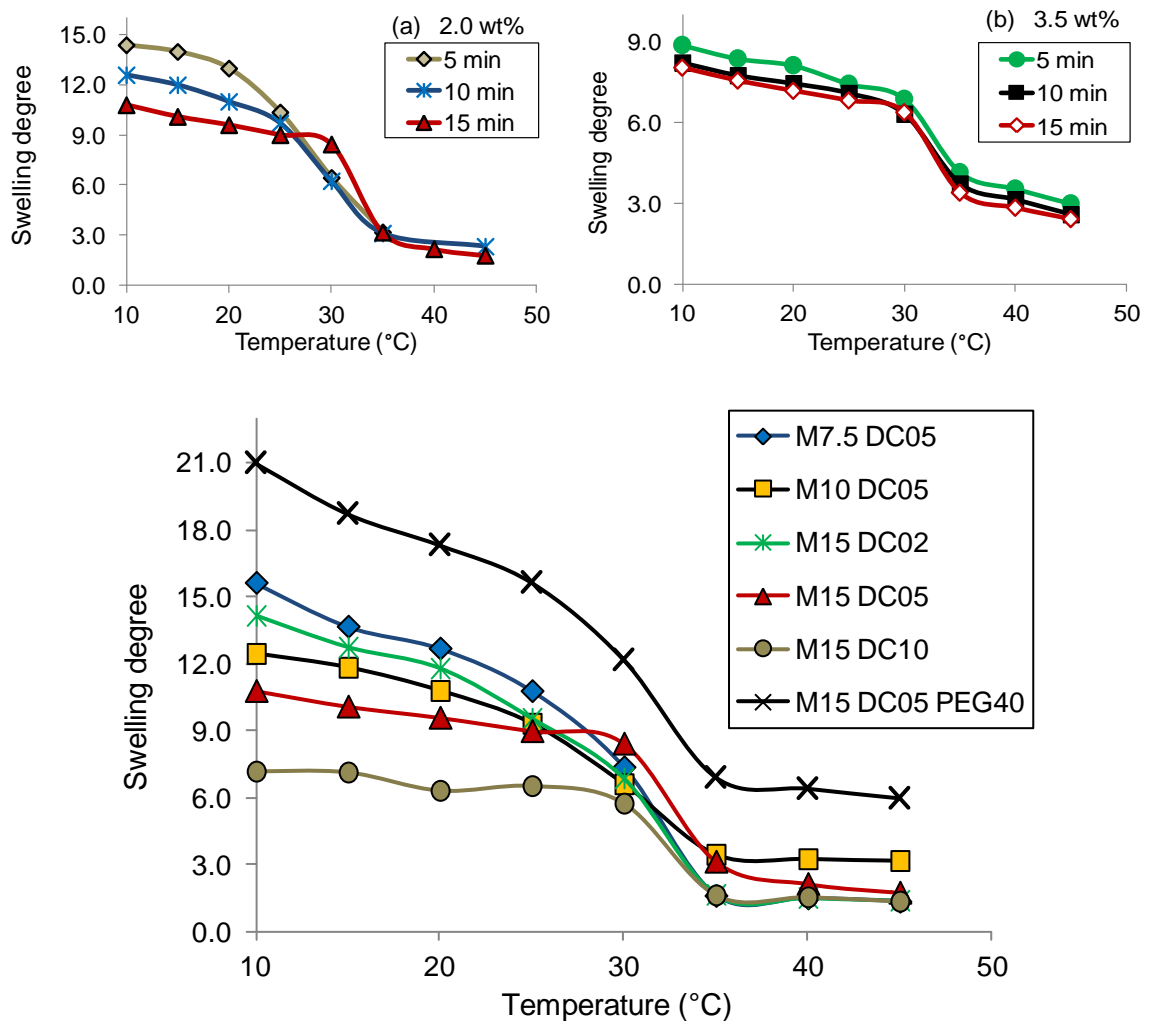


**Figure 4.18** Equilibrium swelling degree of PNIPAAm hydrogels as a function of temperature: influence of irradiation time for hydrogels obtained with (a) 2.0 and (b) 3.5 wt % PI concentration respectively (hydrogel composition: M15DC05); and (c) influence of compositions (hydrogels were obtained using 2.0 wt% PI concentration and 15 min irradiation time).

In addition, Figure 4.18c revealed that the degree of swelling depended both on the temperature and compositions. The monomer and crosslinker contents were varied from 7.5 to 15 wt% and also from 2 to 10 wt% relative to NIPAAm respectively. In case of conventional hydrogels, higher swelling was observed below the LCST for hydrogels with low monomer or crosslinker content. This can be due to the fact that high content of monomer or crosslinker increased the compactness of the hydrogel network and resulted in a mesh size reduction (*c.f.* Table 4.10b). These hydrogels collapsed above LCST, however no clear trend was observed as function of compositions similar to 4.1.1.5. When considering hydrogel composition prepared with a PEG fraction of 40 %, its degree of swelling was significantly higher; around two times higher than the corresponding composition without PEG. This was discussed in details in 4.1.1.5; such behaviour was attributed to its macroporous and heterogeneous network.

The re-swelling was performed in order to find out to what extent the hydrogel can demonstrate a memory effect on its molecular conformation level. The reversibility of swelling and deswelling of PNIPAAm hydrogels is very crucial since small recovery of swelling would limit its practical applications<sup>[36]</sup>. The re-swelling was established for the freeze-dried hydrogel samples and allowed to reach equilibrium similar to swelling conditions (*c.f.* 3.3.3). The average of re-swelling data from three measurement cycles at 20 and 45 °C are shown in Table 4.11 (hydrogel composition: M15DC05). Here, swelling and re-swelling cycles were accompanied with a slight reduction in water uptake especially for re-swelling above LCST. It was reported that the re-swelling process involved three steps: (i) water diffusion, (ii) relaxation of polymer chains, and (iii) expansion of polymer network<sup>[194]</sup>. From this process, water diffusion was the rate-determining step<sup>[195]</sup>. Thus, the water diffusion depends on the state of the polymer chain in its matrix; the re-swelling is more facilitated when the networks are in a loose form than in a aggregated globular structure<sup>[196]</sup>. Nevertheless, data in Table 4.11 suggested that the re-swelling almost completely recovers to the original level indicating that the process is reversible and governed by elasticity and flexibility characteristics of PNIPAAm networks<sup>[197]</sup>.

**Table 4.11 Recovery of swelling of photopolymerized bulk PNIPAAm hydrogel (M15DC05).**

Temperature [°C]	Swelling	Re-swelling	Recovery [%]
25	8.2 ± 0.15	8.0 ± 0.01	97 ± 2
45	1.5 ± 0.07	1.4 ± 0.03	95 ± 5

#### 4.1.2.6 Structure of hydrogels

The interior morphology of swollen freeze-dried hydrogels was analyzed using SEM. These micrographs revealed a network structure with a ‘mesh-like’ morphology that is relatively typical for hydrogels (Figure 4.19). Since the resolution limits of simple electron microscope lies within 10 nm range<sup>[155]</sup>, the mesh-like morphology observed was not the mesh of hydrogel at their molecular scale (2 to 10 nm). Instead, it is a bundle of PNIPAAm chains grouping together of a certain thickness and has been transformed into macrophase separated pores of a larger scale.

Nevertheless, hydrogels from various compositions revealed pronounced morphological differences. First, the level of irregularity increased with increasing crosslinker content. It can also be seen that the size of these pores decreased as the crosslinker content increased from 2 to 10 wt% (Figure 4.19a and b). Thus, highly crosslinked hydrogels have the larger number of pores per unit area and smaller molecular weights between crosslinking (*c.f.* 4.1.1.3.1).

The morphology of conventional hydrogels was rather compact<sup>[194]</sup>. On the contrary, PEG-modified hydrogel showed the formation of macroporous sponge-like structure with a heterogeneously distributed matrix (Figure 4.19c). The macroporous structure of M15DC05PEG40 gel was generated as a result of PIPS; the precipitation of PNIPAAm chains in PEG/water mixture was attributed to the co-nonsolvency effect<sup>[16, 40]</sup> (*c.f.* 4.1.1.3.3).

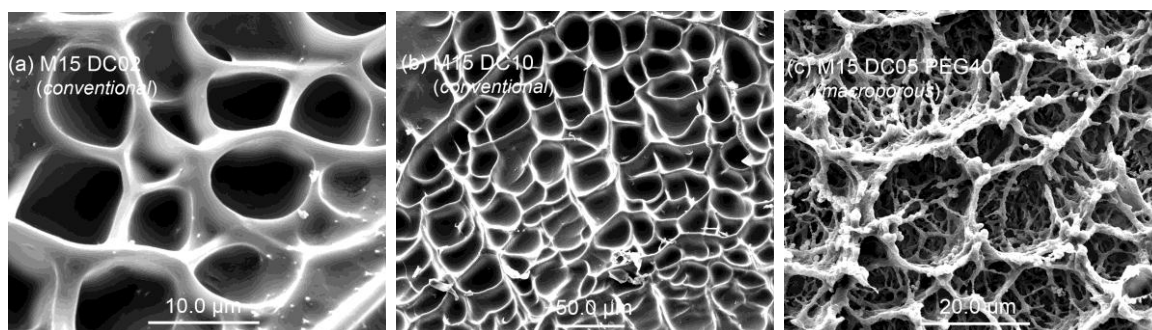


**Figure 4.19** SEM micrographs of swollen hydrogels in freeze-dried state: (a) M15DC02; (b) M15DC10; and (c) M15DC05PEG40.

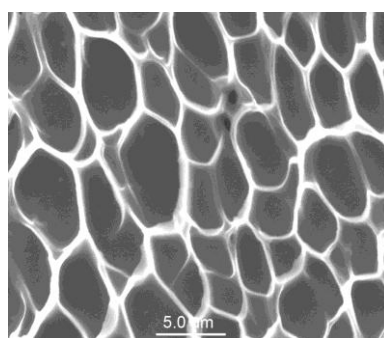


**Figure 4.20** ESEM micrograph of swollen hydrogel in a wet state (M15DC02).

Morphology investigation using ESEM enables the characterization of gels in the wet swollen state. By varying either the temperature or pressure of water vapour in the chamber, the relative humidity in the vicinity of the sample can be controlled. The ability to control the hydration state of the gels allows for correct interpretation of the measurement. The measurement in water as a medium usually reduces the resolution of micrograph. Nevertheless Figure 4.20 revealed the ESEM image with the highest resolution

On one hand, SEM technique produces higher resolution micrographs of the sample in the swollen freeze dried state (Figure 4.19). On the other hand, due to the sudden frozen-in mobility of the chain network, larger pores would be formed in the space originally occupied with water. At the beginning of the freezing process, the inner water started to crystallize and the frames of swollen polymer chains of PNIPAAm hydrogels were fixed, maintaining the original expanded state. However, as the drying continued, the water molecules were removed, polymer chains must move and their mobility is influenced by crosslinking. Subsequent drying will lead to a more porous gel matrix as given in Figure 4.19. The investigation of morphology using freeze-dried samples could lead into an overestimation of the size and the shape of the pores.

#### 4.1.2.7 Partitioning of test solutes

The microstructure of the classical photo gels was investigated from the partitioning coefficient (*c.f.* 3.4.1). The results are expressed in terms of reflection or retention coefficient,  $\sigma$ .

The classical PNIPAAm hydrogels are neutral, whereas the dextran molecules are uncharged. Therefore in the absence of electrostatic interactions between test solutes and polymer mesh, the volume exclusion took place. The mesh size of M15DC05 from swelling experiment was 6.0 nm (*c.f.* Table 4.10). As can be seen in Figure 4.21, partitioning of the test solutes in the constant mesh size was clearly a function of solute size (*c.f.* Table 3.7). The prediction of  $\sigma$  values from an empirical fit of larger solutes should in an ideal case be exactly 100 %. Figure 4.21 and Figure 4.22 show that estimation of  $K$  based on Ogston model for the solutes larger than the mesh size were indeed 100 %. The experimental data show slightly lower  $\sigma$  than the ideal case for the bigger solutes size and vice versa. This deviation can be associated to the broader size distribution of dextran comprising either larger or smaller fraction of small solute, respectively.

The partitioning of charged macromolecules; i.e., protein in the neutral gel give rise to the volume exclusion on the size basis. Figure 4.21 revealed lower reflection coefficient for lysozyme as compared to the dextran. This can be explained by the chain conformation of macromolecules; lysozyme is more compact than dextran with same MW. Overall, the  $\sigma$  values derived from estimation of  $K$  (Equation 11)

were not too far from those experimentally determined (Equation 9). This implied that the Ogston model provides good estimation for  $K$  and  $\sigma$  values.

The reflection coefficients of 4 and 2000 kg/mol dextrans in various gel compositions are shown in Figure 4.22. The estimation of  $\sigma$  based on Ogston model for larger solute than the mesh size of the gels (mesh size of hydrogels from various compositions; *c.f.* Table 4.10) gave rise to the 100 % exclusion. Hydrogels with the smallest mesh size (M15DC02) showed the highest reflection coefficient and vice versa. Indeed the partition data estimated from the Ogston model fit to the physical nature of the gel matrix and the solute quite closely.

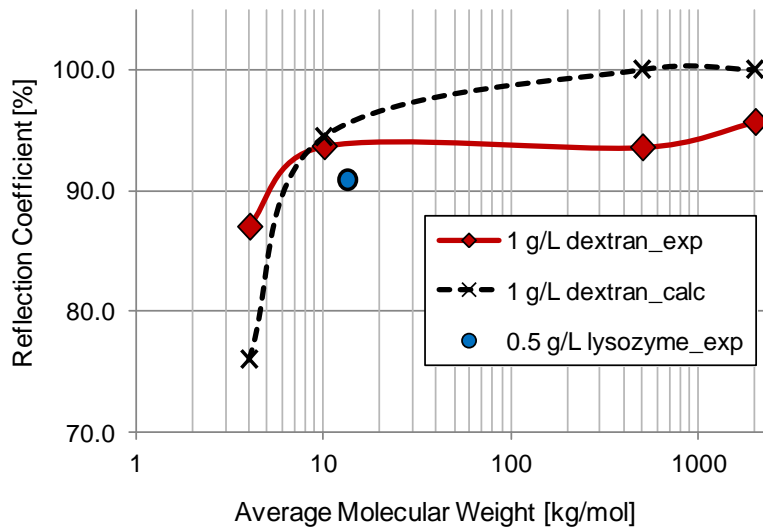


**Figure 4.21** The comparison between experimental (solid line) and calculated data (dashed-line; *c.f.* 2.1.3) of the reflection coefficient of test solutes: (i) dextran from various molecular weights, and (ii) lysozyme, in M15DC05 gel.

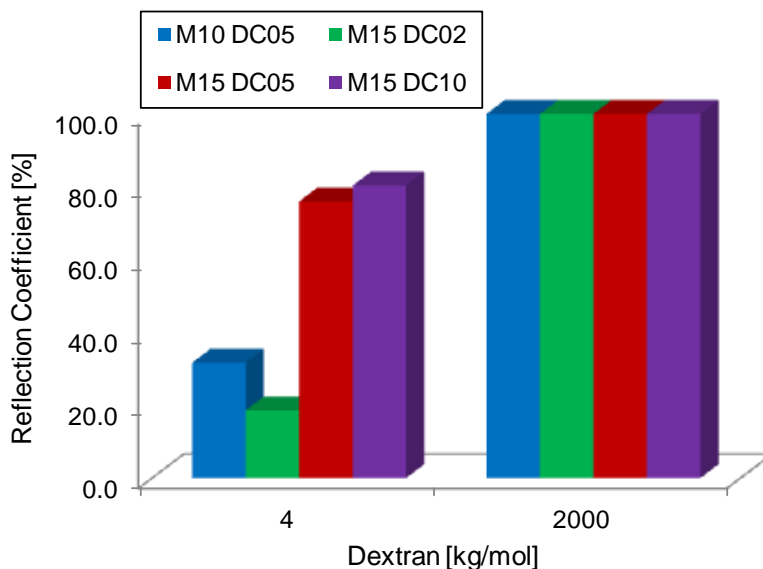


**Figure 4.22** The reflection coefficient of dextran from various gel compositions (calculated data; *c.f.* 2.1.3).



## 4.2 Molecularly Imprinted and Non-Imprinted Poly(*N*-Isopropylacrylamide) Bulk Hydrogels

The MIP and NIP hydrogels were synthesized with various MAA contents relative to the standard precursor solution (M15DC05 *c.f.* 3.2.3). The mesh size of M15DC05 hydrogel (6.0 nm; *c.f.* 4.1.2.4.7) was regarded to give an appropriate crosslinker to functional monomer ratio for lysozyme imprinting (diameter of lysozyme ~ 3 to 4 nm; *c.f.* <sup>[177]</sup>) as suggested in the literature <sup>[24]</sup>.

### 4.2.1 Rheology Investigation of Gelation Kinetics

The gelation kinetics for NIP and MIP hydrogels were investigated rheologically with respect to the variation of template-monomer content; i.e. MAA. For this purpose, the gelation point; the crossover point of storage and loss moduli ( $G' = G''$ ; *c.f.* 4.1.1.4) was recorded as shown in Figure 4.23.

In the previous subsection (4.1.2.4.4) an earlier start of the reaction for higher fraction of main monomer (NIPAAm) was observed. However, in this section, regardless NIP or MIP hydrogels, increasing the fraction of template-monomer resulted into slower gelation. At this point, this was expected result. By increasing content of MAA, the increase amount of ionic species can induce phase separation (*c.f.* <sup>[104]</sup>); thus the gelation in two phases may decelerate gelation kinetics.

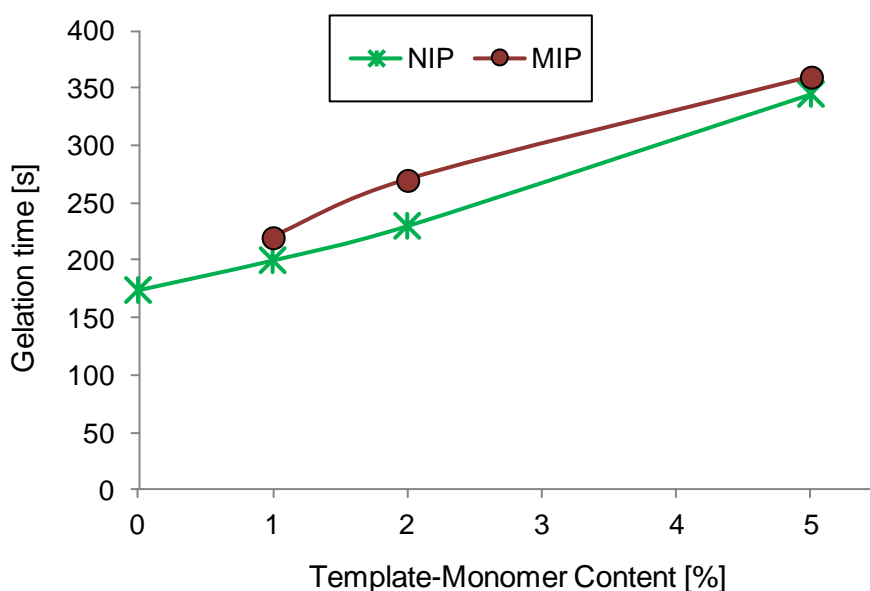


**Figure 4.23** Influence of template-monomer content on the gelation time for NIP and MIP hydrogels. Measurement was performed at constant UV intensity of 1 mW/cm<sup>2</sup> (analogous to Figure 4.12).

The *in situ* rheology experiment could also be used to monitor the influence of protein in the reaction mixture during imprinting. Figure 4.23 revealed that MIP gels have slower gelation kinetics than NIP. This suggested that the presence of the protein thereby spatially hindered the gelation which was related to the complexation of MAA and lysozyme<sup>[126]</sup>. The complexation prevents lysozyme from the attack of free radicals. This implied that the extent of copolymerization of lysozyme with monomers at a controlled kinetic could be reduced significantly. This could in principle facilitate the removal of lysozyme after the polymerization (*c.f.* 4.2.2). In addition, the difference in gelation time between NIP and MIP was found to be the largest for composition prepared with 2 % MAA. This may indicate that rendering the ionic content of the gel through the template-monomer may have an influence for the imprinting efficiency.

#### 4.2.2 Template-Protein Removal and Conversion

Template-protein removal is based on the fact that the interactions between the template and the template binding groups in the polymer can be broken by washing medium. In literature, different NaCl concentrations, usually from 0.1 to 1.0 M, were often used as washing medium. The ionic strength in the washing solution increases the efficiency of protein removal because ionic interactions between the template-protein and functional groups (here carboxylate) can be broken, but this condition might be not optimal. Figure 4.24 shows the effect of washing of both MIP and NIP hydrogels with different salt concentrations. As can be seen, washing with higher salt concentration (1.0 M) lead to shrinkage of the gels, and this was found to be irreversible. This can be associated to lowering the osmotic pressure because of reduced difference between the concentrations of counterions in the network and in the surrounding solution; the resulting aggregation of the hydrophobic network segments may not be fully reversible under aqueous conditions. Thereby, the protein may become entrapped inside the polymeric network. This may also cause negative effects on rebinding process.

The hydrogels were also washed using a lower salt concentration (0.3 M, Figure 4.24). This condition was chosen based on extended preliminary experiments. Note that hydrogels treated under those conditions maintained their integrity (Figure 4.24). Another indication that elution of template-protein took place during the washing process was that the slightly yellowish colour of MIP hydrogel obtained directly after the synthesis decreased significantly to a transparent appearance. However, this was not the case for washing with 1.0 M NaCl.

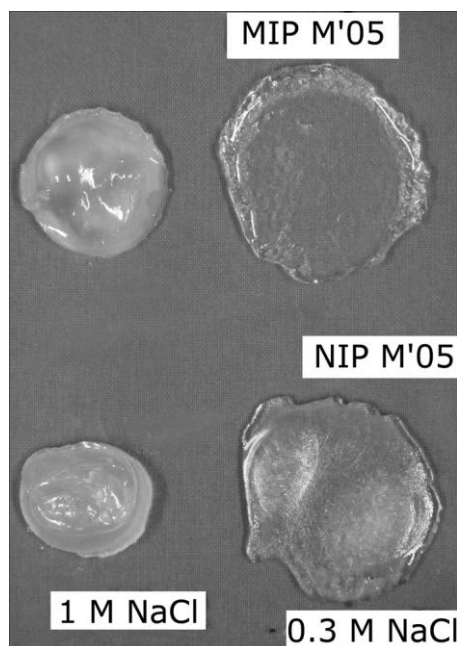


**Figure 4.24** Photograph showing the effect of sodium chloride concentration used for washing of MIP and NIP hydrogels prepared with 5 wt% MAA.

In the literature <sup>[126]</sup>, it had been stated that shielding lysozyme from being copolymerized with monomers has facilitated a relatively easier template-protein removal under mild conditions. It was hypothesized that this was due to complexation of MAA which in turn prevented lysozyme from the attack of free radicals. It was also reported that the fraction of extractable lysozyme increased with increasing MAA content copolymerized to PAAm <sup>[126]</sup>. However this was not the case for PNIPAAm-co-MAA in this study. Presumably, by increasing content of MAA, more electrostatic binding sites may decrease the efficiency of protein removal. A higher strength of interaction can be explained based on coordinated multivalent binding of more than one carboxylic group of the polymer to one protein molecule as seen for the NIP hydrogels (*c.f.* Table 4.13). The incomplete template-protein removal will have a negative influence for recognition binding; it will mask binding sites. It may also impose a resistance towards water uptake or mass transport; that can reduce swelling or binding capacity. In general, an increasing fraction of electrostatic interactions by comonomer segments in the hydrogel makes the material more similar to an ion exchanger matrix.

As shown in Table 4.12, NIP and MIP hydrogels synthesized either with 2 or 5 wt% MAA content relative to NIPAAm achieved a conversion of around 90 %. High degree of monomer conversion is very important due to several factors. The accuracy of network quantification based on statistical models highly depends on the high monomer conversion. Secondly, high conversion will ensure the mechanical stability of hydrogels. In addition, proportionally more ionic sites with increasing MAA content can also only be assured at high monomer conversion.

**Table 4.12 Monomer to hydrogel conversion (TOC) for NIP and MIP gels with various MAA contents after washing in 0.3 M NaCl solution (M'02 and M'05 represent 2 and 5 wt% MAA relative to NIPAAm, respectively).**

Hydrogels	Composition	Conversion [%]
NIP	M15M' <u>02</u> DC05	94
	M15M' <u>05</u> DC05	97
MIP	M15M' <u>02</u> DC05L10	87
	M15M' <u>05</u> DC05L10	92

Assuming that lysozyme is only reversibly bound in the hydrogel, the elution of template-protein (as well as of unreacted monomers) in the washing medium of the NIP and MIP gels can be investigated by monitoring the TOC values. If monomer conversion is the same of MIP and NIP and the template-protein is removed from MIP hydrogels, a correspondingly higher TOC value for MIP than NIP will be measured. However, the source of TOC cannot be distinguished. Overall lower apparent monomer conversion for MIP than for NIP gels was observed (Table 4.12), what could indicate that template-protein was entirely removed.

### 4.2.3 Physical Properties and Temperature-Responsivity

Hydrogels synthesized with various MAA content can be distinguished visually. As shown in Figure 4.25, hydrogels prepared with 5 wt% MAA were transparent (homogeneous gel). In contrast, hydrogels prepared with higher MAA content (i.e. 10 wt%) were opaque. This indicated macroscopic heterogeneities of the network. NIPAAm with isopropyl side group is relatively more hydrophobic than MAA. Thus, with increasing MAA content, phase separated hydrogels were obtained most likely because more ionic groups lead to more water what is bound to MAA-based network segments in the network, competing with the solvation of NIPAAm-based segments *via* hydrogen bonds. In addition, the phase separation could also have taken place as a result of chemical incompatibility of the comonomers during the polymerization <sup>[198]</sup>.

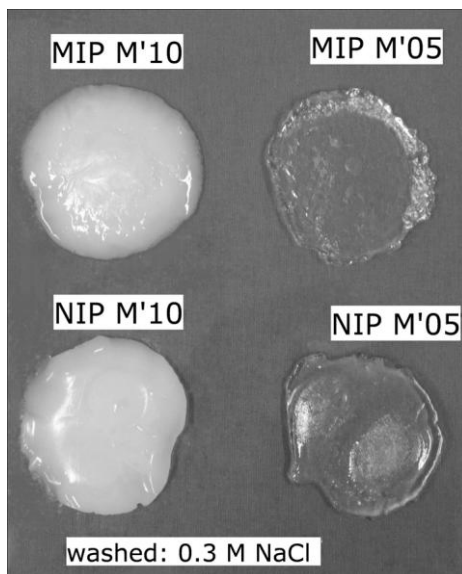


**Figure 4.25** Photograph showing the influence of MAA content on properties of MIP and NIP gels (washing: 0.3 M NaCl).

Figure 4.26 shows the temperature-dependent swelling behaviour of NIP and MIP hydrogels prepared with 2 % template-monomer when the temperature of the buffer increased from 15 to 45 °C. Below the LSCT, all the hydrogels possessed high degree of swelling; a strong decrease of swelling was observed between 30 and 35 °C. This observation is consistent with the classical temperature-responsive behaviour of PNIPAAm homo or copolymers reported in the literature <sup>[14, 15, 40, 41]</sup>.

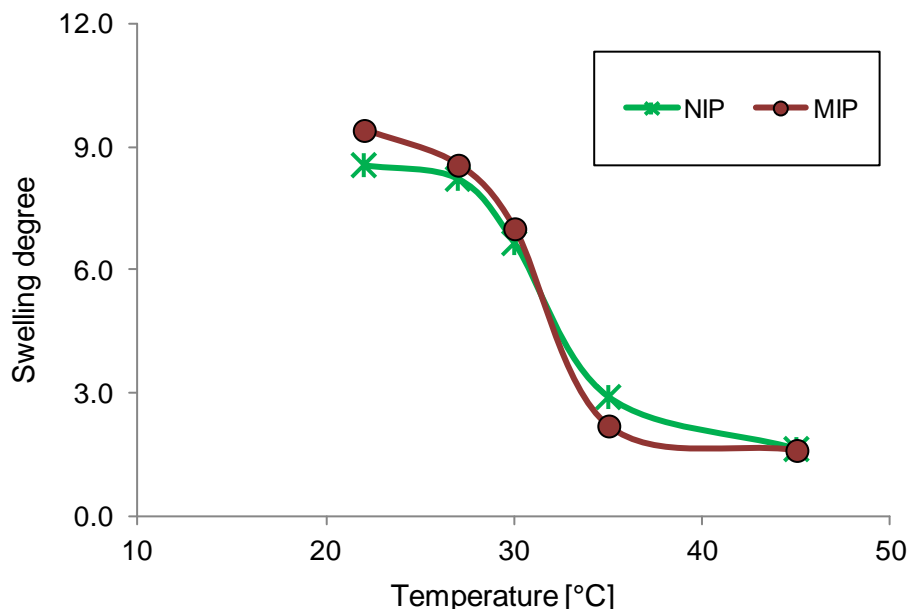


**Figure 4.26** Degree of swelling for MIP and NIP hydrogels prepared with 2 wt% of MAA as a function of temperature.

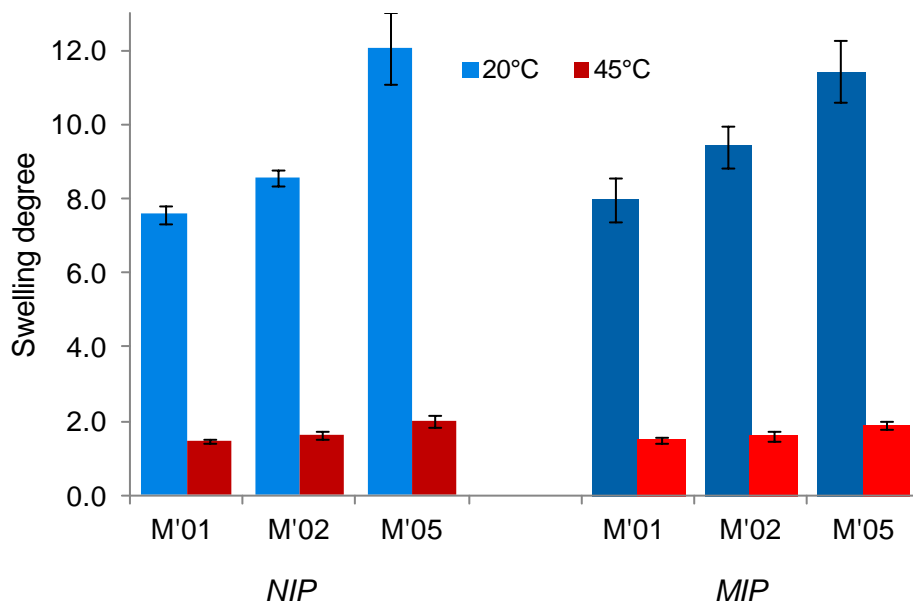


**Figure 4.27** Degree of swelling for MIP and NIP hydrogels at two temperatures as a function of MAA content.

Furthermore, significant differences between swelling degree below and above LCST of PNIPAAm were observed regardless the content of template-binding monomer or presence of protein during synthesis (Figure 4.27). These data confirmed the temperature-responsivity of all NIP/MIP gels synthesized in this work. On one hand, the degree of swelling below critical temperature increases with increasing template-monomer content for both NIP and MIP gels. Increasing template-monomer content could lead to a macroporous structure and increasing ionic group content are the reason for high water uptake. On the other hand, mainly below LCST and also at lower MAA content; i.e., up to 2 wt%, the equilibrium swelling ratio of the MIP hydrogels was higher than that of their NIP counterparts. This is presumably because the molecular imprinting technique creates nanoscale cavities, with additional sites for hydration within the hydrogel matrix (*c.f.* ref. <sup>[137]</sup>). However, this was not case for the MIP hydrogels prepared with the highest template-monomer content; and that lower swelling compared to the NIP gels could be due to incomplete protein removal (*c.f.* 4.2.2). This would be analogous to the effect of protein binding to MIP gels, i.e., a deswelling of the gel (this will be shown and discussed in 4.2.4.1).

## 4.2.4 Protein Binding

### 4.2.4.1 Binding capacity and imprinting factor

The influence of template-binding monomer content onto binding behaviour of hydrogels with the template protein at pH 7 and RT was investigated (Figure 4.28). A very clear correlation between binding capacity and MAA content had been observed; binding capacity increased with increasing template-monomer content.

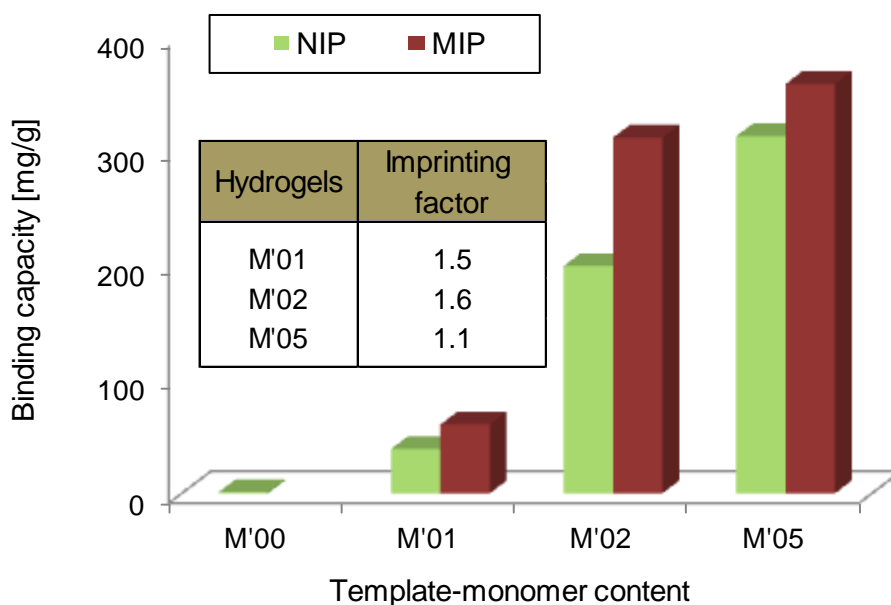


**Figure 4.28** Binding capacities and resulting imprinting factor obtained with 0.5 g/l lysozyme in tris-HCl buffer (10 mM, pH 7.0) at RT.

This trend is analogous to the influence of MAA content on swelling observed in Figure 4.27. At neutral pH, lysozyme is positively charged while MAA has a negative fixed charge due to deprotonation of carboxyl groups. Therefore the template-monomer imposed electrostatic interactions either with water or protein due to their ionic character. Almost no protein binding ( $\sim 1$  mg/g) was observed for the hydrogels prepared without template-monomer (*c.f.* Figure 4.28). This experiment implied that ionic interaction is necessary for binding.

Binding observed for NIP hydrogels was associated only to the non-specific electrostatic interactions. The MIP hydrogels on the other hand bound significantly more protein than NIP hydrogels (Figure 4.28). Imprinting factor is the ratio between binding capacities of MIP and NIP gels. First, the imprinting factor increased with increasing template-binding monomer content. However, a further increased of template-monomer content (5 %) reduced the imprinting factor (*c.f.* Figure 4.28) as a result of increasing the non-specific binding within NIP hydrogels.

The effect of template-binding comonomer content onto the binding capacity of the gel was therefore analyzed. For this purpose, the number of template-monomer molecule ( $N_M$ ) to bind one lysozyme molecule ( $N_{\text{lysozyme}}$ ) was estimated based on the binding data of NIP hydrogels. Table 4.13 shows that more than one MAA molecule in the M'02 and M'05 hydrogels binds one lysozyme molecule. This indicates stronger electrostatic interactions with increasing template-binding comonomer. Thus, it is more likely that at higher MAA content, ion exchanger characteristic of the gel may have stronger influence than just only shielding lysozyme during polymerization (*c.f.* 4.2.2). Even more critical would be the non-specific binding besides recognition in imprinted sites in MIP hydrogels. The non-specific binding can hence be reduced using a lower content of the template-monomer, but this reduced the overall binding capacity. However, the reduction was less pronounced for the MIP hydrogels.

**Table 4.13 Molar ratios between template-binding monomer MAA and lysozyme from protein binding to NIP hydrogels.**

M' [%]	Binding capacity [mg/g]	$N_{(M')} / N_{(\text{lysozyme})}$
1	39	0.6 : 1
2	199	2 : 1
5	313	5 : 1

#### 4.2.4.2 Protein sorption isotherm

Binding capacity was further investigated for hydrogels prepared with 2 % template-monomer content as a function of lysozyme concentration (Figure 4.29). An increase in binding capacity was observed until a saturation level. Overall, MIP exhibited larger binding capacities than NIP hydrogels, especially at low lysozyme concentration. Besides ionic interactions, the higher binding capacity obtained for MIP hydrogels was mainly due to the recognition behaviour towards lysozyme as its template-protein. Thus, recognition favoured a binding process through the fitting of multi binding sites within the hydrogel matrix created by the imprinting procedure and summation of non-covalent interactions such as electrostatic interactions and hydrogen bonding. A steeper curve of MIP hydrogels indicates higher affinity of MIP hydrogels toward its template-protein. Considering the shape of the curve, the data have been fitted to the Langmuir isotherm model in order to estimate the binding constant. The estimated binding constants for NIP and MIP hydrogels in this study ( $3.9 \times 10^5 \text{ M}^{-1}$  and  $7.7 \times 10^4 \text{ M}^{-1}$  respectively) were in a good agreement with those reported in the literature for similar materials ( $4.2 \times 10^5 \text{ M}^{-1}$  and  $9.9 \times 10^4 \text{ M}^{-1}$  respectively; *c.f.* <sup>[131]</sup>).



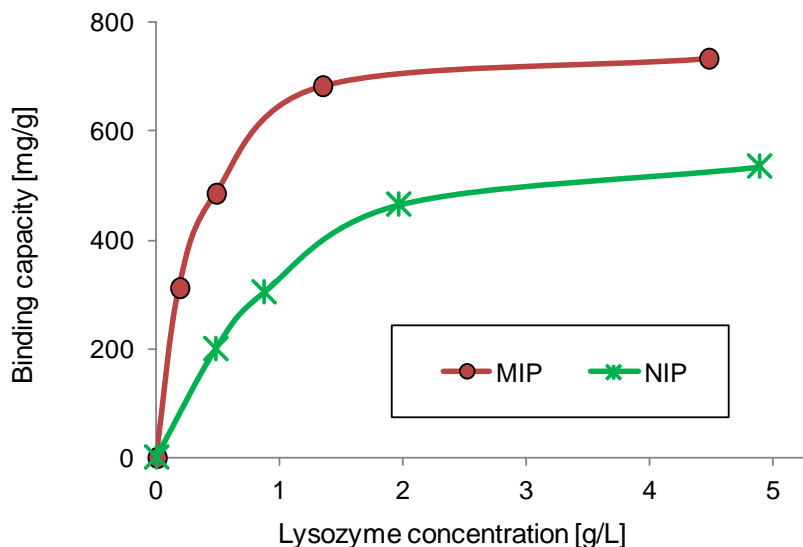


**Figure 4.29** Binding isotherms for MIP and NIP with lysozyme in tris-HCl buffer (10 mM, pH 7.0) at RT; hydrogel composition: M15M'02DC05. Binding constants for MIP and NIP hydrogels were  $3.9 \times 10^5 \text{ M}^{-1}$  and  $7.7 \times 10^4 \text{ M}^{-1}$ , respectively.

#### 4.2.4.3 Protein binding selectivity

In order to determine the selectivity of MIP hydrogel towards its template-protein, a competition sorption test was performed. A protein mixture of 0.5 g/l lysozyme and cytochrome C was used. Cytochrome C was used due to its similar properties compared to lysozyme in terms of size and IEP (*c.f.* Table 3.7). The result of this experiment for hydrogels prepared with 2 % template-monomer is shown Figure 4.30.

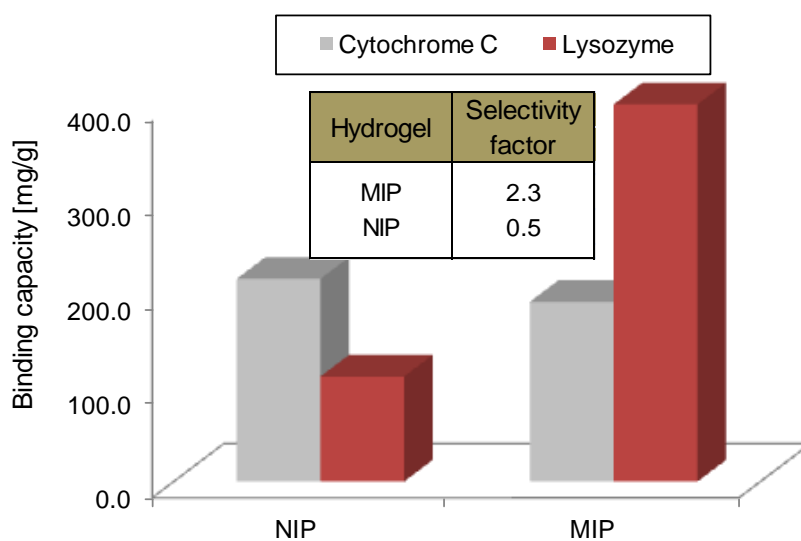


**Figure 4.30** Protein binding selectivity for MIP and NIP hydrogels with total initial protein concentration of 0.5 g/l.

Firstly, NIP and MIP hydrogels demonstrated no significant difference in binding toward the reference protein cytochrome C. This competition experiment clearly indicates that binding was caused by non-specific interactions. It should be noted that the cytochrome C molecule is slightly smaller (*c.f.* Table 3.7) than the lysozyme molecule and, thus, the crosslinked NIP hydrogels could bind more cytochrome C because of better accessibility of the binding sites. For a simple grafted PAAM-based adsorber, somewhat more cytochrome C than lysozyme was bound, what had been related to larger sterical hindrance for the larger protein <sup>[199]</sup>. However, since the difference in size was small, this could not fully justify the relatively large difference in binding for NIP hydrogels. Also, on standard chromatography materials, either cation-exchange or reversed phase, a slightly lower retention of cytochrome C, i.e., slightly weaker binding, than lysozyme is often observed. The two proteins differ with respect to the structure of the basic amino acids: Lysozyme is mainly arginine-based, whereas cytochrome C is mainly lysin-based. This had been used for creating lysozyme selectivity based on polymers with arginine-selective side groups <sup>[199]</sup>. In the same study, the capacity of a grafted cation-exchanger material for the two proteins had been the same <sup>[199]</sup>.

However, most importantly, the data in Figure 4.30 reveal that MIP hydrogels exhibited high selectivity towards lysozyme compared to cytochrome C; i.e., just the opposite compared to the NIPs with the same composition. Even though lysozyme and cytochrome C have similar properties at their molecular level, MIP hydrogels preferentially bind template-protein; i.e., lysozyme to the larger extent than cytochrome C. This is a strong indication that MIP gels can distinguish proteins not simply on the basis of size or charge, but to a large extent due to recognition and binding fitting complementarily to the shape of the template-protein.

#### 4.2.4.4 Temperature-induced binding response

The effect of temperature on protein binding of NIP and MIP hydrogels is shown in Figure 4.31. It can be seen that the binding capacity of both hydrogels decreased as the temperature increased above LCST of PNIPAAm and the lowest binding was observed at highest temperature; i.e. 45 °C. The temperature induced binding response can be explained as follows. The MIP hydrogels serve as the selective recognition element provided that their recognition sites are preserved analogous to the imprinting state. Due to the temperature-responsivity, PNIPAAm based hydrogels collapsed into a compact 3D network and this was not accessible for the protein binding. In addition, deformation of imprinted sites may also have occurred. Nevertheless, MIP hydrogels had overall higher binding capacity than NIP hydrogels also above LCST. This would indicate that a small fraction of imprinted sites was probably on the outer surface of the gel, also at higher temperature with distinct affinity for lysozyme binding.

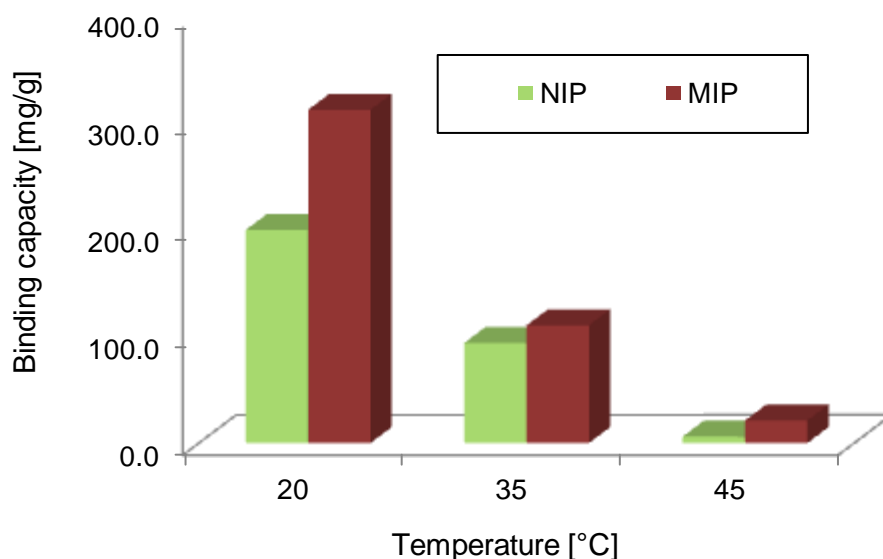


**Figure 4.31** Influence of temperature on binding for MIP and NIP hydrogels. Initial protein concentration 0.5 g/l; hydrogel composition: M15M'02DC05.

#### 4.2.4.5 Specific volume change induced by protein-responsivity

The binding of lysozyme in the MIP hydrogels at a temperature below LCST resulted in a strong decrease in hydrogel volume. This effect was firstly studied for various protein concentrations as shown in Figure 4.32. It can be clearly seen that increasing lysozyme concentration continuously induced shrinking of the MIP hydrogels up to a protein concentration of about 1.2 g/l; then swelling became constant. In case of NIP hydrogels, only slight volume decrease was observed and this occurred only at high lysozyme concentration which is most probably due to non-specific effect of ion pairing. Specific shrinking for MIP gels was observed due to specific interactions between template-protein and imprinting sites and subsequent conformational change within the hydrogel network. Presumably, the best proposed mechanism for this significant specific volume shrinking is that binding to imprinted sites causes local conformation and solvation changes which will ultimately lead to different solvation also in the wider environment of the imprinted sites. Specifically, formation of ion pairs between carboxylate and cationic protein groups will reduce the charge density in the gel and hence lead to lower amount of bound water. The release of bound water could be a strong entropic driving force. This process is started by a recognition sequence of MIP hydrogels followed by adaptation sequence; i.e., conformational adaptation within the network towards the template-protein that ultimately leads to shrinking.

Similarly, the protein-responsivity was also studied for variation of template-binding monomer content as shown in Figure 4.33. Clearly, proportional tendency of volume shrinking and swelling was found.

In the absence of ionic groups, no change of volume was observed. Shrinking became more pronounced with increasing template-monomer content. Several explanations can be offered. It is most likely, that that more bound water can be released from these hydrogels due to an increasing formation of ion pairs between carboxylate and cationic protein groups. Higher template-monomer content introduced more imprinted sites with higher water sorption (*c.f.* 4.2.3) and therefore induced larger degree of shrinkage upon protein binding.

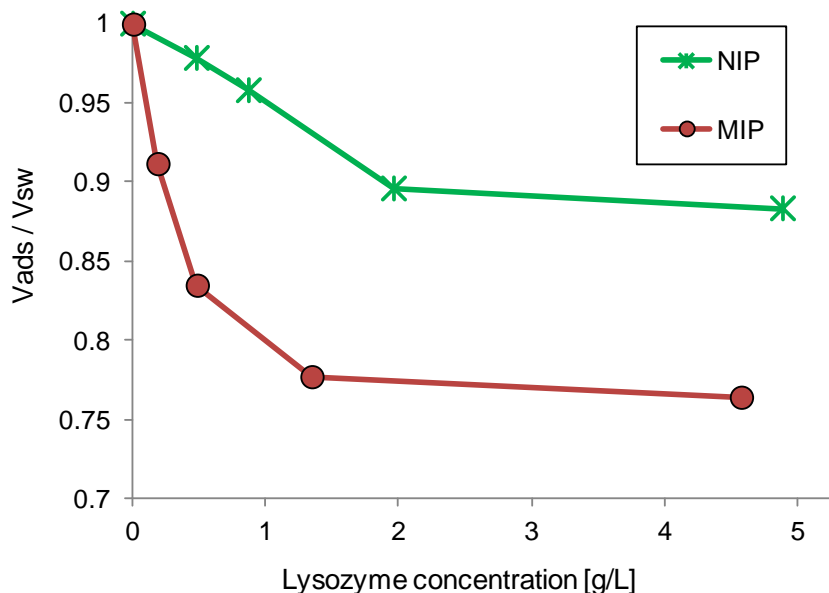


**Figure 4.32** Volume shrinking for MIP and NIP hydrogels as function of lysozyme concentrations in tris-HCl buffer (10 mM, pH 7.0) at RT; hydrogel composition: M15M'02DC05.

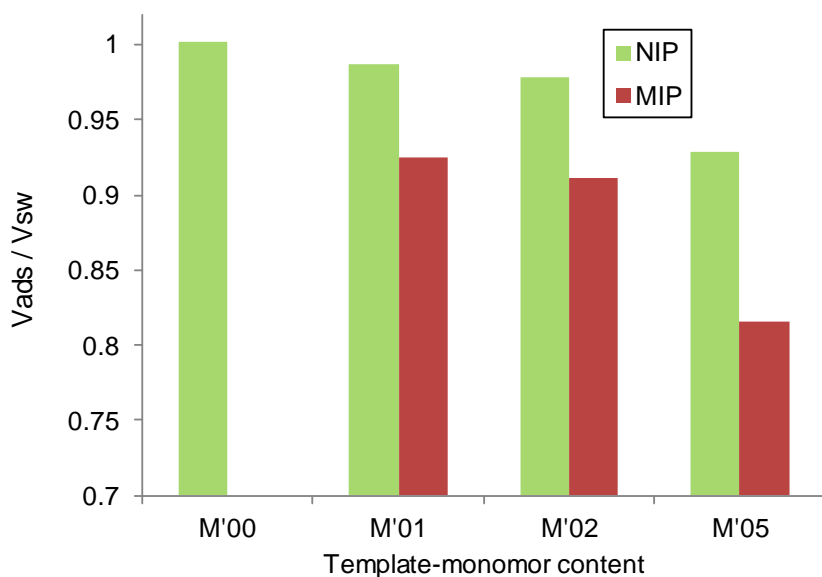


**Figure 4.33** Volume shrinking upon protein binding for MIP and NIP hydrogels with increasing template-monomer content. Initial protein concentration of 0.5 g/l lysozyme in tris-HCl buffer (10 mM, pH 7.0) at RT.

### 4.3 Ion-Selective Poly(*N*-Isopropylacrylamide-*co*-4-vinylbenzo-18-Crown-6) Bulk Hydrogels

The synthesis of PNIPAAm-*co*-vCE hydrogels *via* redox-polymerization (TEMED/APS 4.0 : 1) proceeded through copolymerization of vCE comonomer to the main PNIPAAm backbone, in the presence of MBAAm as a crosslinker. vCE has poor solubility in water. In a water/THF mixture of 4 : 1, the solubility of reaction mixture was improved and the resulting hydrogels appeared to be transparent. As the ratio of THF in a water/THF increased, the obtained hydrogels were opaque; and these gels were not further characterized. In this section, ion-recognition and responsivity properties of resulting hydrogels were explored from the view of conversion and also copolymerization.

#### 4.3.1 Conversion and Copolymerization Efficiency

PNIPAAm-*co*-vCE hydrogels were prepared from moderately and loosely crosslinked networks; i.e. DC05 and DC02 respectively. As shown in Figure 4.34, the degree of monomer conversion of these hydrogels were slightly decreased; from 96 to 83 % with increasing incorporation of vCE units up to 10 wt% relative to NIPAAm. The reduction of conversion was attributed to the steric hindrance imposed by the large ring structure in a CE [28, 29, 138]. It was postulated that copolymerization was relatively facile in a more loosely crosslinked network. Subsequently, a further extent of vCE copolymerization has even reduced the conversion of the hydrogel with lower crosslinker content (Figure 4.34).

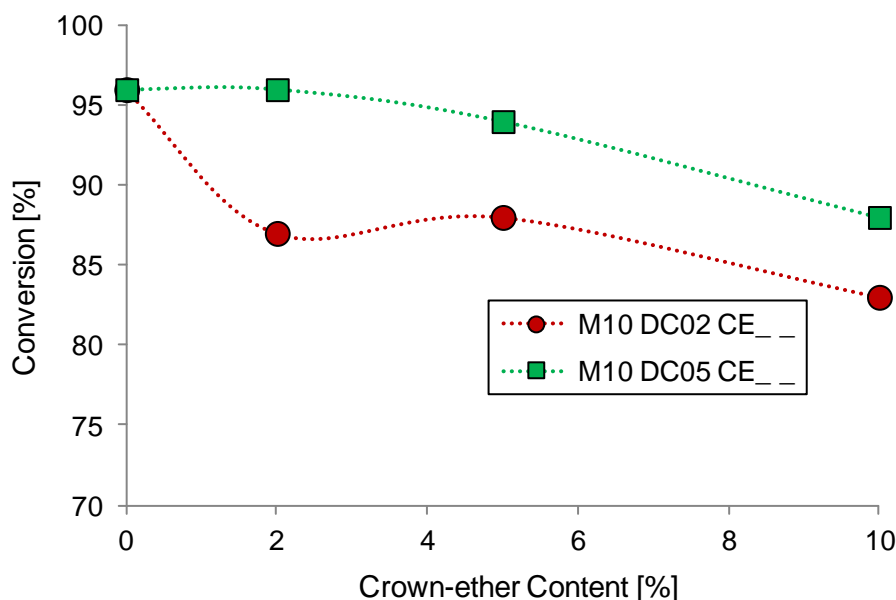


**Figure 4.34** Conversion from TOC to PNIPAAm-*co*-vCE hydrogels with various crown ether content. Hydrogels were obtained using initiator TEMED/APS 4.0 : 1. Other conditions *c.f.* Table 4.4.

The FTIR spectra of PNIPAAm-*co*-vCE hydrogels are shown in Figures 4.35 - 4.37. The characteristic peaks of PNIPAAm were found in each spectrum (1643 and 1534  $\text{cm}^{-1}$  corresponding to amide I and amide II bands respectively). vCE has characteristic peaks at 1052, 1129, 1264 and 1518  $\text{cm}^{-1}$ . For comparison, characteristic peaks of vCE monomer were found only in copolymer containing vCE (Figure 4.35). Furthermore, the peak intensities at 1052, 1129 and 1264  $\text{cm}^{-1}$  appeared gradually with the increasing content of vCE in the M10DC02CE02 to CE10 hydrogels, while the peak at 1518  $\text{cm}^{-1}$  was only noticeable for hydrogel with highest CE content. These were strong evidences that vCE successfully copolymerized to the polymer main chain. In addition, the degree of copolymerization was also strongly dependent on CE content.

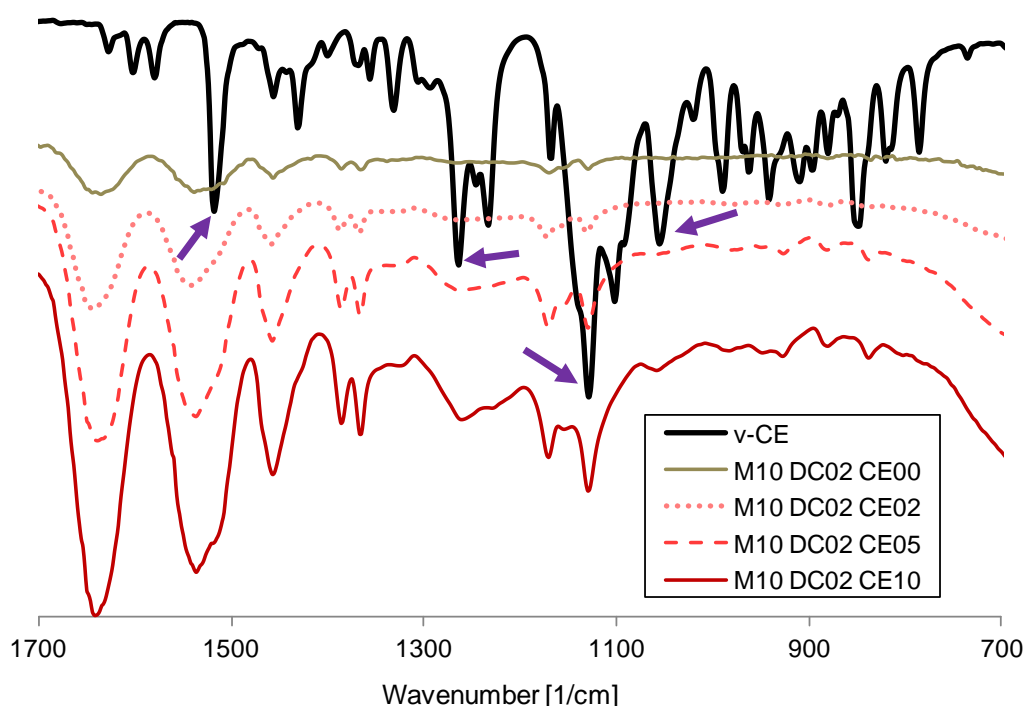


**Figure 4.35** Copolymerization of PNIPAAm-*co*-vCE hydrogels with various crown ether content *via* FTIR analysis at 1052  $\text{cm}^{-1}$  (symmetrical C-O-stretching in Ar-O-R), 1129  $\text{cm}^{-1}$  (asymmetrical C-O-stretching in R'-O-R), 1264  $\text{cm}^{-1}$  (asymmetrical C-O-stretching in Ar-O-R), 1518  $\text{cm}^{-1}$  (C=C-stretching of phenyl ring).

Copolymerization efficiency was also investigated as a function of crosslinker content. As seen from Figure 4.36a and b, hydrogels with lower crosslinker has more pronounced peaks especially at 1129 and 1264  $\text{cm}^{-1}$ . This is due to the fact that higher crosslinker imposed further hindrance of CE monomer to be copolymerized in the networks. In hydrogels with relatively higher crosslinker content, the appearance vCE characteristic peaks suggested that it was also copolymerized to main PNIPAAm chain but copolymerization was less efficient.

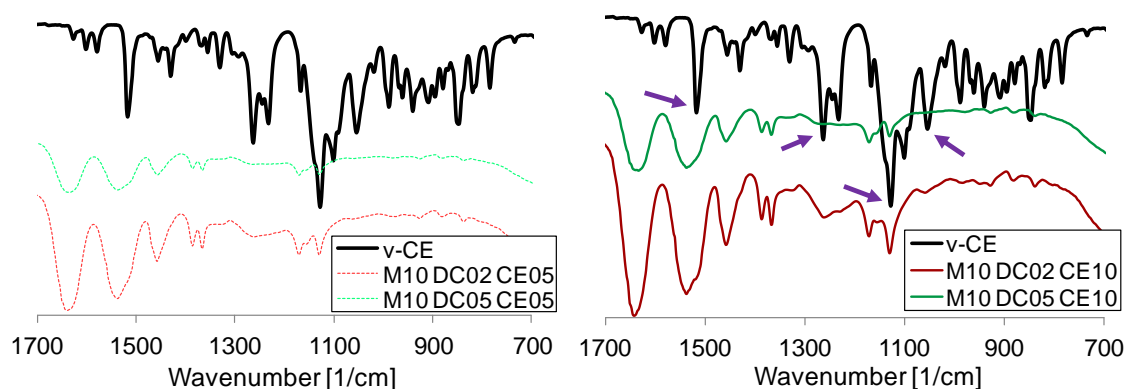


**Figure 4.36** Copolymerization of PNIPAAm-*co*-vCE hydrogels *via* FTIR analysis with various crosslinker content.

### 4.3.2 Rheology Investigation of Gelation Kinetics

The gelation kinetics was investigated rheologically as a function of vCE and crosslinker contents. The gelation kinetics were assessed based on the gelation point; the onset from which the transformation from liquid-like to solid-like properties took place ( $G' = G''$ ; *c.f.* 4.1.1.4).

From Figure 4.37a, a clear tendency can be seen; with increasing vCE the gelation time was delayed. In the absence of vCE, the gelation occurred almost instantaneously. Here, the kinetics of gelation was influenced by the difficulties of vCE copolymerization into the hydrogel network due to the bulky CE rings<sup>[29]</sup>. These results were also analogous to FTIR analyses in 4.3.1.

Overall, the variation of crosslinker does not seem to affect the gelation kinetics of PNIPAAm-*co*-vCE hydrogels, particularly of those with high content of vCE (Figure 4.37b). Again, this can be due to the steric hindrance imposed by vCE unit. In case of hydrogels obtained with the lowest vCE (CE02), the gelation was significantly faster at lower crosslinker content. Obviously, copolymerization is highly promoted in the loosely crosslinked network.

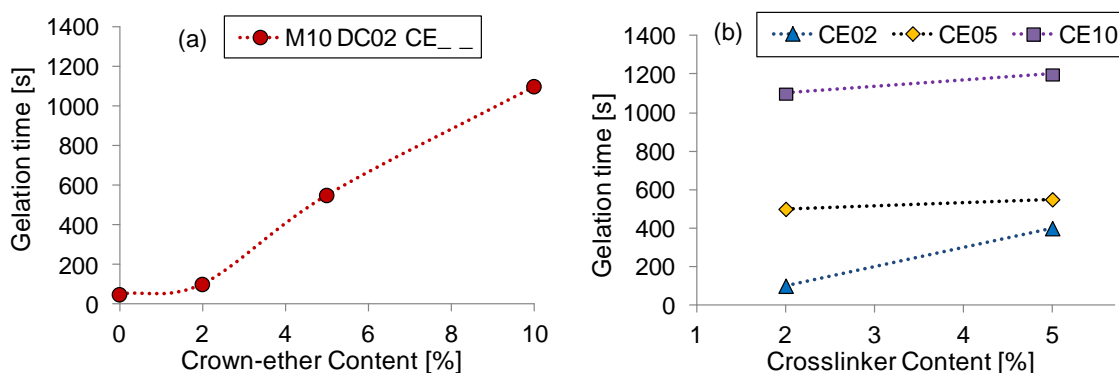


**Figure 4.37** Influence of (a) crown ether content; and (b) crosslinker content on the onset of gelation.

### 4.3.3 Equilibrium Swelling Degree

As a standard procedure, the swelling behaviour in water as a function of temperature was investigated. In water, the temperature-responsive behaviour of PNIPAAm-*co*-vCE hydrogels was analogous to pure PNIPAAm hydrogels (Figure 4.38). This again confirmed the existence of LCST; in which hydrogels were either swollen or collapsed at a temperature below or above it.

Initially, the influence of vCE content on the equilibrium swelling degree was investigated. Figure 4.38a showed an increase in swelling with increasing vCE content. Several explanations can be offered. First, it was due to an enhancement of hydrophilicity of the polymer network that also enhanced the water uptake. The distinct solvation of vCE segment in PNIPAAm-*co*-vCE as compared to pure PNIPAAm was related to the formation of hydrogen bonding between the oxygen atoms in the vCE and hydrogen atoms of water

When the effect of degree of crosslinking was examined, it was found that the loosely crosslinked networks swelled to the larger extent (Figure 4.38b and c). This is due to the fact that loosely crosslinked networks produced larger mesh sizes that allowed for the greatest swelling capacity. And finally, regardless of the vCE content, similar trend of swelling was observed as a function of crosslinker content.

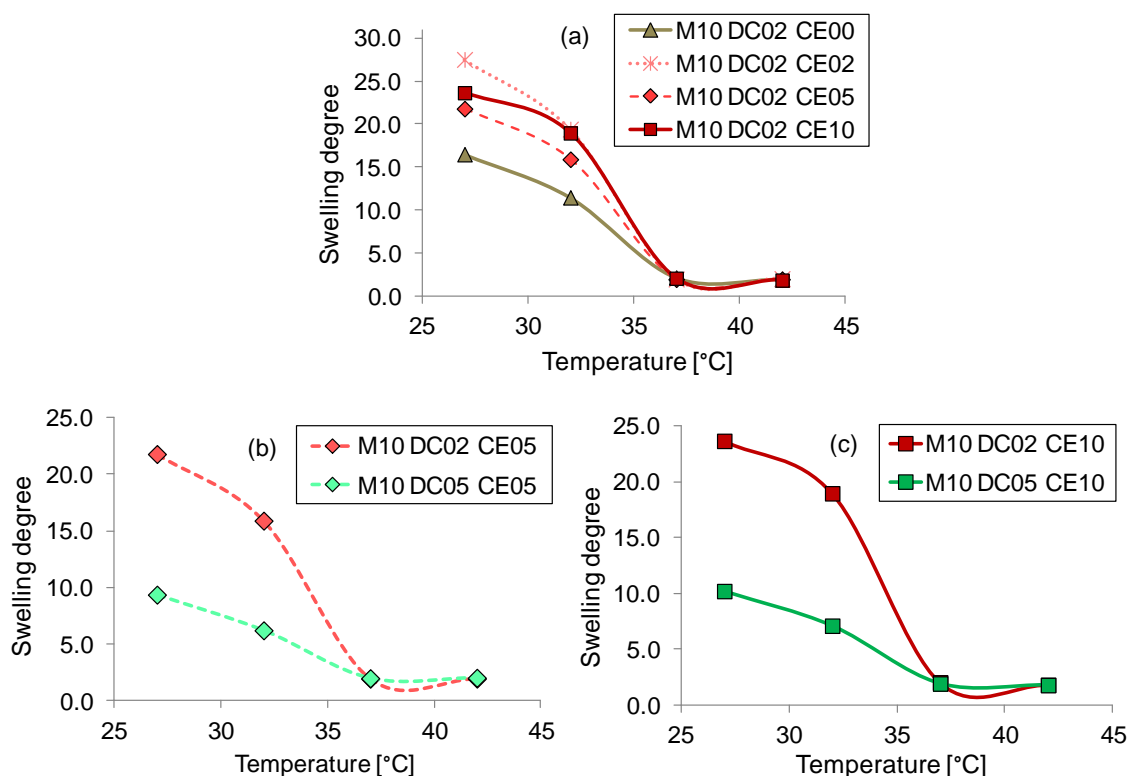


**Figure 4.38** Equilibrium swelling degree of PNIPAAm-*co*-vCE hydrogels as a function of temperature: (a) influence of crown ether content; (b) influence of crosslinker content on hydrogels with 5 % crown ether content; and (c) influence of crosslinker content on hydrogels with 10 % crown ether content.



#### 4.3.4 Ion-Responsivity

The ion recognition properties of PNIPAAm-*co*-vCE hydrogels can be monitored from swelling experiment at 37°C in salt solutions. From Figures 4.39 - 4.41, graphs on the left side represent the influence of swelling degree as function of potassium ion concentrations (0, 0.002 and 0.02 M) while graphs on the right side represent the swelling degree as function of various cations at a constant concentration.

First, the correlation between the vCE content in the hydrogel and the ion sensitivity, i.e. an altered swelling in the presence of certain ions are investigated (Figure 4.39). Interesting observations can be acquired from these graphs. The hydrogel revealed a distinct sensitivity towards potassium ions only at a highest potassium concentration (0.02 M). Subsequently, hydrogels with the highest vCE content swell even more. On one hand, a barium ion sensitivity can already be seen in the hydrogel with 5 wt% of vCE relative to NIPAAm. On the other hand, no significant difference of swelling in sodium salt, and it can therefore be deduced that these hydrogels are not selective to sodium. Considering the complexation of three ions ( $\text{Na}^+$ ,  $\text{K}^+$ ,  $\text{Ba}^{2+}$ ) with vCE units, the barium ion has the highest complexation constant, followed by the potassium and the sodium ions [28, 29, 138, 139, 145, 200]. Complexion with bigger ions like barium to the CE increased the osmotic pressure within hydrogel due to a Donnan potential [139]. This has made the hydrogel to swell more and the tendency is more pronounced for higher vCE copolymer gels. These observations can also be explained by referring to the respective IR spectra. Clearly, ion sensitivities showed a strong correlation with the copolymerization efficiency; being more sensitive in case of higher vCE copolymerized to PNIPAAm backbone.

Evaluation on the Figure 4.40 should demonstrate whether a similar relationship in terms of crosslinker content and the ion sensitivity exists. For this purpose, ion sensitivity measurements were carried out in hydrogels at two different crosslinking level but with fixed vCE content (5 wt% relative to NIPAAm). Overall, in combination with fair vCE composition, the influence of crosslinker content was less pronounced, and thus degree of swelling decreased only slightly. These effects have led into no noticeable ion responsivity features for sodium ion or even potassium ion regardless of its concentration. On the contrary, barium ion sensitivity was displayed in hydrogels with both low and high crosslinker content with no prominent difference (Figure 4.40). The reason for these observations should be associated with the appropriate size of barium ion to form the stable complex even for slightly densely crosslinked hydrogels [139].

Figure 4.41 provides the same connections as the previous diagram (Figure 4.40), represents swelling of PNIPAAm-*co*-vCE hydrogels as a function of the crosslinker content at relatively higher vCE content. Indeed, the same trends are observable and additionally the degree of swelling appeared to be more sensitive for lower crosslinker content. In a relatively less dense network, a sensitivity towards potassium ion can be revealed even in a smaller concentration range. And above all, the measurements

were super sensitive towards barium ions with similar trends in degree of crosslinking. With the increase in the degree of crosslinking, barium ion sensitivities existed on a lesser extent. Also, because of their smaller size, the investigated gels showed no sensitivity with respect to sodium ions <sup>[28, 29]</sup>.

These findings showed a good correlation with the observed swelling behaviour as a function of crosslinker concentration in subsection 4.3.3 and the IR spectra of copolymerization efficiency as a function of vCE content in subsection 4.3.1. From these comparisons, also that the hydrogel from composition M10DC02CE10 showed the supreme recognition and sensitivity for both barium as well as potassium, that surely will be an appropriate choice for future work.

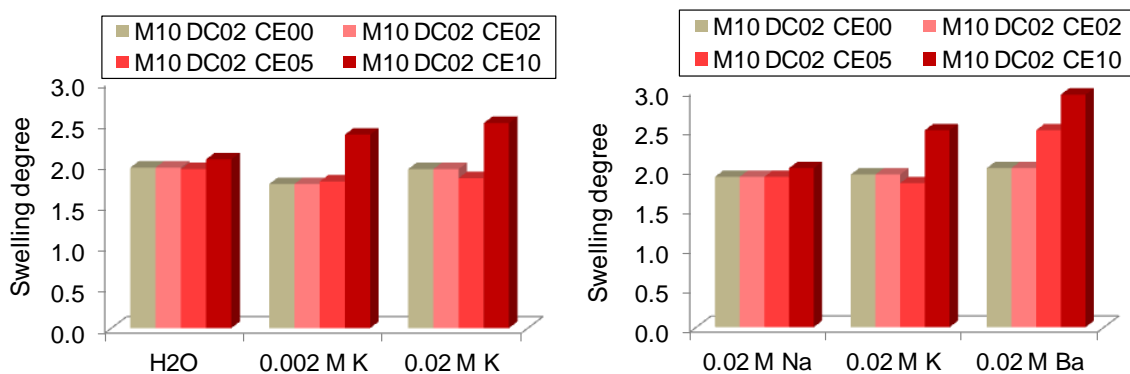


**Figure 4.39** Equilibrium swelling degree of PNIPAAm-*co*-vCE hydrogels with various crown ether content at 37 °C as a function of potassium ion concentration (left); size of ions (right).

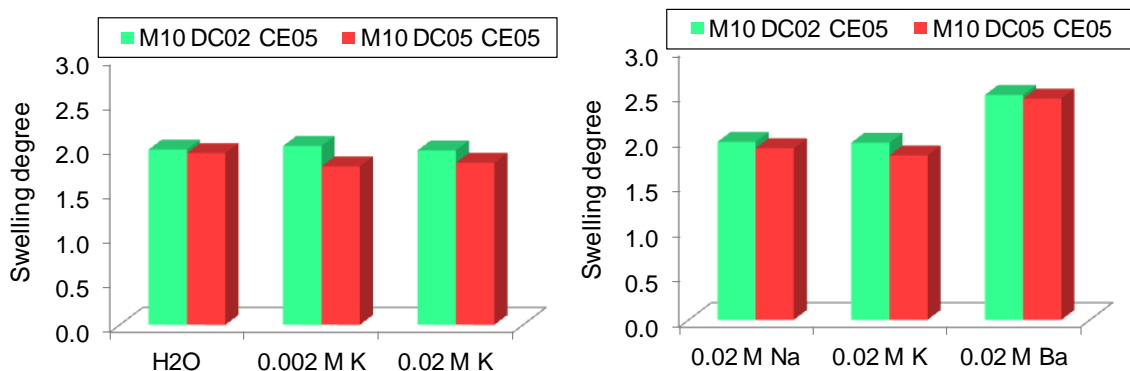


**Figure 4.40** Equilibrium swelling degree of PNIPAAm-*co*-vCE hydrogels with various crosslinker content at 37 °C as a function of potassium ion concentration (left); size of ions (right). Hydrogels obtained with 5 % crown ether content.

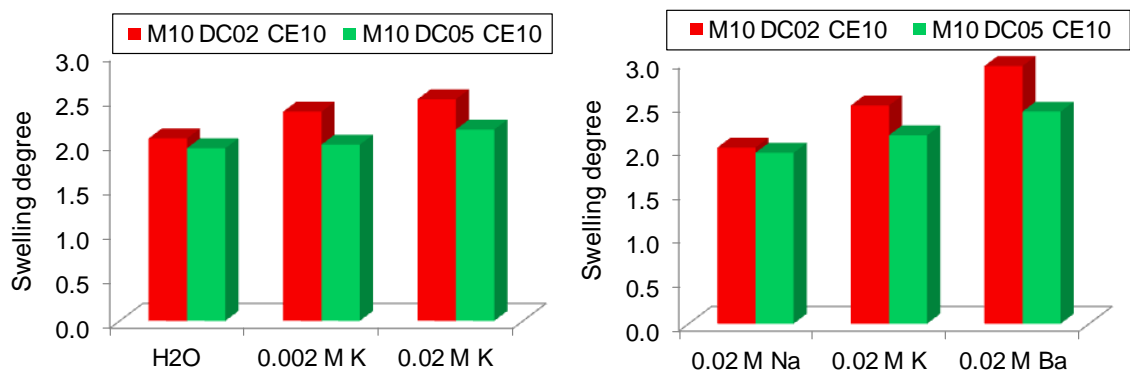


**Figure 4.41** Equilibrium swelling degree of PNIPAAm-*co*-vCE hydrogels with various crosslinker content at 37 °C as a function of potassium ion concentration (left); size of ions (right). Hydrogels obtained with 10 % crown ether content.

## 4.4 Characterization of Base Membranes

Membranes with nominal pore diameter between 200 and 5000 nm were used as base membranes (BM) for pore-filling functionalization. Previous work had already indicated considerable deviations between the nominal and actual pore size for such PET membranes [32, 43]. This section therefore provides data for unmodified membranes.

### 4.4.1 Average Pore Size, Pore Size Distribution and Pore Properties

Verification of the actual pore size and also the pore size distribution was done by means of permoporometry. Figure 4.42 shows the pore size distribution analysis for unmodified BM\_1000 carried out three times. As seen in this figure, some samples had a more narrow size distribution than the others. Nevertheless, data from these three measurements were close to each other; with the peak in the range of 1600 to 1800 nm. However, the average pore size of this membrane was significantly higher than the nominal value. This was attributed from the manufacturing process; over-etching that created double or multiple pores.

Similarly, permoporometry measurements were carried out for each BM. Deviation from the nominal value had been largest for the PET 400 membrane (Figure 4.43). Despite of these deviations, all the BM showed very narrow pore size distributions. This enabled accurate estimation of pore diameter from hydraulic permeability and interpretation of pore size influence on pore-filling.

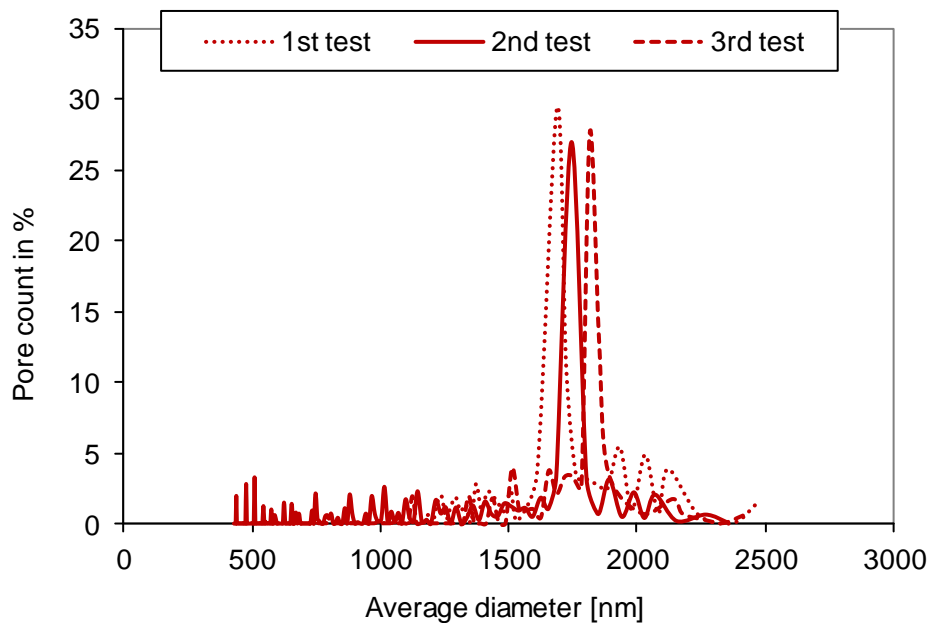


**Figure 4.42** Pore-size distribution measurement of the unmodified PET track-etched base membrane obtained from gas flow / pore dewetting permoporometry; nominal pore diameter 1000 nm.

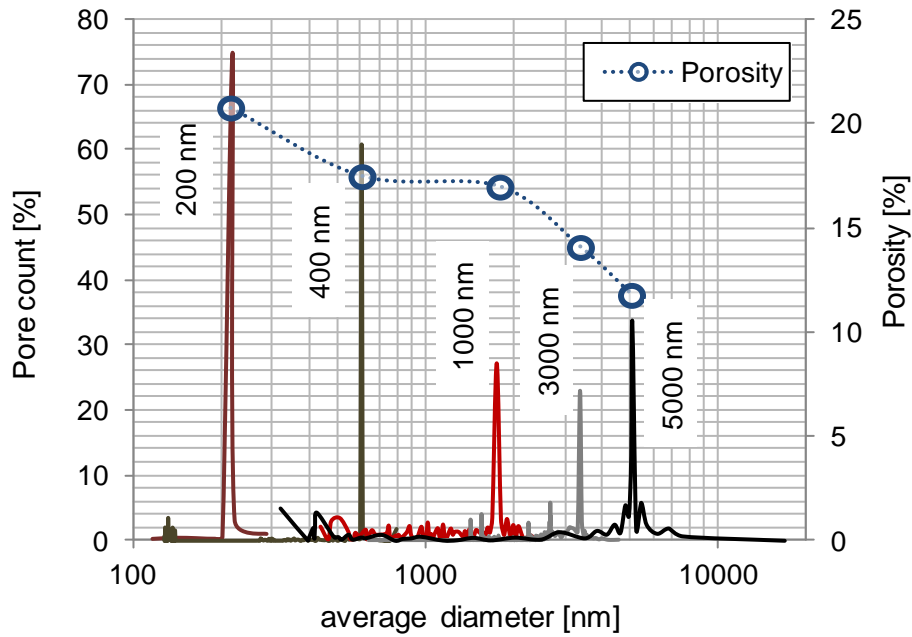


**Figure 4.43** Pore-size distributions of various pore-sizes of unmodified base membranes (analogous to Figure 4.42) and their corresponding porosity.

#### 4.4.2 Water Permeability

The water permeability of the unmodified BM was determined at RT and hydrostatic pressure of about 0.03 bar. The water flux measurements are more reliable compared to permoporometry analysis because they do much better represent the hydrodynamic transmembrane transport <sup>[43]</sup>. As shown in Table 4.14, water permeability increased from about 12000 to 1400000 l/m<sup>2</sup>hbar for BM with nominal pore diameter from 200 to 5000 nm. Permeability data was found to be dependent on pore size; this was used for later comparison with prefunctionalized as well as with pore-filled membranes.

**Table 4.14** Water permeabilities of unmodified base membranes (average of 5 measurements within 10 % standard deviations).

Base Membrane (BM)	Water permeability
	[l/m <sup>2</sup> hbar]
200 nm	12 500
400 nm	41 800
1000 nm	325 000
3000 nm	450 000
5000 nm	1 400 000

## 4.5 Prefunctionalization and Characterization of Prefunctionalized Membranes

The prefunctionalization of the BM was performed to yield a moderate functionalization, i.e., to provide a sufficient anchoring effect to the pore-filled hydrogel without having too much influence on its structure (*c.f.* Figure 1.3). Clearly, in order to achieve that goal, different pore sizes of BM will require different grafted layer thickness. The next subsections contain data and concrete discussion in order to make selections and decisions of suitable prefunctionalization.

### 4.5.1 Selections of Suitable Prefunctionalization

Obviously, prefunctionalization is crucial especially for bigger membrane pores. At the beginning of this work a suitable prefunctionalization was comprehensively explored for BM\_1000 and BM\_5000 using two different prefunctionalization levels respectively (Figure 4.44). In order to achieve different prefunctionalization level, monomer concentration had been varied. Other photografting conditions such as initiator coating or UV time had already before been investigated<sup>[32, 43]</sup> and were kept constant here.

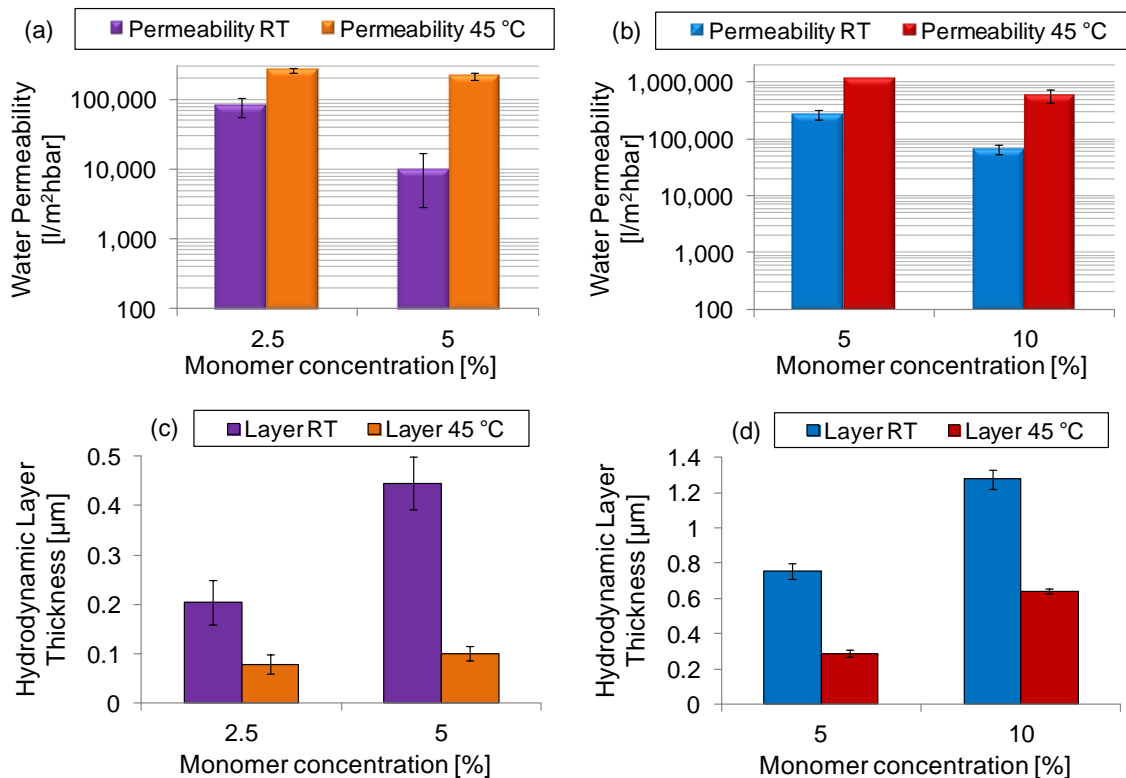


**Figure 4.44** Permeabilities and hydrodynamic layer thicknesses after prefunctionalization step at RT and 45 °C; base membrane: 1000 nm (left) and base membrane 5000 nm (right).

Suitable prefunctionalization was established based on comparison of data for water permeabilities at RT and 45 °C and their respective hydrodynamic layer thicknesses from Figure 4.44. Regardless of monomer concentrations or size of BM, a decrease in water permeability was observed after prefunctionalization. This indicates that PNIPAAm chains were grafted on the pore surface of the BM. A clear dependence between monomer concentrations and the resulting permeabilities at RT was also noticeable; lower permeability was obtained with higher monomer concentration and vice versa.

In case of BM\_1000 (Figure 4.44a), the permeability difference between 2.5 and 5 % prefunctionalized membranes is in the order of one magnitude. This may be explained because higher resistance for water transport was imposed for membranes prefunctionalized with 5 % monomer concentration. This assumption correlates with those corresponding hydrodynamic layer thicknesses (Figure 4.44c) derived from Hagen-Poiseuille model (*c.f.* Figure 2.15). Prefunctionalization with higher monomer concentration caused a doubling of the layer thickness at RT; the pore size had been reduced to about 0.8 and 1.3  $\mu\text{m}$  for prefunctionalization with 5 and 2.5 % respectively. At 45 °C, the collapsed PNIPAAm chains has led into a significant increase in permeability. However, no specific influence from monomer concentration on the resulting permeabilities was seen. Therefore layer thicknesses at 45 °C also differ only slightly from each other despite their different monomer concentration. On the other hand, prefunctionalization with 2.5 % monomer concentration yielded more moderate grafting and also higher reproducibility. Consequently, 2.5 % monomer concentration was chosen for prefunctionalization of BM\_1000.

Prefunctionalization of BM\_5000 revealed a similar trend of permeabilities and layer thicknesses as function of monomer concentration. Besides permeability and layer thickness, selecting optimal prefunctionalization for BM\_5000 was based on the ratio between monomer concentration and pore size obtained for BM\_1000. Thus in this case, with layer thicknesses of about 1.3 and 0.7  $\mu\text{m}$  at RT and 45 °C respectively, 10 % monomer concentration was considered more appropriate for prefunctionalization BM\_5000 (for the influence of prefunctionalization towards stability of HPFCM; *c.f.* 4.6.1.2)

### 4.5.2 Degree of Grafting

Another parameter that should be considered for selecting the optimal prefunctionalization is the so-called degree of functionalization (DOF) or precisely degree of grafting. This parameter was obtained from the mass of polymer grafted on the membrane surface. Despite of various pore sizes of BM, similar DOF was observed (except for BM\_200; Figure 4.45). For these BM between 400 and 5000 nm, DOF were in the range of about 100  $\mu\text{g}/\text{cm}^2$ . The fraction of DOF obtained from prefunctionalization to the total DOF was about 1-15 % (*c.f.* 4.6.2.1). Based on this data, the DOF revealed that moderate prefunctionalization was obtained.

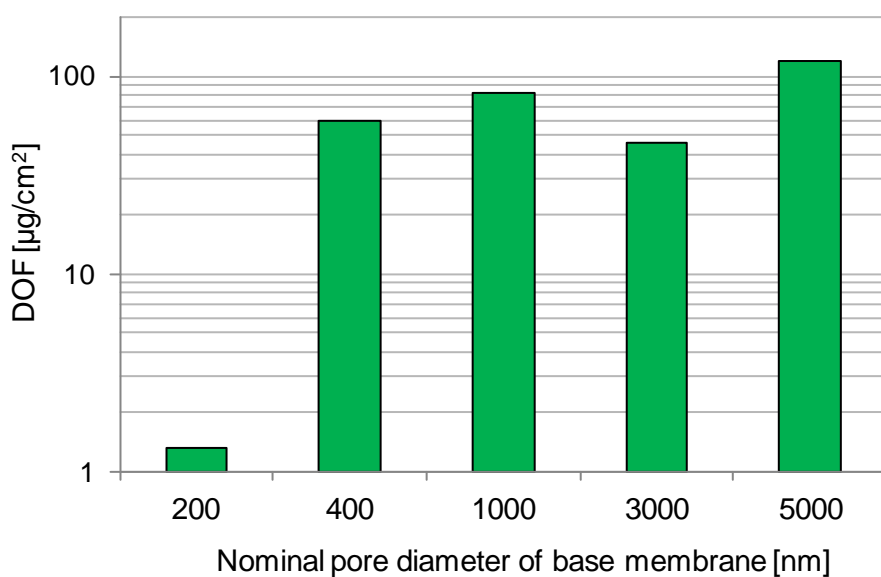


**Figure 4.45** Degree of functionalization (DOF) of grafted PNIPAAm for base membranes with different nominal pore diameter (monomer concentrations [wt %] / nominal pore diameter of base membranes [nm]: 1.0 / 200; 1.5 / 400; 2.5 / 1000; 7.5 / 3000; 10 / 5000).



### 4.5.3 Switchability of Membrane Pore after Prefunctionalization

On one hand, a minimum of some 10 nm layer thickness would provide sufficient probability for chain entanglement between grafted and network polymer. On the other hand, the fraction of grafted polymer should only be small relative to the total polymer in the pore.

With this consideration, the monomer concentration had been varied with the pore size of BM from 1 to 10 wt% in order to adjust the degree of functionalization (Figure 4.45). Compared to unmodified BM, the decrease in water permeability after prefunctionalization step indicated that pore narrowing has taken place. This had been used to calculate the hydrodynamic layer thickness as shown in Figure 4.46. It can clearly be seen that the thickness of grafted layer increased with increasing monomer concentrations which had been adapted to the pore radius of each BM. As a result, similar ratios between layer thickness at RT and pore radius were obtained (Figure 4.46). When examining the data at 45 °C, a considerable decrease in layer thickness was observed. This data had been obtained from water permeability measurements at 45 °C taking the decrease of viscosity into account. This result is associated with the temperature-responsivity of the grafted PNIPAAm chains (*c.f.* <sup>[31, 32, 43]</sup>).

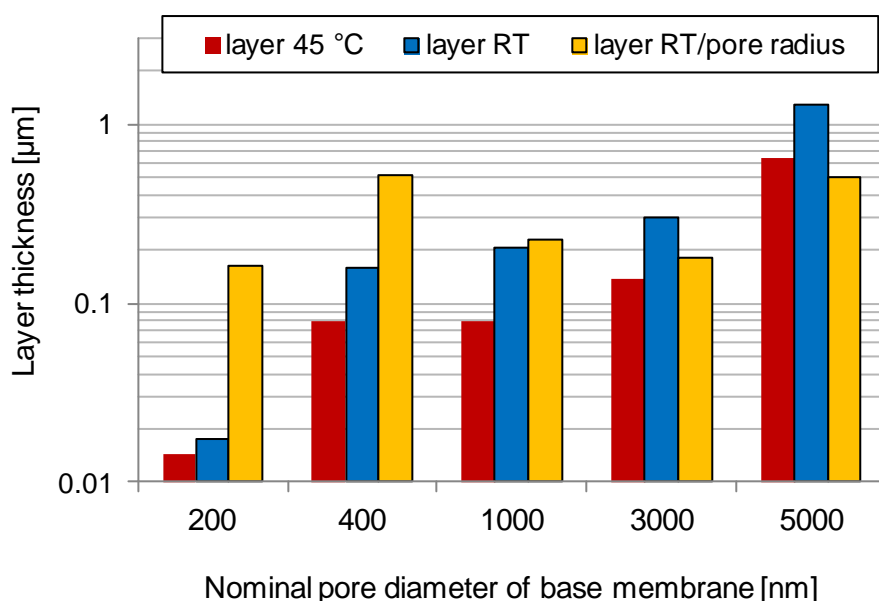


**Figure 4.46** Effective hydrodynamic layer thickness of grafted PNIPAAm at RT and 45 °C (calculated from water permeability before and after prefunctionalization using Hagen-Poiseuille equation; *c.f.* Figure 2.15) for base membranes with different nominal pore diameter.

## 4.6 Pore-Filling and Characterization of Pore-Filled Composite Membranes

The hydrogel network on one hand imposes a sieving structure and may be used to enhance size selectivity processes <sup>[1, 33-35]</sup>. On the other hand, incorporation of smart hydrogels into the membrane matrix *via* pore-filling allows for a tailored and switchable barrier due to stimuli-responsiveness of crosslinked PNIPAAm <sup>[33]</sup>. Therefore, this section focuses onto the selection of appropriate pore-filling conditions of PNIPAAm hydrogels intended for separation applications. Thereafter, a series of characterization was carried out in order to investigate the microstructure of hydrogel networks and separation functions of such novel composite membranes.

### 4.6.1 Pore-Filling under 'Open' System

In the beginning of this work, the pore-filling functionalization of PNIPAAm hydrogels was carried out under 'open' system. Open system means that the equilibration of base membranes with monomer solution took place directly within two glass plates prior to UV irradiation (*c.f.* Figure 3.5). The pore-filling under an open system was done only to BM\_5000 and 15 min UV time using composition M15DC05. The HPFCM with DOF between 90-300  $\mu\text{g}/\text{cm}^2$  were obtained. Other data obtained from these investigations are discussed in 4.6.1.1 to 4.6.1.3.

#### 4.6.1.1 Permeability

The water permeability data obtained after pore-filling with and without prefunctionalization steps are shown in Table 4.15. Here, it can be seen that water permeability after pore-filling was significantly reduced; about 3 fold from values for unmodified BM. The water permeability for HPFCM obtained after prefunctionalization was slightly lower than those prepared without prefunctionalization. This signified that the prefunctionalization did not interfere with the pore-filled hydrogel network to the larger extent.

Despite of its large reduction, these water permeabilities were still considered very high. These data were used to investigate the microstructure of HPFCM using Darcy model (*c.f.* Figure 2.15). As can be seen in Table 4.15, the Darcy mean mesh size for HPFCM obtained under open functionalization system was  $\sim 20$  to 23 times larger than the mesh size of bulk gel from the same composition (6.0 nm; *c.f.* Table 4.10 in 4.1.2.4.7). Since only the average of mesh size could be determined from Darcy model, the apparently large mesh sizes in Table 4.15 may imply that some pores were still open. Hence, the permeability reduction may indicate that the pores of were not completely and evenly filled with hydrogels in its entire volume but somehow the pore entrances were blocked or reduced in size.

Preliminary experiments on the size-selectivity of HPFCM were carried out using dextran molecular probe (2000 kg/mol). A further decrease in permeability was observed; i.e.  $< 20000 \text{ l}/\text{m}^2\text{hbar}$  when

solution of high molecular weight dextran was filtered through the HPFCM (Table 4.15). At this stage pore-filling of the membrane pores was not completely achieved and therefore displayed no size-selectivity.

**Table 4.15 Water and dextran solution permeabilities for HPFCM prepared either with or without prefunctionalization step; base membrane: 5000 nm (hydrostatic pressure).**

HPFCM	Permeability, RT [l/m <sup>2</sup> hbar]		Darcy Mean mesh size at RT [nm]
	Water	Dextran solution 2000 kg/mol	
without prefunctionalization	37 555 ± 8 542	18 002	142 ± 17
5% prefunctionalized	26 943 ± 6 733	12 056	123 ± 13
10% prefunctionalized	22 821 ± 3 919	8 525	119 ± 10

#### 4.6.1.2 Switchability and Stability

Water permeabilities of HPFCM based on BM\_5000 measured at RT and 45 °C revealed a very pronounced temperature-responsive switching effect (Figure 4.47). This implied that the barrier pores of the HPFCM can be enlarged or shrunk as the crosslinked PNIPAAm swells or deswells in the vicinity of its LCST. After each water permeability measurement at 45 °C, the water permeability at 20 °C was re-measured to examine the flux recovery. Here, recovery close to 100 % was observed only for HPFCM prepared with the highest prefunctionalization (10 %). For HPFCM obtained without prefunctionalization, higher permeability regain after permeability measurement at 45 °C suggested that the voids at the interface may form during shrinkage of the gels above LCST. Thus, prefunctionalization step by grafting linear PNIPAAm chains to membrane pore wall is necessary<sup>[45]</sup>. In this case the 10 % prefunctionalization was found to be appropriate to prevent the void formation as well providing the anchoring effect for hydrogels to the membrane pore.

The stability of HPFCM was further explored by measuring the water permeability as a function of pressure (Figure 4.48). The significant decrease in permeability was observed for HPFCM obtained without prefunctionalization. The data suggested that the compression of hydrogel may take place as the pressure increased. Water permeabilities for HPFCM with different prefunctionalization ratio were also compared. Based on Figure 4.48a, less pressure dependence was seen for prefunctionalized HPFCM, which suggested that the hydrogel has been stabilized within the pore through the prefunctionalization. Data provide trustworthy evidence that the gels remained within the porous support. Furthermore, the permeability of prefunctionalized HPFCM was re-measured at low pressure

with good recovery values. Most likely, a slight deformation observed for these composite membranes is reversible. The almost 100 % recovery data also suggested that the hydrogel has been anchored to pore wall by prefunctionalized PNIPAAm chains and remained non-ejectable (Figure 4.48b). The HPFCM which was not prefunctionalized had larger recovery permeability ( $\sim 140\%$ ) as compared to prefunctionalized HPFCM. This implied that this particular composite membrane was less stable; compression effect may impose a permanent deformation to the hydrogel structure.

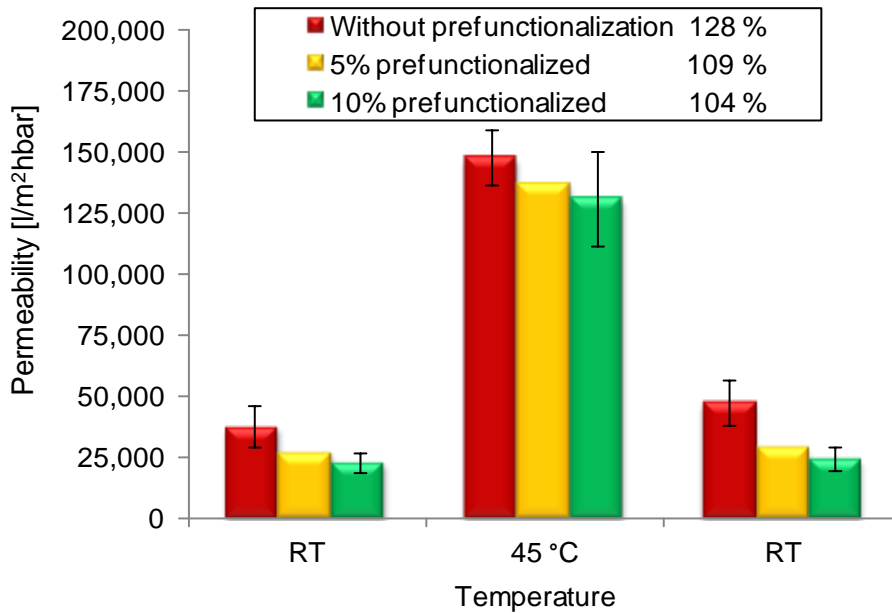


**Figure 4.47** Reversible temperature responsivity of water permeability for HPFCM prepared either with or without prefunctionalization step and their corresponding recovery values; base membrane: 5000 nm (hydrostatic pressure).

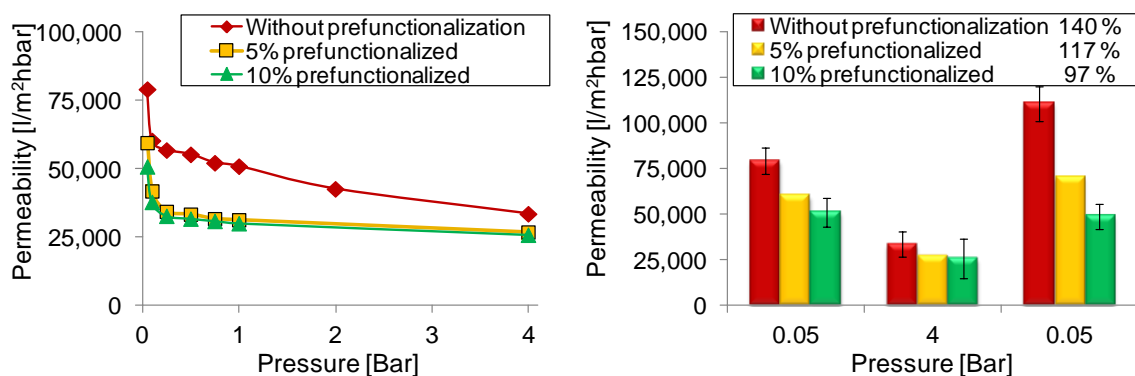


**Figure 4.48** Water permeability for HPFCM prepared either with or without prefunctionalization step as a function of pressure (left) and their corresponding recovery values (right); base membrane: 5000 nm.

#### 4.6.1.3 Scanning electron microscopy

The morphology of composite membranes obtained under open pore-filling system was examined (Figure 4.49). This preparation can minimize the functionalization on the membrane outer surface, but leads to a heterogeneous modified membrane. This may attribute to air leaks between the glass plates and discontinuously distributed filling of monomer solution in the membrane. Thus, it can be clearly seen than some pores were still widely open and some pores were partially filled. Note that, this HPFCM was obtained without prefunctionalization. It is postulated that the precondition of homogeneous pore-filling also relies on prefunctionalization.

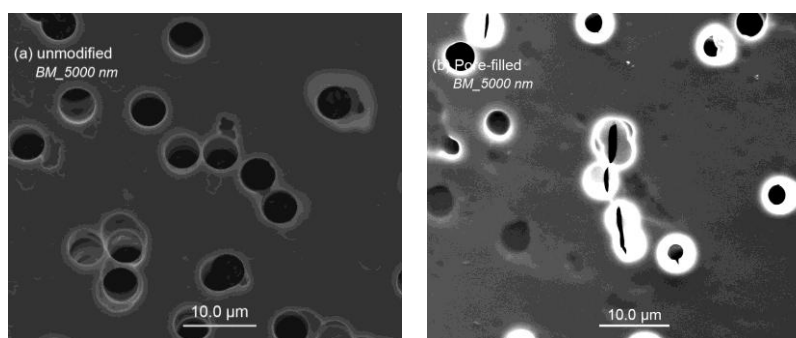


**Figure 4.49** SEM micrographs of the outer surface of unmodified PET membranes (left) and HPFCM after 15 min UV irradiation (hydrogel composition: M15DC05, right); nominal based membrane pore size had been 5000 nm.

#### 4.6.1.4 'Open' pore-filling: some remarks for improvement

The HPFCM data from 4.6.1.1 to 4.6.1.3 clearly revealed that pore-filling under open functionalization system was less successful. This has imposed the needs to optimize the pore-filling conditions in order to achieve complete and homogeneous pore-filling. It is postulated that the crucial step in preparation of HPFCM lies on the equilibration step, during which the filling of the pores with monomer solution takes place. Under open system, air may trap as the upper glass plate is placed onto the equilibrated membrane (*c.f.* Figure 3.5). This may impose the risk of heterogeneous pore-filling; yielding the barrier pores with unpolymerized monomer at the region where air was trapped. Therefore, pore-filling must be designed in such a way that any trapped air bubble can be removed during the filling equilibration prior to *in situ* polymerization (*c.f.* Figure 3.6) and the re-entrance of air is eliminated. Hence, the pore-filling must be done in a close system and considering prefunctionalization as the primary step (*c.f.* 4.6.2). Yet it may be envisioned that the size-selective features can be further enhanced *via* 'closed' pore-filling (*c.f.* 4.6.3.5 and 4.6.3.6).

## 4.6.2 Pore-filling under 'Closed' System: General Characterization

The data in 4.6.1 suggested that pore-filling functionalization must be established under 'closed' system; the equilibrated BM with monomer solution was subjected to UV irradiation under vacuum (*c.f.* Figure 3.6). These subsections reported on general characterization of HPFCM obtained under closed system. Data on membrane performance is reported in the next subsection (4.6.3).

### 4.6.2.1 Degree of pore-filling

Depending on pore size of BM as well as UV irradiation time, DOF values of 520 to 745  $\mu\text{g}/\text{cm}^2$  were obtained (Table 4.16). Comparing the unmodified, prefunctionalized and pore-filled composite membranes, a greater DOF can be observed, which would indicate that functionalization has taken place to a greater extent within the membrane pore rather than their outer surface. For instance, for HPFCM prepared with BM\_1000 and 15 min UV time, a slight increase in thickness ( $\sim 2 \mu\text{m}$ ) had been observed. This observation may indicate that polymer could have been grafted on the outer surface but this was a small fraction compared to the fraction inside the membrane pores. In general, the DOF increased with reaction time and showed a tendency to level off (the difference between 15 and 20 min for BM\_1000 is within error range); this is an indication that full conversion of PNIPAAm into a hydrogel network was achieved <sup>[41]</sup>. For BM\_400, DOF was already at relatively high level after 5 min but further increased with irradiation time. For BM\_200, DOF was significantly smaller for 5 and 10 min of irradiation compared to 15 min. At 15 min of irradiation, similar DOF independent of pore size of BM was observed (*c.f.* Table 4.16). In view of the resulting composite membrane, similar DOF for membranes with similar porosity (*c.f.* Table 3.6 in 3.1.2) can be related to a similar degree of pore-filling. That newly introduced polymer network in the membrane pores should determine the barrier properties because the fraction of grafted polymer introduced in the prefunctionalization step was small, i.e.,  $\sim 1, 8, 10,$  and  $15 \%$  of the total DOF for BM\_200, BM\_400, BM\_1000, and BM\_5000, respectively; *c.f.* Figure 4.45 and Table 4.16).

**Table 4.16 Degree of functionalization for HPFCM prepared from various base membranes and using varied UV irradiation time.**

HPFCM	DOF [ $\mu\text{g}/\text{cm}^2$ ]			
	5 min	10 min	15 min	20 min
BM_200	595 $\pm$ 90	520	730 $\pm$ 30	n.d.
BM_400	525	630	670 $\pm$ 110	n.d.
BM_1000	n.d.	n.d.	720 $\pm$ 45	745
BM_5000	n.d.	n.d.	691 $\pm$ 135	n.d.

*n.d.* ... not done

HPFCM were also obtained from various hydrogel compositions using BM\_1000 and 15 min UV time. The DOF determined for these hydrogels are given in Table 4.17. An increase in DOF with increasing monomer or crosslinker content can be seen. Clearly, higher monomer or crosslinker content attributed to a greater molecular weight of crosslinked polymers provided that degree of conversion is also sufficiently high. Here, the DOF from the composition with the highest crosslinker content (M15DC10) deviated from this general trend. The conversion of this particular hydrogel in its bulk state was relatively low (< 95 %; *c.f.* Table 4.8 in 4.1.2.3) as compared to hydrogel from other compositions which might explain the aforementioned discrepancy. Furthermore, it was most likely that a decrease in DOF for HPFCM with concentrated compositions can be attributed to gel effects; an increase in viscosity imposed hindrance to the further growth of polymer chains especially in a limited volume. Nevertheless, the DOF data suggested a complete and evenly pore-filling functionalization were accomplished.

In the early part of this work, pore-filling was also carried out *via* redox initiation based on the conditions established for bulk, redox-polymerized hydrogel (TEMED/APS 4.0 : 1). The largest DOF was obtained for this HPFCM as shown in Table 4.17. From the rheology data (*c.f.* 4.1.1.4.2), the onset of gelation was < 1 min and the reaction was (~ 5 min) completed sooner than the time required of pore-filling equilibration (10 min). Therefore, the DOF also comprised a fraction of grafted polymer on the membrane outer surface that contributed to an increase of dried layer thickness of about 6-10  $\mu\text{m}$ . The redox pore-filling conditions could be improved using an initiator TEMED/APS 0.5 : 1. But this was not established in this study.

**Table 4.17 Degree of functionalization for HPFCM based on BM\_1000 prepared from various hydrogel compositions. Pore-filling conditions were as for bulk gels (*c.f.* Table 4.8).**

HPFCM	DOF [ $\mu\text{g}/\text{cm}^2$ ]
<b>M10DC05</b>	430 $\pm$ 109
M15DC02	591 $\pm$ 229
M15DC05	720 $\pm$ 45
* M15DC05	780
M15DC10	644 $\pm$ 186

\* *Redox pore-filling*

#### 4.6.2.2 Scanning electron microscopy

The morphology investigation with SEM can be used to elucidate the pore-filling functionalization. Figure 4.50 shows the SEM micrographs of both cross-section and outer surface of the unmodified, prefunctionalized and pore-filled membranes from BM\_1000.

Note that the prefunctionalization steps did not change the pore morphology but, similar to previous work<sup>[201]</sup>, only reduced the size of the membrane pores (Figure 4.50b and e).

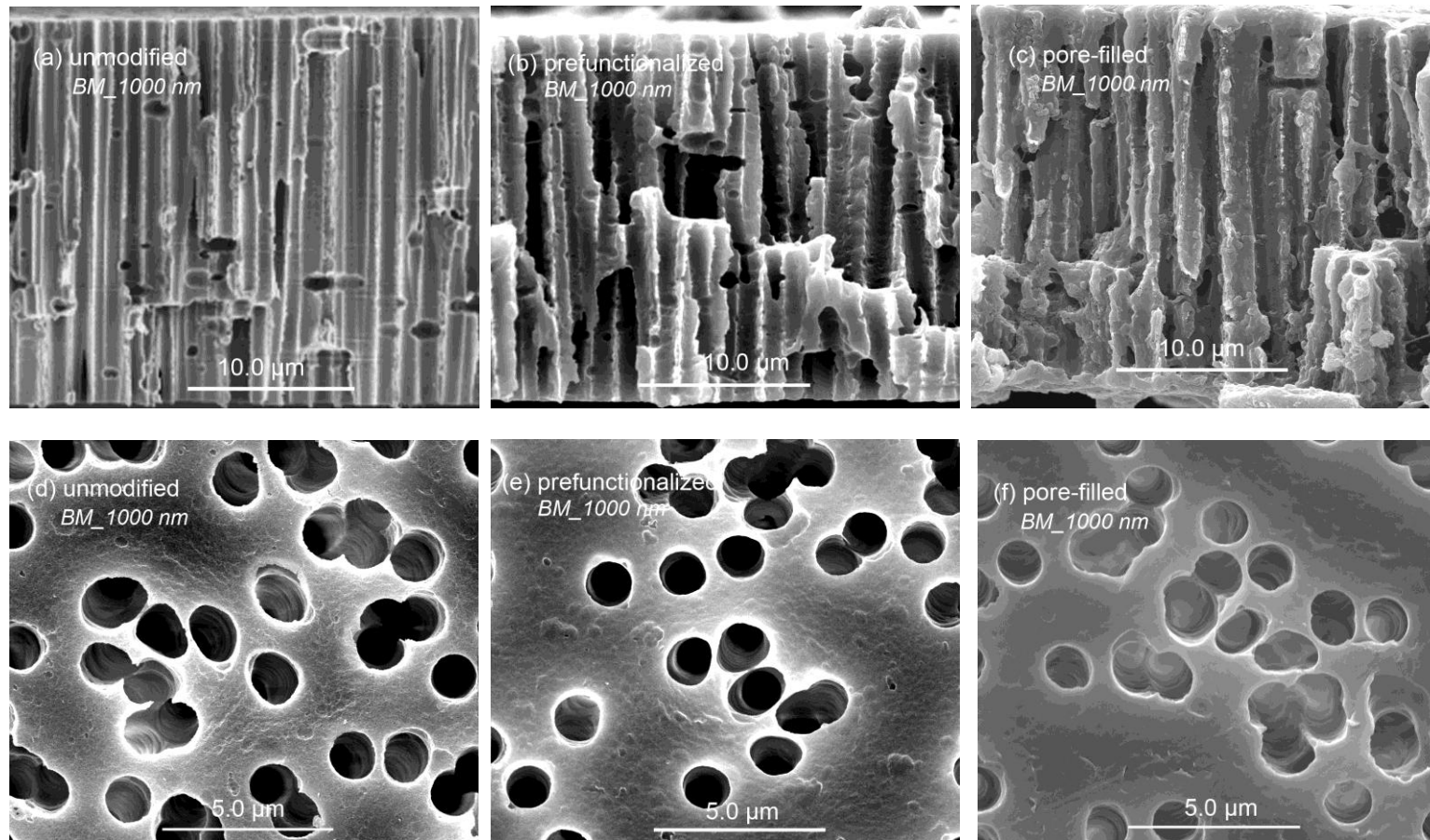


**Figure 4.50** SEM micrographs of the cross sectional view (above) and the outer surface (below) of unmodified membranes (left), of prefunctionalized membranes (middle), and HPFCM after 15 min UV irradiation (hydrogel composition: M15DC05, right); nominal base membrane pore size had been 1000 nm.



Figure 4.51 reveals the morphology of unmodified membranes and HPFCM from BM\_200 and BM\_400 obtained with 80000- and 40000-fold magnification, respectively. Upon close inspection, the filling of the pores due to functionalization can be seen for HPFCM. One can see in the depth of each pore material with a different contrast what is not at all presented in the unmodified membrane. The morphology of hydrogel pore-filled membranes becomes more pronounced particularly within smaller BM membranes (Figure 4.51). The appearance of these newly introduced materials can be related to the morphology of freeze-dried bulk gels which have macropores with a diameter of several  $\mu\text{m}$  and smooth lamellar pore walls (SEM micrograph of bulk hydrogel; *c.f.* Figure 4.19 in 4.1.2.6). In the depth of the membrane pores which have smaller or similar diameter, analogous lamellae would be formed from the pore surface-anchored hydrogel during the freeze-drying process. This observation is in a good agreement with such high DOF ( $> 670 \mu\text{g}/\text{cm}^2$ ). These results could also imply that pore-filling functionalization under close system took place homogeneously over the entire volume of the pores of the membrane. Compared to the base membranes, the HPFCM appeared with slightly smoothed surface which may indicate a very thin layer of hydrogel on the outer membrane surface.

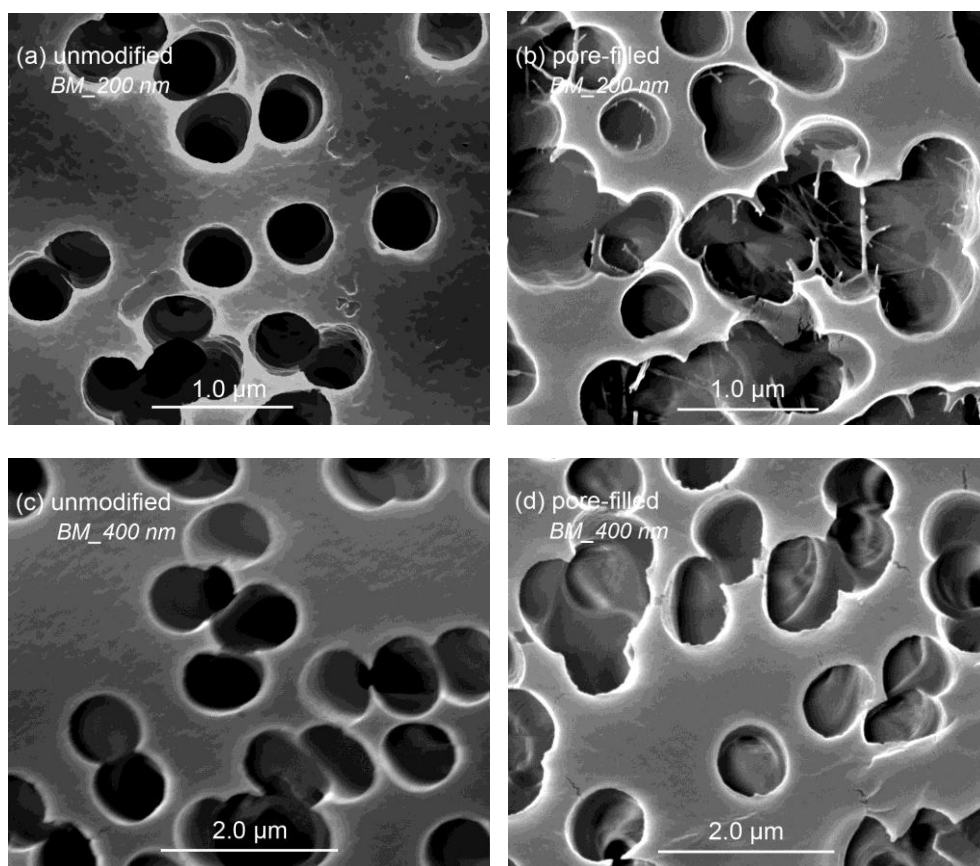


**Figure 4.51** SEM micrographs of the outer surface of unmodified PET membranes (left) and HPFCM after 15 min UV irradiation (hydrogel composition: M15DC05, right); nominal base membrane pore size had been 400 nm (above) and 1000 nm (below).

### 4.6.3 Pore-filling under 'Closed' System: Functional Characterization

#### 4.6.3.1 Water permeability

To further investigate the effect of pore-filling, water permeability data at RT through HPFCM (Figure 4.52) and for unmodified BM (Table 4.14) were compared. The influences of UV irradiation time and of BM pore size onto permeability of HPFCM were concerned. At first glance, a very pronounced decrease in water permeability; i.e., by ~3-5 orders of magnitude relative to the unmodified membranes was observed. It should be noted that this measurement has been done below the LCST of PNIPAAm, where the gel network is in the swollen state and thus expected to impose strong hindrance for convective liquid transport. While the hydrogel is constrained within the BM, transport can occur in the void spacing of hydrophilic chains connected by crosslinking points (*c.f.* Figure 2.15).

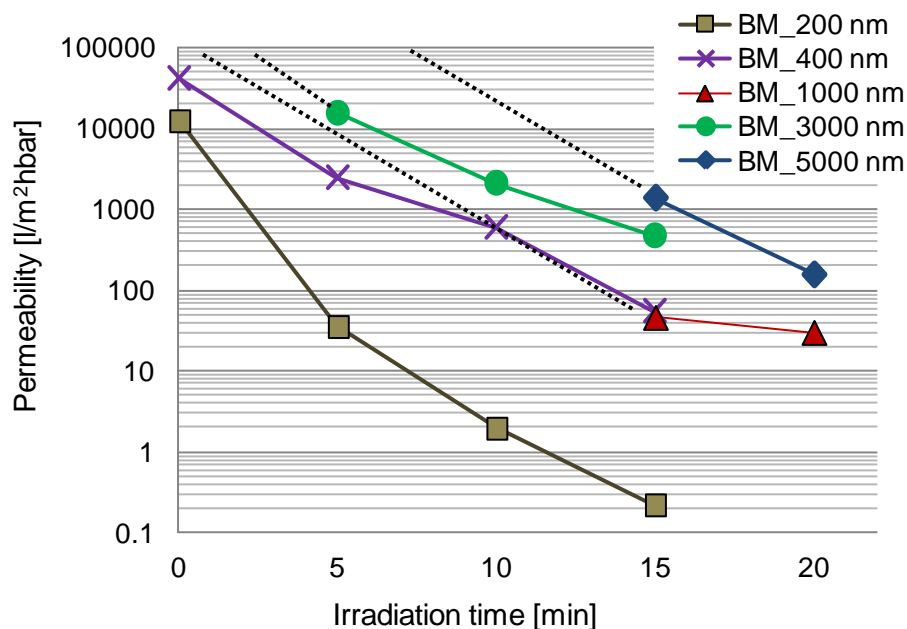


**Figure 4.52** Water permeability at RT of HPFCM based on PET membranes with different nominal pore sizes as function of UV irradiation time during preparation; the dotted lines are projections to the permeabilities of the precursor membranes, i.e., PET membranes after the prefunctionalization step.

As seen in Figure 4.52, the reduction of water permeability was already observed after 5 min of UV irradiation time. This could imply that pore-filling functionalization took place already. BM is relatively thin; thus penetration of UV light is possible and is, together with suited concentration of an efficient PI, enabling *in situ* filling polymerization in short time. Note that increasing the irradiation time

systematically enhanced DOF until 15 min (*c.f.* Table 4.16) and caused also a systematic reduction in permeability. Hence, an increased polymer volume fraction caused that the barrier of HPFCM became denser with longer irradiation time. The most pronounced effect of functionalization was observed at 15 min which was caused by sufficiently high degree of conversion. Such remarkable difference of permeability between unmodified and composite membranes (*i.e.*, between 0 and 15 min irradiation) seemed to have shifted the barrier resistance of the HPFCM into the UF range. A further increase of irradiation time ( $> 15$  min) still considerably changed permeability of HPFCM based on BM\_5000. The resulting permeability of this particular HPFCM was in the range similar to HPFCM based on smaller BM pore sizes (3000 and 1000 nm). This permeability change might be due to a small further increase of monomer conversion or UV effects onto the gel structure leading to a more consolidated hydrogel structure.

The same overall trend of permeability was observed for all HPFCM, but with distinct differences as function of base pore size. The smaller the pores of BM, the stronger reduction of permeabilities was observed. This can be explained by confinement effect. Within too large BM pores (BM\_3000, BM\_5000), the pore-filling was in the regime where insufficient confinement cannot completely immobilize the hydrogel, and thus it may deform under the measurement conditions. As a result, lower resistance towards convective water flow was imposed with bigger BM pores of HPFCM (Figure 4.52). Following the trend in Figure 4.52, the permeabilities of HPFCM based on BM\_400 and BM\_1000 approached each other with increasing UV irradiation time; preparations with 15 min UV time lead to the same barrier property. Apparently these medium pore sizes of BM were in the range where confinement did not affect the swelling and hydraulic resistance much. It is also worth to discuss that the thin hydrogel layers grafted on the BM outer surface during the pore-filling functionalization (*c.f.* 4.5) are less confined compared to the pore-filled hydrogel. The thickness of these layers is also much smaller than the lengths of the gel-filled pores. Thus, the specific flow resistance imposed by this layer is also comparably small. Consequently, the trans-membrane transport was controlled by the hydrogel filled within the membrane pores.

**Table 4.18** Water permeabilities for HPFCM from various compositions; base membrane: 1000 nm. Pore-filling conditions are analogous to Table 4.17.

HPFCM	Water Permeability after Pore-Filling Functionalization, RT [ $l/m^2hbar$ ]
<b>M10DC05</b>	319
M15DC02	24
M15DC05	46
M15DC10	26

Water permeabilities were also measured for HPFCM based on BM\_1000 from various compositions as shown in Table 4.18. Significant permeability dependence on monomer concentration can be seen. Low monomer content was postulated to result in the less dense barrier of HPFCM. The less dense barrier of such compositions leads to higher water permeability. The crosslinker content has also influence towards barrier properties. From bulk hydrogels, it was known that small crosslinker content has led to higher swelling. However, in a membrane formats, the gels are allowed to swell only in vertical direction and this impose resistance towards the transport (Figure 4.53) and resulted in a decrease of permeability (Table 4.18). Subsequently, if the fractions of crosslinker are too high, the denser barrier also imposed transport restrictions.

#### 4.6.3.2 Microstructure of pore-filled hydrogel composite membranes

Using Darcy model (*c.f.* Figure 2.15), the microstructure of pore-filled hydrogel could be estimated; i.e. the average mesh-size between the polymer chains forming the hydrogel network within membrane pore. As seen from Table 4.19, the microstructure of HPFCM from the same composition (M15DC05) remarkably reduced to a smaller mesh-size. It is postulated that microstructure of HPFCM strictly dependent on two factors: (i) the volume expansion behaviour of the hydrogels, and (ii) confinement effect imposed by the BM. As already explained in the previous subsection (4.1.2.3), hydrogel cannot be directly obtained under free swelling equilibrium from its synthesis state in a limited volume. The same will be true for PNIPAAm in the cylindrical pores. For analogous bulk gels (M15DC05) a volume expansion by a factor of 1.33 from the synthesis to equilibrium state had been measured (Table 4.9)<sup>[41]</sup>. The average mesh size estimated from the degree of free swelling was 6.0 nm. Obviously, PNIPAAm gels synthesized in the cylindrical membrane pores therefore have relatively smaller mesh-sizes attributed to their restricted volume expansion.

**Table 4.19 Darcy mean mesh-size for HPFCM prepared from various base membranes (hydrogel composition: M15DC05) determined from Darcy model (*c.f.* Figure 2.15).**

HPFCM	Darcy mean mesh-size [nm]
BM 200_RT	0.4
BM 400_RT	4.7
BM 1000_RT	4.8
BM 1000_45°C	14.6

On the other hand, confinement effect may contribute to the microstructure of pore-filled hydrogel as a function of its BM pore-size. Since all membranes have the same thickness, the aspect ratio is larger for smaller BM pores. Consequently, the effect of suppressed gel swelling in the horizontal direction, i.e., hydrogel confinement, should be more pronounced for smaller pores.

**Table 4.20 Darcy mean mesh-size for HPFCM prepared from various compositions (base membranes: 1000 nm) determined from Darcy model (c.f. Figure 2.15).**

HPFCM	Darcy mean mesh- size	Mesh size of bulk hydrogels from swelling
	[nm]	[nm]
<b>M10DC05</b>	12.8	6.6
<b>M15DC02</b>	3.4	10.9
<b>M15DC05</b>	4.8	6.0
<b>M15DC10</b>	3.9	4.0

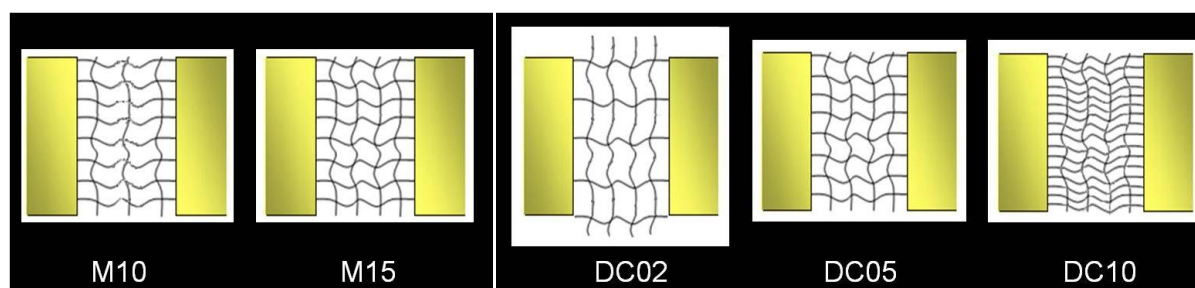


**Figure 4.53 Schematic representations of microstructure of HPFCM and the influence of monomer (M10 and M15) and crosslinker content (DC02, DC05 and DC10). The less crosslinked hydrogels tend to swell in the vertical direction.**

It was also observed that the permeability of HPFCM was largely influenced by monomer content (Table 4.18). The permeability of HPFCM with 10 wt% monomer (M10DC05) is significantly higher as compared to their composition with larger monomer fractions. Both hydrogels had only small difference in their volume expansion factor (Table 4.9). These data therefore suggested that in the less dense hydrogel network, a relatively bigger space is available for the water transport (Table 4.20 and Figure 4.53).

However, the crosslinking ratio imposed not straightforward permeability trend onto mesh-size as compared to monomer content. Even the HPFCM from composition with the lowest crosslinker had a smaller mesh size than the middle composition (M15DC02 vs. M15DC05). Again, the volume expansion factor of hydrogels from various compositions must be referred to. Also, the influence of

crosslinker on the microstructure of HPFCM was explained with the help of Figure 4.53. In this figure, it can be seen that the mesh size from composition M15DC02 relatively larger as compared to their DC05 counterpart. Based on the volume expansion data, hydrogel from composition M15DC02 expanded more than 30 % as compared to composition M15DC05 (*c.f.* Table 4.9). Confining the M15DC02 hydrogel in membrane pores has led into swelling of the network in a vertical direction. This has imposed a greater resistance towards hydraulic permeability (4.6.3.1) which in turns gave rise to an overall average of smaller Darcy mesh-size as compared to their mesh size in the bulk state (Table 4.20).

There were two major remarks with respect to the HPFCM from the composition with highest crosslinker content (M15DC10). First, Darcy mean mesh-size of this particular HPFCM was smaller than HPFCM from composition M15DC05. Based on its water permeability data in Table 4.18 and also the model in Figure 4.53, the explanation is rather straightforward; it was due a denser barrier of HPFCM. And secondly, microstructure of HPFCM from analogous composition was identical to the mesh-size in its bulk state (Table 4.20). Interestingly, this data is in agreement with the negligible volume expansion factor of only 1 % from Table 4.9 (*c.f.* 4.1.2.3)

#### 4.6.3.3 Stability

*Influence of prefunctionalization.* The stability of HPFCM was investigated by studying the flux as a function of TMP. The constant permeability without hysteresis would indicate absence of hydrogel deformation or delamination from the pore wall. For this purpose, the data for the HPFCM prepared with and without prefunctionalization step were compared in Figure 4.54.

The pressure dependent permeability data provide trustworthy evidence that the gels remained within the porous support. Only small pressure dependence of permeability up to 4 bar was observed for HPFCM based on prefunctionalized BM\_5000. No significant changes could be detected for HPFCM based on prefunctionalized BM\_400 and BM\_1000. This difference as function of pore size may be taken as indication for the enhanced gel stabilization in relatively smaller pores. However, changes, i.e., decreasing permeability with increasing pressure, were more pronounced for HPFCM prepared without prefunctionalization. Further, the permeabilities at low pressure were re-measured. A very good recovery was obtained for prefunctionalized HPFCM (92-125 % for all measured samples), while HPFCM without prefunctionalization had much higher fluxes after this cycle of measurements (> 135 % for all measured samples). This means that the pore-filled hydrogels were mechanically stabilized due to the prefunctionalization; i.e., the PNIPAAm hydrogel was fixed on the pore surface of the BM through entanglement with grafted PNIPAAm chains (*c.f.* Figure 1.3).

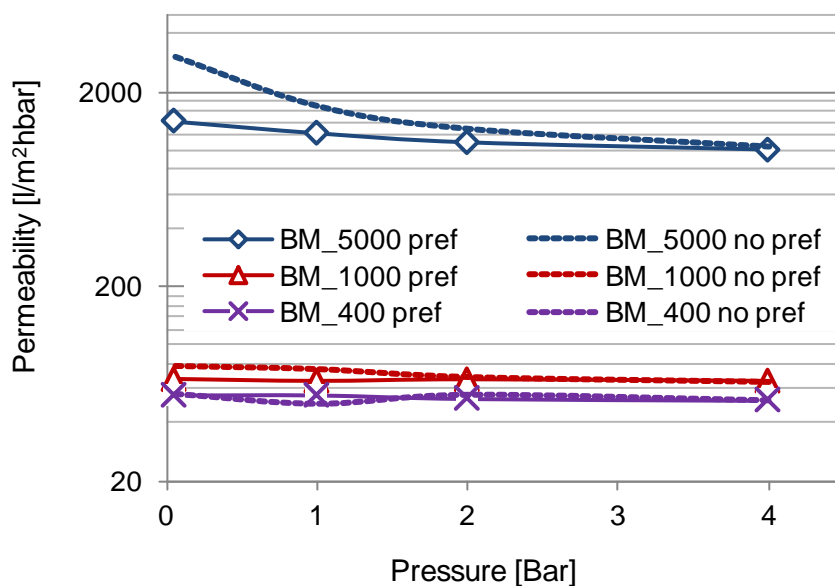


**Figure 4.54** Pressure dependence of water permeability at RT for HPFCM with different base membrane pore size. Measurement has been done by step-wise increasing the pressure (40 min. at each stage) with HPFCM prepared at 15 min of UV irradiation using BM without and with prefunctionalization.

#### 4.6.3.4 Temperature-responsive permeability

Data to illustrate the effect of temperature onto the reversible pore opening of the composite membranes that is triggered by the “smart” pore-filling hydrogel are shown in Figure 4.55. This is done by comparing the water permeability data at RT and beyond LCST of PNIPAAm (45 °C) at constant TMP (0.5 bar).

At a temperature below the LCST of the PNIPAAm, the hydration by water molecules that are bound to the segments of the polymer network leads to a swelling of the hydrogel. At a temperature above the LCST the deswelling process of PNIPAAm gel occurs due to decreasing hydration because of broken hydrogen bonds and increasing agglomeration of hydrophobic moieties. The result was an opening of the pores of the composite membrane. Therefore, the barrier structure of HPFCM can be switched to regulate (increase or decrease) the flux of pure water. The water permeability at RT was again measured after the measurement at 45 °C to determine the water flux recovery. As can be seen in Figure 4.55, recovery values close to 100 % showed that the switching is reversible, and this confirmed also the stability of the hydrogel within the membrane pores. The permeability data for HPFCM based on BM\_1000 at RT and 45 °C measured for at least 3 cycles is shown in Figure 4.56). Such high recovery was observed since the membrane-immobilized hydrogels did presumably not reach a collapsed structure as in the case for free standing bulk hydrogels (*c.f.* Figure 4.57).

As depicted in Figure 4.55b, water permeabilities both at RT and 45 °C were found to be a function of monomer concentrations. Accordingly, the permeability data at these two temperatures differ by several orders of magnitude. Again, this was due to switching of membrane barrier as a function temperature. The switching was from more close to more open structure when the gels collapsed above LCST. The good recovery values of the permeability at RT therefore provide convincing evidence that the switchability was also reversible. In addition, the degree of switching observed was highly dependent on hydrogel structure; higher degree of switching was observed with the lower gel fractions of the composite membrane.

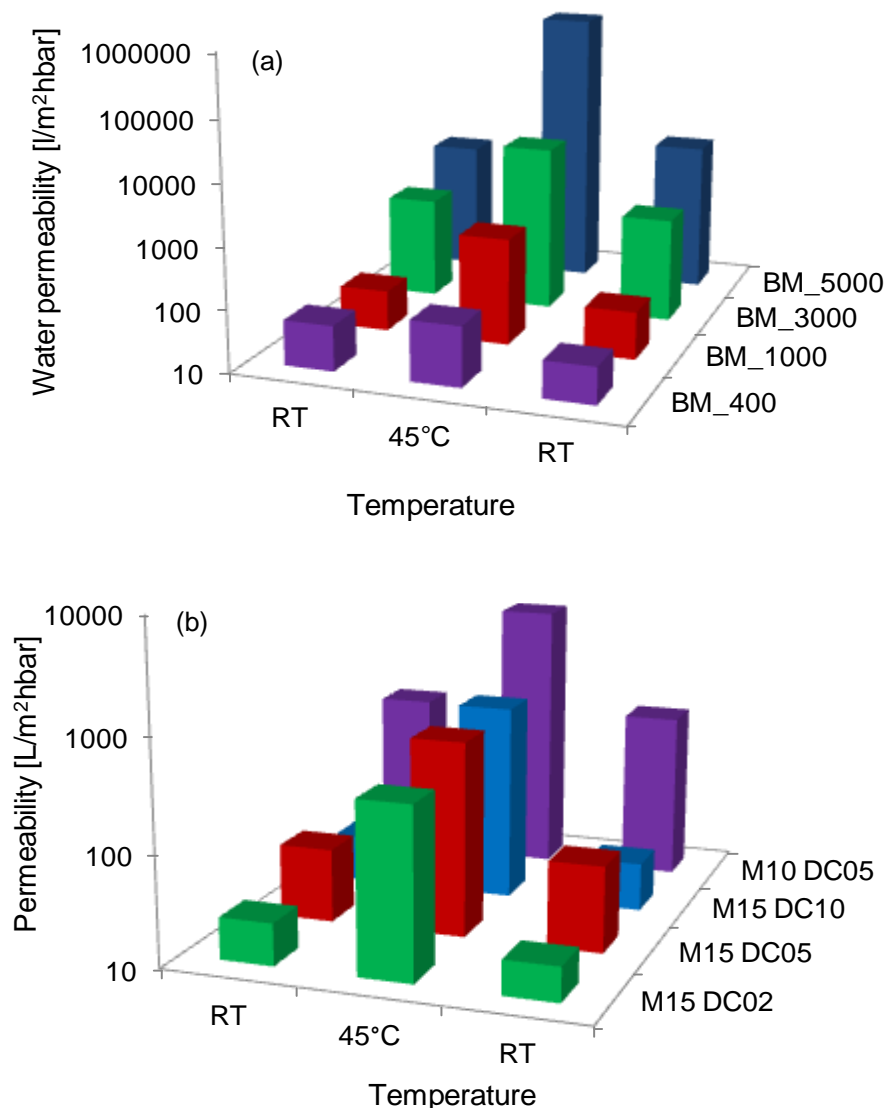


**Figure 4.55** Reversible temperature responsivity of water permeability for HPFCM: (a) with different base membrane pore size (hydrogel composition: M15DC05), and (b) with different compositions (BM\_1000).



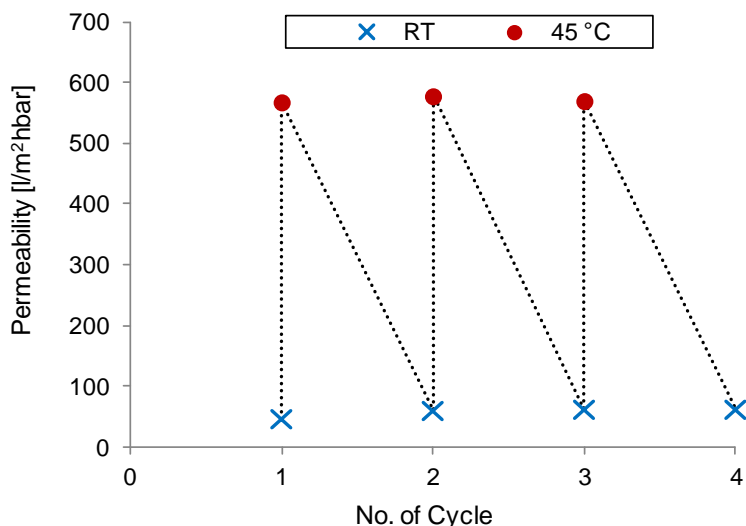


**Figure 4.56** Reversible temperature responsivity of water permeability for HPFCM prepared with base membrane 1000 nm.

Buehler and Anderson <sup>[76]</sup> had already explained the possible collapse mechanism of both types of hydrogels. Consistent to their argumentation, it is more likely that collapsed hydrogels constrained within membrane pores will undergo a microsyreresis rather than macrosyreresis, and this will prevent the material from delamination. Considering the different pore morphologies, an irregular one with very rough surface in case of pore-filled MF membranes and a cylindrical with rather smooth surface for track-etched membranes, the result of this study is even more remarkable. This is another confirmation that the PNIPAAm network chain segments were effectively entangled to the chains of grafted PNIPAAm prepared during prefunctionalization. It should further be noted that the degree of switching was smaller for HPFCM prepared with BM of smaller pore size since a higher degree of restriction to undergo conformational changes upon deswelling is imposed by the contact with the pore walls (confinement). Consequently, the changes of permeability were also much smaller than those observed for pore-filling grafted linear PNIPAAm <sup>[31, 32]</sup>.

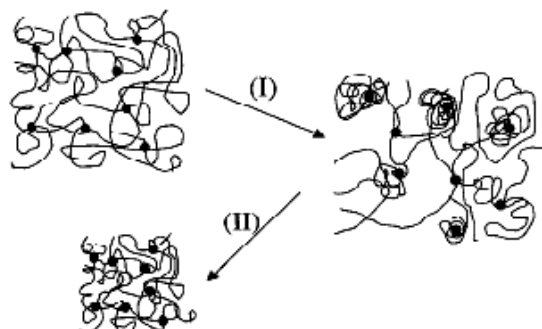


**Figure 4.57** Deswelling of hydrogels: microsyreresis (I) vs. macrosyreresis (II) <sup>[76]</sup>.

#### 4.6.3.5 Size-selectivity of pore-filled composite membranes under diffusion

The transport of macromolecules through HPFCM was studied under diffusion conditions to elucidate the size-selectivity of the resulting composite membranes (Table 4.21). Control experiments were performed with an unmodified PET track-etched membrane with a nominal pore diameter of 30 nm. A mixture of dextran solution with average molecular weights between 4 and 2000 kg/mol (corresponding to Stokes diameters of 3.0 and 54 nm, respectively) was used. The not diffused fraction of molecules after 24 hours diffusion time, expressed in terms of molecular weight cut-off (MWCO), is shown in Table 4.21.

##### 4.6.3.5.1 Effect of base membranes

Even when compared with the 30 nm unmodified PET membrane, the pore-filling functionalization significantly shifted the cut-off to a lower molecular weight. The solute transport was hindered by the hydrogel filled within the membrane pore. For identical hydrogel preparation conditions, the cut-off was much lower for membranes with smaller pore size of the BM. Indeed, the BM imposed confinement effects to pore-filled hydrogels and this was discussed in details in the previous subsection (*c.f.* Table 4.19; in 4.6.3.2). The MWCO was well correlated to the mesh-size determined from Darcy permeability <sup>[34, 35]</sup>. The noticeable MWCO under diffusion condition was therefore due to fractionation of macromolecules performed by sieving features of hydrogels network within the membrane pore. This was confirmed by having unchanged diffusion-based molecular size fractionation at much longer time. The significantly lower effective diffusion coefficients for the HPFCM as compared to the 30 nm track-etched membranes also confirm that the trans-membrane transport is largely controlled by the hydrogel network.

**Table 4.21** Sieving features for unmodified PET membranes (30 nm) and HPFCM from base membranes after 24 h and 1 week diffusion time, expressed in terms of molecular weight cut off (fraction of dextran of which the concentration in the permeate had been reduced by 90 % relative to the feed), revealing their correlation with the microstructure of the hydrogel (*c.f.* Table 4.19), and effective diffusion coefficients of the 4 kg/mol dextran fraction. HPFCM were prepared from composition M15DC05.

Membrane / HPFCM	MWCO after 24 h [g/mol]	MWCO after 1 week [g/mol]	Dextran diffusion coefficient (for 4 kg/mol fraction) $10^{-11}$ * [m <sup>2</sup> /s]
<i>Unmodified</i> BM 30_RT	17 900	n.d.	5.4
<i>HPFCM</i>			
BM 200_RT	6 600	6 600	0.9
BM 400_RT	8 100	8 100	1.4
BM 1000_RT	7 500	n.d.	1.2

#### 4.6.3.5.2 Effect of hydrogel composition

In this study, the effect of hydrogel composition on the distribution of undiffused fraction of dextran molecules in HPFCM was also explored.

**Table 4.22** Sieving features for HPFCM from various compositions after 24 h diffusion time and at RT, revealing their correlation with the microstructure of the hydrogel (*c.f.* Table 4.20), and effective diffusion coefficients of the 4 kg/mol dextran fraction. HPFCM were prepared from base membranes 1000 nm.

HPFCM	MWCO after 24 h [g/mol]		Dextran diffusion coefficient (for 4 kg/mol fraction) $10^{-11}$ * [m <sup>2</sup> /s]	
	RT	45 °C	RT	45 °C
<i>Unmodified</i> BM_30	17 900	19 500	5.4	14.5
M10DC05	15 400	220 000	2.8	3.9
M15DC02	3 000	1 102 000	2.4	3.6
M15DC05	7 500	12 900	1.2	4.4
M15DC10	5 000	5 900	3.3	4.0

At RT, A series of MWCO between about 3000 and 8000 g/mol was obtained for compositions with high monomer content (M15, Table 4.22). From here, the cutoff for highest crosslinker content of HPFCM; DC10 was higher than DC05, which correlates with the calculated Darcy mesh-size in 4.6.3.2. On the contrary, a much lower MWCO was observed for HPFCM from DC02 composition. Presumably, a major resistance in mass transfer and sieving for this composition was attributed to swollen hydrogel network in the vertical direction that shifted MWCO to a lower value. The MWCO obtained for HPFCM from composition with lower monomer content; M10 was comparably high. Once again, a good correlation between MWCO and the previous data on microstructure of HPFCM was noticed (*c.f.* 4.6.3.2).

#### 4.6.3.5.3 *Effect of temperature*

At 45 °C, although faster diffusion was observed as a result of decreased viscosity, almost no effect on MWCO was observed for the unmodified 30 nm PET membrane. The modified membranes changed more strongly due to the temperature-responsive behaviour of the PNIPAAm network. This gave rise to a switching of size-selective barrier properties: a clear shift of the cut off towards higher value was observed (Table 4.22). Note that at higher temperature a significant hindrance towards solute diffusion by the collapsed hydrogel was still observed. This would be in line with the microsineresis evoked (*c.f.* 4.6.3.4); no large openings (“macropores”) throughout the barrier were formed; just the hydrogel void spacing in the lower nm range was modified.

From Table 4.22, it can be seen that the degree of switching is highly dependent on compositions. The degree of switching for HPFCM based on highest polymer fraction (M15DC10) was less pronounced; a change in MWCO was only from 5000 to almost 6000 g/mol. This is attributed to the compactness of the hydrogel network, even when in its collapsed structure, the membrane barrier is relatively obstructed. Following this trend, the MWCO shift of HPFCM was DC10 < DC05 < DC02 and also M15 < M10 (Table 4.22). A significant shift in MWCO was observed for HPFCM from composition with lower monomer as well as crosslinker content (M10DC05 and M15DC02). In case of HPFCM based on M15DC02, such significant MWCO shift corresponds to a degree of switching of the membrane barrier from UF to MF.

#### 4.6.3.6 Size-selectivity of pore-filled composite membranes under ultrafiltration

The fractionation of a polydisperse mixture of macromolecular test substances by HPFCM prepared under varied conditions was studied in more detail under UF conditions. It was evaluated in terms of rejection properties, i.e., MWCO and shape of the rejection curves. The results are presented in Figures 4. 58 - 4.61.

##### 4.6.3.6.1 Effect of UV-irradiation time

The influence of UV time during preparation on the dextran rejection was studied in detail. The measurement was performed for HPFCM based on BM\_1000 nm at RT and at relatively small TMP (0.03 bar; Figure 4.58). At longer UV time, higher fraction of NIPAAm monomer had been converted to PNIPAAm (*c.f.* 4.1.2.4.2 and 4.6.3.1). Very low overall rejection was observed for 5 min. A very pronounced shift of MWCO towards smaller molecular weights with increasing UV time was observed; the steepest curve was obtained after 15 min. UV time for functionalization. However, the results for pore-filling with 20 min. UV time deviated from this trend. In the previous subsection (*c.f.* 4.1.2.2.2) <sup>[41]</sup>, the brittleness of the bulk PNIPAAm hydrogel increased when exposed to UV longer than 15 min. This is again an indication that it is necessary to perform pore-filling with optimized UV irradiation time in order to achieve desired barrier properties. Comparing Table 4.21 and Figure 4.58, the MWCO obtained under UF (~ 36000 g/mol) was significantly larger than the one under diffusion conditions (~ 7500 g/mol).

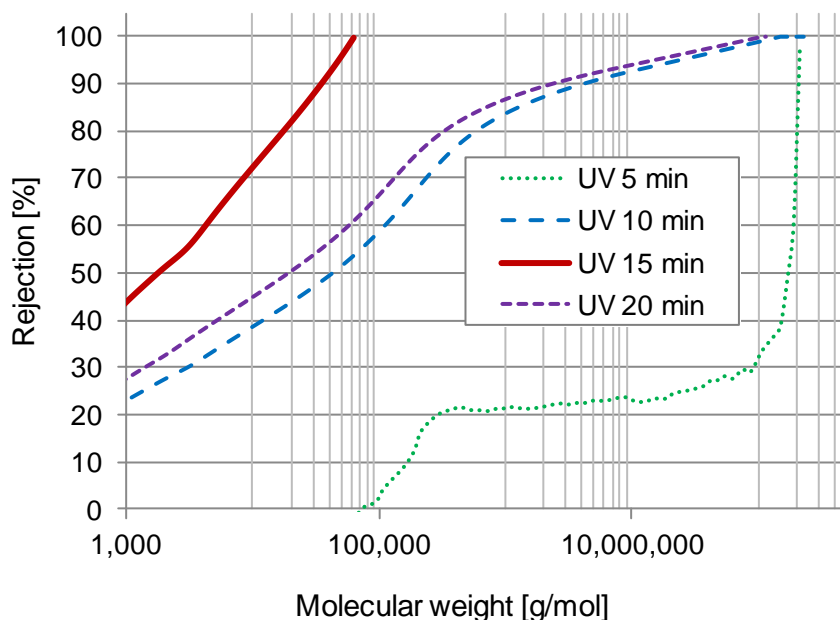


**Figure 4.58** Influence of UV time on ultrafiltration selectivity of HPFCM (base membrane 1000 nm; M15DC05; TMP = 0.03 bar).

#### 4.6.3.6.2 Effect of base membranes

The effect of hydrogel confinement within various pore sizes of BM was also studied under optimized pore-filling conditions, i.e., at 15 min. UV time. At relatively low TMP, smaller MWCO was observed for BM\_200 as compared to BM\_400 and BM\_1000; and this is similar to the results under diffusion conditions. However, all MWCO values were significantly higher than those obtained under diffusion conditions (*c.f.* Table 4.21). Moreover, effectively confining the hydrogel in membrane pores is a precondition for obtaining size-selectivity under convective transport conditions. Analogously, a molecular weight within the 20 to 50 kg/mol range with a systematic trend from BM\_200 nm to BM\_1000 nm had only been seen for a limited base pore size range (Figure 4.59). In contrast, loose fixation of hydrogel in a relatively bigger membrane pore, i.e., within BM\_5000 nm, may lead to too strong deformation the network and ultimately lead to no size-selectivity. This effect can be deduced from the shape of a rejection curve, which shows a very major deviation from other curves.

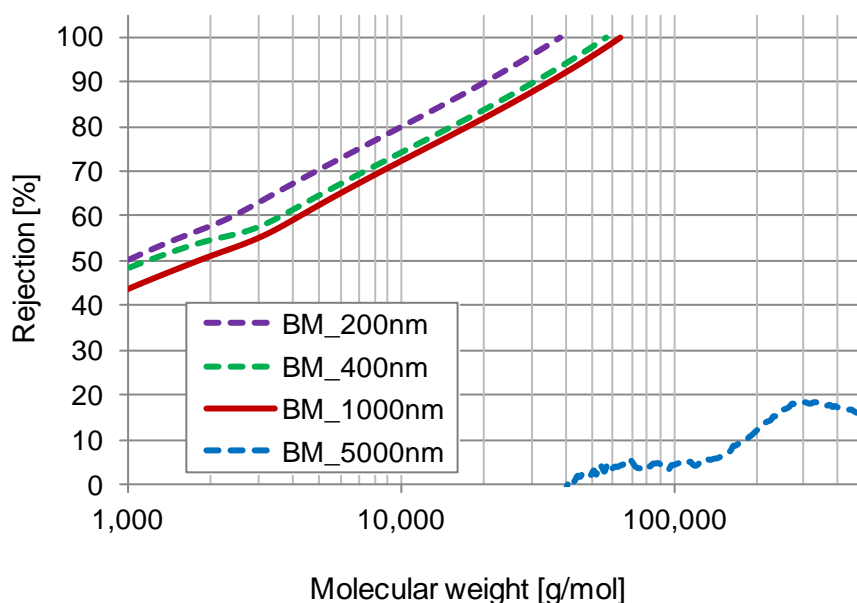


**Figure 4.59** Influence of base membranes pore size on ultrafiltration selectivity of HPFCM (UV time 15 min; M15DC05; TMP = 0.03 bar).

#### 4.6.3.6.3 Effect of transmembrane pressure

To further validate and understand the behavior of a hydrogel network fabricated *via* pore-filling functionalization, UF was investigated as a function of TMP (Figure 4.60). As had already been seen (Figures 4.58 and 4.59 *vs.* Table 4.21), for the HPFCM prepared with the same BM, the MWCO under UF conditions was significantly larger than that obtained under diffusion conditions. Taking a

closer look at the rejection curves presented in Figure 4.60, it can be noticed that the steepest curve was obtained at lowest TMP. The curves showed a strong change, increase of cut-off and stronger deviation from 100 % fractionation for a certain molecular weight, with increasing TMP. This effect became more pronounced in bigger BM pore size (1000 nm). Again, presumably, the hydrogels with same chemical structure were better stabilized in the smaller membrane pore as a result of confinement.

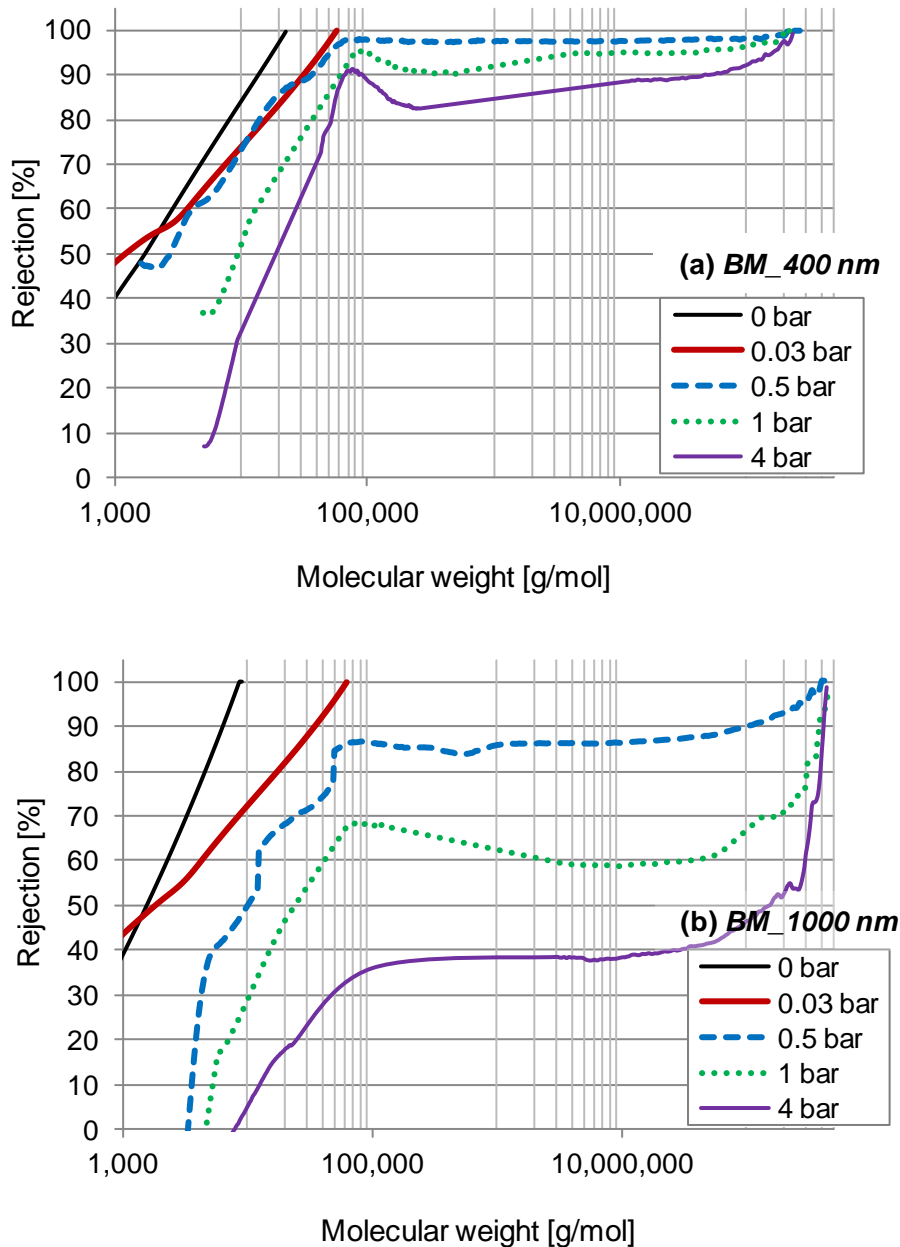


**Figure 4.60** Influence of transmembrane pressure on ultrafiltration selectivity of HPFCM (UV time 15 min; M15DC05) for base membranes with different pore size: (a) 400 nm, (b) 1000 nm.

However, the observed UF results could be explained by two different effects; deformation of dextran molecules during UF or elastic deformation of the hydrogel network. On one hand, with increasing TMP, the ratio between the convective and diffusive transport increased. The increasing convective water flux through the hydrogel imposed also a stronger drag force to the solute molecules. These molecules are not hard spheres; thus, they can be deformed or stretched when dragged and forced through the hydrogel network with increasing viscous flow. Such effects in hydrogel networks are not easy to be measured and no directly related quantitative studies had been found in the literature.

On the other hand, the elastic deformation of the hydrogel is based on the viscoelastic properties of hydrogel network and their entropic origin<sup>[41, 68]</sup>. The hydrogels possess rubber-like elasticity and mesh properties due to crosslinking; either chemical or physical. Thus, a polymer chain in a crosslinked network can be envisioned as an entropic spring. At relatively high TMP, the network is expanded as the polymer chain is stretched. Thus, the less confined hydrogels were more flexible in terms of permitting the convective transport of larger molecules than according to the mesh size of the relaxed hydrogel. Once the external force (i.e., the TMP) is removed the hydrogel network can return to its not deformed state. That this is the case for the HPFCM can be taken from the full recovery of MWCO when the membranes were re-measured at lower TMP or under diffusive conditions after UF at larger TMP (Figure 4.61). Due to the large magnitude of the effects, we believed that drag onto solutes is not the main reason for the pressure / flux effects onto selectivity. To the best of our knowledge, analogous investigations on the changed size-selectivity of transport enabled by the elasticity of hydrogel networks have not yet been reported.

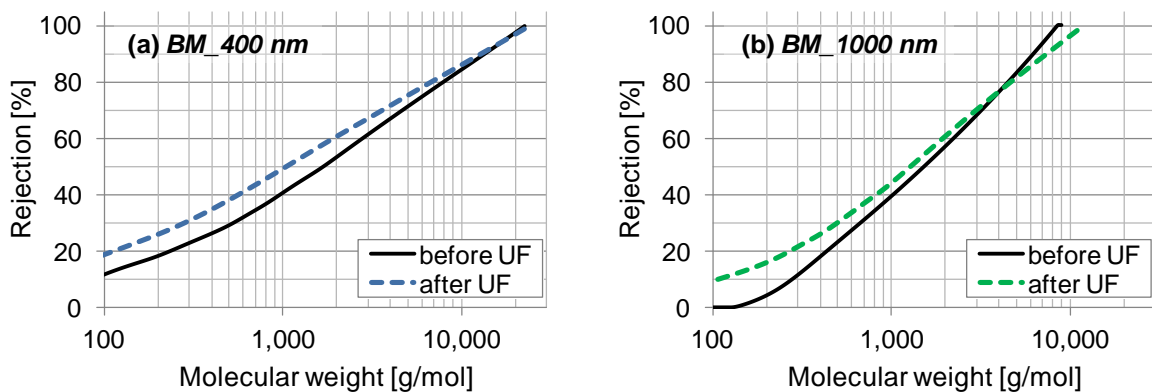


**Figure 4.61** Recovery of MWCO measured before and after ultrafiltration (UV time 15 min; M15DC05; TMP = 0 bar) for base membranes with different pore size: (a) 400 nm, (b) 1000 nm.



#### 4.6.3.6.4 Effect of temperature

Due to the filling functionalization of the membrane pores with the “smart” gels, the barrier properties of the membrane became also switchable as function of the swelling/deswelling transition of the crosslinked PNIPAAm at its LCST. Thus, a shift of MWCO by several orders towards higher value was observed when increasing the temperature to 45 °C (Figure 4.62). Above LCST, the collapsed PNIPAAm hydrogel had also lead to much higher water permeability (*c.f.* Figures 4.55 and 4.56). However, this result is probably even more important because the barrier properties of HPFCM can be switched from macromolecule-size selective UF to MF or even filtration (passage of all macromolecules) just by changing the temperature.

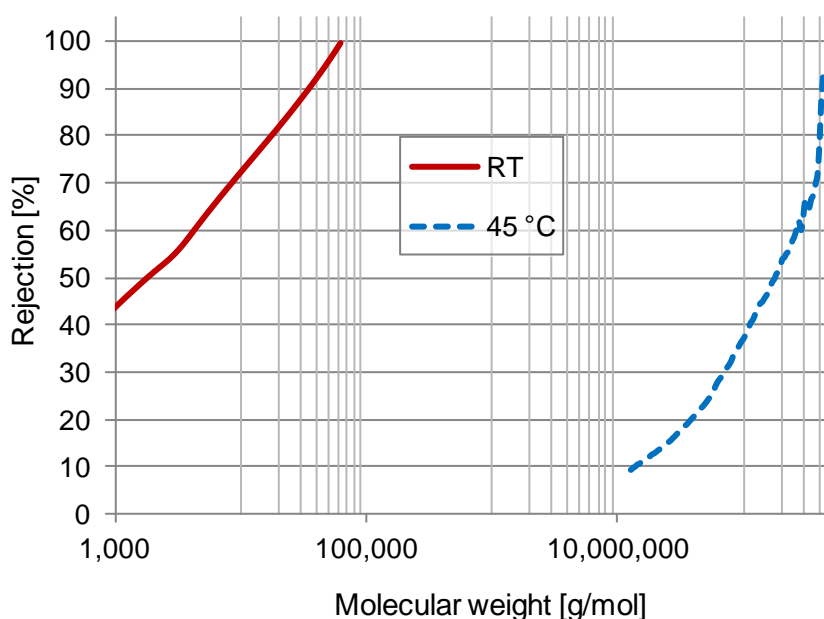


**Figure 4.62** Influence of temperature on ultrafiltration selectivity of HPFCM (UV time 15 min; base membrane 1000 nm; M15DC05, TMP = 0.03 bar).

#### 4.6.3.6.5 Effect of composition

MWCO can be easily tuned by adjusting the sieving coefficient of hydrogel <sup>[1]</sup>. Therefore, the most straightforward strategy to tailor the hydrogel network properties is by obtaining HPFCM from various hydrogel compositions.

Note that all MWCO values were significantly higher than those obtained under diffusion conditions (*c.f.* Table 4.22) analogous to observation in 4.6.3.6.2. This was already explained in details in the same subsection.

Figure 4.63 illustrates the size-selectivity features of HPFCM as function of compositions at relatively low TMP. Here, a clear dependency between the composition and MWCO could be extracted. The smallest MWCO was obtained from HPFCM based on composition M15DC10; composition with the highest monomer and crosslinker content. The obtained MWCO for HPFCM from analogous composition was even smaller than the MWCO for HPFCM from composition M15DC05 based on BM\_200 (Figure 4.59 and Figure 4.63). Besides, the corresponding curve was the steepest among all other compositions of HPFCM. These observations were attributed the mechanical stronger hydrogel network (and yet flexible) obtained from the monomer-rich composition.

Lowering the polymer fraction or crosslinker content signified a large influence on the MWCO as well as the shape of the curves. An intense change of the curves including increment of cut-off and fractionation for a certain molecular weight was less than 100 %. This may imply a lack of stability of the monomer-poor composition. Nevertheless, these data already indicated that the sieving coefficient may eventually be tuned based on the diversification of hydrogel networks as function of HPFCM compositions. It is also foreseen that preparation of HPFCM from various compositions in a smaller BM pore-size will enhanced the overall size-selectivity.

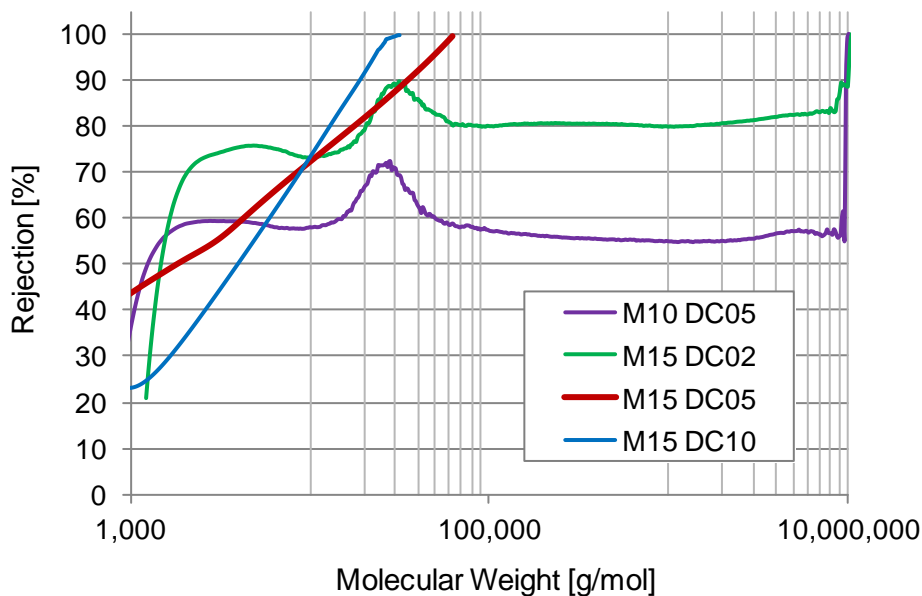


**Figure 4.63** Influence of compositions on ultrafiltration selectivity of HPFCM (UV time 15 min; base membrane 1000 nm, TMP = 0.03 bar).

#### 4.6.3.7 Mechanism for tunable and switchable size-selectivity of composite membranes

In a general view, the transport through HPFCM (Figure 4.64), can be influenced by three consecutive steps; (i) convective flow (or diffusion) until macropore entrance, (ii) the molecules which are larger than the mesh of the hydrogel are rejected from the pores by size-exclusion mechanism, and (iii) convection (or diffusion) of smaller molecules through the swollen network of membrane-confined hydrogels (rate-determining step).

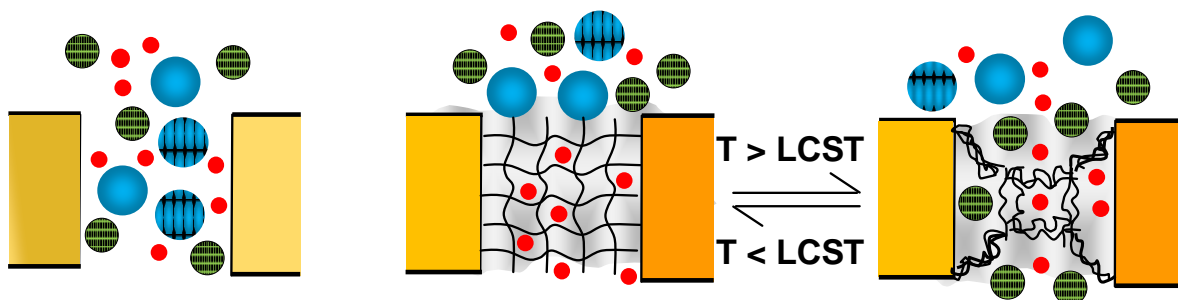


**Figure 4.64** Size-selective separation by hydrogel pore-filled composite membrane compared with unmodified base membrane.

Hydrogels have very high free water content (70-90 %). Thus, the hydrogel network imposes a porous-like structure with the void spacing between hydrophilic chains connected by crosslinking points defining the porosity of the gel, where the permeation of solutes can occur. In literature, this is known as pore mechanism<sup>[19]</sup>. Provided that no affinity between solutes and gel networks is imparted, exclusion of solutes due to "pore" mechanism takes place based on size and shape<sup>[75]</sup>.

The transport of solute toward the space between fibers imposed steric hindrance and hydrodynamic interactions between the solute and the fibers, thereby increasing the friction coefficient for the solute molecule and decreasing its mobility. Due to the steric hindrance imposed by the hydrogel network, the effective diffusion coefficient is always smaller than the free (Stokes-Einstein) diffusion coefficient. In the absence of elastic deformation, mobility of diffusing solute (here macromolecule; *c.f.* 4.6.3.5) is related to the Darcy permeability giving an average value of the mesh-size of the hydrogel network of about 5 nm or smaller. This is the basis for tuning the size-selectivity of the composite membranes *via* variation of preparation conditions, e.g. fraction of crosslinker monomer. In addition, confinement effects due to pore size will have an additional influence (*c.f.* 4.6.3.6.2).

Furthermore, with increasing convective flow, the proposed elastic behavior of the pore-immobilized hydrogels can lead to changed size-selectivity (*c.f.* 4.6.3.6). Above LCST, collapse of membrane confined hydrogel occurs *via* microsineresis, rather than *via* macrosineresis for bulk gels (Figure 4.57; *c.f.* 4.6.3.4). This will largely enhance the mobility of solute and solvent, and facilitate the mass transport through the heterogeneous polymer network with much larger voids than in the swollen state.

One consequence is the very pronounced switching from UF to MF or filter barrier properties (*c.f.* Figure 4.62). In addition to the resulting very interesting composite materials properties, pore-filling functionalization in track-etched membranes provides very interesting insights into hydrogel microstructure in order to understand the mechanisms of tunable permeability and size-selectivity features (*c.f.* 4.6.3.2).

## 5. CONCLUSIONS

In this work, the study of hydrogels was divided into their stimuli-responsivity and smart properties in the bulk state and their separation functions in the membrane formats.

First, PNIPAAm hydrogels were prepared as bulk materials (*ex situ*) and within a rheometry system (*in situ*). The final properties of these hydrogels were greatly influenced by the way the initiation triggered the polymerization. It was demonstrated that either manipulating the accelerator/initiator ratio for redox polymerization or tuning PI concentration and UV irradiation time for photopolymerization can well control the kinetics of reaction and optimize the reaction conditions.

Monitoring the polymerization toward bulk hydrogels with conventional methods was valuable, but limited with respect to quantitative information. Deeper insights were gained through the time-resolved monitoring of the conversion of NIPAAm to PNIPAAm using rheology. The results have shown that this technique was highly reproducible and reliable. Rheology enabled detailed assessment on the gelation mechanism by monitoring the evolution of liquid- ( $G''$ ) and solid- ( $G'$ ) related properties. Knowledge gained from these measurements can be summarized as follows. *Via* redox-initiation, manipulating the TEMED/APS ratio had improved the overall polymerization kinetics. In contrast, obtaining hydrogels with tailored properties *via in situ* photopolymerization was much easier and faster. The control over photopolymerization through the initiation step triggered upon UV irradiation enabled the generation of free radicals at the desired rate; this was illustrated by syntheses using interrupted UV irradiation. *In situ* rheological measurement also enabled the exploration of the parameter structure relationships upon changing the UV intensity or irradiation time.

Overall, these data suggested that synthesis of hydrogels *via* photopolymerization is more suitable for preparation under challenging conditions, e.g. in microsystems; redox-initiated polymerization is less favourable due to its autocatalytic nature. The advantages of photopolymerization include: i) rapid polymerization time to achieve complete conversion; ii) the reaction will not start without UV as a trigger; the elapsed time prior to polymerization can be manipulated; and iii) photopolymerization can be very selective since the reaction occurs only at certain wavelength. Therefore, this method had been used to prepare pore-filling temperature-responsive hydrogels in membranes with pore diameters between 0.5 and 5  $\mu\text{m}$  and pore lengths of  $\sim 20 \mu\text{m}$  (*c.f.* below).

Rheological measurements do not only provide detailed information about the polymerization but can also be used as a characterization tool of the hydrogel structure. The “perfect” behaviour of hydrogels obtained at sufficiently high monomer conversion was elucidated from frequency sweep measurements.

The mesh size determination from rheology experiments fitted very well with those derived from equilibrium swelling data. Based on temperature programmed rheometry, one could also observe the LCST and the pronounced changes of modulus upon deswelling the hydrogel at higher temperature. Characterization of mesh size of hydrogels is important because it can be used to deduce sieving property of the hydrogel network.

The separation functions for classical bulk PNIPAAm hydrogels was explored from partitioning of test solutes and presented in terms of reflection coefficient. The macromolecular solute exclusion within neutral hydrogel network was observed based on their size; regardless either charged or uncharged character. The partitioning was also estimated based on Ogston's excluded volume model. The empirical relationships between reflection coefficient and solute size from this model were close to those experimentally determined. The excluded-volume effect depends not only on the size of the solute, but also on the volume fraction of the polymer forming the network.

PNIPAAm-based NIP and lysozyme MIP hydrogels were synthesized *via* photo-initiated free radical copolymerization. To our knowledge, photopolymerized MIP hydrogels for protein recognition had not been reported before. Photopolymerization techniques offer several advantages, especially for *in situ* fabrication or integration of hydrogels within microsystems. The weak cation-exchange template-binding monomer (MAA) was used to introduce electrostatic interactions towards a cationic template-protein (lysozyme). Optimization of ionic content of MIP hydrogels at sufficient degree of monomer conversion increased the efficiency of template-protein removal even using a moderate NaCl concentration. It has been shown that MIP hydrogels showed higher protein binding capacity and selectivity towards lysozyme than NIP hydrogels. The temperature-responsive swelling-deswelling modulated the binding ability. Most importantly, specific volume shrinking was observed due to specific interactions between template-protein and imprinted sites, most probably as a result of ion pairing effect between carboxylate and cationic protein groups that induced conformational change and desolvation within hydrogel networks. Due to these interesting properties, this approach is envisioned to facilitate establishment of biomimetic materials. As such, preparation of MIP hydrogels *via* photopolymerization can be adapted to a macroporous support, for instance *via* pore-filling functionalization in order to obtain MIP hydrogels as recognition in a protein-selective membrane.

Furthermore, crosslinked PNIPAAm-*co*-vCE hydrogels having both ion-recognition and temperature-responsivity were successfully prepared *via* redox-initiated free radical copolymerization. The FTIR analysis implied that the vCE was more efficiently copolymerized in the loosely crosslinked hydrogel network. From swelling measurements, a clear trend between ion-recognition properties and vCE fraction in the hydrogel was discovered. The hydrogel copolymers swelled at a larger degree in  $\text{Ba}^{2+} > \text{K}^+$  solutions than in pure water as function of ion concentrations. The dual temperature- and ion-responsive properties of PNIPAAm-*co*-vCE hydrogels are beneficial for the development of smart chemosensors, actuators, metal ion extractors and etc.

Up to date, only a very limited number of works had been reported on the microstructure of hydrogels as "sieving networks" within a confined membrane support. Using track-etched membranes for pore-filling with hydrogel had not been done before; however, it is also fundamentally interesting because different from the MF membranes with irregular porosity, relationships to pore size can easily be developed. In this work, a simple and yet effective strategy to approach this goal was studied. HPFCM with tunable size-selectivity and temperature-responsive features were prepared via photoinitiated pore-filling functionalization of track-etched membranes with "smart" PNIPAAm hydrogels. Identifying suitable pore-filling conditions was necessary to achieve these composite membranes with the desired transport properties. The microstructure of HPFCM was easily tailored by selecting proper photopolymerization conditions and the synergistic function of hydrogel confinement in various membrane pore sizes. Anchoring the pore-filled hydrogels to the membrane pore was achieved *via* a prefunctionalization with linear grafted PNIPAAm and enhanced mechanical stabilization over wide range of operating conditions (including pressure-driven permeability measurements). The barrier properties of HPFCM can be adjusted as the crosslinked PNIPAAm swells or deswells by decreasing or increasing temperature in the vicinity of its LCST (32 °C). Thus large and reversible switching of hydraulic permeability, solute diffusion and UF performance including MWCO was observed. Higher degree of switching was observed for HPFCM fabricated with larger BM pore sizes since these hydrogels collapsed to higher extent. Diffusion measurements demonstrated size selectivity as function of hydrogel microstructure and correlation between Darcy permeability and size of dextran. A significant shift of MWCO towards higher values was observed under UF conditions. Two possible qualitative explanations were proposed: i) drag force imposed on solute molecules (dextran) with increasing contribution of convective flow leading to solute deformation and thereby forcing it through the hydrogel network, or (ii) increasing elastic deformation of the hydrogel network with increasing TMP and thus permitting the convective transport of larger molecules than corresponding to the mesh size of the not deformed hydrogel. A mechanism for tunable size-selectivity features was also discussed in order to elucidate the understandings of hydrogels as size-exclusion devices and their interplay with a confined membrane support. The novel composite membranes are easy to prepare; hence variations of hydrogel structure and compositions are straightforward, and their key features revealed feasibility and novelty to obtain membranes with tunable and switchable permeability and selectivity. Such a novel approach is very important since it could overcome the limitations of MF or UF processes with conventional membranes, but the composite material concept has also broader implications, for instance, for applications in controlled release or microfluidic systems.

## REFERENCES

- [1] Q. Yang, N. Adrus, F. Tomicki and M. Ulbricht, *J. Mater. Chem.*, 2011, **21**, 2783.
- [2] Medical Department Stores, Hydrogel Wound Dressing, available in <http://www.medicaldepartmentstore.com/Hydrogel-Wound-Dressing-s/295.htm>
- [3] Endo Pharmaceuticals, Vantas® Implant, available in <http://www.endo.com/Vantas.aspx>
- [4] Pall Corporation, Ion-Exchange Chromatographic Resin, available in <http://www.pall.com/main/Laboratory/Literature-Library-Details.page?id=49521>
- [5] P. C. Nicolson and J. Vogt, *Biomaterials*, 2001, **22**, 3273.
- [6] A. C. Jen, C. M. Wake and A. G. Mikos, *Biotechnol. Bioeng.*, 1996, **50**, 357.
- [7] N. A. Peppas and A. R. Khare, *Adv. Drug Delivery Rev.*, 1993, **11**, 1.
- [8] C.-C. Lin and A. T. Metters, *Adv. Drug Delivery Rev.*, 2006, **58** 1379.
- [9] L.-J. Yan and M. J. Forster, *Anal. Biochem.*, 2009, **389**, 143.
- [10] H. Ju, B. D. McCloskey, A. C. Sagle, V. A. Kusuma and B. D. Freeman, *J. Membr. Sci.*, 2009, **330**, 180.
- [11] A. Kumar, A. Srivastava, I. Y. Galaev and B. Mattiasson, *Prog. Polym. Sci.*, 2007, **32**, 1205.
- [12] L. Chen, M. Liu, L. Lin, T. Zhang, J. Ma, Y. Song and L. Jiang, *Soft Matter*, 2010, **6**, 2708.
- [13] M. A. Cohen Stuart, W. T. S. Huck, J. Genzer, M. Müller, C. Ober, M. Stamm, G. B. Sukhorukov, I. Szleifer, V. V. Tsukruk, M. Urban, F. Winnik, S. Zauscher, I. Luzinov and S. Minko, *Nature Mat.*, 2010, **9**, 101.
- [14] C. Fänger, H. Wack and M. Ulbricht, *Macromol. Biosci.*, 2006, **6**, 393.
- [15] X.-Z. Zhang, D.-Q. Wu and C.-C. Chu, *J. Polym. Sci. B: Polym. Phys.*, 2003, **41**, 582.
- [16] X.-Z. Zhang and C.-C. Chu, *Chem. Commun.*, 2004, 350.
- [17] X. S. Wu, A. S. Hoffman and P. Yager, *J. Polym. Sci. A: Polym. Chem.*, 1992, **30**, 2121.
- [18] X.-Z. Zhang, Y.-Y. Yang, T.-S. Chung and K.-X. Ma, *Langmuir*, 2001, **17**, 6094.
- [19] L. C. Dong, A. S. Hoffman and Q. Yan, *J. Biomater. Sci. Polym. Ed.*, 1994, **5**, 473.
- [20] L.-C. Dong and A. S. Hoffman, *J. Contr. Rel.*, 1990, **13**, 21.
- [21] Y.-X. Wang, X.-F. Wang and S.-W. Song, *Adv. Mater. Res.*, 2006, **11-12**, 737.
- [22] D. J. Beebe, J. S. Moore, J. M. Bauer, Q. Yu, R. H. Liu, C. Devadoss and B.-H. Jo, *Nature*, 2000, **404**, 588.
- [23] M. E. Harmon, M. Tang and C. W. Frank, *Polymer*, 2003, **44**, 4547.
- [24] M. E. Byrne, K. Park and N. A. Peppas, *Adv. Drug Delivery Rev.*, 2002, **54**, 149.



- [25] N. Adrus and M. Ulbricht, *Polymer*, 2012, submitted.
- [26] L. Qin, X.-W. He, W. Zhang, W.-Y. Li and Y.-K. Zhang, *Anal. Chem.*, 2009, **81**, 7206.
- [27] Z. Hua, Z. Chen, Y. Li and M. Zhao, *Langmuir*, 2008, **24**, 5773.
- [28] K. Kosik, E. Wilk, E. Geissler and K. László, *J. Phys. Chem. B*, 2008, **112**, 1065.
- [29] X.-Z. Zhang, J.-T. Zhang, R.-X. Zhuo and C.-C. Chu, *Polymer*, 2002, **43**, 4823.
- [30] K. Yagi, J. A. Ruiz and M. C. Sanchez, *Macromol. Rapid Commun.*, 1980, **1**, 263.
- [31] A. Friebe and M. Ulbricht, *Langmuir*, 2007, **23**, 10316.
- [32] C. Geismann, A. Yaroshchuk and M. Ulbricht, *Langmuir*, 2007, **23**, 76.
- [33] N. Adrus and M. Ulbricht, *J. Mater. Chem.*, 2012, **22**, 3088.
- [34] V. Kapur, J. Charkoudian and J. L. Anderson, *J. Membr. Sci.*, 1997, **131**, 143.
- [35] V. Kapur, J. C. Charkoudian, S. B. Kessler and J. L. Anderson, *Ind. Eng. Chem. Res.*, 1996, **35**, 3179.
- [36] X.-Z. Zhang and C.-C. Chu, *J. Mater. Chem.*, 2003, **13**, 2457.
- [37] X.-Z. Zhang, X.-D. Xu, S.-X. Cheng and R.-X. Zhuo, *Soft Matter*, 2008, **4**, 385.
- [38] L. E. Niță, A. P. Chiriac, M. Bercea and I. Neamțu, *Rheol. Acta*, 2007, **46**, 595.
- [39] O. Okay, *Prog. Polym. Sci.*, 2000, **25**, 711.
- [40] D. Singh, D. Kuckling, V. Choudhary, H.-J. Adler and V. Koul, *Polym. Adv. Technol.*, 2006, **17**, 186.
- [41] N. Adrus and M. Ulbricht, *React. Func. Polym.*, 2012, submitted.
- [42] C. Yu, F. Svec and J. M. J. Fréchet, *Electrophoresis*, 2000, **21**, 120.
- [43] C. Geismann and M. Ulbricht, *Macromol. Chem. Phys.*, 2005, **206**, 268.
- [44] M. Ulbricht, *Polymer*, 2006, **47**, 2217.
- [45] A. Salam and M. Ulbricht, *Macromol. Mater. Eng.*, 2007, **292**, 310.
- [46] T. Miyata and T. Urugami, "Biological Stimulus-Responsive Hydrogels", in *Polymeric Biomaterials*, 2nd edition, S. Dumitriu, Ed., Dekker, New York, 2002.
- [47] N. A. Peppas, P. Bures, W. Leobandung and H. Ichikawa, *Eur. J. Pharm. Biopharm.*, 2000, **50**, 27.
- [48] N. A. Peppas, CRC-Press, Boca Raton, Florida, 1987.
- [49] M. Shibayama and T. Tanaka, "Volume phase transition and related phenomena of polymer gels", in *Advances in Polymer Science [Responsive Gels: Volume Transitions I]*, K. Dušek, Ed., Springer, Berlin, 1993, p. 1.

- [50] H. G. Schild, *Prog. Polym. Sci.*, 1992, **17**, 163.
- [51] H. Kubota and A. Fukuda, *J. Appl. Polym. Sci.*, 1997, **65**, 1313.
- [52] M. Ulbricht, *React. Funct. Polym.*, 1996, **31**, 165.
- [53] C. Yan and D. J. Pochan, *Chem. Soc. Rev.*, 2010, **39**, 3528.
- [54] R. H. Colby, L. J. Fetters, W. G. Funk and W. W. Graessley, *Macromolecules*, 1991, **24**, 3873.
- [55] B. Nyström, H. Walderhaug, F. K. Hansen and B. Lindman, *Langmuir* 1995, **11**, 750.
- [56] A. Chenite, M. Buschmann, D. Wang, C. Chaput and N. Kandani, *Carbohydr. Polym.*, 2001, **46**, 39.
- [57] A. Montembault, C. Viton and A. Domard, *Biomacromolecules*, 2005, **6**, 653.
- [58] L. Weng, X. Chen and W. Chen, *Biomacromolecules*, 2007, **8**, 1109.
- [59] O. Okay and W. Oppermann, *Macromolecules*, 2007, **40**, 3378.
- [60] D. Calvet, J. Y. Wong and S. Giasson, *Macromolecules*, 2004, 7762.
- [61] J. L. Trompette, E. Fabrègue and G. Cassanas, *J. Polym. Sci. B: Polym. Phys.*, 1997, **35**, 2535.
- [62] J. Wang and V. M. Ugaz, *Electrophoresis*, 2006, **27**, 3349.
- [63] Y. Zhao, Y. Cao, Y. Yang and C. Wu, *Macromolecules*, 2003, **36**, 855.
- [64] H. Senff and W. Richtering, *J. Chem. Phys.*, 1999, **111**, 1705.
- [65] J. Jagur-Grodzinski, *Polym. Adv. Technol.*, 2010, **21**, 27.
- [66] L. E. Nielsen, *J. Macromol. Sci. C*, 1969, **3**, 69.
- [67] P. Flory and R. Rehner, Jr., *J. Chem. Phys.*, 1943, **11**, 521.
- [68] T. Canal and N. A. Peppas, *J. Biomed. Mater. Res.*, 1989, **23**, 1183.
- [69] R. Yoshida, Y. Okuyama, K. Sakai, T. Okano and Y. Sakurai, *J. Membr. Sci.*, 1994, **89**, 267.
- [70] D. Kuckling, J. Hoffmann, M. Plötner, D. Ferse, K. Kretschmer, H.-J. P. Adler, K.-F. Arndt and R. Reichelt, *Polymer*, 2003, **44**, 4455.
- [71] T. Tanaka and D. J. Fillmore, *J. Chem. Phys.*, 1979, **70**, 1214.
- [72] N. A. Peppas, J. Z. Hilt, A. Khademhosseini and R. Langer, *Adv. Mater.*, 2006, **18**, 1345.
- [73] R. H. Colby, L. J. Fetters and W. W. Graessley, *Macromolecules*, 1987, **20**, 2226.
- [74] M. Marchetti and E. L. Cussler, *Sep. Purif. Rev.*, 1989, **18**, 177.
- [75] J. Tong and J. L. Anderson, *Biophys. J.*, 1996, **70**, 1505.
- [76] K. L. Buehler and J. L. Anderson, *Ind. Eng. Chem. Res.*, 2002, **41**, 464.

- [77] M. L. White, *J. Phys. Chem.*, 1960, **64** 1563.
- [78] J. J. Kim and K. Park, *Bioseparation*, 1999, **7**, 177.
- [79] P. G. Righetti and C. Gelfi, *J. Chromatogr. B*, 1997, **699**, 63.
- [80] J. L. Anderson, *J. Theor. Biol.*, 1981, **90**, 405.
- [81] M. A. Fernandez and G. Carta, *J. Chromatogr. A*, 1996, **746**, 169.
- [82] E. Boschetti, *J. Chromatogr. A*, 1994, **658**, 207.
- [83] A. G. Ogston, *Trans. Faraday Soc.*, 1958, **54**, 1754.
- [84] G. W. Jackson and D. F. James, *The Can. J. Chem. Eng.*, 1986, **64**, 364.
- [85] V. Y. Grinberg, A. S. Dubovik, Dmitry V. Kuznetsov, N. V. Grinberg, A. Y. Grosberg and T. Tanaka, *Macromolecules*, 2000, **33**, 8685.
- [86] B. Zhao and J. S. Moore, *Langmuir*, 2001, **17**, 4758.
- [87] K. Otake, H. Inomata, M. Konno and S. Saito, *Macromolecules*, 1990, **23**, 283.
- [88] C. K. Han and Y. H. Bae, *Polymer* 1998, **39**, 2809.
- [89] Y. H. Bae, T. Okano and S. W. Kim, *J. Polym. Sci. B: Polym. Phys.*, 1990, **28**, 923.
- [90] H. Feil, Y. H. Bae, J. Feijen and S. W. Kim, *Macromolecules*, 1993, **26**, 2496.
- [91] T. Tokuhira, T. Amiya, A. Mamada and T. Tanaka, *Macromolecules*, 1991, **24**, 2936.
- [92] G. Bokias, D. Hourdet, L. Iliopoulos, G. Staikos and R. Audebert, *Macromolecules*, 1997, **30**, 8293.
- [93] L. D. Taylor and L. D. Cerankowski, *J. Polym. Sci. Polym.: Chem. Ed.*, 1975, **13**, 2551.
- [94] I. C. Kwon, Y. H. Bae, T. Okano and S. W. Kim, *J. Contr. Rel.*, 1991, **17**, 149.
- [95] D. De Rossi, K. Kajiwara, Y. Osada and A. Yamauchi, Plenum, New York, 1991.
- [96] E. C. Muniz and G. Geuskens, *Macromolecules*, 2001, **34**, 4480.
- [97] Y. Katsumoto, T. Tanaka, H. Sato and Y. Ozaki, *J. Phys. Chem. A*, 2002, **106**, 3429.
- [98] H. M. Zareie, E. Volga Bulmus, A. P. Gunning, A. S. Hoffman, E. Piskin and V. J. Morris, *Polymer*, 2000, **41**, 6723.
- [99] X. Wang, X. Qiu and C. Wu, *Macromolecules*, 1998, **31**, 2972.
- [100] M. Shibayama, T. Tanaka and C. C. Han, *J. Chem. Phys.*, 1992, **97**, 6842.
- [101] A. Lendlein, Lecture Notes, available in <http://www.chem.uni-potsdam.de/lendlein/downlmakrochem.htm>
- [102] S. Hirotsu, Y. Hirokawa and T. Tanaka, *J. Chem. Phys.*, 1987, **87**, 1392.

- [103] D. Asnaghi, M. Giglio, A. Bossi and P. Righetti, *J. Mol. Struct.*, 1996, **383**, 37.
- [104] A. Y. Kwok, G. G. Qiao and D. H. Solomon, *Polymer*, 2003, **44**, 6195.
- [105] H. Oxley, P. H. Corkhill, J. H. Fitton and B. J. Tighe, *Biomaterials*, 1993, **14**, 1064.
- [106] H. W. Kang, Y. Tabata and Y. Ikada, *Biomaterials*, 1999, **20**, 1339.
- [107] M. Komiyama, T. Takeuchi, T. Mukawa and H. Asanuma, "*Molecular Imprinting: From Fundamentals to Applications*", Wiley-VCH, Weinheim, 2003.
- [108] C. Alexander, H. S. Andersson, L. I. Andersson, R. J. Ansell, N. Kirsch, I. A. Nicholls, J. O'Mahony and M. J. Whitcombe, *J. Mol. Recognit.*, 2006, **19**, 106.
- [109] B. Sellergren, *Trends Anal. Chem.*, 1997, **16**, 310.
- [110] G. Wulff, T. Gross, R. Schönfeld, T. Schrader and C. Kirsten, "Molecular Imprinting for the Preparation of Enzyme-Analogous Polymers", in *Molecular and Ionic Recognition with Imprinted Polymers*, ACS Symposium Series; American Chemical Society, 1998, p. 10.
- [111] I. Andersson Lars, A. Nicholls Ian and K. Mosbach, "Antibody Mimics Obtained by Noncovalent Molecular Imprinting", in *Immunoanalysis of Agrochemicals*, American Chemical Society, 1995, p. 89.
- [112] D. Cai, L. Ren, H. Zhao, C. Xu, L. Zhang, Y. Yu, H. Wang, Y. Lan, M. F. Roberts, J. H. Chuang, M. J. Naughton, Z. Ren and T. C. Chiles, *Nature Nanotech.*, 2010, **5**, 597.
- [113] Z. X. Xu, H. J. Gao, L. M. Zhang, X. Q. Chen and X. G. Qiao, *J. Food Sci.*, 2011, **76**, R69.
- [114] B. Sellergren, "Separation of enantiomers using molecularly imprinted polymers", in *Chiral Separation Techniques*, 3rd edition, G. Subramanian, Ed., Wiley-VCH Verlag GmbH & Co. KGaA, Weinheim, 2007, p. 399.
- [115] K. Haupt, *Anal. Chem.*, 2003, **75**, 376 A.
- [116] A. Kugimiya, Y. Kuwada and T. Takeuchi, *J. Chromatogr. A*, 2001, **938**, 131.
- [117] T. Ikegami, W.-S. Lee, H. Nariai and T. Takeuchi, *Anal. Bioanal. Chem.*, 2004, **378**, 1898.
- [118] G. Vlatakis, L. I. Andersson, R. Muller and K. Mosbach, *Nature*, 1993, **361**, 645.
- [119] N. M. Bergmann and N. A. Peppas, *Ind. Eng. Chem. Res.*, 2008, **47**, 9099.
- [120] R. A. Scott and N. A. Peppas, *Macromolecules*, 1999, **32**, 8674.
- [121] K. A. Stancil, M. S. Feld and M. Kardar, *J. Phys. Chem. B*, 2005, **109**, 6636.
- [122] S. Hjertén, *J. Chromatogr. A*, 1973, **87**, 325.
- [123] S. Hjertén, J. Liao, K. Nakazato, Y. Wang, G. Zamaratskaia and H. Zhang, *Chromatographia*, 1997, **44**, 227.
- [124] D. S. Janiak, O. B. Ayyub and P. Kofinas, *Macromolecules*, 2009, **42**, 1703.
- [125] D. S. Janiak, O. B. Ayyub and P. Kofinas, *Polymer*, 2010, **51**, 665.

- [126] S. H. Ou, M. C. Wu, T. C. Chou and C. C. Liu, *Anal. Chim. Acta*, 2004, **504**, 163.
- [127] K. Hirayama, Y. Sakai and K. Kameoka, *J. Appl. Polym. Sci.*, 2001, **81**, 3378.
- [128] Y.-Q. Xia, T.-Y. Guo, M.-D. Song, B.-H. Zhang and B.-L. Zhang, *Biomacromolecules*, 2005, **6**, 2601.
- [129] J. L. Liao, Y. Wang and S. Hjertén, *Chromatographia*, 1996, **42**, 259.
- [130] E. Turan, G. Özçetin and T. Caykara, *Macromol. Biosci.*, 2009, **9**, 421.
- [131] Z. Chen, Z. Hua, L. Xu, Y. Huang, M. Zhao and Y. Li, *J. Mol. Recognit.*, 2008, **21**, 71.
- [132] A. Uysal, G. Demirel, E. Turan and T. Çaykara, *Anal. Chim. Acta*, 2008, **625**, 110.
- [133] X. Kan, Q. Zhao, D. Shao, Z. Geng, Z. Wang and J.-J. Zhu, *J. Phys. Chem. B*, 2010, **114**, 3999.
- [134] M. Watanabe, T. Akahoshi, Y. Tabata and D. Nakayama, *J. Am. Chem. Soc.*, 1998, **120**, 5577.
- [135] T. Miyata, M. Jige, T. Nakaminami and T. Urugami, *Proc. Natl. Acad. Sci. U.S.A.*, 2006, **103**, 1190.
- [136] Sarhan and G. Wulff, *Makromol. Chem.*, 1982, **183**, 85.
- [137] N. Bereli, M. Andaç, G. Baydemir, R. Say, I. Y. Galaev and A. Denizli, *J. Chromatogr. A*, 2008, **1190** 18.
- [138] P. Mi, L.-Y. Chu, X.-J. Ju and C. H. Niu, *Macromol. Rapid Commun.*, 2008, **29**, 27.
- [139] X.-J. Ju, L.-Y. Chu, L. Liu, P. Mi and Y. M. Lee, *J. Phys. Chem. B*, 2008, **112**, 1112.
- [140] T. Ito, Y. Sato, T. Yamaguchi and S.-I. Nakao, *Macromolecules*, 2004, **37**, 3407.
- [141] S. Okajima, Y. Sakai and T. Yamaguchi, *Langmuir* 2005, **21**, 4043.
- [142] G. Gockel, "*Crown Ethers and Cryptands*", The Royal Society of Chemistry, Cambridge, England, 1991.
- [143] Y. Inoue and G. W. Gockel, "*Cation Binding by Macrocycles: Complexation of Cationic Species by Crown Ethers*", Marcel Dekker Inc., New York, USA, 1990.
- [144] T. Ito, T. Hioki, T. Yamaguchi, T. Shibo, S.-I. Nakao and S. Kimura, *J. Am. Chem. Soc.*, 2002, **124**, 7840.
- [145] D. Kuckling and P. Pareek, *J. Polym. Sci. A: Polym. Chem.*, 2003, **41**, 1594.
- [146] M. Irie, Y. Misumi and T. Tanaka, *Polymer*, 1993, **34**, 4531.
- [147] Q. Luo, Y. Guan, Y. Zhang and M. Siddiq, *J. Polym. Sci. A: Polym. Chem.*, 2010, **48**, 4120.
- [148] T. Ito and T. Yamaguchi, *Langmuir*, 2006, **22**, 3945.
- [149] T. Ito and T. Yamaguchi, *J. Am. Chem. Soc.*, 2004, **126**, 6202.
- [150] T. Ito and T. Yamaguchi, *Angew. Chem. Int. Ed.*, 2006, **45**, 5630.

- [151] M. C. Porter, Noyes Publication, New Jersey, USA, 1990.
- [152] R. E. Kesting, McGraw-Hill, USA, 1971.
- [153] R. W. Baker, 2nd edition, Wiley, West Sussex, England, 2004.
- [154] T. Matsuura, CRC Press, Boca Raton, Florida, 1994.
- [155] M. Mulder, "*Basic Principles of Membrane Technology*", 2nd edition, Kluwer Academic Publishers, Dordrecht, Netherland, 2003.
- [156] Z. Chen, M. Deng, Y. Chen, G. He, M. Wu and J. Wang, *J. Membr. Sci.*, 2004, **235**, 73.
- [157] T. Kitamura, S. Okabe, M. Tanigaki, K.-I. Kurumada, M. Oshima and S.-I. Kanaza, *Polym. Eng. Sci.*, 2000, **40**, 809.
- [158] L. Liang, X. Feng, L. Peurrung and V. Viswanathan, *J. Membr. Sci.*, 1999, **162**, 235.
- [159] G. V. Rama Rao, M. E. Krug, S. Balamurugan, H. Xu, Q. Xu and G. P. López, *Chem. Mater.*, 2002, **14**, 5075.
- [160] L.-Y. Chu, T. Niitsuma, T. Yamaguchi and S.-I. Nakao, *AIChE Journal*, 2003, **49**, 896.
- [161] H. Susanto and M. Ulbricht, *Water Res.*, 2008, **42**, 2827.
- [162] H. Susanto and M. Ulbricht, *Langmuir*, 2007, **23**, 7818.
- [163] T. Yamaguchi, S.-I. Nakao and S. Kimura, *Macromolecules*, 1991, **24**, 5522.
- [164] A. M. Mika and R. F. Childs, *Ind. Eng. Chem. Res.*, 2001, **40**, 1694.
- [165] E. M. Johnson, D. A. Berk, R. K. Jain and W. M. Deen, *Biophys. J.*, 1996 **70**, 1017.
- [166] L. J. Zeeman and A. L. Zydney, Marcel Dekker Inc, New York, 1996.
- [167] A. M. Mika, R. F. Childs and J. M. Dickson, *J. Membr. Sci.*, 1999, **153** 45.
- [168] J. Zhou, R. F. Childs and A. M. Mika, *J. Membr. Sci.*, 2005, **254**, 89.
- [169] T. Yamaguchi, S.-I. Nakao and S. Kimura, *Ind. Eng. Chem. Res.*, 1993, **32**, 848.
- [170] Q. Yu, J. M. Bauer, J. S. Moore and D. Beebe, *Appl. Phys. Lett.*, 2001, **78**, 2589.
- [171] T. Rohr, E. F. Hilder, J. J. Donovan, F. Svec and J. M. J. Fréchet, *Macromolecules*, 2003, **36**, 1677.
- [172] I. Nischang, O. Brueggemann and F. Svec, *Anal. Bioanal. Chem.*, 2010, **397**, 953.
- [173] S. P. Pappas, "*UV Curing Science and Technology*", Plenum Press, New York, 1992.
- [174] M. Tokita, "Friction coefficient of polymer networks of gels", in *Advances in Polymer Science [Responsive Gels: Volume Transitions II]*, K. Dušek, Ed., Springer, Berlin, 1993.
- [175] M. Ulbricht and H. H. Schwarz, *J. Membr. Sci.*, 1997, **136**, 25.

- [176] A. L. Buyanov, L. G. Revel'skaya, E. Y. Rosova and G. K. Elyashevich, *J. Appl. Polym. Sci.*, 2004, **94**, 1461.
- [177] J. M. Kisler, G. W. Steven and A. J. O'Connor, *Mater. Phys. Mech.*, 2001, **4**, 89.
- [178] A. Bonincontro, S. Cinelli, G. Onori and A. Stravato, *Biophys. J.*, 2004, **86**, 1118.
- [179] Wikipedia, Rate Equation, available in [http://en.wikipedia.org/wiki/Rate\\_equation](http://en.wikipedia.org/wiki/Rate_equation)
- [180] X.-Z. Zhang and C.-C. Chu, *J. Mater. Sci. Mater. Med.*, 2007, **18**, 1771.
- [181] X.-Z. Zhang, F.-J. Wang and C.-C. Chu, *J. Mater. Sci. Mater. Med.*, 2003, **14**, 451.
- [182] A. M. Hecht, R. Duplessix and E. Geissler, *Macromolecules*, 1985, **18**, 2167.
- [183] Y. Suzuki, K. Nozaki, T. Yamamoto, K. Itoh and I. Nishio, *J. Chem. Phys.*, 1992, **97**, 3808.
- [184] Y. Cohen, O. Ramon, I. J. Kopelman and S. Mizrahi, *J. Polym. Sci. B: Polym. Phys.*, 1992, **30**, 1055.
- [185] M. V. Badiger, M. E. McNeill and N. B. Graham, *Biomaterials*, 1993, **14**, 1059.
- [186] X. D. Feng, X. Q. Guo and K. Y. Qiu, *Makromol. Chem.*, 1988, **189**, 77.
- [187] G. Moad and D. H. Solomon, "*The Chemistry of Radical Polymerization*", 2nd edition, Elsevier, Oxford, UK, 2006.
- [188] CIBA, available in <http://www.xtgchem.cn/upload/20110629045632.PDF>
- [189] J. D. Ferry, "*Viscoelastic Properties of Polymers*", John Wiley and Sons, Canada, 1980.
- [190] P. G. Righetti, C. Gelfi and A. B. Bosisio, *Electrophoresis*, 1981, **2**, 213.
- [191] P. G. Righetti, C. Gelfi and A. B. Bosisio, *Electrophoresis*, 1981, **2**, 220.
- [192] P. G. Righetti, C. Gelfi and A. B. Bosisio, *Electrophoresis*, 1981, **2**, 291.
- [193] A. Ewa, *Prog. Polym. Sci.*, 2001, **26**, 605.
- [194] X.-Z. Zhang, Y.-Y. Yang and T.-S. Chung, *J. Colloid Interface Sci.*, 2002, **246**, 105.
- [195] X. Zhang and R. Zhuo, *J. Colloid Interface Sci.*, 2000, **223**, 311.
- [196] C. S. Biswas, V. K. Patel, N. K. Vishwakarma, A. K. Mishra and B. Ray, *J. Appl. Polym. Sci.*, 2011, **121**, 2422.
- [197] C.-J. Cheng, L.-Y. Chu, J. Zhang, H.-D. Wang and G. Wei, *Colloid Polym. Sci.*, 2008, **286**, 571.
- [198] E. Turan, S. Demirci and T. Caykara, *J. Polym. Sci. B: Polym. Phys.*, 2008, **46**, 1713.
- [199] D. He, W. Sun, T. Schrader and M. Ulbricht, *J. Mater. Chem.*, 2009, **19**, 253.
- [200] P. Mi, X.-J. Ju, R. Xie, H.-G. Wu, J. Ma and L.-Y. Chu, *Polymer*, 2010, **51**, 1648.
- [201] F. Tomicki, D. Krix, H. Nienhaus and M. Ulbricht, *J. Membr. Sci.*, 2011, **377**, 124.

## Abbreviations and Symbols

3D	Three-dimensional
$A$	Membrane outer surface area [ $\text{m}^2$ ]
$Abs$	Absorbance
$A_{eff}$	Effective membrane area [ $\text{m}^2$ ]
APS	Ammonium persulfate
BM	Base membranes
$c$	Concentration [M]
C	Carbon
$c^{gel}$	Equilibrium concentration in the gel (based on total gel volume) [g/l]
$c^{sol}$	Concentration in the solution [g/l]
CE	Crown ether
CE-12,4	2-crown-4
CE-15,5	15-crown-5
CE-18,6	18-crown-6
$c_F$	Concentration in the feed solution [g/l]
$C_N$	Characteristic ratio (for acrylates = 6.9)
$c_P$	Concentration in the permeate solution [g/l]
$c_{x,0}$	Initial concentration of species $x$ [M]
$c_x$	Concentrations of species $x$ [M]
$c_y$	Concentrations of species $y$ [M]
$D$	Effective diffusion coefficient [ $\text{m}^2/\text{s}$ ]
DC	Degree of crosslinking
DOF	Degree of functionalization
$d_{p,0}$	Pore diameter of the unmodified membrane [nm]
$d_{pref}$	Pore diameter of the prefunctionalized membrane [nm]
ESEM	Environmental scanning electron microscopy
$F_N$	Normal force [N]
FTIR	Fourier transform infrared
$G'$	Storage (elastic) modulus [Pa]
$G''$	Loss (viscous) modulus [Pa]
HCl	Hydrochloric acid
HPC	Hydroxypropyl cellulose
HPFCM	Hydrogel pore-filled composite membranes
IEP	Isoelectric point



---

$J$	Water flux through the membrane [ $l/m^2h$ ]
$K$	Partition coefficient of a solute molecule [-]
$k$	Reaction-rate constant [ $s^{-1}$ ]
$k_{gel}$	Darcy permeability of the gel [ $m^2$ ]
$k_{mem}$	Darcy hydrodynamic permeability of pore-filled gel membrane
$\sqrt{k_{mem}}$	Darcy void spacing or mesh size
$l_C$	The length of C-C single bond (= 0.154 nm)
$l$	Path length
LCST	Lower critical solution temperature
$l_h$	Hydrodynamic layer thickness of the grafted polymer [nm]
$L_P$	Permeability [ $l/m^2hbar$ ]
M	Main monomer content
$M$	Molecular weight of the two monomers and their ratio in the gel
$M'$	Ionic comonomer content
$M(MBAAm)$	Molecular weight of MBAAm
$M(NIPAAm)$	Molecular weight of NIPAAm
MAA	Methacrylic acid
MBAAm	$N,N'$ -methylenebisacrylamide
$M_c$	Number average molecular weight between crosslinks
$m_{c,cl}$	Mass of carbon in crosslinker
$m_{c,co-mon}$	Mass of carbon in comonomer
$m_{c,gel}$	Mass of carbon in gel.
$m_{c,inert}$	Mass of carbon in inert material; i.e., co-solvent
$m_{c,mon}$	Mass of carbon in main monomer
$m_d$	Mass of the dry network
MF	Microfiltration
MIP	Molecularly imprinted polymers
$m_{res,net}$	Net mass residues of carbon in the washing water
$m_{res,tot}$	Summation mass residues of carbon
$m_s$	Mass of the swollen network
MW	Molecular weight
MWCO	Molecular weight cut-off
MWD	Molecular weight distribution
$n_{cl}$	Number of elastically effective crosslinking points
$n$	Number of washing
$n(MBAAm)$	Mol of MBAAm

---

$n(\text{NIPAAm})$	Mol of NIPAAm
$N_A$	Avogadro's number.
NaCl	Sodium chloride
NF	Nanofiltration
$N_{(\text{lysozyme})}$	Number of lysozyme molecule
$N_{(M)}$	Number of template-monomer molecule
NIP	Non-imprinted polymers
NIPAAm	<i>N</i> -isopropylacrylamide
PAAm	Polyacrylamide
PAm	Polyamide
PAN	Polyacrylonitrile
PC	Polycarbonate
PE	Polyethylene
PEG	Polyethylene glycol
PES	Polyethersulfone
PET	Polyethylene terephthalate
PHEMA	Poly(2-hydroxyethyl methacrylate)
PI	Type I photoinitiator ( Irgacure 2959 <sup>®</sup> )
PIPS	Polymerization-induced phase separation
PNIPAAm	Poly( <i>N</i> -isopropylacrylamide)
PNIPAAm- <i>co</i> -MAA	Poly( <i>N</i> -isopropylacrylamide- <i>co</i> -methacrylic acid)
PNIPAAm- <i>co</i> -vCE	Poly( <i>N</i> -isopropylacrylamide- <i>co</i> -4-vinylbenzo-18-crown-6)
PP	Polypropylene
PPG	Polypropylene glycol
Pref	Prefunctionalization
PSu	Polysulfone
PTFE	Poly(tetrafluoroethylene)
PVDF	Poly(vinylidene fluoride)
$Q$	Degree of swelling
$r$	Distance between two crosslinking points
$R$	Universal gas constant
Ref.	Reference
$r_f$	Radius of the polymer fiber
$r_s$	Radius of the solute
RT	Room temperature ( $23 \pm 2$ °C)
SEM	Scanning electron microscopy

---

SRH	Stimuli-responsive hydrogels
$T$	Absolute experimental temperature
$t_{1/2}$	half-life
$\tan \delta$	Dissipation factor
TEMED	<i>N,N,N',N'</i> -tetramethylethylenediamine
THF	Tetrahydrofuran
TIPS	Temperature-induced phase separation
TMP	Transmembrane pressure
TOC	Total organic carbon
UF	Ultrafiltration
$V$	Volume of permeate [l]
vCE	4-vinylbenzo-18-crown-6
$V_{wash}$	Volume of washing medium [l]
$x$	Reactant species
$y$	Product species
$\gamma$	Strain deformation [%]
$\Delta G$	Gibbs free energy
$\Delta H$	Enthalpy
$\Delta N$	Amount of material [mol]
$\Delta P$	Transmembrane pressure [bar]
$\Delta S$	Entropy
$\Delta t$	Time [s]
$\Delta x$	Membrane thickness [m].
$\varepsilon_{mem}$	Membrane porosity [%]
$\varepsilon$	Molar absorptivity [l/mM.cm]
$\varepsilon_x$	Molar absorptivity of species $x$ [l/mM.cm]
$\varepsilon_y$	Molar absorptivity of species $y$ [l/mM.cm]
$\eta$	Viscosity of water [Pa.s]
$\lambda$	Wavelength
$\zeta$	Mesh size of bulk hydrogel
$\sigma$	Retention or reflection coefficient
$v_{2,s}$	Polymer volume fraction
$\omega$	Angular frequency [rad/s]

## *List of Awards and Publications*

### **Award:**

- 1) Oral presentation awards in Summer School Romania 2010; worth EUR 300 and certificate.
- 2) Sponsorship to take part in a conference for POLYDAYS 2010, Berlin from the *Gesellschaft Deutscher Chemiker GDCh (The German Chemical Society)*; worth EUR 150.
- 3) Travel Awards to take part in a conference; ICOM 2011; Amsterdam from the *European Membrane Society*; worth EUR 250.

### **Review Article:**

Q. Yang, **N. Adrus**, F. Tomicki & M. Ulbricht. Composites of functional polymeric hydrogels and porous membranes. *J. Mater. Chem.* 2011, 21, 2783.

### **Paper in Journal (Peer-reviewed):**

- 1) **N. Adrus** and M. Ulbricht. Rheological studies on PNIPAAm hydrogel synthesis *via in situ* polymerization and on resulting viscoelastic properties, *React. Func. Polym.* (2012) submitted.
- 2) **N. Adrus** and M. Ulbricht. Novel hydrogel pore-filled composite membranes with tunable and temperature-responsive size-selectivity, *J. Mater. Chem.* **12** (2012) 3088.
- 3) **N. Adrus** and M. Ulbricht. Molecularly imprinted stimuli-responsive hydrogels for protein recognition, *Polymer* (2012) submitted.
- 4) **N. Adrus**, T. Hennecke and M. Ulbricht. Performance of hydrogel pore-filled composite membranes as tunable ultrafiltration device, *J. Membr. Sci.* (2012) in preparation.

### **Invited talk on occasion of Neujahrskolloquium (New Year Colloquium):**

**N. Adrus**. Smart hydrogel pore-filled composite membranes: features and performance, Faculty of Chemistry, Universität Duisburg-Essen, January 2011.

**Oral presentation in conferences:**

- 1) **N. Adrus** and M. Ulbricht.  
Development of Pore-Filling Stimuli-Responsive Membranes with Polymer Hydrogel Systems.  
1<sup>st</sup> Regional Conference on Materials (RCM 2009), Penang, Malaysia.
- 2) **N. Adrus**, T. Hennecke and M. Ulbricht.  
Transport through tailored & switchable barrier of HPFCM.  
European Membrane Society Summer School (EMS-SS 2010), Bucharest, Romania.
- 3) **N. Adrus** and M. Ulbricht.  
Temperature-Responsive and Protein-Selective Hydrogels *via* Molecular Imprinting.  
Zsigmondy Colloquium 2011, Münster, Germany.
- 4) **N. Adrus** and M. Ulbricht.  
Molecularly imprinted stimuli-responsive hydrogels for protein recognition.  
Frontiers in Biomedical Polymers (FBPS 2011), Funchal, Portugal.
- 5) **N. Adrus** and M. Ulbricht.  
Novel composite membranes with switchable ultrafiltration functions.  
International Congress on Membranes and Membrane Processes (ICOM 2011),  
Amsterdam, The Netherlands

**Poster presentation in conferences:**

- 1) **N. Adrus** and M. Ulbricht.  
Photopolymerization of *N*-isopropylacrylamide Hydrogel Towards Preparation of Functional  
Pore-Filling Composite Membrane.  
International Symposium on Macro- and Supramolecular Architectures and Materials  
(MAM 2008), Düsseldorf, Germany.
- 2) **N. Adrus** and M. Ulbricht.  
Transport through Temperature-Responsive Hydrogels with Improved Mechanical Stability  
Prepared by Reactive Membrane Pore-Filling.  
European Polymer Congress (EPF 2009), Graz, Austria.
- 3) **N. Adrus** and M. Ulbricht.  
Smart Performance of Hydrogel Pore-Filled Stimuli Responsive Membranes.  
EUROMEMBRANE 2009, Montpellier, France.

- 4) **N. Adrus** and M. Ulbricht.  
Separation Performance of Hydrogel Pore-Filled Composite Membranes.  
Informationtag Membrantechnik (DECHEMA 2011), Frankfurt, Germany.
- 5) **N. Adrus** and M. Ulbricht.  
Transport of biomacromolecules through temperature-responsive HPFCM.  
GDCh Polymers in Biomedicine and Electronics (POLYDAYS 2010), Berlin, Germany.

## ***Curriculum Vitae***

Name : Nadia binti Adrus  
Nationality : Malaysian  
Date/Place of Birth : 15 July 1978/ *in* Perlis Malaysia



### **Education**

1996 - 2000 : *Bachelor of Chemical Engineering*  
Universiti Teknologi Malaysia, Johor, MALAYSIA

2005 - 2007 : *M.Sc. Applied Polymer Science*  
Martin Luther Universität, Halle-Witternberg, GERMANY

2007 - 2012 : *Dr. rer. nat. (Research in Stimuli-Responsive Polymers/Membranes)*  
Universität Duisburg-Essen, GERMANY

### **Professional career**

Nov 2000 – Dec 2001 : *Associate Research Officer*  
SIRIM Berhad, Shah Alam, Malaysia

April 2002 – June 2003 : *QA Engineer*  
Mardec Polymers Sdn Bhd, Penang, Malaysia

July 2003 – to date : *Lecturer*  
Universiti Teknologi Malaysia, Johor

### **Scholarships**

Mac 2005 – Sept 2007 : **Malaysian Government Scholarship** - for master studies  
*sponsored by* Universiti Teknologi Malaysia

Nov 2007 – Oct 2011 : **Malaysian Government Scholarship** - for doctoral studies  
*sponsored by* Ministry of Higher Education Malaysia